INVESTIGATION OF MICROBIAL EXOELECTROGENICITY FOR ELECTROCHEMICAL ENERGY CONVERSION

by

NARENDRAN SEKAR

(Under the Direction of Ramaraja P. Ramasamy)

ABSTRACT

The ability of microorganisms to transfer electrons to electron acceptors present outside their cellular envelope is called exoelectrogenicity. This study focuses on investigating exoelectrogenicity of cyanobacteria (CB) to generate electricity in a photo-bioelectrochemical cell. Investigation using site-specific photosynthesis inhibitors revealed that the electrons were redirected predominantly from photosystem II to the electrode via plastoquinone pool. Despite having huge advantages for solar energy conversion, CB could not efficiently perform extracellular electron transfer (EET). The reasons being, (1) unlike natural exoelectrogens, CB did not possess any special features on outer membrane to exhibit EET and (2) electrons generated in photosynthetic electron transport chain were channeled into respiratory pathways rather than to the electrode. To overcome the first caveat, CB named *Synechococcus elongatus*

PCC7942 was genetically engineered to express outer membrane c-type cytochrome (OmcS). The genetically engineered CB (*omcs*) was found to exhibit two-fold greater rate of ferricyanide reduction and generated ~ nine-fold higher photocurrent compared to the wild-type (*wt*). To address the second issue, each of three respiratory terminal oxidases present in *S. elongatus* was knocked-out and their role towards EET was investigated. The mutant *cyd*$^{-}$ (strain lacking bd-quinol oxidase) was observed to exhibit higher EET than *wt* as evident from its higher ferricyanide reduction rate. This result clearly corroborated the fact that bd-quinol oxidase distracted more electrons from the plastoquinone pool. Further, the strain *cyd*$^{-}$*omcs* (i.e., CB that contained OmcS and lacked bd-quinol oxidase) was observed to generate the most photocurrents compared to *wt*, *cyd*$^{-}$ and *omcs*. In addition to enhancing the exoelectrogenicity of CB, EET of a hyperthermophilic archaeon named *Pyrococcus furiosus* was explored by studying its ability to (1) reduce exogenously added ferric oxide and ferric citrate, and (2) generate electricity in a two-chamber microbial fuel cell operated at 90 ^{o}C. As a concluding note, a mathematical model has been developed to study the effect of incident light intensity on performance of a biofilm-based anode. Results and findings presented in this dissertation could make significant contributions to the existing knowledge of microbial exoelectrogenicity and benefit advancing the technology of sustainable electricity generation from microorganisms.

INDEX WORDS: Exoelectrogenicity, Cyanobacteria, Microbial Fuel Cell, Pyrococcus furiosus, Outer Membrane Cytochrome, Respiratory Terminal Oxidases, Mathematical Modeling

INVESTIGATION OF MICROBIAL EXOELECTROGENICITY FOR ELECTROCHEMICAL ENERGY CONVERSION

by

NARENDRAN SEKAR

B. TECH., Anna University, Chennai, India, 2009

M.S., Anna University, Chennai, India, 2012

A Dissertation Submitted to the Graduate Faculty of The University of Georgia in Partial Fulfillment of the Requirements for the Degree

DOCTOR OF PHILOSOPHY

ATHENS, GEORGIA

2016

INVESTIGATION OF MICROBIAL EXOELECTROGENICITY FOR ELECTROCHEMICAL ENERGY CONVERSION

by

NARENDRAN SEKAR

Major Professor: Ramaraja P. Ramasamy

Committee: Yajun Yan
Michael W. W. Adams
William B. Whitman

Electronic Version Approved:

Suzanne Barbour
Dean of the Graduate School
The University of Georgia
December 2016

DEDICATION

to my mom, dad and grandparents

Arise! Awake! and stop not until the goal is reached!

-Swami Vivekananda

ACKNOWLEDGEMENTS

First and foremost, I would like to thank GOD (OM NAMA SIVAYA) for giving me energy courage and confidence in all actions and deeds that I perceive in both my professional and personal life.

I would like to extend my sincere gratitude to my PhD supervisor Dr. Ramaraja P. Ramasamy. Since the day I joined his research group at UGA, he has been a continuous support throughout my career as a PhD student at UGA. In addition to his guidance for my PhD research work, he trained me in multiple aspects such as writing manuscripts, patents and grants and honed my multitasking ability. Next, I would like to thank my PhD dissertation committee members: Dr. Yajun Yan, Dr. Michael W. W. Adams and Dr. William B. Whitman for their advice, suggestions and comments, that motivated me throughout my research work. For a graduate student, the lab would eventually become a second-home. I am very thankful to my friends, colleagues and labmates: Yi Fang and Yan Zhou who made the lab environment cheerful and happy to work in. It is my pleasure to thank my friend and our earlier post-doc Dr. Yogeswaran Umasankar, who helped me during my initial phase of the PhD work. I greatly appreciate the help offered by all of my friends and collaborators Rachit, Perry, Jackie and Dr. Manjinder Singh without whom my PhD work would not be finished in entirety. I wish to thank all of my teachers who instructed me at Anna University and UGA. You are the greatest asset that I earned through my academic career as a student. I thank all my friends at Riverbend and UGA who directly and/or indirectly helped and motivated me through the course of my PhD work. I wish to make a

special mention about the UGA-Georgia iGEM teams 2012-2016, with whom I acquainted with as one of the instructors during my graduate studies at UGA and learnt how to do science with fun.

It gives me an immense pleasure to thank my macha Suraj, who has been my well-wisher and a great support morally and spiritually. Suraj has been motivating and advising me, right from taking the decision to join PhD at UGA until proof-reading the dissertation. And, my entire acknowledgment session would not complete without mentioning my dear friends Ahil anna, Ronald macha and Kabi macha, who are always cheering me up overseas. Last, but not least, I would love to dedicate this work to my mom, dad, grandparents, my sisters, including my little nephew Tejesh and all my family members who always pray for me and wish all the good things to happen in my life. Thank you all.

TABLE OF CONTENTS

CHAPTER 1

INTRODUCTION

This chapter contains text modified from the following two publications:

Narendran Sekar and Ramaraja P. Ramasamy. 2015. *Journal of Photochemistry and Photobiology C: Photochemistry Reviews*. 22:19–33.

Reprinted here with permission of the publisher.

Narendran Sekar and Ramaraja P. Ramasamy. 2015. *ElectroChemical Society Interface*. Fall Issue:67-73.

Reprinted here with permission of the publisher.

The ability of microorganisms to transfer electrons to electron acceptors present outside their cellular envelope is called exoelectrogenicity. This process of extracellular electron transfer is being utilized by the most primitive microorganisms, evolved on the earlier Earth, as one of the major modes of energy conservation. For example, microorganisms that thrive in iron rich sediments use insoluble iron-oxides (Fe(III) oxide) as electron acceptors via extracellular electron transfer. This has a huge impact on biogeochemistry of the Earth and continuously sculpts the biosphere that we are living in, which is clearly evident from the central role of Fe in active site of almost, if not all, redox proteins that you can think of. The microbial exoelectrogenicity is being exploited in numerous ways to benefit humankind such as in microbial fuel cell (MFC) to produce electricity in sustainable manner, bioremediation to convert the toxic form of heavy metals to less-harmful form, bio-sensing and quorum signalling applications.

The research work reported in this dissertation is focussed on exploring exoelectrogenicity, especially for generating electricity, of two different microorganisms that are diverse in their physiology, metabolism and evolutionary traits.

1) Cyanobacteria – photosynthetic microorganisms that are ancestors for today's chloroplast and are known to perform the first oxygenic photosynthesis in the planet Earth.
2) Hyperthermophilic Archaea – microorganisms that thrive in extreme hot environments with temperature nearing 100 °C.

In addition to exploring the cyanobacterial exoelectrogenicity, a successful and novel attempt has been made to enhance its exoelectrogenicity by genetically modifying them. On the other hand, a pure culture of hyperthermophilic microorganism has been demonstrated, for the first time, to generate electricity in a MFC that was operated at a higher temperature of 90 °C. The following sections provide an elaborate background for the need, the state of the art and the knowledge gap in using cyanobacteria to generate electricity, followed by introducing the hyperthermophile *Pyrococcus furiosus* and its unique metabolism that proven to be a better candidate to exhibit exoelectrogenicity and generate current in the MFC.

1.1 Green Electricity

1.1.1. Solar Energy Conversion

Energy crisis is one of the most important issues that mankind facing in the 21st century. A great deal of ongoing research is focused on developing renewable, self-sustainable and environment friendly sources of energy. The currently available renewable resources include sunlight, wind, rain, tides and geothermal heat, accounting for around 16% of the global energy usage. Among these renewable sources, sunlight is the most abundant, ubiquitous and reliable energy source. Earth receives about 120,000 TW of solar energy each year, which far exceeds our current global annual demand of ~16 TW (Hoffert et al. 2002). The major routes through which solar energy conversion is currently achieved are photosynthesis in nature and photovoltaics.

Photosynthesis is an incredible aspect of nature's ability to convert solar energy into chemical energy and has an evolutionary significance on existence of today's life. The primitive photosynthetic bacteria such as purple sulfur bacteria and green sulfur bacteria carry out anoxygenic photosynthesis that produces elemental sulfur from hydrogen sulfide with the help of sunlight. On the other hand, cyanobacteria, algae and plants carry out oxygenic photosynthesis to convert water and carbon dioxide to sugars with the help of sunlight and releasing oxygen as a byproduct. In fact, oxygenic photosynthesis is the only natural process known on earth to form oxygen from water. Further, fossil fuels such as coal, petroleum and natural gas are formed from the remains of buried dead plants by exposure to heat and pressure in the earth's crust over millions of years. With increasing energy crisis and environmental issues lately, now is the time to revisit photosynthesis in order to address these two burgeoning issues.

Photovoltaic devices such as solar panels generate electrical power by converting solar radiation into direct current electricity using semiconductors. Solar cells include: (1) first generation conventional wafer–based cells made up of crystalline silicon; (2) second generation thin film solar cells made up of amorphous silicon, cadmium telluride and copper indium gallium selenide and (3) third generation emerging solar cells such as organic solar cells, dye sensitized solar cells (DSSC) and quantum dots solar cells, each with their own efficiency limits, advantages and disadvantages.

1.1.2. Photosynthesis versus Photovoltaics

Photosynthesis converts light energy into chemical energy and the energy is stored within chemical bonds like biofuels or biomass. There is various consensuses about the definition of efficiency with respect to photosynthesis. All the numbers reported in literature, ranging from as low as ~ 1% to as high as ~ 100 %, are in fact correct with respect to the definition of efficiency. The internal quantum efficiency of charge separation step in natural photosynthesis process is ~ 100% at optimal conditions (Wraight and Clayton 1973), i.e., for every single photon absorbed by chlorophyll molecule, an excited electron is generated within the reaction center of photosystem. The light-biomass conversion efficiency is ~ 1 % for higher plants and ~ 3 % for microalgae. A lot of factors such as non-bioavailable photon waste (energy outside photosynthetic action spectrum), wavelength-mismatch, incomplete absorption, reflectivity of leaf, etc., contribute to the losses and reduce the efficiency. Chlorophyll-a, the primary photosynthetic pigment in both the photosystems (PSI and PSII), competes with the same wavelength, drastically reducing the photosynthetic efficiency by half. It is also important to note that the energy conserved in the form of ATP (cellular energy currency) are used for the maintenance, repair and self-heal from damage, and growth. Another fascinating aspect of photosynthesis is that the CO_2, one of the major greenhouse gases, is sequestered during the process in the form of sugars.

PVs converts light energy directly into electrical energy and the energy is stored in batteries and are then transmitted. The energy conversion efficiency of PV based devices is around 18 ± 2 % for the direct electricity generations (Green et al. 2010). With the advancement of engineering

design and optimizations, so far, the efficiency has been pushed to ~ 45 % (gallium arsenide based multiple junction solar cells (Luque and Hegedus 2003). PVs can absorb a wide range of electromagnetic radiations such as ultraviolet, infrared in addition to visible light. In a two junction PV (similar to two photosystems in photosynthesis), the band-gap of semiconductors can be manipulated to absorb photons of two different wavelengths. The materials and components of the PV system must come from limited global resources and are not 100% recyclable. The PV technology can never sequester CO_2 and no artificial system, yet devised, including PVs can self-heal or repair from the damage.

By and large, the energy conversion efficiency of current photovoltaic cell can be compared with that of a living photosynthetic cell and both the systems work very differently (Blankenship et al. 2011). However, this can be somehow resolved by considering a PV based water electrolysis system, in which the electrical energy converted from the light energy by a PV device is used for hydrolyzing water into oxygen and hydrogen with a reported efficiency of ~ 11% (Blankenship et al. 2011). Yet, other aspects such as CO_2 fixation, self-repair and healing, and growth of a photosynthetic cell can never overweigh the artificial PV device.

1.1.3. Photosynthetic Electron Transport Chain

In higher plants, photosynthesis takes place in compartmentalized organelle called chloroplasts. The inner matrix of chloroplast is called stroma in which thylakoids are organized into a structure similar to a stack of coins called granum (plural: grana) as shown in Figure 1.1. All the protein complexes involved in the photosynthetic electron transport chain (P-ETC) are arranged

in the thylakoid membrane. Photosynthesis consists of two sequences of reactions: 1) light reactions and 2) dark reactions.

Linear Electron Transport Chain (Z-Scheme)

With the help of light harvesting complexes and protein complexes present in the thylakoid membranes, plants produce reducing equivalents (NADPH) and energy currencies (ATP) through light-induced splitting of water into protons and oxygen. The P-ETC consists of several multi-subunit protein complexes in the thylakoid membrane such as photosystem II (PSII), cytochrome b_6f (Cyt b_6f), plastocyanin (PC), photosystem I (PSI), ferredoxin (Fd), ferredoxin-$NADP^+$ reductase (FNR) and ATP synthase. The PSII and the PSI are the major energy transducing photosystems. A pair of chlorophyll-a (Chl-a) molecules is present in both the reaction center P_{680} and P_{700} of PSII and PSI respectively. When a photon reaches the P_{680} reaction center of PSII complex, resonance energy is produced, thereby inducing a charge separation, which generates an excited electron and transfers it on to a bound plastoquinone (PQ) on Q_A site of the PSII complex. Meanwhile, the oxygen-evolving complex (OEC) of PSII oxidizes water into oxygen, electrons and protons. The electron released by OEC is used to replace the initial electron that was split from the P_{680} Chl-a molecule of PSII during the photon excitation. PQ at Q_A site of PSII transfers electron to loosely bound PQ on the Q_B site of PSII. From Q_B site of PSII, PQ transfers the electron to Cyt b_6f, which then use the electrons to reduce PC. PC is the electron donor for the P_{700} reaction center of PSI complex. In PS1, capture of another photon excites the complex to a higher energy state, which then transfers the electrons to Fd. Fd reduces FNR forming NADPH from $NADP^+$. In addition to transferring electron from

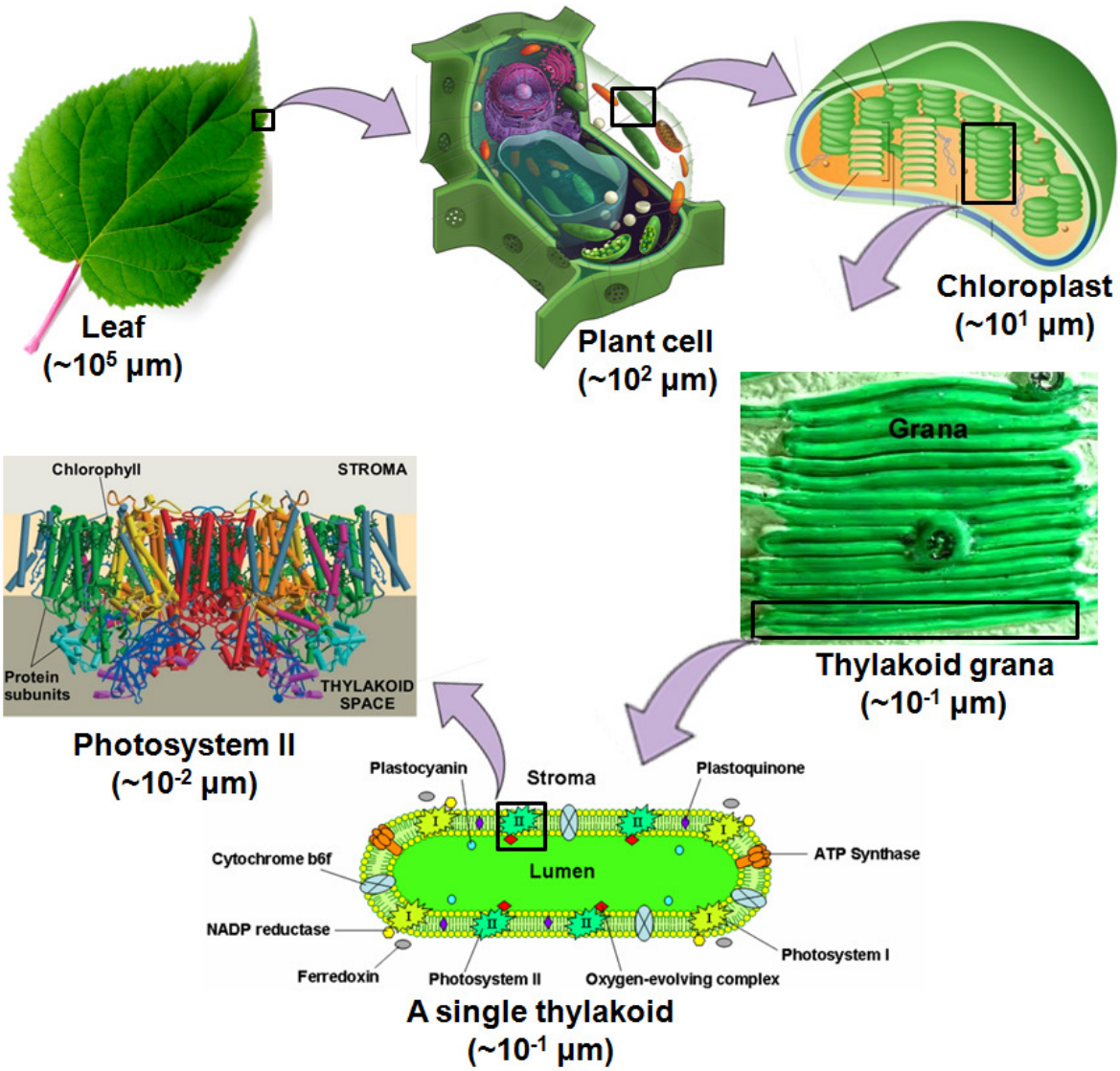

Figure 1.1: Hierarchical organization of photosynthetic machinery in thylakoids inside the chloroplast of plant cell with relative dimensions mentioned in micrometer (Sekar and Ramasamy, 2015)

PSII to PSI in the P-ETC, the Cyt b_6f also helps in translocating protons from the cytoplasmic to the luminal side of the thylakoid membrane; thereby generating proton motive force across the thylakoid membrane to help drive the ATP production through ATP synthase. The entire set of reactions called the 'Z scheme' or 'linear electron transport chain' as shown in Figure 1.2, is explained in greater detail in most biochemistry textbooks (David L. Nelson 2008).

In the dark reactions, also called Calvin cycle, plants utilize the ATP and NADPH, which are produced during the light reactions, to fix CO_2 captured from the atmosphere and synthesize carbohydrates. The net reaction of photosynthesis is the synthesis of carbohydrates using sunlight, water and CO_2 while oxygen is released as byproduct.

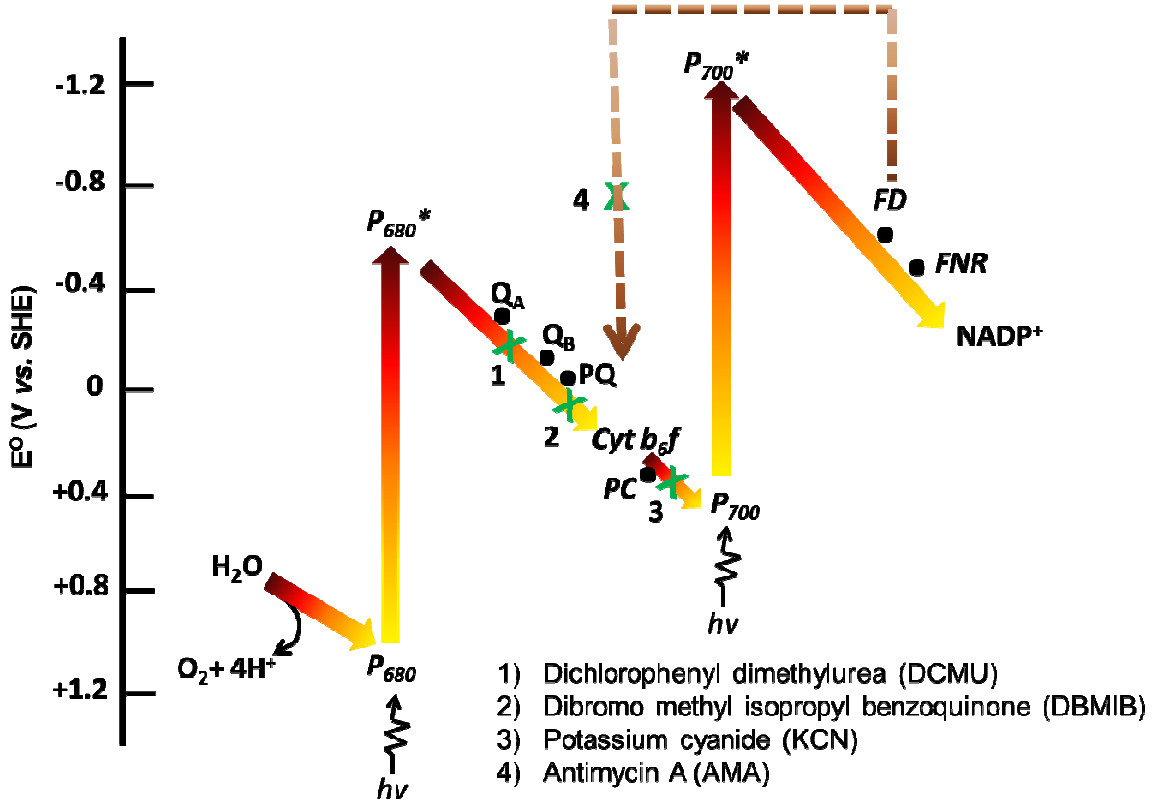

Figure 1.2: Z- scheme of linear photosynthetic electron transport chain (solid arrow) and cyclic electron transport chain around PSI (broken arrow) with all the components expressed along the redox potential scale; the green cross marks (1-4) represent the specific sites inhibited by the photosynthesis inhibitors such as DCMU, DBMIB, KCN and AMA. (Abbreviations: P_{680}: photosystem II; P_{680}*: excited photosystem II; Q_A: Q_A site of photosystem II; Q_B: Q_B site of photosystem II; PQ: plastoquinone; Cyt b_6f: cytochrome b_6f complex; PC: plastocyanin; P_{700}: photosystem I; P_{700}^*: excited photosystem I; FD: ferredoxin; FNR: ferredoxin NADPH reductase; $NADP^+$: oxidised form of NADPH

Cyclic Electron Transport Chain

In the linear electron transport chain (Z-scheme), for every four electrons transported, two $NADP^+$ molecules are reduced to two NADPH molecules. Simultaneously, two molecules of ATP are generated through photo-phosphorylation. However, two molecules of NADPH and three molecules of ATP are required to reduce one molecule of CO_2 in the dark reaction, which results in a higher demand for ATP. The cyclic electron transport chain is used to meet this demand by redirecting electrons from Fd back to Cyt b_6f through the plastoquinone (PQ) pool, which then transfers the electron to PSI complex as shown in Figure 1.2. While NADPH is not produced in the cyclic electron transport chain, it facilitates more protons to be transported into the lumen side of the thylakoid membrane during the reduction of PQ, thereby increasing the proton gradient across the thylakoid membrane generating more ATP. The complete pathway of the cyclic electron transport chain is believed to be facilitated by ferredoxin-plastoquinone reductase (Bendall and Manasse 1995), the mechanism of which still remains unclear. Recent studies suggest that Fd is not only involved in linear and cyclic electron transport chains, but also can transfer electrons to at least six other enzymes to facilitate with enzyme regulation and other biosynthetic pathways. Certain isoforms of Fd are encoded as new electron acceptors from PSI, thereby serve as redox enzymes for other pathways under certain extreme environmental conditions (Hanke and Hase 2008; Jacobs et al. 2009; Terauchi et al. 2009). Such deviation from the usual routes of P-ETC is usually induced by a change in micro-environment of the enzyme. The following section explains how the photosynthesis can be exploited for benefit of humankind.

1.1.4. Exploiting Photosynthesis for Humankind

The photosynthesis process can be effectively utilized for energy conversion applications in a variety of ways as shown in Figure 1.3: direct generation of electricity, hydrogen or biofuels. For electricity and hydrogen generation, light reaction is of the major concern; however, for the production of energy rich carbon based fuels, dark reaction and central carbon metabolism are exploited. Figure 1.4 shows different schemes of electricity generation in photo-bioelectrochemical cells (PBEC). The PBEC is an electrochemical device consisting of two compartments: anode containing a biocatalyst that carries out photosynthesis and transfers electrons from P-ETC to the electrode; cathode containing enzymes such as laccase or bilirubin oxidase that catalyze the reduction of oxygen to water. When such anodes are coupled with cathodes containing enzymes such as hydrogenase or nitrogenase, the system generates hydrogen. In either case, water and light are the only raw materials used by the biocatalyst to generate electricity or hydrogen, thereby making the system sustainable, economic and environment friendly. On the other hand, the pathways in the Calvin cycle and the central carbon metabolism are manipulated to produce carbon based biofuels like ethanol, propanol and butanol. The research work reported in this dissertation is exclusively focused on photosynthesis based electricity generation, also known as photocurrent generation.

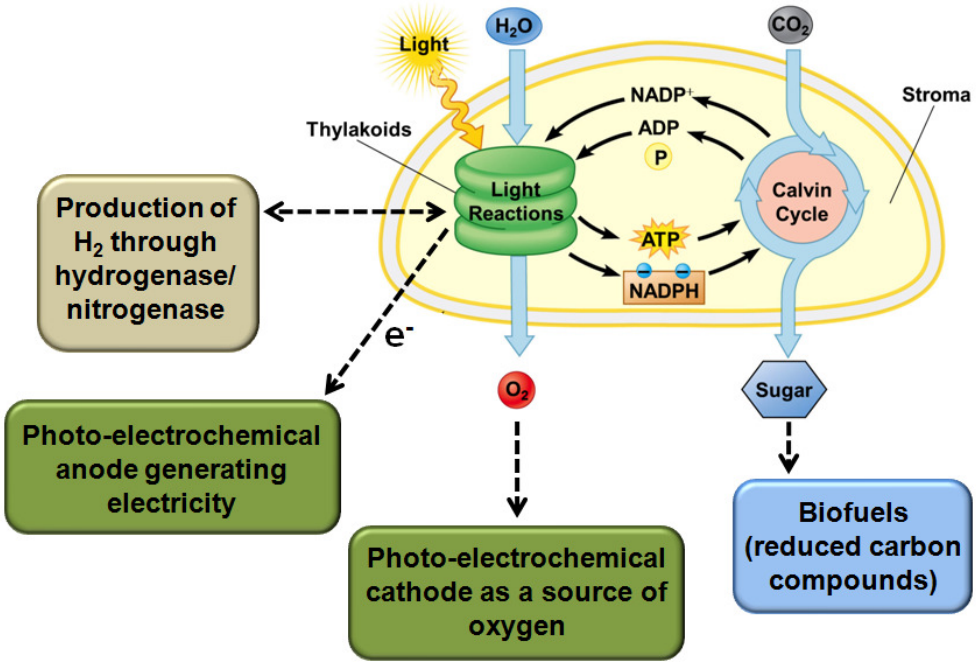

Figure 1.3: Chloroplast showing light reaction in thylakoid and dark reaction in stroma and utilization of these reactions for various applications such as generation of electricity, hydrogen and carbon based biofuels

1.1.5. Manipulating Photosynthesis for Electricity Generation

Direct conversion of light to electricity can be achieved in PBEC using natural photosynthetic machineries as biocatalysts. The photosynthetic machineries include bacterial photosynthetic reaction center (RC), photosystem I and II (PSI and PSII) complexes, organelles such as thylakoids that are isolated from algae and plants, whole cell photosynthetic microorganisms such as cyanobacteria and microalgae (Figure 1.4). Each of these machineries has its specific advantages and disadvantages. Research based on these machineries are also complementing and/or advancing the development of each other's. Like any other bio-electrochemical system, the primary challenge in getting the photosynthetic machineries, especially thylakoids and

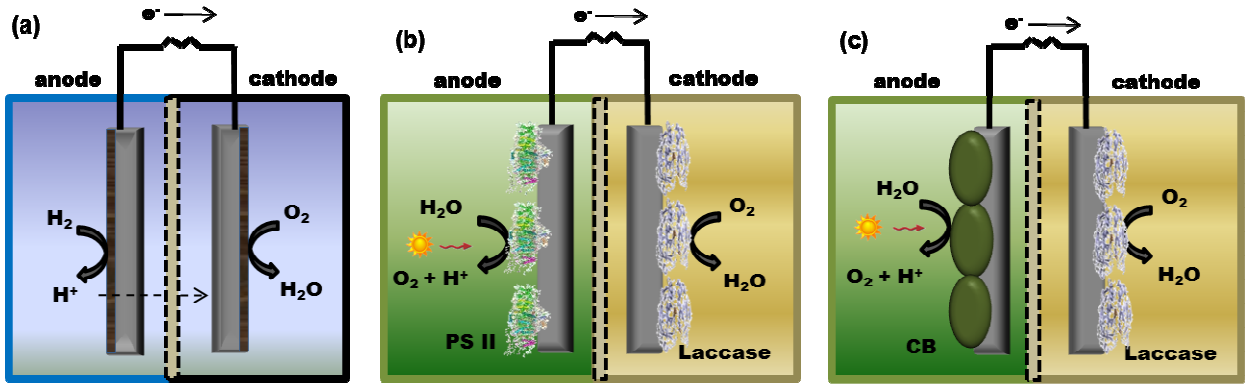

Figure 1.4: Schematic representation of various forms of fuel cells: (a) conventional hydrogen fuel cells with Pt as catalyst on both anode and cathode, (b) and (c) are photo-biochemical fuel cells: (b) shows isolated photosystems (PSII) on the anode and (c) shows photosynthetic microorganisms such as green algae or cyanobacteria (CB); both employ the enzymatic cathode for the reduction of oxygen to water via laccase. PSII and CB are not drawn to scale

photosystems, to work on the electrode relies on the electrical communication between the biocatalyst and the electrode. The electrical communication is greatly dependent on the effectiveness of attachment between the electrode and the biocatalyst and therefore the type of immobilization is of prime importance. The immobilization method determines how effectively the biocatalysts (thylakoids, PSI and PSII complexes) are tethered onto the electrode. An effective immobilization confers structural stability and retains biocatalyst activity. Moreover, the immobilization strategy is essential in dictating the orientation of biocatalyst on the surface of the electrode. These two factors are important for an efficient electrochemical reaction, because the electron transport pathway inside the huge PSI and PSII complexes is strictly vectorial.

Thylakoids as photo-biocatalysts

The major advantage of using thylakoids to harness photocurrent is that the integral membrane protein complexes are retained in their native environment during the isolation processes. This leads to a greater stability of the biocatalyst with higher yield (current density) than that can be achieved using isolated protein complexes such as PSII, PSI or bacterial reaction centers. Moreover, since thylakoid membranes contain multiple redox protein complexes, the electron transfer pathways can be manipulated at more than one location along the P-ETC on the thylakoid membrane (for example from both PSII and PSI). Various attempts have been made to immobilize the isolated thylakoids onto different support matrices such as albumin-glutaraldehyde cross-linked matrix (Carpentier et al. 1989), multi-walled carbon nanotubes (Calkins et al. 2013), encapsulating the thylakoid membrane vesicles onto conductive nanofibers by electro-spinning (Bedford et al. 2011) and vapor deposition of thin layer of silica onto the thylakoid layer (Rasmussen and Minteer 2014).

In addition to the whole thylakoid membranes, specific photosystems have also been examined and tested for photocurrent generation by several research groups. The advantages of using photosystems include: less interference of other redox enzymes from the electron donor sites thereby reducing the competition for electron capture from the donor sites, closer orientation of the donor site to the electrode to help establish direct electron transfer and a better manipulation of the electron transport pathway due to clear identification of redox potentials at electron transfer sites. Further, from an electrochemical perspective, the excited photosystems offer

greater prospects for harvesting electrons directly from a higher energy state, thereby increasing the electrochemical cell voltage.

Photosystem I as photo-biocatalysts

PSI complex captures light by an internal antenna system comprising of more than 110 cofactors, which is a unique feature of PSI, not present in any other known protein in nature, representing the vital evolution for high efficiency of energy transduction. The structure of PSI of *Synechococcus elongatus* consists of 12 protein subunits, 96 Chl-a molecules, 22 carotenoids, three [4Fe-4S] clusters, two phylloquinones and four intrinsic lipid components. The whole complex of PSI exists as a trimer in the native membrane with a molecular mass of 1068 kDa (Fromme et al. 2001). Light energy is transferred from the antenna system to the core of the PSI complex (P_{700} reaction center) with an efficiency of more than 99.99%, driving the electron transfer from the soluble electron carrier (PC) at the luminal side of the thylakoid membrane to Fd at the stromal side. PSI complexes have been immobilized using several different strategies such as gold nanoparticle (GNP) modified electrode (Faulkner et al. 2008), functionalized nano-porous gold leaf electrodes (Ciesielski et al. 2008), PSI-GNP hybrid electrode modified with 3-mercapto-1-propanesulfonic acid (Terasaki et al. 2006) and via self-assembly onto zinc oxide nanomaterials (Mershin et al. 2012). Despite being a good photo-biocatalyst, the usage of PSI has a few drawbacks compared to the thylakoids in terms of stability. PSI is a huge protein complex that incorporates major constraints on purification as well as stability of the purified protein complex. Another important limitation to be considered is that the oxidized PSI requires

an external electron donor (plastocyanin in intact thylakoid) to proceed with continuous electron transfer, thereby making it a system dependent on additional electron source for its reduction.

Photosystem II as photo-biocatalysts

The major advantage of using PSII over PSI is that the fuel needed to drive electron transfer is water, which is abundantly available. Unlike PSI, which requires an electron donor to replenish the excited electron, PSII possess intrinsic oxygen evolving complex (OEC) and is dependent only on water and light. PSII is the site of both charge separation and water oxidation by OEC. The crystal structure of PSII complex from *S. elongatus* shows that the complex is homo-dimeric protein with the membrane-intrinsic subunits (D1 and D2) containing CP47 and CP43 antenna proteins which bind to the chlorophylls Chl-a 13 and Chl-a 16 respectively (Guskov et al. 2009) The antenna proteins help funnel the absorbed photon to the reaction centers in the subunits D1 and D2 where charge separation occurs, that causes the oxidation of P_{680} (Guskov et al. 2009). Further, the OEC subsequently replenishes the electron-hole pair that was generated by the photon via the oxidation of water with the help of Mn-cluster, which makes PSII a self-replenishing source of energy as long as water and light are present (Kern and Renger 2007). The excited electron from P_{680} is transferred via resonance energy to pheophytin (Phe) and then to the PQ pool to follow the electron transport chain (Figure 1.2) (Boghossian et al. 2011). Ideally, replacing Phe with another equally reactive electron acceptor (electrode) will allow the highest energy conversion in a photosynthesis-based solar cell (Enami et al. 1991). Further, the reduction of PQ at Q_B site of PSII by two electrons from PQ at the Q_A site of PSII and diffusion of the reduced quinone into the membrane are the major rate-limiting steps (de Wijn and van Gorkom

2001). Therefore it is hypothesized that water oxidation via PSII could be accelerated if electrons are efficiently extracted from Q_A^- to an external electron acceptor (Ulas and Brudvig 2011). Accordingly, in order to collect the photochemical energy from PSII, the complex needs to come in contact with the electrode surface for direct electron transfer, otherwise the electron transfer must be facilitated via a mediator. The direct electron transfer from PSII to the electrode is difficult to establish, because the Phe-PQ binding site is located deep within the PSII (Badura et al. 2008).

A poly-histidine (His) tag and Ni(II)-nitrilotriacetic acid (Ni-NTA) system has been found to be profoundly useful in immobilizing PSII for its efficient photo-electrochemistry (Badura et al. 2006; Das et al. 2004; Goldsmith and Boxer 1996; Noji et al. 2011; Vittadello et al. 2010). Other significant improvements are witnessed by immobilizing PSII in osmium-containing redox polymer based on poly(1-vinylimidazole)(Badura et al. 2008) and a matrix of 2-mercapto-1,4-benzoquinone (MBQ), electro-polymerized on the gold surface (Yehezkeli et al. 2012). Multiple attempts have also been made to increase the stability of PSII as well as to optimize the electron transfer from PSII to a collection source (Badura et al. 2008; Enami et al. 1991; Vittadello et al. 2010).

Both the photosystems (PSII and PSI) are highly susceptible to photo-inhibition and the damaged photosystems are effectively repaired by protective mechanisms inside the chloroplast. It is obvious that the stability of purified photosystems will be hampered once they are isolated from their native stable environment. Further, the purified PSII is very unstable relative to PSI and greater current densities were achieved using the relatively more stable PSI (Table 1.1). Further,

a lot of effort has been undertaken to maintain the activity of the isolated thylakoids and photosystems by mimicking the natural environment on the electrode (Das et al. 2004; Mershin et al. 2012) or by preventing the loss of activity through catalytic quenching of reactive oxygen species which otherwise reduces the activity of the photosynthetic machineries (Sjoholm et al. 2012).

Table 1.1: Comparison of photocurrent density of various photosynthesis based anodes

S. No	Electrode	Photocurrent density	Reference	System
1	Zinc oxide nanostructured semiconductor with PS I	362 µA cm^{-2}	(Mershin et al. 2012)	PS I
2	Au/MWNT/thylakoids	68 µA cm^{-2}	(Calkins et al. 2013)	Thylakoids
3	Au/Os-poly (vinyl) imidazole/PS II	45 µA cm^{-2}	(Badura et al. 2008)	PS II
4	Au/Ni-NTA/His tagged PS II	43 µA cm^{-2}	(Vittadello et al. 2010)	PS II
5	Au/poly MBQ/PS II	3.1 µA cm^{-2}	(Yehezkeli et al. 2012)	PS II
6	Au-3-mercapto-1-propane sulfonic acid/GNP/PS I	1.6 µA cm^{-2}	(Terasaki et al. 2006)	PS I
7	Au-thylakoids	1.1 µA cm^{-2}	(Lam et al. 2006b)	Thylakoids
8	Functionalized nano-porous gold leaf electrodes/PS I	0.3 µA cm^{-2}	(Ciesielski et al. 2008)	PS I
9	Pt/native thylakoids	0.25 µA cm^{-2}	(Carpentier et al. 1989)	Thylakoids
10	Au/Self assembled amino-alkane-thiol/thylakoid	0.2 µA cm^{-2}	(Ahmed et al. 2009)	Thylakoids
11	Au/PS I monolayer	0.1 µA cm^{-2}	(Faulkner et al. 2008)	PS I
12	Au-Self assembled monolayer/reaction center	0.2 µA	(Lebedev et al. 2006)	Bacterial reaction center
13	Carbon coated Au/reaction center	0.05 µA	(Trammell et al. 2006)	Bacterial reaction center

MWNT – Multiwalled carbon nanotubes, Ni-NTA - Nickel-nitrilotriacetic acid, MBQ - mercapto-p-benzoquinone, GNP - Gold nanoparticles

Photosynthetic microorganism as photo-biocatalysts

While relatively higher power densities were achieved using isolated photosynthetic machineries such as bacterial reaction centers, PSI, PSII or thylakoids, they are not amenable for practical applications mainly due to the following reasons: (1) requirement of laborious and skillful isolation procedure; (2) requirement of specific environmental conditions (pH, temperature, ionic concentration of surrounding media etc.,) to ensure the stability of the isolated entities; (3) instability caused by photo damage; (4) inability to self-repair upon photo damage, since they are present in an artificial environment devoid of their natural counterparts. All the above caveats can be overcome by employing the whole cell photosynthetic microorganisms in PBEC. The whole cells retain all their native biological functions and therefore possess superior stability upon immobilization on electrode surfaces.

1.1.6. Why Cyanobacteria?

Among the photosynthetic microorganisms, cyanobacteria possess greater advantages than others such as follows:

(1) *Robustness*: Cyanobacteria are the ancient ancestor of chloroplasts and perform oxygenic photosynthesis similar to higher plants and algae;

(2) *Stability:* Cyanobacteria are evolved 3.5 billion years ago and are still existing in almost all terrestrial and aquatic environment on Earth and relatively more stable and withstand extreme environmental conditions such as light intensity, temperature, dryness and CO_2 level;

(3) *Scope for engineering:* Compared to algae and plants, cyanobacteria are simple prokaryotic life-forms. Cyanobacteria such as *Synechococcus* and *Synechocystis* are model microorganisms to explore fundamental biological process such as photosynthesis, circadian clock, etc., The whole genome of these two cyanobacteria was sequenced and molecular biology tools are available for manipulation at molecular and genetic level;

Cyanobacteria such as *Synechococcus elongatus* (Yagishita et al. 1993), *Synechocystis* sp. (Bombelli et al. 2011; Zou et al. 2009), *Anabaena variabilis* (Tanaka et al. 1985) and *Spirulina platensis* (Lin et al. 2013) and green algae such as *Chlamydomonas reinhardtii* (Rosenbaum et al. 2005b), *Chlorella vulgaris* (Velasquez-Orta et al. 2009), *and Ulva lactuca* (Velasquez-Orta et al. 2009) are employed in the PBEC for light induced photocurrent generation. Compared to growing the culture of cyanobacteria in PMFC with bare untreated electrode (Zou et al. 2009), growing cyanobacterial biofilm or immobilizing the cyanobacterial cells onto the electrodes modified with nanostructure based support matrix such as polyaniline (Furukawa et al. 2006), polypyrrole (Pisciotta et al. 2010) and electrodes modified with osmium redox polymer (Hasan et al. 2014), indium tin oxide (McCormick et al. 2011) have been shown to significantly improve the power density of the PBEC. The advantage of PBEC over conventional microbial fuel cells (MFC) is that the PBEC requires only light and water, whereas MFCs that harbor dissimilatory metal reducing bacteria like *Geobacter*, *Shewanella*, etc., require organic carbon source like glucose/lactate and produce CO_2 as end-product.

1.1.7. Cyanobacterial Membrane Systems

Cyanobacteria are prokaryotes and do not contain membrane bound organelles unlike their eukaryotic counterparts such as algae and plant cell. Yet, the two fundamental processes that generate ATP such as photosynthesis and respiration occur in the cyanobacterial cell in the extended membrane system of cyanobacteria. Cyanobacteria possess cell wall similar to Gram-negative bacteria. In addition to the cytoplasmic membrane (or cell membrane or plasma membrane), cyanobacteria possess an extended thylakoid membrane system throughout the cytoplasm (Figure 1.5). While the cytoplasmic membrane contains only respiratory electron transport chain (R-ETC), the extended thylakoid membranes in the cyanobacteria contain both P-ETC and R-ETC, an interesting feature unique to cyanobacteria. The P-ETC of cyanobacteria is very much similar to that of higher plants as shown in Figure 1.2. The R-ETC of cyanobacteria shares some commonalities with the well-known mitochondrial respiratory chain including NADH dehydrogenase, succinate dehydrogenase, plastoquinone pool, cytochrome b_6f complex, cytochrome c_6, cytochrome oxidases, quinol oxidases and ATP synthase with appropriate modification specific to cyanobacteria (Bryant 1994; Herrero and Flores 2008). The overall reaction is the transfer of electrons from the NADH and succinate to O_2 thereby generating H_2O and the transmembrane proton motive force drives the synthesis of ATP through oxidative phosphorylation. The P-ETC and R-ETC share certain components such as plastoquinone pool,

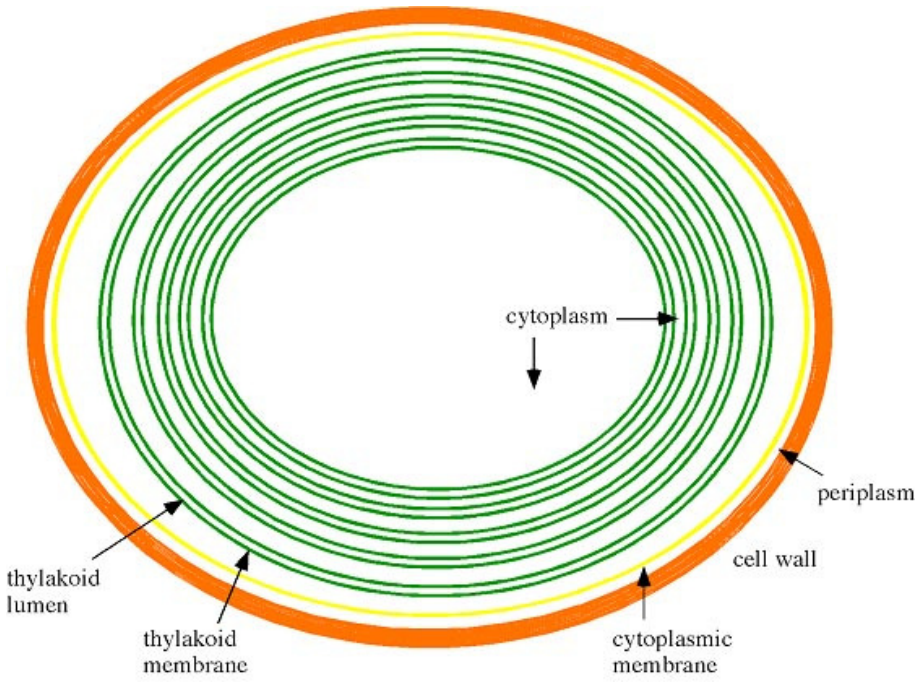

Figure 1.5: Schematic overview of a cyanobacterial cell. Thylakoid membranes, shown in green, contain photosynthetic and respiratory complexes and separate the cytoplasm from the lumen; cytoplasmic membrane, shown in yellow, separates the cytoplasm from the periplasm; and cell wall shown in orange (Adopted from Cyanobacteria project website of Arizona State University)

cytochrome b_6f complex and cytochrome c_6 or plastocyanin (Vermaas 2001). This peculiar organization in cyanobacteria is the primary reason for its capability to generate electricity under both light and dark conditions (Sekar et al. 2014) unlike PBEC based on isolated thylakoids, PSI and PSII, which can generate electricity only in the presence of light. Indeed the overlapping of P-ETC and R-ETC is a protective mechanism evolved by cyanobacteria to handle excess electrons (Pisciotta et al. 2011; Trubitsin et al. 2005), when the surrounding light intensity is higher than that sustained by the P-ETC. The photocurrent generated by live cyanobacteria in PBEC can be attributed to the overflow of the excess electrons from the P-ETC on exposure to excessive light (Pisciotta et al. 2011).

1.1.8. Elucidation of Electron Transfer Pathways Using Site-Specific Photosynthesis Inhibitors

Investigating electron transfer pathways during photocurrent generation would greatly help to understand the major pathways by which electrons are transferred from the P-ETC to the electrode. It also facilitates to identify the bottlenecks in the system thereby further optimizations can be carried out for enhancing photocurrent in PBEC. This can be accomplished with the help of certain site-specific photosynthesis inhibitors that block a specific pathway in P-ETC (Figure 1.2). 3-(3,4-Dichlorophenyl)-1,1-Dimethylurea (DCMU) is known to block the P-ETC immediately downstream of PSII at its Q_B binding site by competing with quinones and has been reported to inhibit linear electron transport at concentrations as low as 1 μM (Duysens 1963). 2,5-dibromo-3-methyl-6-isopropyl benzoquinone (DBMIB) occupies the Q_o site of the Cyt b_6f complex and alters the Rieske iron-sulfur protein of the complex arresting the electron flow from PSII to PSI (Roberts et al. 2004) (Roberts and Kramer 2001). High concentrations of potassium cyanide (KCN) (>10 mM) at high pH values (>7.5) is believed to inhibit the copper containing plastocyanin in linear electron transport chain (Ouitrakul and Izawa 1973). In the case of PSI, an inhibitor called bipyridillum (paraquate) acts as a competitor to Fd and inhibits electron flow from PSI to Fd (Summers 1980) (Fuerst and Norman 1991). Antimycin-A (AMA) inhibits the FNR thereby disrupting the cyclic electron flow around PSI (Hosler and Yocum 1987; Joet et al. 2001) and is highly useful to study the contribution of photocurrent from cyclic ETC. The source of electron for the photocurrent generation and the major electron transfer from the photosynthetic machinery to the electrode had been investigated using these site specific inhibitors in both isolated thylakoids (Calkins et al. 2013) as well as in cyanobacteria (Torimura

et al. 2001; Yagishita et al. 1993). Such fundamental studies assist in advancing our understandings towards manipulating the natural P-ETC to redirect more electrons for photocurrent generation.

1.1.9. Redirecting Electrons from P-ETC with Redox-Active Compounds

Unlike inhibitors that block the electron transport chain at specific site, certain redox active compounds are known to accept the electrons from specific site of P-ETC as dictated by its redox potential. Such studies will be helpful to understand the presence of possible electron sinks that might otherwise be able to contact directly with the electrode to generate photocurrent. The redox active sites of metalloproteins will be usually buried inside, for example, Q_A site of PSII (Acharya et al. 2012) and only a specific substrate can find its way and binds the active site. Similarly, when redox proteins are immobilized on the electrode for fuel cell applications, accessibility of the electrode to the internally buried electron transfer sites would be limited and hinders the electron transfer. This limitation can be overcome by redirecting the electron from the protein interior to the surface using metal complexes such as Co, Ni. Further, since redirecting the electrons form the initial steps of P-ETC will be more beneficial, much of the research has been focused on redirecting the electrons from PSII to an immobilization support. For example, Larom et al (2010) successfully redirected electrons from Q_A^- in PSII of cyanobacteria *Synechocystis* PCC 6803 to engineered collection sites approximately 13 Å away on the stromal side of the membrane (Larom et al. 2010). This redirection along with the addition of an herbicide blocking Q_B resulted in reduced oxidative damage due to decrease in Q_A/Q_B intermediate transfer time. Further, cationic redox-active metal complexes were recently used to

redirect electrons from Q_A^- at a distance of 9 Å (Ulas and Brudvig 2011). The complexes needed a well-poised redox potential for efficient electron transfer from Q_A^- (Robinson and Crofts 1983; Shibamoto et al. 2009). Ulas and Brudvig (2011) also used Co^{III} complexes small enough to fit in a 5 Å diameter negatively charged patch along the stromal side of the membrane to redirect the electron from PSII (Ulas and Brudvig 2011). In addition to these metal complexes, certain redox mediators can also be used to help facilitate electron transfer from its source to the electrode (Fultz and Durst 1982). Typically, mediators should have a slightly lower redox potential than the electron source, which is needed to help drive its reduction and the mediators shuttle the electrons between the electron source and electrode. Mediators such as 1, 4-benzoquinone (BQ), 2,6-dimethyl-1-benzoquinone (DMBIB), 2-hydroxy-1,4-napthaquinone (HNQ) have been used to collect electrons from the photosynthetic electron transport pathways in cyanobacteria (Torimura et al. 2001; Yagishita et al. 1993).

1.1.10. Knowledge Gap - Exoelectrogenicity of Cyanobacteria

The extracellular electron transport flux from P-ETC of cyanobacteria to the electrode is fairly low compared to that of dissimilatory metal reducing bacteria (DMRB) such as *Geobacter* and *Shewanella* in microbial fuel cells (MFC) (Lovley 2008; Yang et al. 2012). The reason being that the cyanobacteria are not evolved to perform exoelectrogenicity, rather they are smart oxygenic photosynthesizer. One way to overcome this limitation is through the use of redox mediators such as 1,4-benzoquinone (Torimura et al. 2001), 2,6-dimethyl-1,4-benzoquinone (Torimura et al. 2001; Tsujimura et al. 2001), 2-hydroxy-1,4-napthaquinone (Yagishita et al. 1993) or phenazine methosulfate (Yu et al. 2014) that are permeable to outer membrane of the living cell

and could greatly enhance the photocurrent generation. However, from an electrochemical standpoint, the use of redox mediators decreases the overall cell voltage and therefore is not beneficial. Moreover, mediators must be regenerated constantly, which introduces additional complexity to the system.

1.1.11. Prospective Solution through Genetic Engineering

Regardless of the mode of extracellular electron transport (direct or mediated), the cyanobacterial PBEC generally suffers from a lower extracellular electron flux because the electrons must be diverted from their native routes (overlapping P-ETC and R-ETC) to alternate pathways to reach the electrode. A robust approach to efficiently establish the alternative electron harvesting pathways by genetically modifying the cyanobacterium would be the most welcoming strategy to improve the performance of PBEC. With the advancement of genetic engineering and synthetic biology, these smart microorganisms can be made smarter to benefit our need to generate more electricity in PBEC. Accomplishing such challenging tasks has been undertaken during my PhD research work as reported in this dissertation.

1.2 Hot Electricity

1.1.12. Pyrococcus furiosus

Pyrococcus furiosus is a hyperthermophilic archaeon that grows anaerobically at an optimal temperature of 100 ^{0}C by consuming a wide range of sugars such as maltose, cellobiose, laminarin and chitin, and peptides (Koning et al. 2001; Lee et al. 2006) as primary carbon source.

During growth on sugars and in absence of S^0, *P. furiosus* produces acetate, CO_2 and H_2 and does not produce any fermentation products such as lactate or ethanol which suggests that all of the reducing equivalents are disposed of as H_2 (Figure 1.6) (Schut et al. 2013). Contrasting to cyanobacteria, that have complex and overlapping electron transport chains, *P. furiosus* exhibits the simplest respiratory electron transport chain involving ferredoxin (Fd) as electron carrier which shuttles electron between glycolytic intermediates of the central carbon metabolism and a membrane bound protein complex called hydrogenase (Mbh). Mbh does not require an additional electron acceptor because it catalyzes the reduction of protons, the simplest of electron acceptors, to molecular hydrogen. Mbh also pumps ions (H^+/Na^+) outside the membrane generating ion gradient for the synthesis of ATP. The usage of ferredoxin as reducing equivalents instead of the usual NADH enables *P. furiosus* to conserve more energy (ATP) through hydrogen production (Sapra et al. 2003). The transfer of electron from ferredoxin (E_m = -480 mV, pH 7.0) to protons (E_m = -420 mV, pH 7.0) is thermodynamically more favorable compared to that from NADH (E_m = -320 mV, pH 7.0) (Schut et al. 2013). Further, the coupling of hydrogen production to the energy conservation facilitates *P. furiosus* to have greater growth yield which is much higher compared to the ATP production by usual substrate level phosphorylation. Two other cytosolic hydrogenases (SHI and SHII) are also functional in *P. furiosus* which catalyze the reversible formation of H_2 using NADPH as electron donor. However, in the presence of elemental sulfur (S^0), *P. furiosus* does not express Mbh, rather reduces S^0 to H_2S with the help of another membrane bound oxidoreductase termed as Mbx (Figure 1.6). Similar to Mbh, Mbx accepts electron from ferredoxin and generates ion gradient, but its expression is regulated by S^0. ΔMbx mutant strain that lacks the catalytic subunit L neither did grow nor reduce S^0 suggesting that Mbx is highly essential for the S^0 reduction

system (Schut et al. 2013). However, Mbx does not directly forms H_2S, but rather couples the oxidation of ferredoxin with the formation of NADPH, which in turn donates electron to another protein called NADPH S^0 reductase (Nsr) (Schut et al. 2007) and H_2S is formed as shown in Figure 1.6. Expression of Nsr is also up-regulated in the presence of S^0.

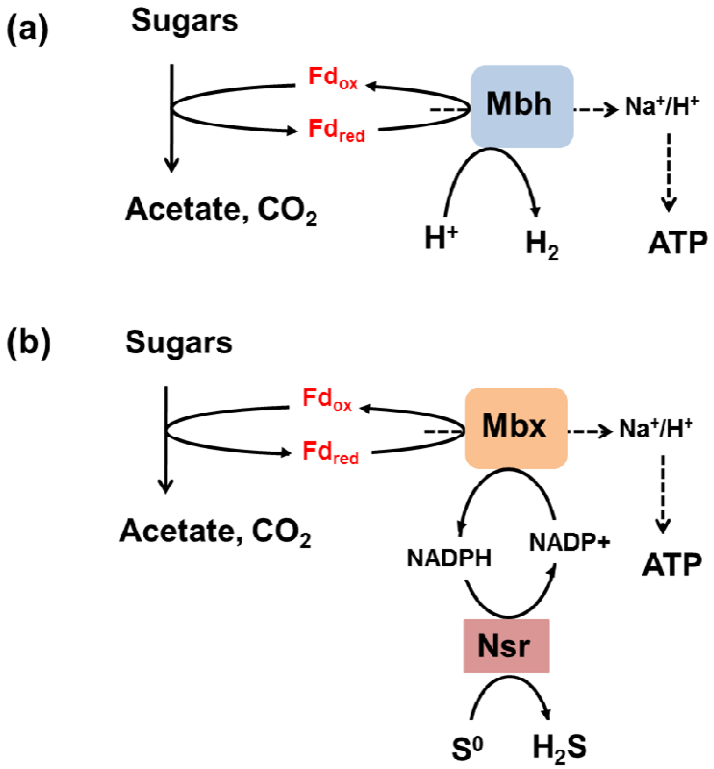

Figure 1.6: Schematics of metabolic pathways in *Pyrococcus furiosus* showing (a) production of H_2 in the absence of S^0 by Mbh complex and (b) production of H_2S in the presence of S^0 by Mbx complex and Nsr. Dotted black lines represent the generation of ion gradient for the production of ATP; (Abbreviations: Mbh: membrane bound hydrogenase; Mbx: membrane bound oxidoreductase; Fd_{ox}: oxidized from of ferredoxin; Fd_{red}: reduced form of ferredoxin; Nsr: NADPH elemental sulfur reductase)

The response of *P. furiosus* to the availability of S^0 and its metabolism of hydrogen and S^0 through Mbh/Mbx complexes are highly regulated by SurR regulon which is a unique evolutionary feature seen in Thermococcales such as *P. furiosus* (Lipscomb et al. 2009). In the

absence of S^0, SurR up-regulates all the three hydrogenases: Mbh, SHI and SHII, and represses Mbx; however, in the presence of S^0, SurR represses the hydrogenases and expresses Mbx. The mutant ΔMbh that lacks functional membrane bound hydrogenase cannot grow without the addition of S^0. Similarly, when the sulfur grown *P. furiosus* cells with active Mbx are exposed to an environment devoid of S^0, they cannot survive without an alternative electron sink.

Growth temperature is an important parameter affecting the physiological state and the optimal growth of *P. furiosus*. While *P. furiosus* grows optimally at 100 ^{0}C, it can grow up to 105 ^{0}C and tolerate as low as 70 ^{0}C. At 70 ^{0}C, so called cold shock condition for *P. furiosus*, the growth is much slower (generation time of 1 h at 98 ^{0}C versus 7 h at 72 ^{0}C) (Weinberg et al. 2005). The microorganism slows down its metabolic activity, but performs efficient bio-catalysis using the heterogeneously expressed enzyme that works at that lower temperature (Basen et al. 2012).

P. furiosus is also shown to establish cell-cell connections and adhesion to the abiotic surfaces with the help of flagella (Schopf et al. 2008), which is of greater concern in the proposed work, since cell-cell adhesion is essential for formation of biofilm on the anode of MFCs. A single *P. furiosus* cell contains up to 50 flagella originating from one pole of the coccus which are aggregated to form a cable-like structure through which the other cell is attached. Further, with the help of flagella, *P. furiosus* cells could adhere to carbon-coated gold grids used for electron microscopy, to sand grains collected from the original habitat, and to various other surfaces (Nather et al. 2006). Hence the biofilm forming ability of *P. furiosus* is an additional advantage for exploiting this microorganism for microbial fuel cell applications.

Therefore, the simplest respiratory electron transport chain of *P. furiosus* involving Fd/Mbh in the absence of S^0 and Fd/NADPH/Mbx in the presence of S^0 as well as its physiological characteristics of forming biofilm with the help of its flagella makes it an interesting candidate to explore its extracellular electron transfer for energy applications. Fewer the steps involved in electron transfer chain, lesser would be the energy loss at each step; thereby achieving more efficient energy conservation.

1.3 Specific Objectives and Organization of Chapters

Chapter 2: PHOTOCURRENT GENERATION BY IMMOBILIZED CYANOBACTERIA VIA DIRECT ELECTRON TRANSPORT IN PHOTO-BIOELECTROCHEMICAL CELLS

a) Exploring photocurrent generation from cyanobacteria named *Nostoc* sp. using an efficient immobilization strategy i.e., multi-walled carbon nanotubes.
b) Characterizing electrochemical response of cyanobacterial anode through electrochemical techniques such as chronoamperometry and impedance spectroscopy.
c) Studying electrochemical response of cyanobacterial anode at varying light intensities, monochromatic lights of different wavelengths, various biocatalyst loading (*Nostoc* cells).
d) Elucidating extracellular electron transport pathways in cyanobacteria using site-specific photosynthesis inhibitors.
e) Evaluating performance of a PBEC containing cyanobacterial anode and enzyme based cathode for direct and mediated electron transfer.

Chapter 3: ENHANCED PHOTO-BIOELECTROCHEMICAL ENERGY CONVERSION BY GENETICALLY ENGINEERED CYANOBACTERIA

The exoelectrogenicity of dissimilatory metal reducing bacteria (DMRB) such as *Geobacter* and *Shewanella* are predominantly attributed to c-type cytochromes present in their outer membrane. Enhancing the exoelectrogenicity of cyanobacteria by genetically engineering them to express the outer membrane cytochrome (OmcS) has been reported in this chapter. This novel strategy and the results from this research work have been filed as an US-Patent. (Ramasamy and Sekar 2015).

a) Expression of heterologous gene (*omcS*) in *Synechococcus elongatus* PCC 7942.
b) Biochemical and electrochemical characterization of enhanced exoelectrogenicity of the genetically engineered *S. elongatus.*
c) Demonstration of enhanced performance of the PBEC containing genetically engineered *S. elongatus* compared to that generated by the wild type cyanobacterium.

Chapter 4: ROLE OF RESPIRATORY TERMINAL OXIDASES IN CYANOBACTERIA TOWARDS EXTRACELLULAR ELECTRON TRANSFER

From an electrochemical perspective, the respiratory electron transport chain of cyanobacteria can be considered as competing pathways that decrease the electron flux from photosynthetic electron transport chain to the electrode and negatively impact the photocurrent generation. The

role of respiratory terminal oxidases (RTO) for exoelectrogenicity has been investigated by creating knock-out mutants for each of these RTOs in this chapter.

a) Construction of three single knock-out mutants for each of the three respiratory terminal oxidases in *S. elongatus* PCC 7942
b) Evaluating the knock-out mutants for exoelectrogenicity

Chapter 5: ELECTRICITY GENERATION BY *PYROCOCCUS FURIOSUS* IN MICROBIAL FUEL CELL OPERATED AT 90 °C

a) Studying exoelectrogenicity of *P. furiosus* via biochemical reduction of alternate electron acceptors such as ferric oxide and ferric citrate at 90 °C
b) Exploring current generation from *P. furiosus* in a microbial fuel cell operated at a higher temperature of 90 °C – this is the first reported case of using a pure culture of hyperthermophile to study current generation in MFC
c) Hypothesizing extracellular electron transfer pathways in *P. furiosus*

Chapter 6: STUDYING EFFECT OF LIGHT INTENSITY ON PERFORMANCE OF BIOFILM-BASED ANODE THROUGH A MATHEMATICAL MODEL

a) Developing a first principle mathematical model to describe the performance of a biofilm-based anode by incorporating the influence of incident light intensity

b) Simulating the effect of incident light intensity on current generation using the developed model

Chapter 7: CONCLUSIONS AND FUTURE DIRECTIONS

All the protocols used in the entire PhD work are listed in the appendices (Appendix A-K).

CHAPTER 2

PHOTOCURRENT GENERATION BY IMMOBILIZED CYANOBACTERIA VIA DIRECT ELECTRON TRANSPORT IN PHOTO-BIOELECTROCHEMICAL CELLS

Narendran Sekar, Yogeswaran Umasankar and Ramaraja P. Ramasamy. 2014. *Physical Chemistry Chemical Physics*. 16:7862-7871.

Reprinted here with permission of the publisher.

Abstract

Cyanobacteria possess unique and exciting features among photosynthetic microorganisms for energy conversion applications. This study focuses on production of direct electricity using a cyanobacterium called *Nostoc* sp. (NOS) as photo-biocatalyst immobilized on carbon nanotube on the anode of photo-bioelectrochemical cells. By illuminating with light (intensity 76 mW cm^{-2}) the NOS immobilized on carbon nanotubes (CNT) modified electrode generated a photocurrent density of 30 mA m^{-2} at 0.2 V (vs. Ag/AgCl). The contribution of different photosynthetic pigments in NOS to the light capture was analyzed and chlorophyll-a was found to be the major contributor to light capture followed by phycocyanin. Further investigation using a set of inhibitors revealed that the electrons were redirected predominantly from PSII to the CNT through plastoquinone pool. A rudimentary design photosynthetic electrochemical cell has been constructed using NOS/CNT on the anode and laccase/CNT on the cathode as catalysts. The cell generated a maximum current density of 250 mA m^{-2} and a peak power density of 35 mW m^{-2} without any mediator. With the addition of 1,4-benzoquinone as a redox mediator, the electricity generation capability was significantly enhanced to a current density of 2300 mA m^{-2} and power density of 100 mW m^{-2}. The power densities achieved in this work are the highest among 'non-engineered' cyanobacteria based electrochemical systems reported yet.

Keywords: Cyanobacteria, Nostoc, Anabaena variabilis, Electron transport pathway, Direct electron transfer, Mediated electron transfer.

1.4 Introduction

Cyanobacteria are commonly used in the production of fuels, hydrogen and other value-added chemicals (Quintana et al. 2011). A relatively simpler cellular organization and ease of genetic manipulations in cyanobacteria have given a competitive edge over their photosynthetic counterpart (green algae) for these applications (Rosenbaum et al. 2010). In particular, the electrogenic properties of cyanobacteria are being explored for direct electricity generation in photo-bioelectrochemical cells (Pisciotta et al. 2010; Rosenbaum et al. 2010). The direct electricity generation using cyanobacteria features greater advantages over the green algae or other dissimilatory metal reducing microorganisms such as *Geobacter* sp. and *Shewanella* sp., because cyanobacteria can operate without any external fuel to generate electricity from photosynthetic electron transport chain (P-ETC). Moreover, cyanobacteria being evolved over 2.5 billion years ago, has greater evolutionary significance to make it easily adapt to varying environmental conditions and are excellent candidates for solar based energy conversion processes. Though the photosynthetic electrochemical cell technology is not mature enough for practical applications, continuous advancements in the area could potentially make this technology an alternative to present day photo-voltaics or similar technologies in the future. Photosynthetic electrochemical cells offer unique advantages over any parallel technology in terms of biodegradability, low-cost and non-dependency on inorganic materials.

Photosynthesis based energy conversion has been explored using isolated photosynthetic reaction centers (PSRC) (Katz 1994; Katz et al. 1990; Katz et al. 1989; Solov'ev et al. 1991) such as thylakoids (Calkins et al. 2013; Carpentier et al. 1989; Lam et al. 2006a; Sjoholm et al. 2012) or

photosystems: PSII (Badura et al. 2008; Vittadello et al. 2010; Yehezkeli et al. 2012) and PSI (Faulkner et al. 2008; Mershin et al. 2012; Terasaki et al. 2006; Ulas and Brudvig 2011) in the anode of photo-electrochemical cells. However, there are major drawbacks of using PSRC as they require expensive, labor-intensive procedures for isolation, employ complex immobilization strategies (Lebedev et al. 2006), expensive metals as immobilization support and exhibit inferior long-term stability for practical applications. The use of whole cell of cyanobacterium as photo-biocatalyst in electrochemical cells would overcome these caveats. Cyanobacteria contain both P-ETC and respiratory electron transport chain (R-ETC) reactions occurring in their thylakoid membranes, while the higher plant thylakoid membranes carry out only P-ETC reactions. The excess light energy quenched by PSII can be dissipated to the respiratory terminal oxidases of R-ETC in cyanobacteria, thereby providing greater stability on electrode surfaces compared to isolated PSRCs or thylakoids of higher plants.

Previously, cyanobacteria such as *Anabaena variabilis* (Tanaka et al. 1985), *Synechococcus* sp. (Yagishita et al. 1993), *Synechocystis* sp. (Zou et al. 2009), and other fresh water photosynthetic organisms have been used to illustrate photo-electrochemical response in aerobic photosynthetic microbial fuel cells (PMFC) (Pisciotta et al. 2010; Torimura et al. 2001; Yagishita et al. 1993; Zou et al. 2009). While these early attempts formed a basis for utilizing cyanobacteria in PMFC for the generation of electric current, majority of the work in this area were focused on employing redox-mediators to carry out extracellular electron transport between the cyanobacteria and the electrode. From a power generation standpoint, direct electron transfer (DET) is always beneficial over mediated transfer as it minimizes the over-potential losses for bio-electrochemical reactions and simplifies the electrochemical cell design and operation.

Cyanobacteria are capable for extracellular electron transfer through membrane bound cytochromes similar to that of metal reducing microorganisms (McCormick et al. 2011; Pisciotta et al. 2011). Moreover, Gorby *et. al.,* discovered the presence of electrically conductive nanowires in cyanobacterium *Synechocystis* PCC 6803 using scanning tunneling microscopy (Gorby et al. 2006), which would highly facilitate the extracellular electron transport through DET. In our previous work we demonstrated photocurrent generation using spinach-thylakoids immobilized on carbon nanotube modified electrodes as photo-biocatalysts in photo-electrochemical cells (Calkins et al. 2013). In this work, we investigated the DET ability of a cyanobacterium called *Nostoc* sp. ATCC 27893 (NOS) for photocurrent generation in a photo-electrochemical cell. This was achieved by immobilizing NOS on carbon nanotube modified electrodes. To our knowledge, there are no previous reports on wiring cyanobacteria onto carbon nanotubes for electricity production. The schematic of NOS immobilized on the carbon nanotube modified electrode and the relevant electron transfer pathways are illustrated in Figure 2.1.

1.5 Materials and Methods

2.2.1 Materials

Multi walled carbon nanotubes (CNT), 10 nm diameter and 1-2 µm length (Dropsens, Spain), were used as immobilization support and 1-pyrenebutanoic acid succinimidyl ester (PBSE) (Anaspec) was used as molecular tethering agent to attach *laccase* enzyme (*Trametes versicolor*, Sigma) to the CNT. 3-(3,4-dichlorophenyl)-1,1-dimethylurea (DCMU) (Tokyo Chemical Industry), 2,5-dibromo-3-methyl-6-isopropylbenzoquinone (DBMIB) (Aldrich),

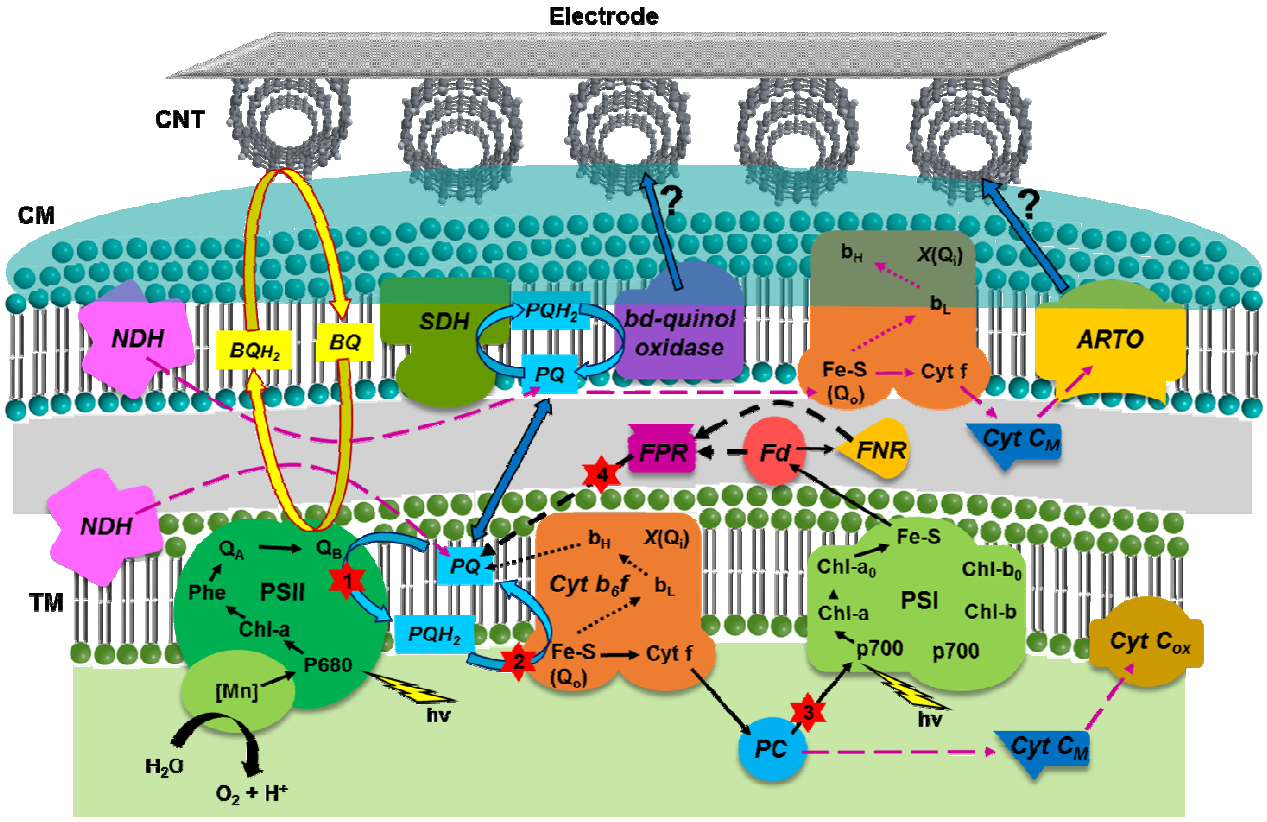

Figure 2.1: Schematic of electron transport pathways in a cyanobacterium immobilized on a CNT modified electrode. Black solid arrows represent the photosynthetic linear electron transport chain, black broken arrows represent the cyclic electron transport pathway in photosynthesis, pink broken arrows represent the respiratory electron transport chain, and red stars represent blocking sites of inhibitors: (1) DCMU, (2) DBMIB, (3) KCN and (4) antimycin A. The extracellular electron transport pathways from P-ETC to CNT are identified using site-specific photosynthesis inhibitors. Dark blue block arrows represent extracellular electron transport from PSII to CNT via the PQ pool, and yellow block arrows represent mediated electron transport between BQ and CNT. (Abbreviations: CM: cytoplasmic membrane; TM: thylakoid membrane; NDH: NADH dehydrogenase; SDH: succinate dehydrogenase; ARTO: alternate respiratory transport oxidase; Cyt Cox: cytochrome C oxidase; PSII: photosystem II; Cyt b_6f: cytochrome b_6f complex; PC: plastocyanin; PSI: photosystem I; Fd: ferredoxin; FNR: ferredoxin $NADP^+$ reductase; FPR: ferredoxin plastoquinone reductase; PQ: plastoquinone; PQH_2: plastoquinol; BQ: 1,4-benzoquinone oxidized form; BQH_2: hydroquinone)

potassium cyanide (KCN) (Fisher Scientific), antimycin A (AMA) (Sigma Scientific) were the photosynthesis inhibitors used in this study. All other chemicals were purchased from Amresco,

EMD, Acros Organics, J T Baker or Alfa Aesar. Monobasic and dibasic salts of potassium phosphate (BDH) were used to prepare the phosphate buffer solutions. All buffers were prepared using nanopure distilled water (dd water).

2.2.2 Cyanobacterial Culture

Fresh cultures of *Nostoc* sp. ATCC 27893 (NOS) and *Anabaena variabilis* ATCC 29413 (AV) were procured from Biorefining and carbon cycling research laboratory at the University of Georgia. The cultures were propagated in 100 mL shake flask cultures using modified BG11 medium. The BG11 medium (per L) consists of 0.02 g Na_2CO_3, 1.07 g $NaNO_3$, 10 mL of stock solution I (0.1 g L^{-1} Na_2Mg EDTA, 0.6 g L^{-1} ferric ammonium citrate, 0.6 g L^{-1} citric acid.$1H_2O$, 3.6 g L^{-1} $CaCl_2.2H_2O$), 10 mL of stock solution II (7.5 g L^{-1} $MgSO_4.7H_2O$), 10 mL of stock solution III (6.1 g L^{-1} K_2HPO_4) and 1 mL of microelement solution (2.86 g L^{-1} H_3BO_3, 1.81g L^{-1} $MnCl_2.4H_2O$, 0.222 g L^{-1} $ZnSO_4.7H_2O$, 0.079 g L^{-1} $CuSO_4.5H_2O$, 0.05 g L^{-1} $CoCl_2.6H_2O$, 0.018 g L^{-1} $NaMoO_4$). The cyanobacterial cultures were inoculated in the autoclaved media and grown at 25±2 ^oC and 100 rpm in 12:12 h light/dark cycles illuminated by fluorescent lamps (80 µmol m^{-2} s^{-1}). The growth was monitored by measuring optical density of the cultures at 750 nm using UV-Vis spectrophotometer (Genesys 10S, Thermo Scientific).

2.2.3 Electrode Preparation

SpectraCarb 2050-L carbon paper (CP) was used as the base electrode. The CP was treated with a boiling mixture of 1M HNO_3 and 0.5 M H_2SO_4 (1:4 ratio) for an hour and washed with dd

water. The geometric surface area of CP was 0.0254 cm^2. The CNT solution (1 mg mL^{-1}) was prepared in dimethyl formamide and suspended to uniform slurry by sonicating it for 15 min in ultrasonic homogenizer. 5 µL of CNT was drop casted on the CP, dried in oven to make CNT modified CP. The fresh cyanobacterial culture was washed using phosphate buffer (100 mM, pH 7) and resuspended in the same buffer. 5 µL of the culture was loaded onto CNT modified CP and allowed to air dry at room temperature. The NOS(or AV)/CNT modified CP was used as the working electrode (or photo-anode in full cell) for the electrochemical experiments.

2.2.4 Electrochemical Studies

Electrolyte solutions were purged with N_2 for 30 min to remove dissolved oxygen. Open circuit potential (OCP), current *vs*. time (*i-t* curve) and electrochemical impedance spectroscopy (EIS) studies were conducted using a CHI potentiostat (920c and 401a models, CH Instruments Inc). Ag/AgCl/Sat. KCl was used as reference electrode and a platinum wire was used as counter electrode. A Dolan-Jenner Industries Fibre-Lite lamp (model 190) with a light intensity of 76 mW cm^{-2} was used for illumination. Bacterial cell loading was optimized by measuring the photocurrent generated upon loading various amounts (5, 10, 15, 20, 25 µL) of culture on the CNT modified CP electrode. The stability of the cyanobacteria immobilized anode was tested by measuring its photocurrent generating capability every day until 10 days. The absorption spectrums of NOS and AV were measured using UV-Vis spectrophotometer in the range between 400 nm and 700 nm. The monochromatic light from monochromator (Oriel QE/IPCE measurement kit, Newport) was used to illuminate light of different wavelengths. For the inhibitor studies, the fresh culture was incubated with the inhibitor for 1 hour, and washed with

phosphate buffer (100 mM, pH 7) before immobilizing on the CNT and then the photocurrent density was measured electrochemically. Solutions of DCMU, DBMIB and AMA were made in 100% ethanol, and KCN solution was prepared in dd water and appropriate dilutions were made to vary the concentration of inhibitors. The photo-electrochemical full cell was developed using NOS/CNT modified CP as anode and *laccase*/CNT as enzymatic cathode. A molecular tethering approach developed in our previous work was used to immobilize *laccase* on to CNT (Parimi et al. 2012; Ramasamy et al. 2010; Roy et al. 2012). 100 mM phosphate buffer with pH 5.8 was used as the electrolyte in the full cell.

1.6 Results and Discussions

2.3.1 Characterization of Immobilized Cyanobacteria on CNT

The immobilization of cyanobacteria on CNT modified CP has been characterized using scanning electron microscopy (FEI Inspect F FEG-SEM) and the images are shown in Figure 2.2. Figure 2.2a shows the image of the CNT modified CP; Figure 2.2b and 2.2c show the images of NOS and AV on CNT modified CP respectively. Figure 2.2b and 2.2c clearly show the direct physical attachment of the outer membrane of NOS and AV with the underlying CNT. Immobilization of cyanobacteria directly on CP with CNT modification established such intimate connection through multiple attachment sites. Here, CNT serves both as an immobilization support and a current collector. The physical attachment of bacteria with CNT would help in extracellular electron transport from the cells to the CNT through the outer membrane redox proteins.

2.3.2 Photo-Electrochemical Activity

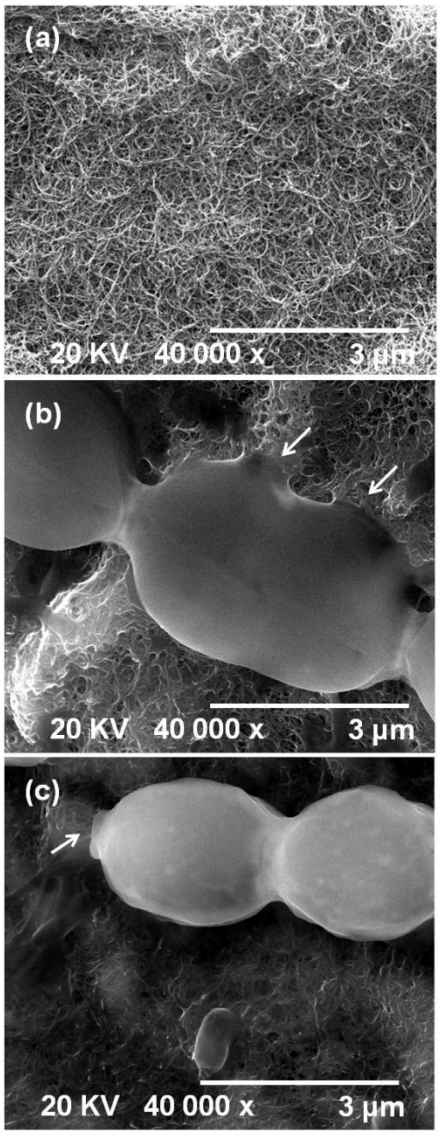

Figure 2.2: Scanning electron microscopy images of (a) CNT modified CP, (b) NOS immobilized on CNT modified CP and (c) AV immobilized on CNT modified CP. The attachment sites indicated by arrows can be clearly seen from the images in (b) and (c)

Figure 2.3a shows the comparison of the open circuit potential (OCP) profiles of bare electrodes and NOS or AV immobilized electrodes under alternative light-dark conditions. As shown in

Figure 2.3a, the OCP decreased upon illumination by light, and increased when light was switched off (dark) for both NOS and AV. By comparison, the OCP of bare CNT control electrodes (no cyanobacteria) was unaltered in both dark/light phases.

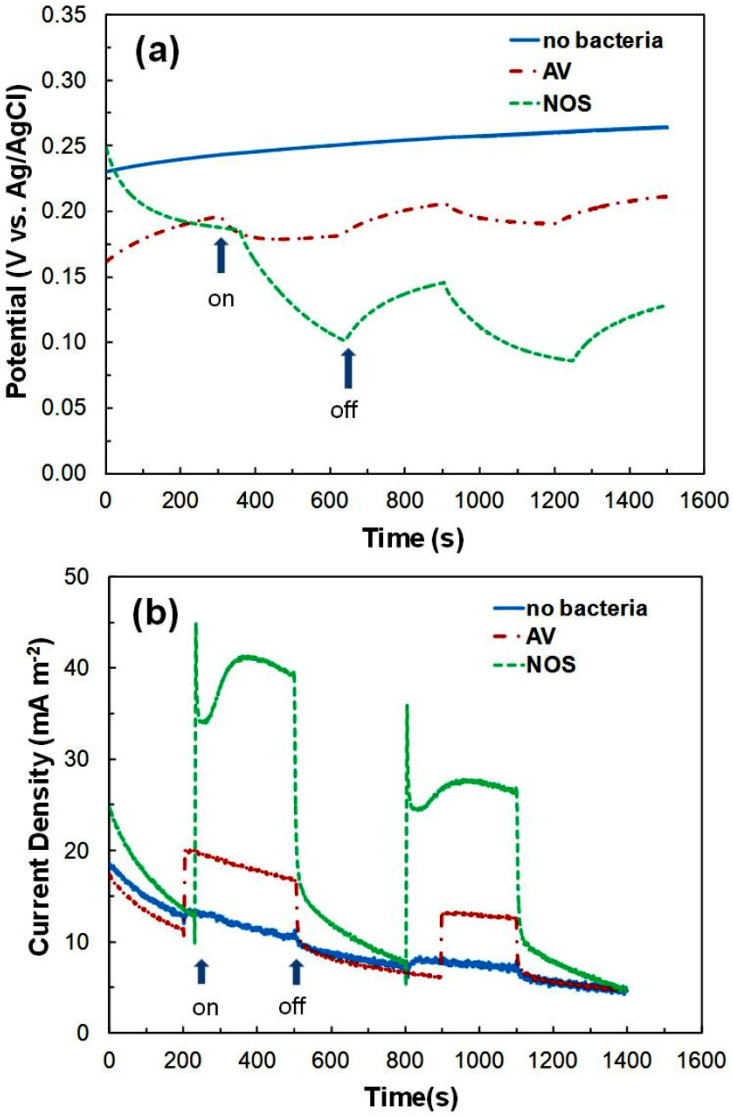

Figure 2.3: Electrochemical characterization of NOS and AV immobilized on CNT modified CP under alternative light and dark conditions. (a) Comparison of open circuit potential variations of NOS/CNT, AV/CNT and bare CNT modified CPs. (b) Photocurrent densities measured as a function of time at an applied voltage of 0.2 V (vs. Ag/AgCl) for NOS/CNT, AV/CNT and bare CNT modified CPs

The decrease in the OCP caused by light in cyanobacteria immobilized electrodes is due to the mixed potential effect caused by the oxygen released due to the photosynthetic activity of cyanobacteria and is similar to the effect we have observed in our previous study with plant-thylakoids (Calkins et al. 2013). The effect of photosynthesis on the extracellular electron transport in cyanobacteria is clearly manifested in the amperometric response of the NOS and AV immobilized electrodes under alternate light/dark phases as shown in Figure 2.3b. The photo induced current generation increased when illuminated with light and decreased during dark due to a completely shut off of light driven electron transport reactions in the linear photosynthetic pathway. In a separate set of experiments, the loading of cyanobacteria on CNT electrodes was optimized for the highest current generation and the results are given in the supplementary information (Figure 2.S1). The photocurrents peaked at a loading of 2.2 mg cm^{-2} for NOS and 5 mg cm^{-2} for AV, beyond which the photocurrents decreased possibly due to the formation of a thick non-conducting mat of cells on the CNT. The variation in both OCP and current density during light/dark cycles were higher for NOS compared to AV. This concurs with previous reports suggesting higher electrogenic activity for NOS compared to other cyanobacteria studied (Pisciotta et al. 2010). For this reason, the following studies were carried out only using NOS immobilized electrodes for further investigations.

The impedance characteristics of NOS immobilized electrode was studied using electrochemical impedance spectroscopy in a three-electrode system. Figure 2.4 shows the Nyquist plot obtained with NOS/CNT in light and dark conditions. The diameter of the semicircle in the Nyquist plot represents the polarization resistance (R_p). From Figure 2.4, it is clear that R_p of the NOS/CNT anode (8.2 kΩ cm^2) was less than that of the control (CNT without bacteria (22 kΩ cm^2)).

Similarly, the R_p of NOS/CNT was lower in light conditions (8.2 kΩ cm^2) compared to dark (14.2 kΩ cm^2), suggesting the enhancement of electro-kinetics under light due to photosynthesis.

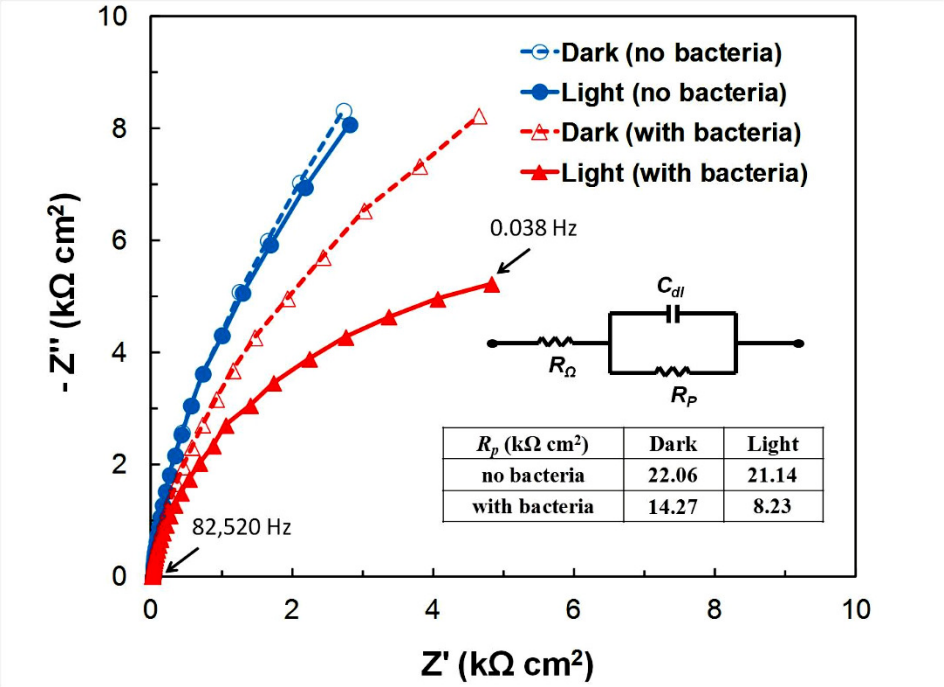

Figure 2.4: Nyquist plot showing impedance behaviour of CNT modified CP with and without NOS under light and dark conditions. The insets are the simple Randles circuit used to fit the impedance data and the insert-table shows polarization resistance of the different electrodes under study

2.3.3 Photocurrent Stability

It is noteworthy to point out that *Nostoc sp.* could withstand desiccation (nutrient and water deprivation) to a significant extent. Particularly the mechanism of desiccation tolerance has been extensively studied in *Nostoc* sp.(Potts 1999), therefore making it an excellent candidate for long term generation of photocurrent. This has been experimentally verified in our 'accelerated' stability studies, where the photocurrent generation of NOS immobilized electrodes was monitored at 0.2 V (vs. Ag/AgCl) for a period of 10 days using forced desiccation. It can be

observed from Figure 2.5 that the generated photocurrents stabilized after the first day, for up to 5 days after which the cells became inactive. However, upon immersing the electrode to a nutrient containing BG11 medium on day 6, almost all the photo-activity resumed on day 7. This result suggests that when continuously provided with minimal nutrients (note that nutrients are different from fuel or substrate), the cyanobacteria can retain almost all of its activity for a prolonged period, which is critical in designing practical power generation systems based on cyanobacteria.

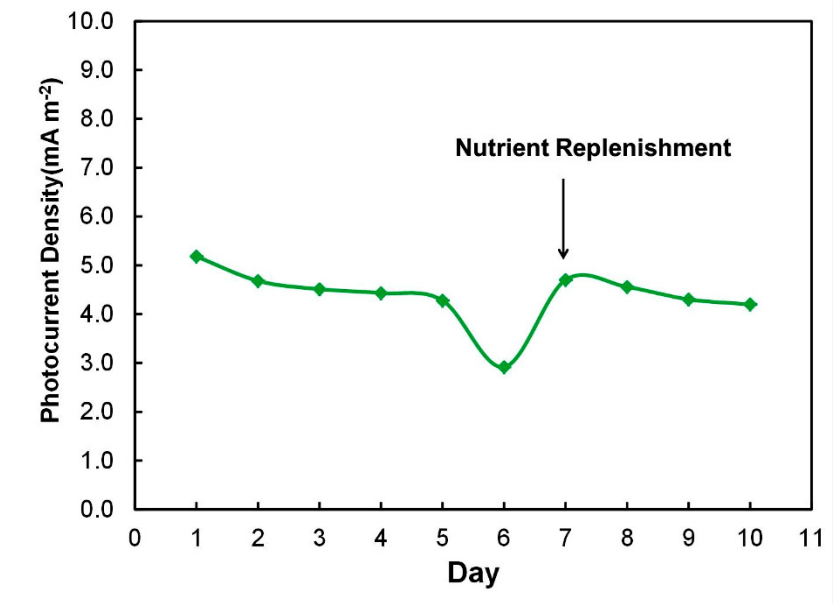

Figure 2.5: Stability of photocurrent generation in the NOS immobilized electrode

2.3.4 Role of Individual Photosynthetic Pigments

The photosynthetic pigments play a crucial role in capturing the sunlight and initiate the charge separation inside the reaction centers of photosystems. The proportion of different pigments present in a cyanobacterium is under regulation of light. The major photosynthetic pigment present in cyanobacteria is chlorophyll-a (*Chl-a*), which is present as special pair of chlorophylls

in both PSII and PSI. In addition, cyanobacteria also possess accessory pigments such as phycocyanin (*PhyC*), phycoerythrin (*PhyE*) and allophycocyanin, which together form a fluorescent antenna complex called phycobilisome (MacColl 1998). In association with both PSII and PSI, the phycobilisomes capture light in a range of wavelength not utilized by *Chl-a* and transfer the energy to *Chl-a*. The absorption spectrum of NOS in the visible region is shown in Figure 2.6b. The peaks at wavelength 440 nm and 680 nm correspond to *Chl-a* and peaks at 500 nm and 640 nm correspond to *PhyE* and *PhyC* respectively. In order to investigate the contribution of different photosynthetic pigments towards the photocurrent generation, the current density was measured by illuminating NOS with monochromatic light of different wavelengths such as 440, 500, 550, 600, 640 and 680 nm as shown in Figure 2.6a. It was observed that the monochromatic light of wavelength 640 nm resulted in the maximum photocurrent, followed by 440, 680, 500 and 550 nm in that order. No appreciable current had been observed with 600 nm light. Since the intensity of light varies with the wavelength, the measured photocurrent density was normalized with the light intensity at the corresponding wavelength, and the normalized photocurrent profiles are shown in Figure 2.6b. The photocurrent generated at wavelengths of *Chl-a* (both 440 and 680 nm) was found to be maximum followed by that of *PhyC*. It was evident that *Chl-a* contributed largely towards the light energy capture leading to greater photocurrent generation. Among the phycobiliproteins, *PhyC* captured the most light. This observation was also confirmed by fluorescence measurements as shown in Table 2.S1 (supplementary information). NOS produced significant fluorescence at excitation/emission pair of 590±10 nm/645±20 nm, corresponding to C-phycocyanin and 530±12.5 nm/645±20 nm corresponding to R-phycocyanin (Herrero and Flores 2008). No such fluorescence was seen in the control samples. Though *PhyC* contributes to the

light energy capture, it is important to note that unlike *Chl-a* of PSII or PSI, *PhyC* by itself could not induce the charge separation and initiate the electron transfer. It rather just captures the light at 640 nm and transfers the energy to *Chl-a*.

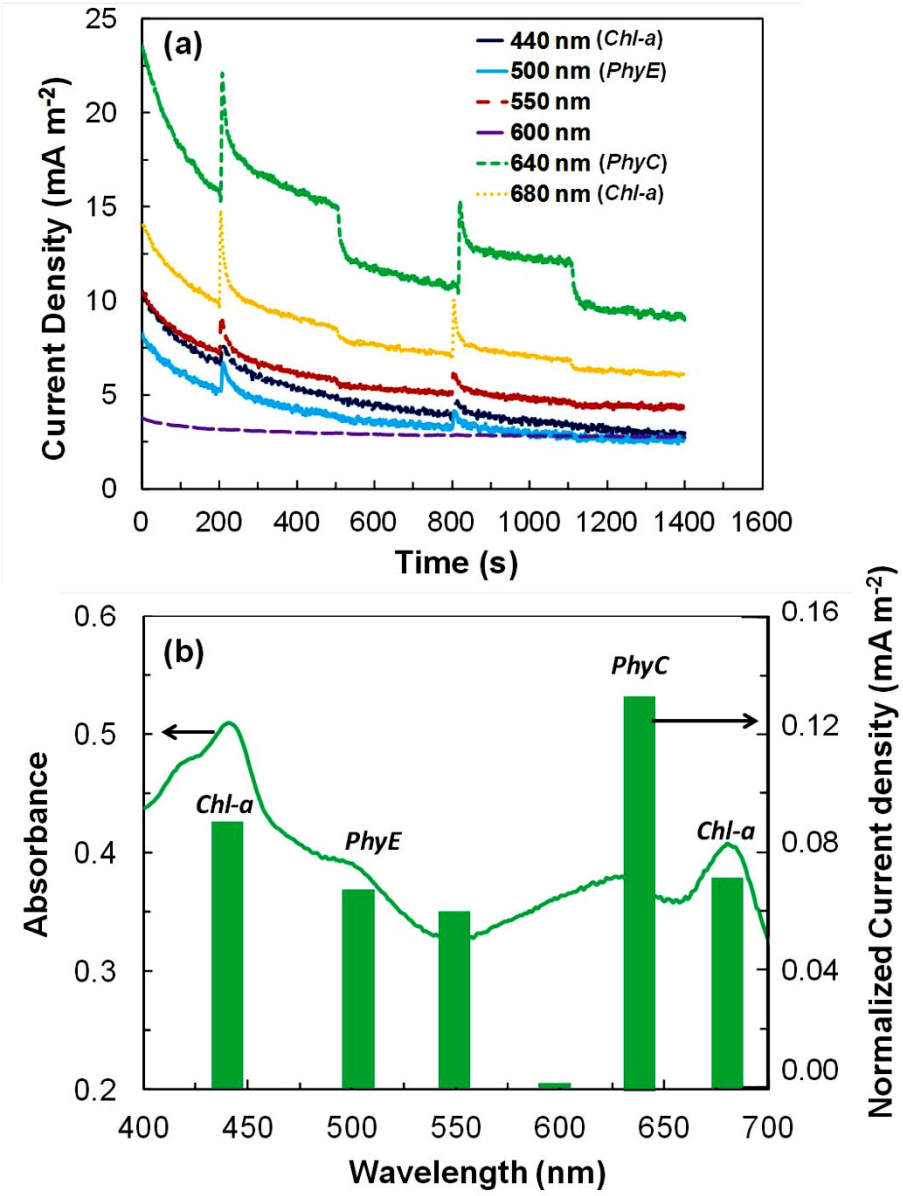

Figure 2.6: (a) Photocurrent response of NOS/CNT modified CP to monochromatic lights of different wavelengths. (b) Line chart shows the absorption spectrum of NOS in the visible region and the bars represent normalized current density generated by NOS in the wavelengths studied (refer text). The photosynthetic pigment Chl-a contributed maximum to the light capture followed by PhyC

Besides *Chl-a* and *PhyC*, *PhyE* also contributed significantly leading to photocurrent generation as seen in Figure 2.6a. Exploring the role of these photosynthetic pigments in greater detail is beyond the scope of this work and hence was reserved for a future study.

2.3.5 Extracellular Electron Transfer Pathways

Detailed mechanistic analyses of energy capture and extracellular electron transfer in cyanobacteria at the molecular level would provide meaningful insights into their photo-bioelectrochemical characteristics. This has been accomplished with the help of site-specific photosynthesis inhibitors that can be used to envisage the possible electron transfer pathways from the bacteria to the electrode. The fresh culture of NOS was treated with various site-specific photosynthesis inhibitors before immobilization on the CNT/CP, and electrochemical studies were performed to monitor photo-electrochemical activity. Figure 2.7a shows the photocurrent generated by NOS treated with various concentrations of DCMU (0.05, 0.1, 0.5 and 1 mM). Compared to the control (NOS without inhibitor), the photocurrents of DCMU-inhibited NOS fell by nearly 80% for all concentrations of DCMU examined. DCMU is known to bind to both Q_A and Q_B sites in PSII, arresting the transfer of electron from PSII to plastoquinone (PQ) (site 1 in Figure 2.1). While the binding of DCMU to both quinone sites are mutually exclusive (i.e, cannot bind to both the sites at the same time), binding to Q_B completely blocks the electron transfer; whereas binding to Q_A only slows down the electron transfer and it requires high DCMU concentration (Hsu et al. 1986). Since the inhibition was found to be maximal even with a ultra-low concentration of DCMU (0.05 mM), it could be concluded that DCMU was bound to Q_B site and inhibited the electron flow in our case (Trebst 1978). The greatest evolutionary

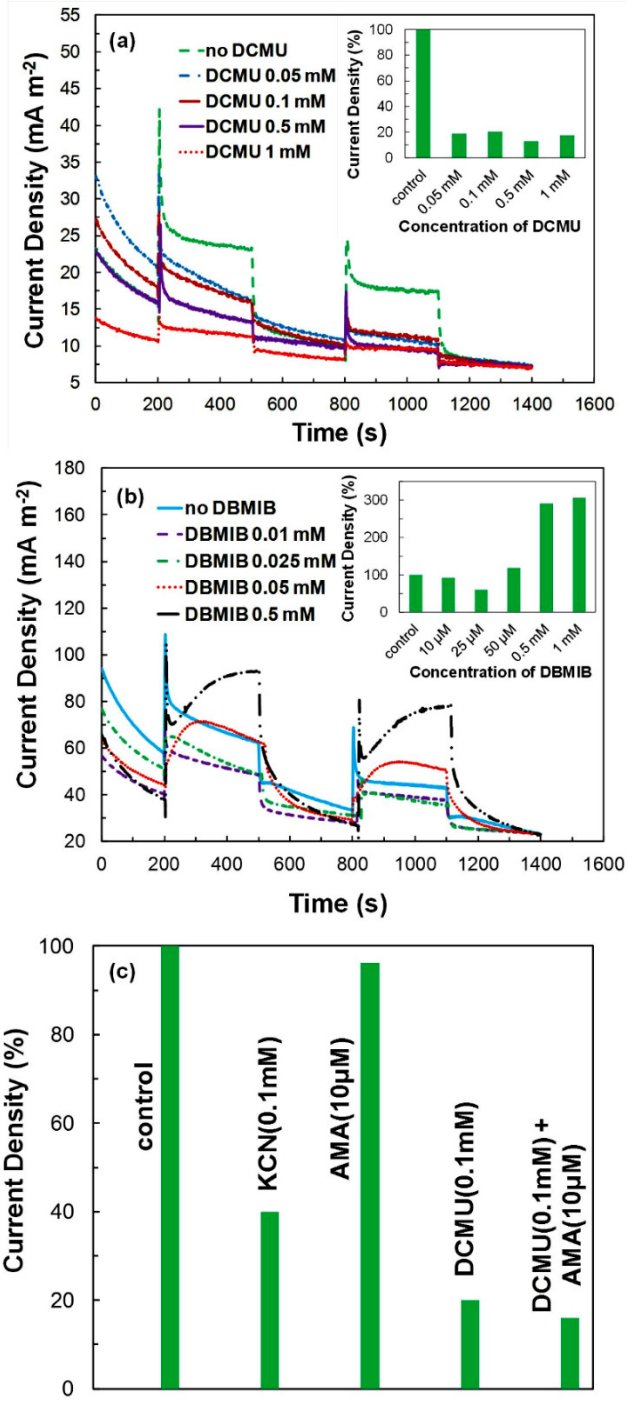

Figure 2.7: Effects of site-specific photosynthesis inhibitors on the photocurrent generation in NOS: (a) DCMU, (b) DBMIB, and (c) KCN, AMA and AMA + DCMU. The insets in (a) and (b) represent the percentage of photocurrent inhibition by NOS at different concentrations of inhibitors. Control represents no inhibitor case

advantage of cyanobacteria is that they possess intersecting P-ETC and R-ETC in thylakoid membranes (Katz et al. 1989). While both photosynthesis and respiration takes place in the thylakoid membranes, only respiration occurs in the cytoplasmic membrane. The *PQ* pool, cytochrome b_6f (*Cyt* b_6f) and *PC* are shared by both the photosynthesis and respiration in thylakoid membranes (Figure 2.1). This organization offers competitive advantage for the cyanobacteria to redirect the excess electrons from P-ETC towards R-ETC if the *PQ* pool is over-reduced (to PQH_2). This is not possible in higher plants and algae where photosynthesis and respiration are spatially separated from each other and happen in two different organelles called chloroplast and mitochondria respectively. The transfer of electron from *PQ* to *Cyt* b_6f is the rate-limiting step in the photosynthesis (Katz et al. 1990). When PSII is exposed to high intensity light, the *PQ* pool will be predominantly in reduced form leading to photo-damage of PSII. However, the cyanobacteria combat this phenomenon by elevating the level of antioxidant pigments such as carotenoids (Solov'ev et al. 1991) and/or by oxidizing the PQH_2 through a terminal oxidase called *bd-quinol oxidase* (Katz 1994). The same concept was also witnessed by Pisciotta *et. al.,* who correlated the electrogenic activity of cyanobacteria with overflow metabolism, when the cells are exposed to high intensity light (Pisciotta et al. 2011). Further *bd-quinol oxidase* is present in both thylakoid and cytoplasmic membranes (Potts 1999). In our case we believe that the reduced *PQ* pool was being oxidized by *bd- quinol oxidase*, which might deliver the electrons to CNT thereby generating photocurrent. Other terminal oxidases such as alternate terminal oxidases (ARTO) were also found to present in cytoplasmic membrane. The electron transfer pathways from *PQ* to CNT could not be ascertained with the observed experimental data. However, from Figure 2.7a, it could be confirmed that most of the photocurrent was contributed by the PSII via *PQ* pool. Figure 2.7b shows the effect of various

concentration of DBMIB (10 μM, 25 μM, 50 μM, 0.5 mM, 1 mM) on the photocurrent generation by NOS. The photocurrents decreased by up to 40% at low concentrations of DBMIB (10 and 25 μM) compared to the no-inhibitor case, but increased at higher concentrations. This enhancement in photocurrent by up to 200% at high DBMIB concentrations is quite interesting and can be attributed to the redox properties of the compound, which acts as an electron transfer mediator between the cyanobacteria and the electrode. Similar observations about DBMIB have been made by others (Pisciotta et al. 2010; Yagishita et al. 1997). DBMIB is a *PQ* analogue and exhibits its effect by binding to the Q_o site of *Cyt* b_6f complex (Figure 2.1), where DBMIB has multiple functions depending on the concentration.

Case (i) DBMIB binding at Q_o ***site of Cyt*** b_6f***:*** At low concentrations, DBMIB inhibition at Q_o site of *Cyt* b_6f (site 2 in Figure 2.1) prevents the oxidation of PQH_2 to *PQ*, thereby preventing the transfer of electrons from *PQ* to *Cyt* b_6f complex(Roberts et al. 2004; Roberts and Kramer 2001). Since the electron transfer from *PQ* to *Cyt* b_6f is rate-limiting(Katz et al. 1990), the blocking of *Cyt* b_6f by DBMIB would redirect the electrons from *PQ* to electrode (dark blue block arrows in Figure 2.1).

Case (ii) DBMIB binding at Q_B ***site of PSII:*** However, at high concentrations, DBMIB also displaces *PQ* at the Q_B site of PSII (site 1 in Figure 2.1), thereby '*out-circuiting the PQ pool*' and accepts electrons directly from Q_B (Guikema and Yocum 1978; Kouchkovsky and Kouchkovsky 1974). In such a situation it can act as a redox shuttle and transfer electrons to an external electron acceptor or directly to the electrode itself as observed in our results. A control experiment with DBMIB in the absence of cyanobacteria showed direct electrochemical redox

activity for DBMIB on the electrode (supplementary information Figure 2.S2).

Case (iii) DBMIB binding at Q_i site of Cyt b_6f: Further, there also exists an extra heme called *heme-x* (*X* in Figure 2.1) in *Cyt* b_6f complex at the Q_i site, which involves in cyclic electron transfer from ferredoxin (*Fd*) or ferredoxin $NADP^+$ reductase (*FNR*) to *PQ* through ferredoxin plastoquinone reductase (*FPR*) (broken black arrows in Figure 2.1), thereby completing the Q cycle(Cape et al. 2006; Zhang et al. 2004). If high DBMIB concentration displaces the *PQ* from Q_B site of PSII, then it could likely displace *PQ* from Q_i site of *Cyt* b_6f complex, thereby shuttling the electrons as a mediator directly from *heme-x* to external electron acceptor or electrode without the assistance from *PQ* as given in case (ii).

It was found that incubating NOS in KCN containing media resulted in ~40 % decrease in photocurrent densities (Figure 2.7c), but the results did not show a definitive concentration dependent trend as with that of other inhibitors (data not shown). KCN is known to inhibit the copper containing *PC* and arrest the transfer of electrons from *Cyt* b_6f complex to PSI (Izawa et al. 1973; Ouitrakul and Izawa 1973) (site 3 in Figure 2.1). KCN inhibition can also be used to qualitatively identify the contribution of PSI to the overall photocurrent generation (Calkins et al. 2013). Since KCN inhibition resulted in decreased photocurrents, it is fair to conclude that PSI also contributed towards the measured photocurrents in our experiments.

Figure 2.7c represents the photocurrent produced by NOS in the presence of either AMA or DCMU or both. AMA inhibits the *FPR*, thereby hinders the cyclic electron transport (Figure 2.1) (Hosler and Yocum 1987; Joet et al. 2001). The AMA (10 μM) inhibition decreased the

photocurrents by only 10%, hence it can be concluded that the contribution of cyclic electron transport to the measured photocurrents is marginal (~10%) compared to the contribution from PSII (~80%). No additional inhibitory effect was found at higher (>10 μM) AMA concentrations (data not shown). It is also important to note that the addition of both AMA (10 μM) and DCMU (0.1 mM) did not completely block the photocurrents, suggesting that in addition to PSII and cyclic electron transport, there could be other sources (such as PSI) contributing to the photocurrent generation to a small extent (see Figure 2.7c). This hypothesis has also been supported by the fact that KCN treated NOS produced more than 10% of photocurrent, which enforces us to believe that inhibition of cyclic electron transport chain at *PC* (by KCN) and *FPR* (by AMA) are completely different. The inhibition by KCN produces more current than the inhibition by AMA, which implies that the electrons are also exiting from a site downstream of PC and upstream of *FPR*, more likely from either Fe-S of PSI or *Fd* or *FNR*.

2.3.6 Power Generation in a Photo-Bioelectrochemical Cell

A rudimentary photo-bioelectrochemical cell was constructed using NOS/CNT modified CP as the anode and *laccase*/CNT modified CP as the cathode. *Laccase* and other multicopper oxidases have been demonstrated to catalyze bio-electrochemical oxygen reduction with high efficiency on CNT supports (Lau et al. 2012; Parimi et al. 2012; Ramasamy et al. 2009; Ramasamy et al. 2010; Roy et al. 2012). The electrolyte was 0.1 M, pH 5.8 phosphate buffer. No external mediator was added to the system. Upon illumination by light, water was oxidized at the anode generating protons, electrons and oxygen. While the anode captures the electrons for photo-electricity generation, the protons and oxygen move towards cathode through the electrolyte. At

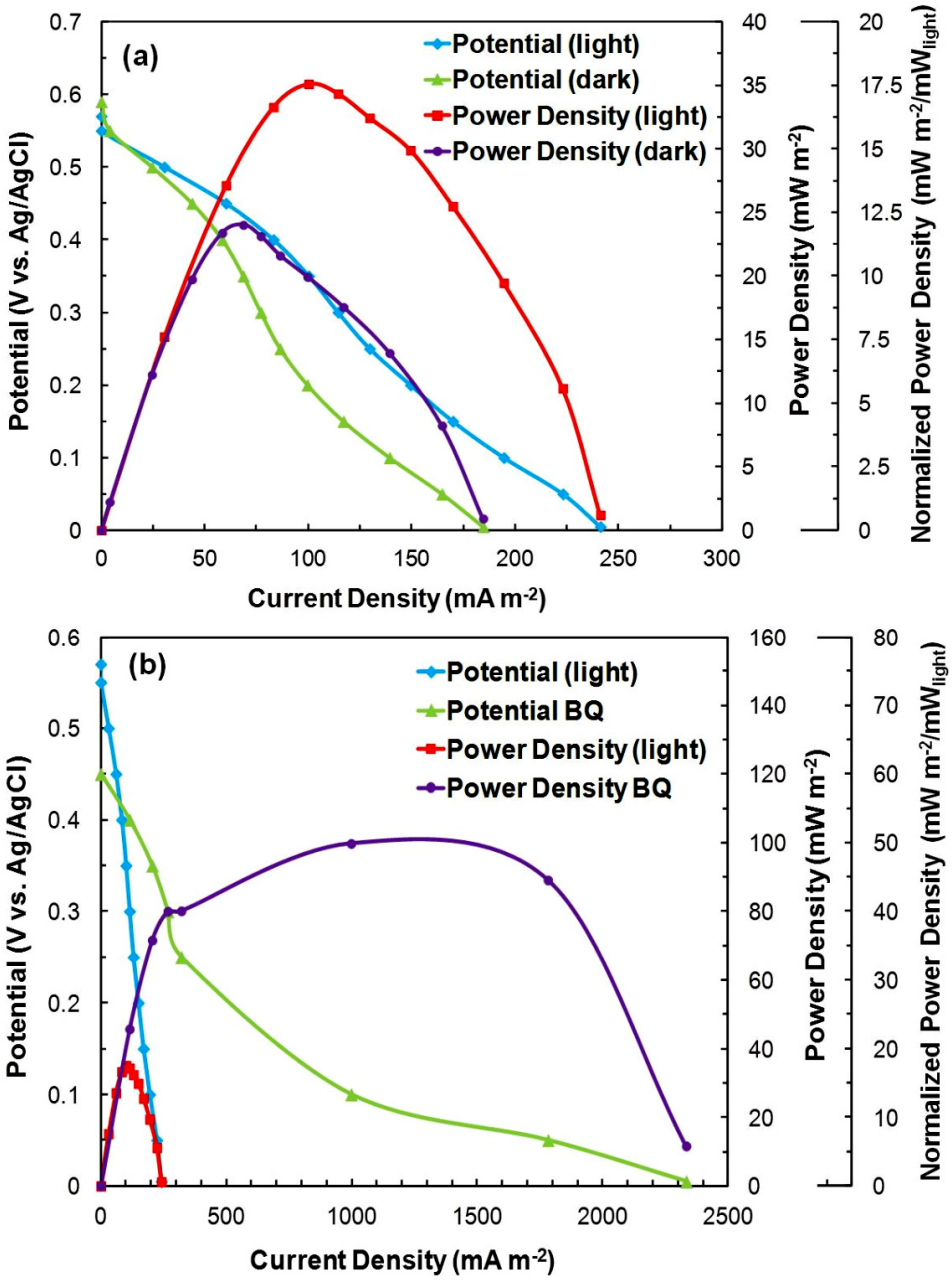

Figure 2.8: Polarization and power density curves of the photo-bioelectrochemical cell with a NOS/CNT anode and a laccase/CNT cathode. (a) DET based power generation without any mediator under light and dark conditions. (b) Comparison of DET and mediated electron transfer using BQ as a mediator

the cathode, protons, oxygen and electrons combine to form water through a bio-electrochemical reduction reaction catalyzed by *laccase*. The overall process generates electricity from light

using photosynthesis carried out by NOS. It should be noted that we did not provide any additional CO_2 to the cyanobacteria other than that is naturally available in the headspace. Polarization tests were performed at different applied voltages and the steady state photocurrents were measured at each voltage under both light (76 mW m^{-2}) and dark conditions. The OCP was found to be 0.57 V and 0.59 V in light and dark conditions respectively. As shown in Figure 2.8a, maximum current density of 240 mA m^{-2} in the light and 180 mA m^{-2} in the dark conditions were achieved. The peak power densities were 35 mW m^{-2} and 24 mW m^{-2} in light and the dark conditions without the addition of any mediators. This is the highest power density reported for any 'non-engineered' cyanobacteria based photo-bioelectrochemical systems power generation using direct electron transport.

The spent electrolyte after electrochemical experiments was also tested for the presence of any redox mediator secreted by NOS using cyclic voltammetry. As found in our previous work, the electrochemical technique has been found to be very effective in detecting even sub-nanomolar concentrations of mediators in the anolyte of microbial fuel cells (Ramasamy et al. 2009; Roy et al. 2012). In this work, no representative redox peaks were seen in the voltammograms of the spent electrolyte (Supplementary information Figure 2.S3), which confirms that the cyanobacteria do not utilize any redox mediators for external electron transport in our system and the role of direct electron transfer in photocurrent generation in NOS immobilized electrodes is substantiated. While the photocurrent generated in presence of light was due to photosynthesis, the current generated in the dark can be attributed to the extracellular electron transport resulting from respiratory electron transport pathway. Cyanobacteria are known to contain functional R-ETC in both the outer membrane and the thylakoid membrane. With NADH or succinate as

substrate, quinones and c-type cytochromes of the R-ETC might transfer electrons extracellularly and contributed to the anode current observed in dark conditions.

Table 2.1: Comparison of photo-electrochemical cell power densities reported using cyanobacteria as the photo-biocatalyst on the anode via direct electron transport

S. No.	Cyanobacteria	Anode	Cathode	Current density (mA m^{-2})	Power density (mW m^{-2})	Light intensity normalized power density (mW m^{-2} mW_{light}^{-1})[a]	Reference
1	*Nostoc* sp.	CNT/CP	Laccase/CNT/ CP	240	35	18.13	This work
2	Freshwater photosynthetic biofilm	Poly pyrrole/ carbon paint	Pt/carbon cloth	30	1.3	1.78	Zhou et al (2009)
3	Mixed photosynthetic bacteria	Nanostructures poly pyrrole/ carbon paint	Pt/carbon cloth	120	6	5.71	Pisciotta et al (2010)
4	*Synechococcus* sp. WH 5701	ITO-PET		93	8.5	0.68	McCormick et al (2011)

ITO-PET: Indium tin-oxide coated polyethylene terephthalate. Calculated from the power density, light intensity and electrode area given in the respective paper.

Table 2.2: Comparison of photo-electrochemical cell power densities reported using cyanobacteria as the photo-biocatalyst on the anode via direct electron transport

S. No.	Cyanobacteria	Anode	Cathode	Mediator	Current density (mA m^{-2})	Power density (mW m^{-2})	Light intensity normalized power density (mW m^{-2} mW_{light}^{-1})[a]	Reference
1	*Nostoc* sp.	CNT/CP	Laccase/CNT/ CP	BQ	2334	100	51.8	This work
2	*Synechococcus*	Carbon felt	ABTS/BOX/ carbon felt	DMBQ	444	58	17.2	Tsujimura et al (2001)

BOX: bilirubin oxidase; DMBQ: 2,6-dimethyl-1,4-benzoquinone; ABTS: 2,20-azino-bis(3-ethylbenzthiazoline-6-sulfonic acid). a Calculated from the power density, light intensity and electrode area given in the respective paper.

Redox mediators are generally used to facilitate the electron transport between the bacteria and the electrode under conditions where DET is ineffective. Even though, the DET was established in the case of NOS/CNT in the current study, 1,4-benzoqinone (*BQ*) was used as a supplement to examine the effect of mediator on power generation. Figure 2.8b shows the polarization and power density curves obtained from the full cell using BQ (2 mM) as mediator. As seen in Figure 2.8b, a maximum current density of 2330 mA m^{-2} and peak power density of 100 mW m^{-2} were achieved, which is a huge enhancement by the addition of *BQ* as a mediator in the electrolyte. It is noteworthy to point out that the electrochemical cell was neither optimized for power generation nor was enriched with CO_2 for increased photosynthetic activity. Benzoquinone is similar in structure to the *PQ* except in lacking the isoprene chain of *PQ*. *BQ* being lipophilic might diffuse through both outer membrane and thylakoid membranes of cyanobacteria and gets reduced by the electrons from P-ETC (Torimura et al. 2001). *BQ* could possibly compete with *PQ* in electron collection sites as explained in the section 2.3.5 i.e., Q_B site of PSII, *heme-x* in the Q_i site of *Cyt* b_6f and mimic the role of highly concentrated DBMIB (see Figure 2.7b), thereby enhancing the power density to nearly two orders of magnitude. Table 2.1 and 2.2 compare the power and current densities obtained in this study with the values reported in the literature so far for cyanobacteria based electrochemical systems based on direct and mediated electron transport. The power density achieved with *BQ* mediator for NOS/CNT is the highest ever achieved with similar systems studied so far.

1.7 Conclusions

We have demonstrated direct electron transfer based electrogenic activity of *Nostoc* sp. for

photosynthesis-assisted power generation in an electrochemical cell. The contribution of different photosynthetic pigments to photocurrent generation has been found to vary greatly, with chlorophyll-a being the major contributor. The extracellular electron transfer pathways between the cyanobacterium and the CNT have been elucidated with the help of photosynthesis inhibitors. The route $H_2O \rightarrow$ PSII $\rightarrow$ *PQ* $\rightarrow$ *protein ?*$\rightarrow$ CNT has been found to be the major pathway by which the light induced electrons generate photocurrent by direct electron transport. The cyclic electron transport chain also contributed to the photocurrent generation in smaller amount. The photo-electrochemical cell developed using immobilized *Nostoc* sp. as photo-biocatalyst on the anode, and *laccase* modified CNT on the cathode generated an average power density of 35 mW m^{-2} (18 mW m^{-2}/mW_{light}) without any exogenous mediator, which is highest among the 'non-engineered' photo-electrochemical systems to this date. The photo-electrochemical cell demonstrated is rudimentary, which has not been engineered for geometry, electrode shape, size, physical properties, internal impedance, fluid flow, mass transport, or other parameters. However, engineering optimizations such as better cell design, usage of three dimensional brush electrodes, reduced electrode spacing, etc., could result in much higher power densities than reported here and would be part of our future research. The photocurrent generation was found to be fairly stable in our studies if the nutrient supply is not deprived. Upon addition of 1,4-benzoquinone mediator, the power density increased by nearly two orders of magnitude. This work also demonstrates that photo-bio anodes made of whole cells of microorganisms such as NOS would be highly beneficial for fuel cell applications than using isolated thylakoids or photosystems which require intensive isolation procedures, as well as suffer from high degree of instability when immobilized on electrodes. Moreover, cyanobacteria are also known to survive in different environmental conditions such as varying levels of CO_2,

light exposure and dryness and therefore offer many advantages for practical photosynthesis based energy conversion applications. Research on antenna pigments and light harvesting complexes are crucial in revealing the natures astounding capability of solar energy conversion. Detailed investigation of the mechanism of electron transport and the localization of redox active proteins in various membrane systems of the cyanobacteria would be highly useful in developing genetically-engineered cyanobacteria with controllable electron transfer pathways and enhanced electrogenic capabilities.

1.8 Supplementary Data

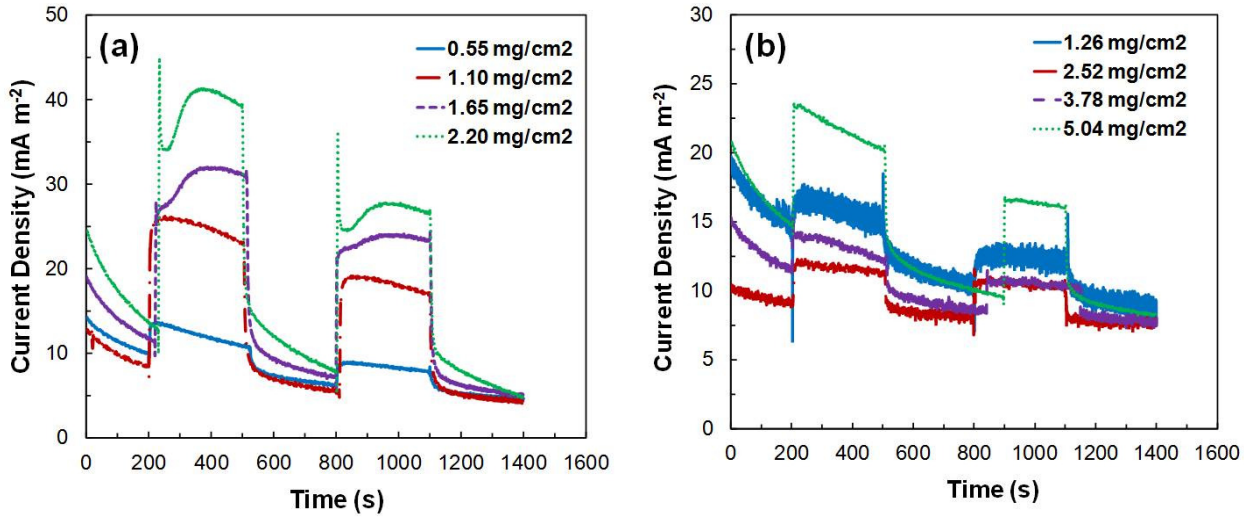

Figure 2.S1: Optimization of cyanobacteria loading on the CNT modified electrodes for the photocurrent generation: (a) NOS and (b) AV. The photocurrent density increased loading until 2.2 mg cm^{-2} and 5.04 mg cm^{-2} for both NOS and AV respectively beyond which the photocurrents decreased

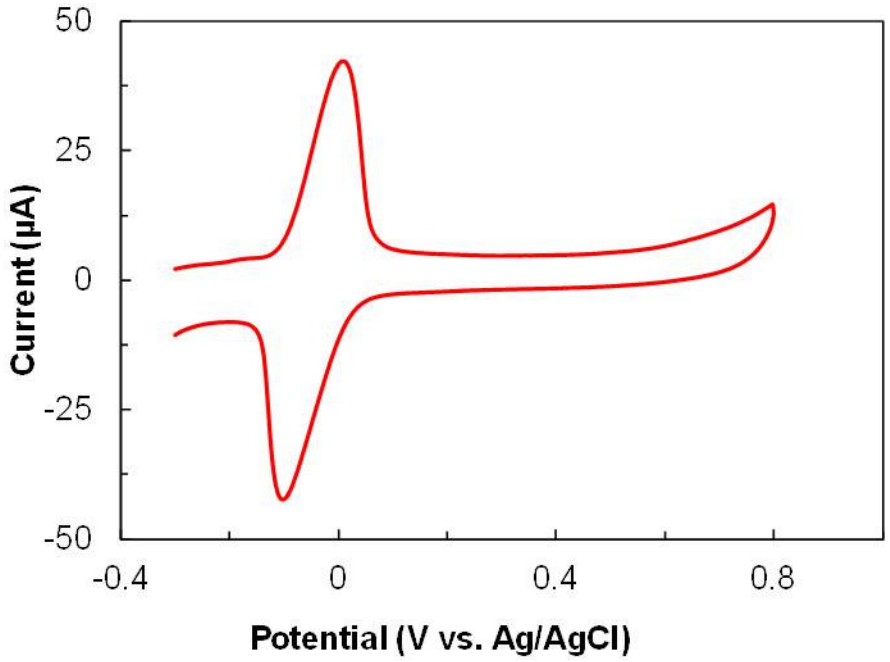

Figure 2.S2: Cyclic voltammogram showing redox peaks of DBMIB

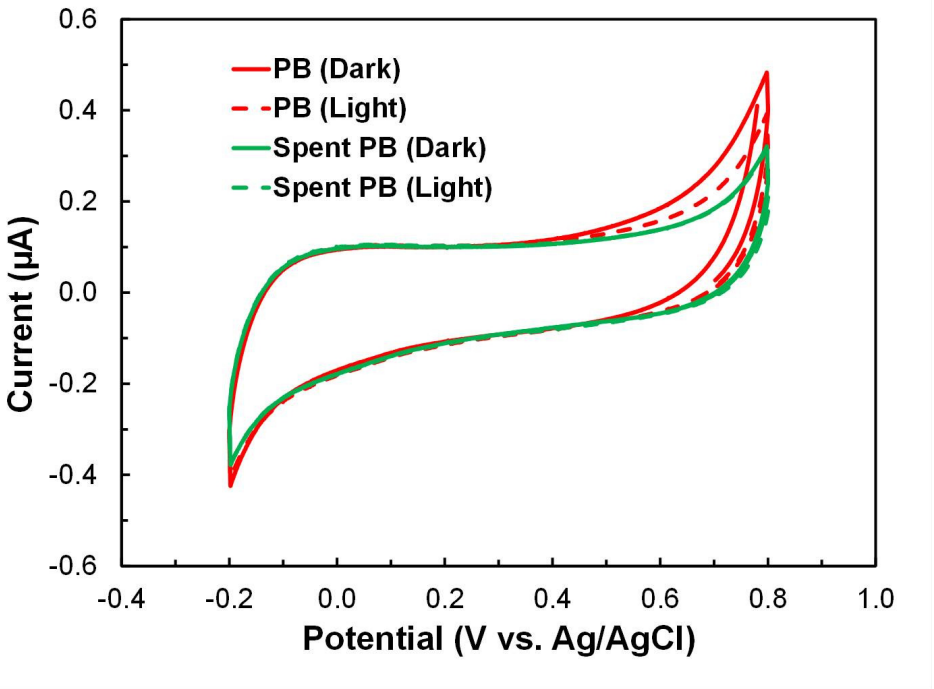

Figure 2.S3: Cyclic voltammograms of fresh phosphate buffer (PB) and spent phosphate buffer (Spent PB) under dark and light conditions

Table 2.S1: Fluorescence measurement of NOS for examining the accessory photosynthetic pigments

S. No.	Excitation wavelength	Emission wavelength	Control	NOS	Fluorophore
1	590 (±10)	645 (±20)	0	370	C-Phycocyanin
2	530 (±12.5)	645 (±20)	0	91	R-Phycocyanin
3	530 (±12.5)	590 (±17.5)	0	22	B-Phycoerythrin

CHAPTER 3

ENHANCED PHOTO-BIOELECTROCHEMICAL ENERGY CONVERSION BY GENETICALLY ENGINEERED CYANOBACTERIA

This chapter contains text modified from the following two publications:

Narendran Sekar, Rachit Jain, Yajun Yan and Ramaraja P. Ramasamy. 2016. *Biotechnology and Bioengineering*. 113: 675–679.

Narendran Sekar and Ramaraja P. Ramasamy. 2015. *ElectroChemical Society Transactions*. 69 (34): 1-8.

Abstract

Photosynthetic energy conversion using natural systems is increasingly being investigated in the recent years. Photosynthetic microorganisms such as cyanobacteria exhibit light dependent electrogenic characteristics in photo bio-electrochemical cells (PBEC) that generate substantial photocurrents, yet the current densities are lower than their photovoltaic counterparts. Recently we demonstrated that a cyanobacterium named *Nostoc* sp. employed in PBEC could generate up to 35 mW m^{-2} even in a non-engineered PBEC. With the insights obtained from our previous research, a novel and successful attempt has been made in the current study to genetically engineer the cyanobacteria to further enhance its extracellular electron transfer. The cyanobacterium *Synechococcus elongatus* PCC 7942 was genetically engineered to express a non-native redox protein called outer membrane cytochrome S (OmcS). OmcS is predominantly responsible for metal reducing abilities of exoelectrogens such as *Geobacter* sp. The engineered *S. elongatus* exhibited higher extracellular electron transfer ability resulting in ~ 9-fold higher photocurrent generation on the anode of a PBEC than the corresponding wild-type cyanobacterium. Further, power density generated by the genetically engineered cyanobacteria in a rudimentary PBEC was found to be five times higher than that generated by the wild-type. This work highlights the scope for enhancing photocurrent generation in cyanobacteria thereby benefiting faster advancement of the photosynthetic microbial fuel cell technology.

Keywords: *Synechococcus elongatus*, outer membrane cytochrome, photocurrent, extracellular electron transfer, genetic engineering, photosynthetic microbial fuel cell

1.9 Introduction

Microorganisms that are capable of transferring electrons to extracellular electron acceptors as a part of their metabolism are called exoelectrogens. The extracellular electron transfer (EET) capability of microorganisms has been exploited in microbial fuel cells (MFC) to generate electricity using organics as fuel. When deprived of their cellular terminal electron acceptor, these microorganisms prefer to transfer their electrons to the electrode, thereby using it as an alternate electron sink. In MFC, the commonly used exoelectrogens such as *Geobacter* sp. and *Shewanella* sp. consume organic carbon sources such as acetate or lactate as their reductant and transfer the electrons from their respiratory electron transport chain to the anode while simultaneously releasing CO_2. On the contrary, photosynthesis based electricity generation using plant thylakoids (Calkins et al. 2013), cyanobacteria (Sekar et al. 2014) requires only light and water without the need of any external organic carbon source and therefore offers huge potential for development of a clean, renewable and environment friendly alternate energy source (Sekar and Ramasamy 2015). Cyanobacteria have inherent ability to perform EET and are shown to generate electricity in photo-bioelectrochemical fuel cells (Pisciotta et al. 2010). However, the power density achieved using cyanobacteria (~ 0.035 W m^{-2} of electrode surface) (Sekar et al. 2014) is two orders of magnitude lower compared to that produced by the exoelectrogens in MFC (~ 7 W m^{-2} of electrode surface) (Logan 2009). In order to make them competitive against biofuel cell and photovoltaic technologies, the current densities of cyanobacteria based PBECs must be improved greatly. Such an improvement could be realized through genetic engineering (Blankenship et al. 2011).

The EET ability of exoelectrogens can be primarily attributed to their dissimilatory metal reducing properties in anaerobic environment. *Geobacter* and *Shewanella* exhibit their dissimilatory metal reducing capability with the help of numerous c-type cytochromes that are present on their outer membrane called outer membrane cytochromes (Omc) (Yang et al. 2012), which execute the electron transfer across the cell membrane. Recently, detailed pathways by which these bacteria perform EET through their Omc are elucidated on both biochemical and genetic basis (Lovley 2008). *Geobacter* sp. expresses an array of Omc when they are grown in medium containing insoluble terminal electron acceptors such as Fe(III) oxide and Mn(IV) oxide (Mehta et al. 2005). Particularly, outer membrane cytochrome S (OmcS) has been found to play a predominant role in EET in *Geobacter sulfurreducens* (Qian et al. 2011). The pili of *G. sulfurreducens* was found to be aligned with numerous OmcS that help transfer the electrons extracellularly (Leang et al. 2010). Cyanobacteria (CB) do not contain any of these Omc therefore are not on par with exoelectrogens for EET, despite their tremendous photosynthetic energy conversion ability with high internal quantum efficiency of ~100% (Blankenship et al. 2011). We hypothesize that combining the desired properties of both organisms could result in an engineered strain with unique properties for photo-bio-electrochemical energy conversion.

In the present work, we genetically engineered heterologous *omcS* in *Synechococcus elongatus* PCC 7942 to enhance the cyanobacterial extracellular electron transfer to alternate electron acceptors (Figure 3.1). The idea of genetically engineering cyanobacteria for enhancing EET is novel (Ramasamy and Sekar 2015) and has not yet been reported so far in literature to the best of our knowledge.

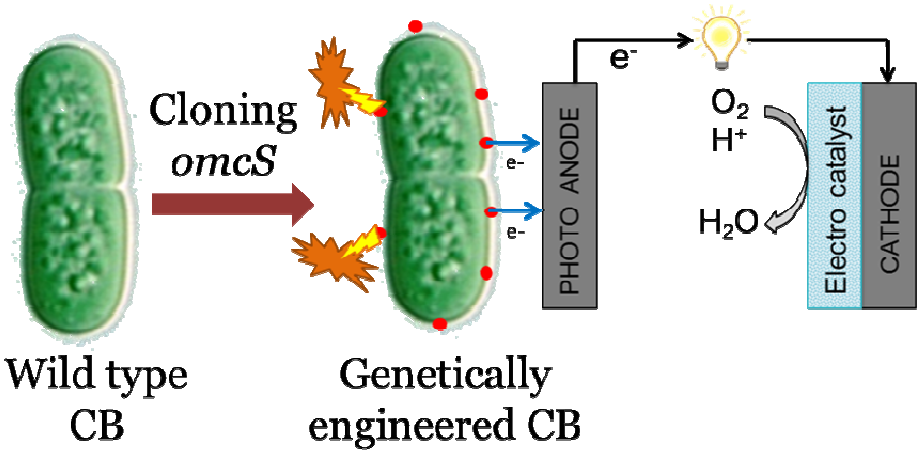

Figure 3.1: Schematic showing the concept of enhancing exoelectrogenicity of cyanobacteria (CB) by genetic engineering them to express the outer membrane cytochrome S (*omcS*)

1.10 Materials and Methods

3.2.1. Materials and Bacterial Strain

Carbon paper (SpectraCarb 2050-L) was used as base electrode (3 mm diameter) onto which a slurry of multi-walled carbon nanotube (CNT) of 10 nm diameter and 1–2 mm length (Dropsens, Spain) were drop-casted as immobilization support for cyanobacteria. 1-pyrenebutanoic acid succinimidyl ester (PBSE) (Anaspec) was used as a molecular tethering agent to attach the laccase enzyme (Trametes versicolor, Sigma) to the CNT. Monobasic and dibasic salts of potassium phosphate (BDH) were used to prepare the phosphate buffer solutions of appropriate pH. All buffers were prepared using nanopure distilled water (dd water). All other chemicals were purchased from either Amresco, EMD, Acros Organics, J. T. Baker or Alfa Aesar. *Synechococcus elongatus* PCC 7942 strain and pAM2991 plasmid were obtained from Dr. Susan S. Golden (University of California, San Diego).

3.2.2. Cloning of *omcS* Gene in *S. elongatus*

The wild type *Synechococcus elongatus* PCC 7942 was used as a model organism for our study. Both the wild-type (Wild-CB) and the genetically engineered *S. elongatus* (Eng-CB) were grown in modified BG11 medium as shown in our previous work (Sekar et al. 2014). The cyanobacterial cultures were inoculated in the autoclaved media and grown at 30 ± 2 ^{0}C at 100 rpm under continuous illumination using fluorescent lamps (80 µmol $m^{-2}s^{-1}$). The coding sequence of *omcS* gene from *G. sulfurreducens* PCA strain (NC_002939.5) was codon optimized for expression in *S. elongatus* and synthesized by Genscript. We constructed pNR1 by cloning the *omcS* gene into neutral site I (NSI) targeting pAM2991 vector (Ivleva et al. 2005) that harbors spectinomycin resistance gene ($spec^{R}$) as an antibiotic selection marker (Figure 3.2a). The expression of *omcS* gene was under the control of P_{trc} and was inducible by the addition of isopropyl β-D-1-thiogalactopyranoside (IPTG). The vector pNR1 was transformed into *S. elongatus* PCC 7942 following the transformation protocol given by Invitrogen, Life Technologies. The colonies were screened in BG11-agar plates with 50 µg/ml spectinomycin and the presence of *omcS* in the positive colonies was confirmed by PCR using the primers 5'GGGAAA**GAATTC**GAAGGAGTATACCTATACATGAAGAAAGGCATGAAAGTTAGT CTGA 3' and 5'GGGAAA**GGATCC**TTAATCTTTGGCGTGGCATTTGTTAC 3'. The Eng-CB grown in modified BG11 was induced at an OD_{750} of 0.6 with 1mM IPTG and the sample was collected after 24 hours for heme staining in non-denaturing SDS-PAGE (Thomas et al. 1976).

3.2.3. Ferricyanide Reduction Assay

Ferricyanide reduction assay was carried out to evaluate the extracellular electron transfer of the cyanobacterium. Both the Wild-CB and the Eng-CB cultures were harvested at an OD_{750} of 0.6 by centrifuging the cells at 5000 rpm for 10 minutes at room temperature and re-suspended in fresh BG11 medium. Following induction with 1mM IPTG, 1 mM potassium ferricyanide (in BG11 medium) was added and the culture was split into two halves; One-half was incubated in light and the other was covered with aluminum foil and incubated in dark to assess the reduction of potassium ferricyanide in both light and dark conditions. Samples were collected every 4 hours for 48 hours. The sample was centrifuged at 10,000 rpm for 5 minutes at room temperature and the absorbance of supernatant was measured at 420 nm to calculate the concentration of residual potassium ferricyanide. The rate of ferricyanide reduction for 12 hours was then normalized with the average chlorophyll content (Bradley et al. 2013).

3.2.4. Electrochemical Experiments

Electrochemical experiments were conducted with Wild-CB and Eng-CB to investigate the photocurrent generation. Briefly, the cells were harvested by centrifugation and physisorbed onto carbon paper (CP) modified with multi-walled carbon nanotubes (MWNT) as shown in our previous work (Sekar et al. 2014). Same amount of cells was drop-casted onto the electrode for comparing the performance of Wild-CB and Eng-CB. Half-cell electrochemical system with either CP/MWNT/Wild-CB or CP/MWNT/Eng-CB as working electrode, Ag/AgCl, sat. KCl as reference electrode and platinum wire as counter electrode was employed to measure open

circuit potential (OCP) and current generated at an applied voltage (an overpotential of 0.1 V vs. Ag/AgCl) using CHI potentiostat (401a models, CH Instruments Inc). All potentials reported here are with respect to Ag/AgCl electrode. 100 mM potassium phosphate buffer (pH 7) was used as electrolyte. A Dolan-Jenner Industries Fibre-Lite lamp (model 190) with a light intensity of 76 mW cm^{-2} was used for illumination.

The photo-bioelectrochemical full cell was developed using CP/CNT/Wild-CB or CP/CNT/Eng-CB as anode and CP/CNT/Laccase as the enzymatic cathode. A molecular tethering approach using PBSE was used to immobilize laccase onto CNT. Potassium phosphate buffer (100 mM, pH 5.8) was used as the electrolyte in the full cell. In the presence of light, CB oxidizes water and transfers electron to the anode and the oxygen is enzymatically reduced on the cathode to form water. Polarization curve was generated by measuring the current at different applied potential. A Dolan–Jenner Industries Fibre-Lite lamp (model 190: quartz-halogen vibration less light source, 3100 K color temperature) with a light intensity of 76 mW/cm^2 was used for illumination.

1.11 Results and Discussion

S. elongatus PCC 7942 was the first cyanobacterium demonstrated to be reliably transformable by exogenously added DNA. Figure 3.2a shows the schematic of cloning procedure used to express *omcS* gene in *S. elongatus*. Following transformation, *omcS* was integrated into the NSI site in genomic DNA of *S. elongatus* by homologous recombination as shown in Figure 3.2b. The presence of *omcS* in the *S. elongatus* was evident from its ability to grow in the

spectinomycin BG11 agar plates and was confirmed subsequently by PCR (Figure 3.2c) using the primers given in section 3.2.2. The growth characteristic of Eng-CB was similar to that of Wild-CB implying that the expression of heterologous *omcS* has no detrimental effect on the cyanobacterium (Figure 3.3a). The log phase Eng-CB culture (OD_{750} of ~ 0.6) was induced with IPTG (1mM) and expression of *omcS* was confirmed in non-denaturing PAGE followed by heme staining (Figure 3.3b) which specifically stains multi-heme proteins such as OmcS.

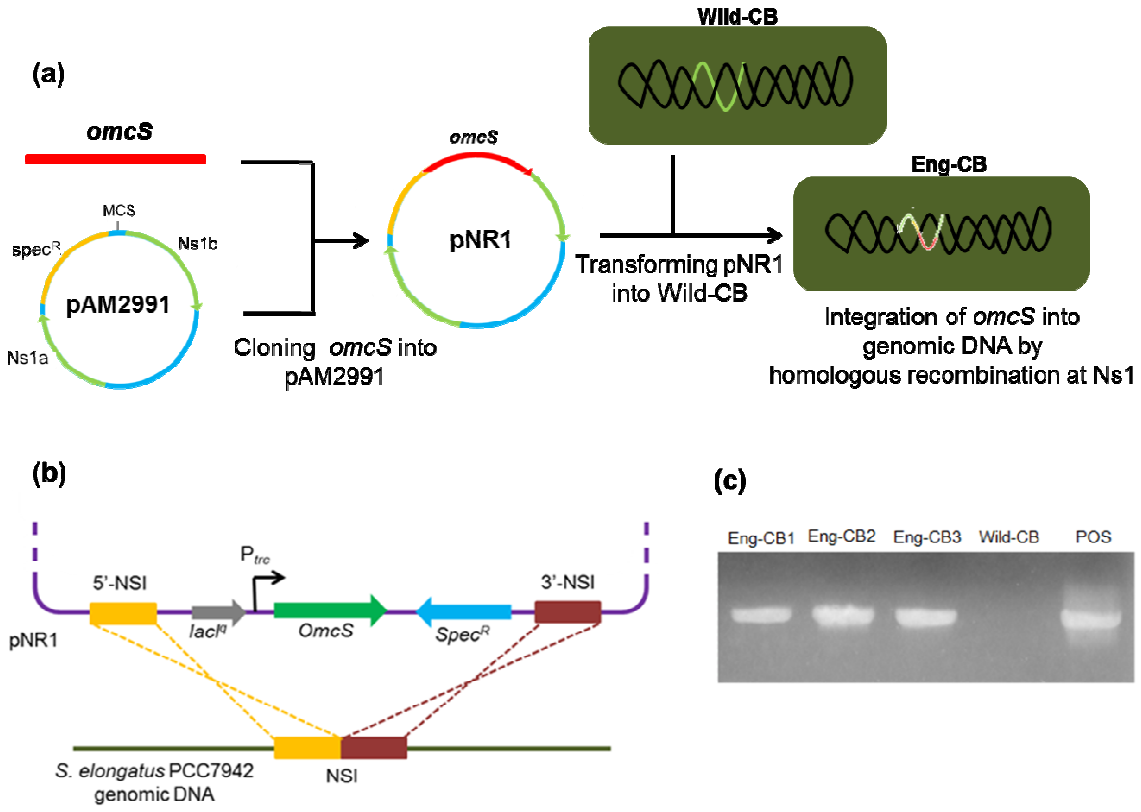

Figure 3.2: (a) Schematic showing the cloning of *omcS* gene into *S. elongatus*: construction of pNR1 by cloning *omcS* into pAM2991, transformation of pNR1 into wild type *S. elongatus* (Wild-CB) and integration of *omcS* into genomic DNA of CB; (b) Schematic showing chromosomal integration of *omcS* in *S. elongatus* by homologous recombination. NSI: neutral site I; $Spec^R$: spectinomycin resistance gene; P_{trc}: IPTG inducible trc promoter; (c) Confirmation of successful cloning of *omcS* by PCR. Eng-CB1/2/3: three different colonies screened and found to be positive; Wild-CB: wild type *S. elongatus*; POS: pNR1 vector positive control

The heme staining confirmed that the OmcS was active, because the appearance of distinct band on the activity gel was solely based on peroxidase activity of the active heme protein. The significant band was seen only in the soluble fraction of Eng-CB, but not in the insoluble fraction, which is meaningful considering the fact that OmcS is not an integral membrane protein but a peripheral membrane protein that is loosely attached to the outer membrane. However, the precise localization of OmcS has yet to be confirmed by specifically analyzing the various membrane fractions that would be addressed in our future research.

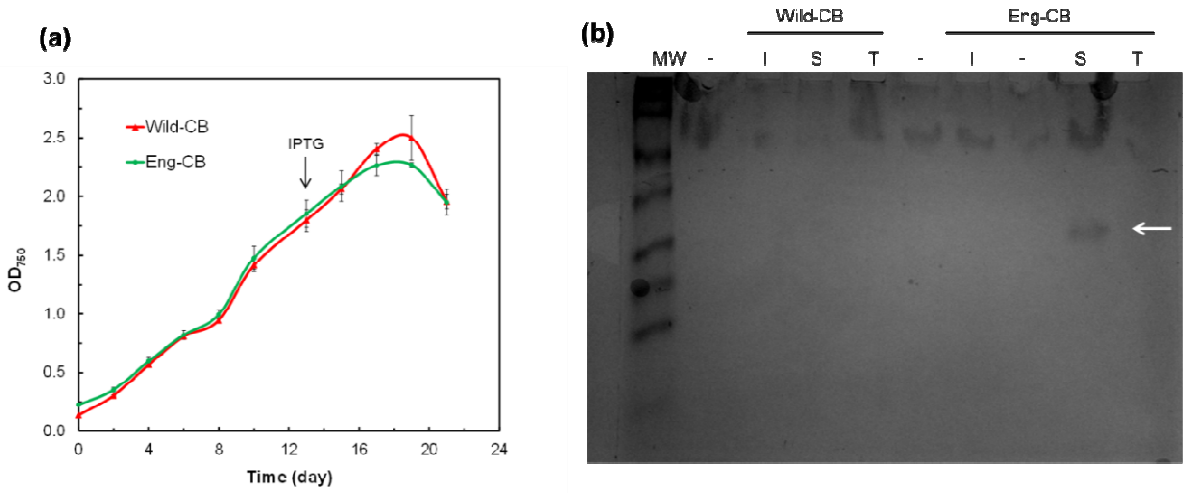

Figure 3.3: (a) Growth curve of Wild-CB or Eng-CB. Eng-CB culture was induced with 1 mM IPTG at 13th hour; (b) heme staining following the separation of total protein on non-denaturing polyacrylamide gel. MW: standard molecular weight marker; I: insoluble protein in the pellet; S: soluble protein in the supernatant; T: total protein (I+S). The white solid arrow represents the active OmcS in the soluble fraction of Eng-CB

Upon confirming the expression of active *omcS*, the ability of Eng-CB to reduce the exogenously added potassium ferricyanide was studied and compared with that of Wild-CB. Being highly water soluble, ferricyanide cannot cross the outer membrane of cyanobacteria and is highly appropriate to study the extracellular electron transfer (Bombelli et al. 2011). Thus, the rate of ferricyanide reduction of Wild-CB and Eng-CB was measured in both light and dark condition as

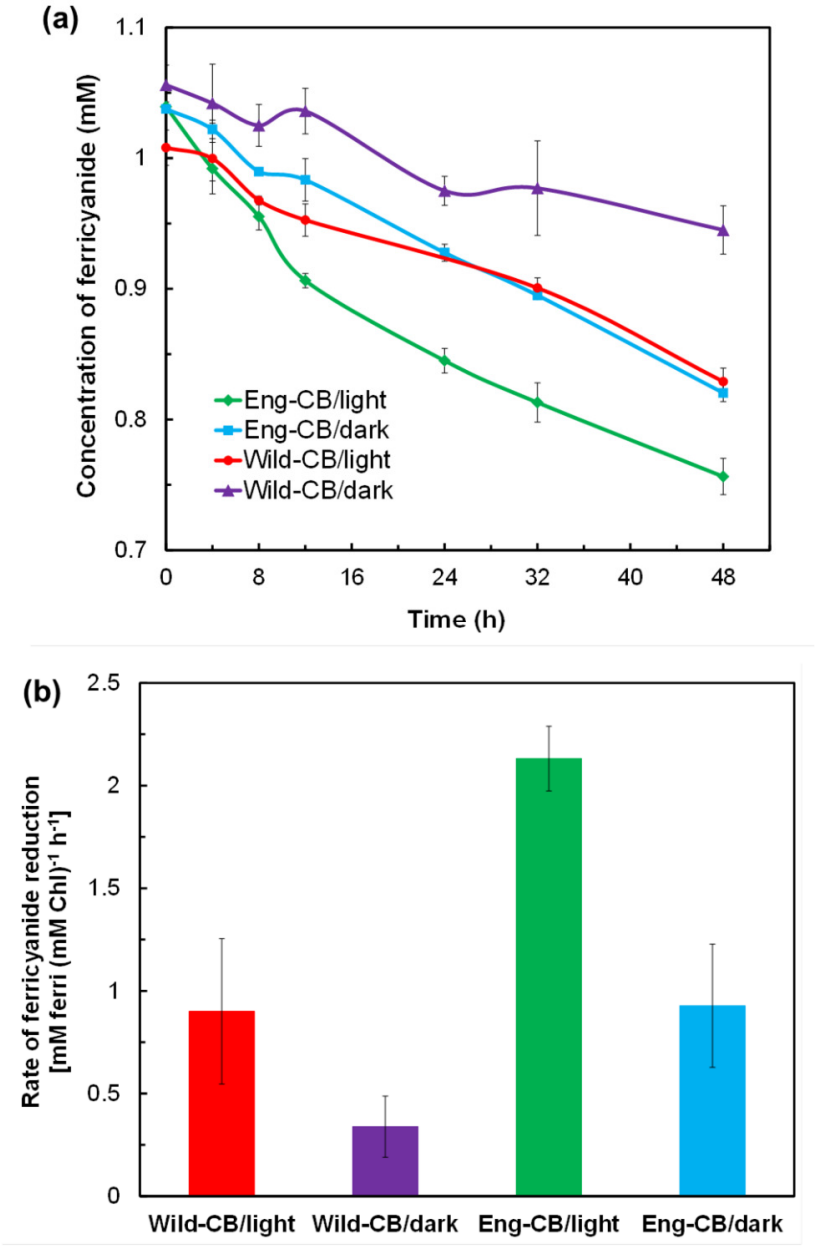

Figure 3.4: (a) Reduction of potassium ferricyanide by Wild-CB and Eng-CB over 48 hours in both light and dark conditions. (b) Rate of ferricyanide reduction (normalized with the average chlorophyll content) of Wild-CB and Eng-CB calculated using the raw data in Figure 3.4a over the first 12 hours in both light and dark conditions. Each data point/bar shown is average of three independent experiments with SD as error bars

shown in Figure 3.4a. Although potassium ferricyanide is light sensitive, it was found to be more stable without any significant reduction during the short period of our control experiments in the

absence of cyanobacterium under light condition. Cyanobacteria such as *S. elongatus* has already been proven to exhibit light dependent electrogenic activity in the presence of various redox mediators such as hydroxyl napthoquinone and dimethyl benzoquinone. Both Wild-CB and Eng-CB strains reduced ferricyanide under light as well as dark conditions (Figure 3.4a). The ferricyanide reduction in the light and dark was attributed to the electrons channeling from photosynthetic (P-ETC) and respiratory electron transport chain (R-ETC) respectively. The rate of ferricyanide reduction by Eng-CB in light was found to be ~ 2 fold higher than that of Wild-CB in light (Figure 3.4b), which clearly corroborates that the heterogeneously expressed *omcS* enhanced the EET in the Eng-CB. Further, it is also interesting to note that the rate of ferricyanide reduction of Eng-CB in dark was also observed to be ~2.5 fold higher compared to that of Wild-CB in dark (Figure 3.4b), supporting evidently that the OmcS interacted with both the P-ETC and R-ETC.

The photocurrent generation by the genetically modified *S. elongatus* was investigated using amperometric i-t curve in a photo bio-electrochemical half-cell (Figure 3.5) using the cyanobacterial anode as explained in the experimental procedures. The electrode harboring Eng-CB showed a lower open circuit potential (OCP) compared to that of Wild-CB which is indicative of Eng-CB being a better anode (Figure 3.5a). Once light is turned on, the OCP significantly reduced in both Eng-CB and Wild-CB which is consistent with our previous observation in *Nostoc* sp. (Sekar et al. 2014). Upon absorbing light energy, the redox potential of both PSII and PSI reaches a more negative value from ~ +0.1V to ~ -0.1 V for PSII and from ~ +0.2 V to ~ -1.4 V for PSI (all redox potentials are expressed with respect to Ag/AgCl) and is solely responsible for the decrease in OCP during the light phase. Similarly, upon shutting off

the light, the OCP stabilized in both Eng-CB and Wild-CB which altogether illustrated that the response can be primarily attributed to the photo-electrochemical reactions of cyanobacteria on the electrode. The current generated by Eng-CB and Wild-CB was measured by applying over-potential of 0.1 V (vs. Ag/AgCl) for both (0.2 V for Eng-CB and 0.25 V for Wild-CB) based on our previous experience in *Nostoc* sp. (Sekar et al. 2014). Eng-CB was observed to generate ~9-fold higher current compared to Wild-CB as shown in Figure 3.6b.

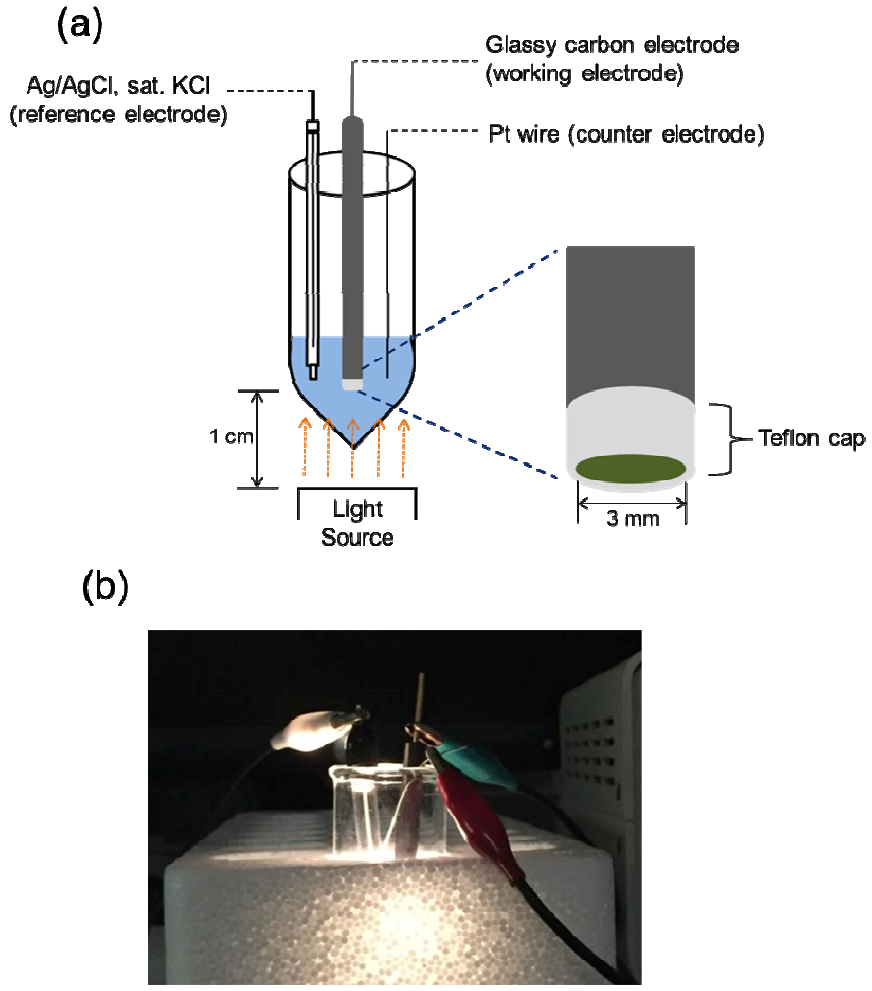

Figure 3.5: (a) Schematic of electrochemical cell used in present study; (b) photograph of the electrochemical cell showing the three electrode system: CP/CNT/CB working electrode (green), Ag/AgCl reference electrode (white) and Pt wire counter electrode (red) used in the present study

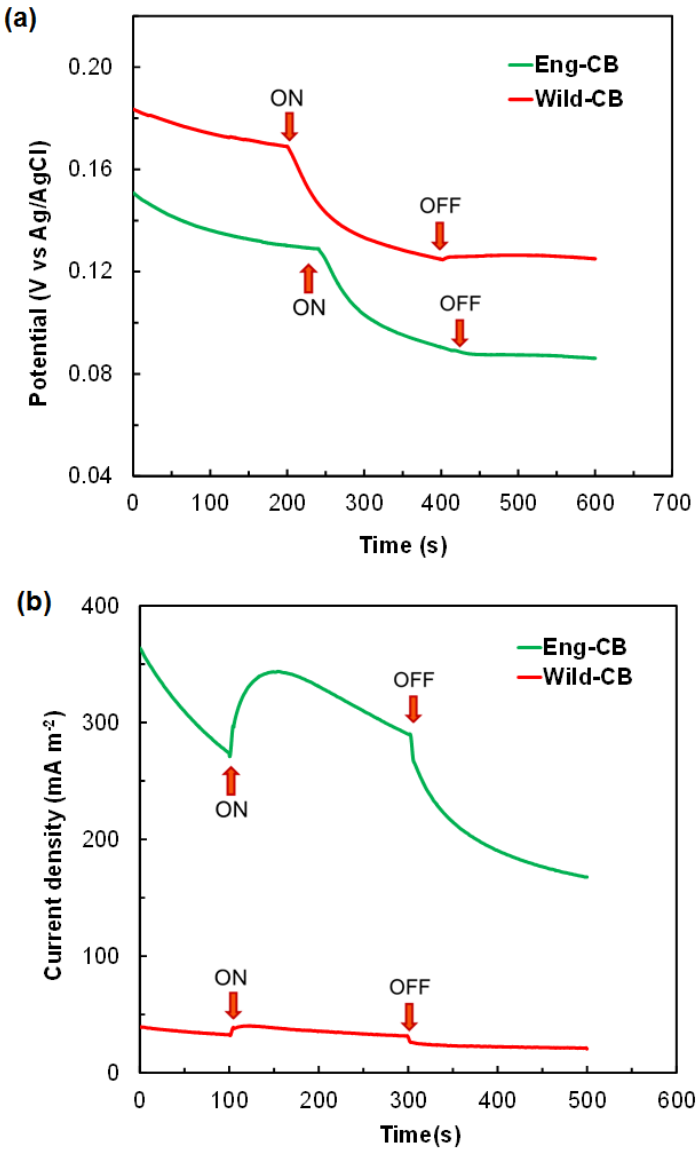

Figure 3.6: (a) Measurement of open circuit potential (OCP) of the electrode with Wild-CB or Eng-CB using Ag/AgCl as a reference electrode in light and dark phases; (b) Measurement of current generated by Wild-CB and Eng-CB by applying an over-potential of 0.1 V (vs Ag/AgCl) in light and dark phases

In addition to the enhanced DET shown by Eng-CB, its mediated electron transfer ability was also evaluated using 1,4-benzoquinone (1 µM) as a redox mediator as shown in Figure 3.7. 1,4-benzoquinone mimics the plastoquinone naturally present in the P-ETC and has been demonstrated to enhance mediated EET in our previous work. Tremendous increase in current

was observed by adding 1,4-benzoquinone as mediator in the presence of light (Figure 3.7). Taken together both the biochemical reduction of potassium ferricyanide and the electrochemical measurement of photocurrent strongly confirmed that the heterogeneously expressed *omcS* significantly enhanced the direct extracellular electron transfer ability of *S. elongatus*.

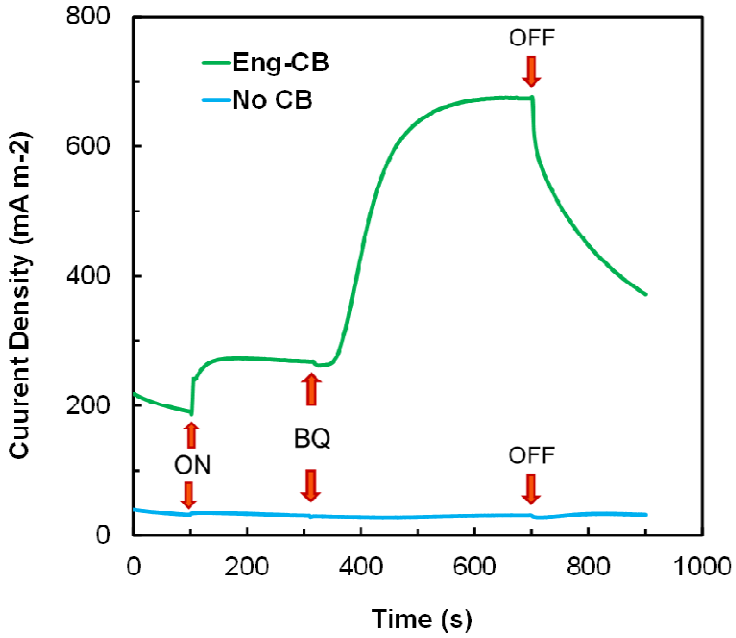

Figure 3.7: Mediated electron transfer exhibited by Eng-CB using 1,4- benzoquinone (BQ) as redox mediator. Upon addition of BQ (1µM) during light phase, Eng-CB generated a higher current compared to the direct electron transfer

Cyclic voltammogram technique with a scan rate as low as 1 mV/s has been used in microbial fuel cells to probe the electrochemistry of redox proteins on bacterial outer membrane that are in direct contact with the electrode. Similar study was conducted to characterize the Eng-CB in a three electrode system using Eng-CB, immobilized on multi-walled carbon nanotubes (MWCNT) modified glassy carbon electrode, as a working electrode, Ag/AgCl (sat. KCl) as a reference electrode and platinum wire as a counter electrode. As shown in Figure 3.8, the

Eng-CB showed a specific oxidation peak at 0.1 V (vs. Ag/AgCl) and the same was not observed in the Wild-CB. The redox peak observed in Eng-CB in Figure 3.8 corresponds to the heterologously expressed OmcS, which further proved that the enhanced photo-electrochemical activity of Eng-CB was mainly due to the presence of OmcS on the outer membrane of Eng-CB.

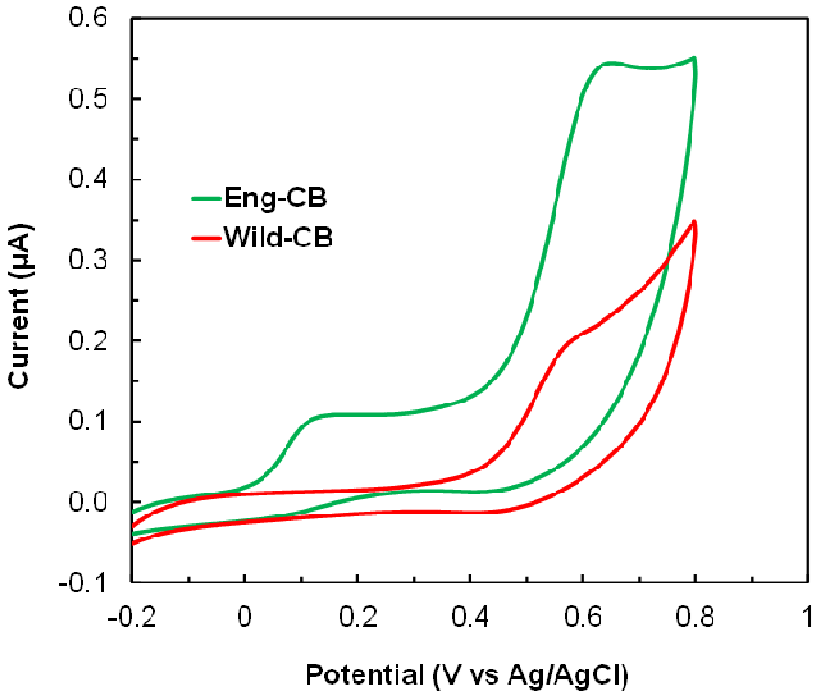

Figure 3.8: Cyclic voltammograms showing the enhanced direct electron transfer by Eng-CB (green) compared with that by Wild-CB (red); Scan rate: 1 mV/s

The photo-bioelectrochemical cell (PBEC) is a self-sustainable system using only water and light as fuel without the necessity for any external organic carbon source. CB on the anode do photosynthesis in the presence of light and transfer electrons from the P-ETC to the electrode. The oxygen generated as the by-product of photosynthesis is enzymatically reduced at the cathode to form water (Figure 3.9a). Figure 3.9b shows the current density and the power density

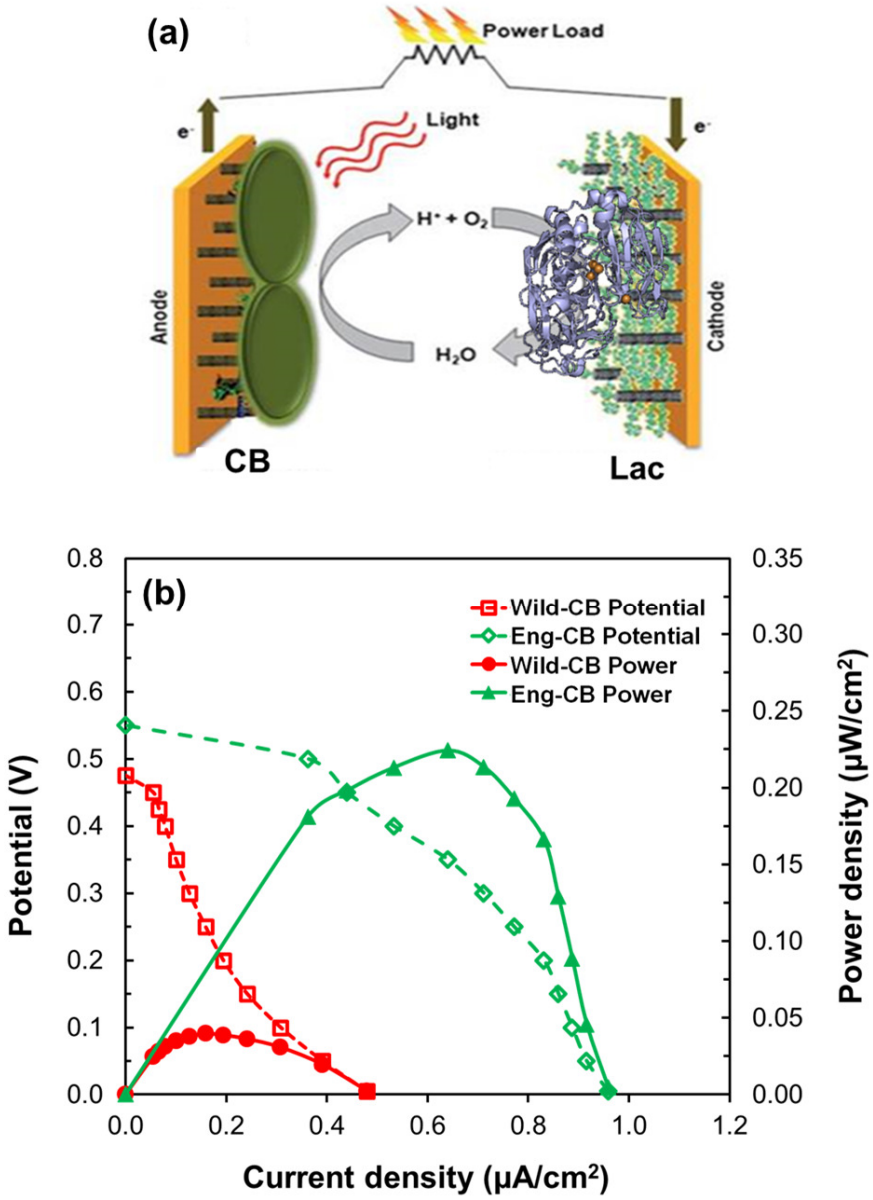

Figure 3.9: (a) Schematic showing power generation in PBEC with cyanobacteria (CB) immobilized anode and laccase based bio-cathode; (b) Polarization and power density curves of PBEC with anode: CP/MWCNT/Wild-CB (red) or CP/MWCNT/Eng-CB (green) and cathode: Carbon/MWCNT/laccase

generated by Wild-CB and Eng-CB in the PBEC. It is evident that the peak power density generated by Eng-CB (0.22 μW/cm^2) is nearly five times higher than that generated by Wild-CB

(0.04 μW/cm^2). The maximum current density generated by Eng-CB (1 μA/cm^2) is twice as that generated by the Wild-CB (0.5 μA/cm^2). It is to be noted that the peak power density and the maximum current density reported here were not the maximum reported in the literature of cyanobacterial photo-electrochemistry. The cell design/experimental set up used in the present study was very rudimentary without any engineering optimization. This study is a proof of concept to show that the Eng-CB performed better than the Wild-CB in photocurrent generation due to the heterologous expression of OmcS. However, engineering optimizations such as better cell design, usage of three dimensional brush electrodes, etc., could result in much higher power densities than that reported here.

At this juncture, it is useful to note that in *Geobacter* sp., OmcS is a predominant terminal cytochrome that transfers electron from cytochrome bc complex in cytoplasmic membrane to the external *milieu* with the help of other intermediate periplasmic c-type cytochromes such as MacA and PpcA. Both cytochrome bc complex of *G. sulfurreducens* and cytochromes b_6f complex (Cyt b_6f) of *S. elongatus* are functionally related and belong to the highly conserved Rieske/cytochromes b complexes (Cape et al. 2006). Further, certain c-type cytochromes such as cytochromes c_6 (Cyt c_6) are also found in periplasmic space of cyanobacteria (Obinger et al. 1990) that might have functionally complemented the requirement of MacA and PpcA. Both these evidences led us to hypothesize that electrons from Cyt b_6f were transferred to OmcS through Cyt c_6 (Figure 3.10). Further, Cyt b_6f is involved in both P-ETC and R-ETC which appropriately correlated with our observation that the OmcS enhanced EET under both light and dark conditions (Figure 3.4b). It is noteworthy that, in addition to Cyt b_6f and Cyt c_6, plastoquinones are also shared between both P-ETC and R-ETC (Vermaas 2001). When the

photosystems absorb more light than that can be handled by P-ETC, the more reduced plastoquinone pool buffers the P-ETC by channelling the excess electrons to respiratory terminal oxidases such as bd type quinol oxidase (bd Q) and alternate respiratory terminal oxidase (ARTO) (Pisciotta et al. 2011). Equally likely, we also postulate that this overflow mechanism

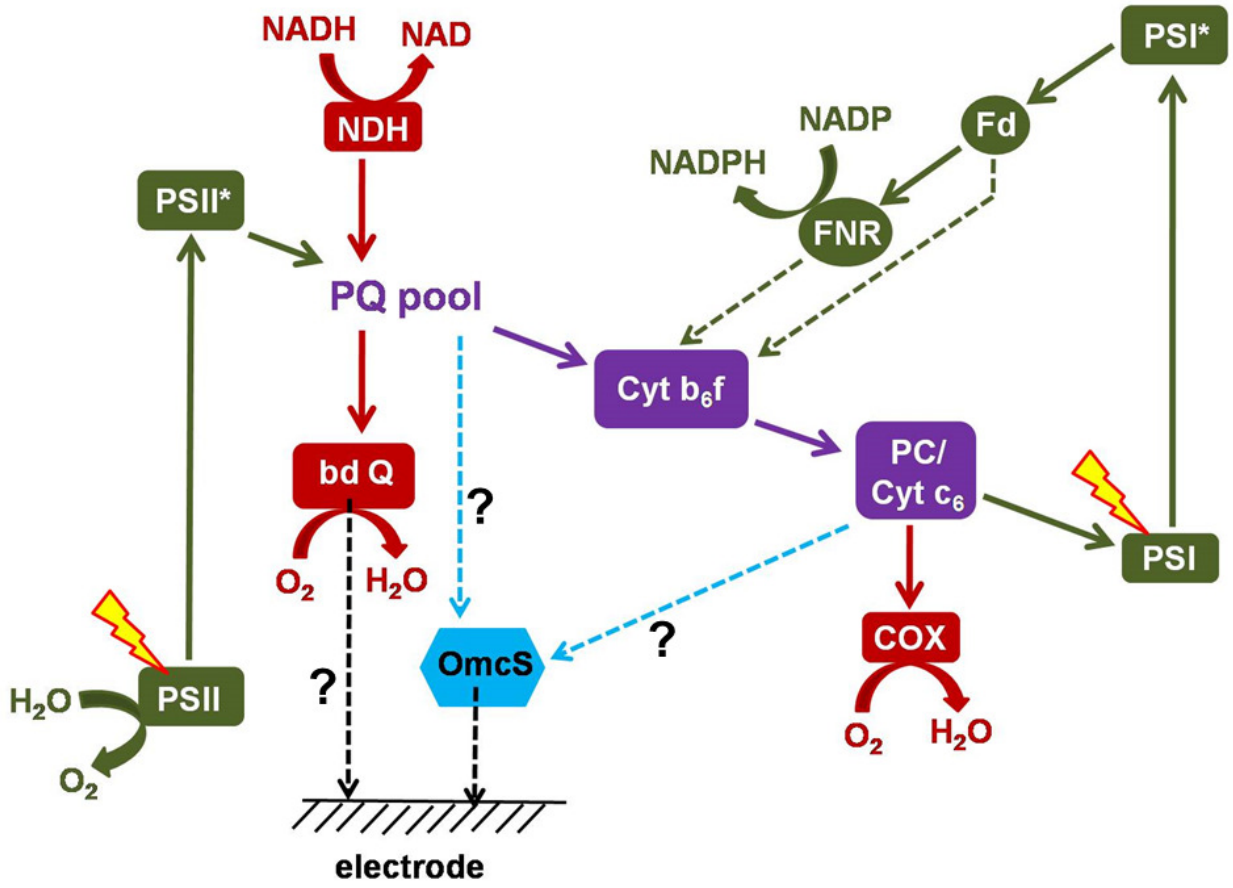

Figure 3.10: Schematic showing the proposed electron transfer pathways from photosynthetic (P-ETC) and respiratory electron transport chain (R-ETC) to OmcS. Green solid arrows: P-ETC; green broken arrows: cyclic P-ETC; red solid arrows: R-ETC; purple solid arrows: pathway shared by both P-ETC and R-ETC; blue broken arrows: hypothesized electron transfer pathways from P-ETC and R-ETC to OmcS; black broken arrows: extracellular electron transfer to the electrode; (Abbreviations: PSII: photosystem II; PSII*: excited photosystem II; PQ pool: plastoquinone pool; Cyt b_6f: cytochrome b_6f complex; PC: plastocyanin; Cyt C_6: cytochrome c_6; PSI: photosystem I; PSI*: excited photosystem I; Fd: ferredoxin; FNR: ferredoxin NADP reductase; NDH: NADH dehydrogenase; bd Q: bd type quinol oxidase; COX: cytochrome c oxidase)

by plastoquinones might have extended to the OmcS leading to more EET (Figure 3.10) in Eng-CB, but the specific interaction of OmcS with the components of ETC could not be ascertained.

1.12 Conclusions

S. elongatus was genetically engineered to express heterologous *omcS* gene and expression of the active OmcS was confirmed through heme staining. Eng-CB was found to exhibit enhanced extracellular electron transfer as evident from both the higher rate of ferricyanide reduction (~2 fold) and higher photocurrent generation (~ 9 fold) compared to the wild-type cyanobacterium. The higher rate of ferricyanide reduction under both light and dark conditions by Eng-CB underlines the fact that the OmcS interacted with both photosynthetic and respiratory electron transport chain of cyanobacteria. In a rudimentary photo-bioelectrochemical full cell, the Eng-CB was observed to generate ~ 5-fold higher power density than that generated by the wild-type. Further, exploring the electron transfer pathways with the help of site specific inhibitors and other knock-out mutants would reveal the key players involved in the pathway leading to enhanced EET, which is our goal for future work. No actual electrochemical optimizations/engineering aspects (such as better reactor design) have been done to maximize the photocurrent density. Doing so (in our future work) could result in remarkable improvement in power generation ability. This work underlines the novel concept that interdisciplinary approaches such as genetic engineering can be employed to enhance the exoelectrogenicity of the microorganisms used in the photosynthetic microbial fuel cells.

CHAPTER 4

ROLE OF RESPIRATORY TERMINAL OXIDASES IN CYANOBACTERIA TOWARDS EXTRACELLULAR ELECTRON TRANSFER

To be submitted to Biotechnology and Bioengineering.

1.13 Introduction

Cyanobacteria (CB) are well known for their evolutionary significance as the most primitive microorganisms to perform oxygenic photosynthesis. The electrogenic characteristics of cyanobacteria have been exploited in the photo-bioelectrochemical cells (PBEC) to generate electricity in a sustainable, economic and environmental friendly manner (Pisciotta et al. 2010; Zou et al. 2009). Although, the concept of electricity generation using CB had been reported as early as 1980s (Tanaka et al. 1985), the mechanistic understanding of electron transfer pathways that transport electrons from photosynthetic electron transport chain to the electrode present outside the CB is still lacking. While, a few research attempts have been made to elucidate the extracellular electron transfer pathways in CB using site-specific photosynthesis inhibitors (Pisciotta et al. 2011; Sekar et al. 2014; Torimura et al. 2001; Yagishita et al. 1993), a clear interpretation at the molecular level is absent, warranting a need for further investigation on the basis of cellular physiology.

Unlike oxygenic photosynthesizers such as algae and plants, CB do not contain a well defined membrane-bound organelles such as chloroplasts. Therefore the light reactions along the photosynthetic electron transport chain (P-ETC) take place in an extended system of thylakoid membranes that are distributed in the cytoplasm inside the cell membrane. In the presence of light, cellular energy currencies in the form of ATP are generated by P-ETC in the thylakoid membrane. However in the absence of light, ATP are generated via respiratory electron transport chain (R-ETC) reactions that occur in both thylakoid and cytoplasmic membranes. In CB, the reactions of P-ETC and R-ETC are not spatially separated between distinct organelles (such as chloroplast and mitochondria) but rather occur in thylakoid membranes distributed throughout

the cytoplasm. Some components of ETC such as plastoquinone, cytochrome b_6f and plastocyanin are shared between P-ETC and R-ETC pathways in the thylakoid membranes, which are the only site of both photosynthesis (during light) and respiration (dark). Therefore it can be expected of CB to generate current on the anode of a bio-electrochemical cell under both light and dark conditions during photosynthesis and respiration respectively.

Light dependent electrogenic activity of CB has been reported to be responsible for photocurrent generation under light conditions (Pisciotta et al. 2010; Zou et al. 2009) in photo-bioelectrochemical cells. Nevertheless, current generation was also observed under dark conditions in our earlier work (Sekar et al. 2014) on CB, which further corroborates that the R-ETC of CB contributes to the current generation as anode catalyst in electrochemical cells. In either case, the current generated by CB (normalized per unit electrode area) is less than that generated by dissimilatory metal reducing bacteria (DMRB) as anode catalyst in microbial fuel cells. The major reason for this difference is that unlike DMRBs, CB do not possess any terminal reductases on their outer membrane which could assist in the transfer of electrons from inside the cell to an external electron acceptor, through a process commonly known as extracellular electron transfer (EET). We have demonstrated that expressing the non-native outer membrane c-type cytochrome S (OmcS) obtained from *Geobacter sulfurreducens* in *Synechococcus elongatus* PCC7924 significantly improved its EET (Sekar et al. 2016). The genetically engineered *S. elongatus* generated nearly five times higher power density than the corresponding wild type *S. elongatus*.

From an evolutionary perspective, a cellular assembly consisting of intersecting P-ETC and R-ETC is greatly beneficial for CB, because, at high light intensities, the over-reduced P-ETC could be re-oxidized by R-ETC, so as to continually operate the light reactions without causing photo damage. However, from engineering perspective, the overflow of electron from the P-ETC to R-ETC is considered as a loss of useful electrons, which could otherwise be used to generate electricity if carefully channeled outside the membrane to an electrode. Accordingly the R-ETC could be considered as a competing pathway for photo-electrochemical energy conversion. Eliminating this competing R-ETC pathway by knocking-out the respiratory terminal oxidases (RTO) present in the pathway could potentially increase the electron flow in P-ETC. Even though this strategy might seem detrimental to the cell survival at high light intensities, we hypothesize that combining this knock-out strategy with our earlier strategy (Sekar et al. 2016) of expressing outer membrane cytochrome could increase the electron flux from the over-reduced P-ETC towards the electrode via extra cellular electron transport (EET), thereby generating high photocurrent as well as increasing the fitness of the cell.

Three different types of RTOs have been reported to be present in *S. elongatus* PCC7942 namely bd-type quinol oxidase encoded by *cydBA*, aa_3-type cytochrome oxidase encoded by *coxBAC* and cbb_3-type cytochrome oxidase encoded by *ccoNQ* (Burgstaller 2012). In this work, the above-mentioned respiratory terminal oxidases in *S. elongatus* PCC7942 were knocked-out, one at a time, in both wild type-CB and omcs-CB (work from (Sekar et al. 2016), chapter 3 in this dissertation) in order to understand the contribution of these RTOs towards extracellular electron transfer of cyanobacteria.

1.14 Materials and Methods

4.2.1. Materials

All the chemicals and reagents used in the study were of analytical grade with maximum purity as claimed by the manufacturer. Standard molecular biology and cloning protocols were used for the construction of knock-out mutants as explained in detail in Appendices B and D.

4.2.2. Bacterial Strains and Culture

The cyanobacterium *Synechococcus elongatus* PCC7942 (*S. elongatus*) was used in all genetic manipulations. The wild type *S. elongatus* (*wt*), and the *S. elongatus* that were genetically engineered to express outer membrane cytochrome S (*omcs*) (Sekar et al. 2016) as well as all the knock-out mutants (*cyd*$^-$, *cox*$^-$ and *cco*$^-$) were grown in modified BG-11 medium, the composition of which is as given in Sekar et al 2014. Appropriate antibiotics were added to the growth medium at a final working concentration as given in Table 4.1 and Table 4.2. The strains were inoculated into sterile BG11 medium and incubated at 32 °C, 100 rpm (thermos scientific) with continuous illumination conditions (80 µmol m^{-2} s^{-1}) using white fluorescent lamps (6400 K, T5 fluorescent tubes).

Table 4.1: Antibiotics and its working concentration used to grow *E. coli* containing different knock-out plasmids

Plasmid present in the Strain	Antibiotic	Working Concentration (µg/mL)
pHBUV10 (cyd)	Kanamycin	50
pHBUV9 (cox)	Streptomycin	50
UGS3- F2 P11 (ccoN)	Ampicillin	50
pNR2 (cox)	Erythromycin	300

Table 4.2: Antibiotics and its working concentration used to grow *S. elongatus* containing different knock-out plasmids

Plasmid present in the Strain	Antibiotic	Working Concentration (µg/mL)
pHBUV10 (cyd)	Kanamycin	40
UGS3- F2 P11 (ccoN)	chloramphenicol	7.5
pNR2 (cox)	Erythromycin	10

4.2.3. Construction of Knock-out Mutants

Three *E. coli* cultures, each containing the knock-out plasmid specific to one of the three different respiratory terminal oxidases were received from Dr. Susan Golden at the University of California, San Diego. The plasmid pHBUV10 contained kanamycin resistance gene cassette with flanking *cydB* and *cydA* sequences, which are the genes encoding the bd-quinol oxidase in *S. elongatus*. The plasmid pHBUV9 contained spectinomycin resistance gene cassette with flanking *coxB* and *coxC* sequences, thereby the *coxBAC*, the genes encoding aa3-type cytochrome oxidase would be knocked-out. The plasmid UGS3- F2-P11 contained chloramphenicol resistance gene cassette with flanking *ccoN* sequences, which is the gene encoding the cbb3-type oxidase cytochrome oxidase in *S. elongatus*. Since *omcs* (Sekar et al. 2016) was already equipped with the spectinomycin resistance gene, plasmid pNR2 was constructed from the plasmid pHBUV9, in which the spectinomycin resistance gene was replaced with erythromycin resistance gene. The erythromycin resistance gene was obtained from the plasmid pTRKH2 (Addgene) through PCR using erm_F and erm_R primers. All the three plasmids pHBUV10, pNR2 and UGS3-F2-P11 were transformed into *wt* and *omcs* to get

six combinations of knock-out mutants: three with *wt* background and three with *omcs* background using standardized transformation protocol given by Golden's lab (Burgstaller 2012). The genes in cyanobacterial genomic DNA would be replaced with the corresponding antibiotic resistance gene cassette by double homologous recombination as shown in Figure 4.1. Transformed colonies were picked from corresponding antibiotic selective BG11-agar plates and grown into shake flask cultures. The genomic DNA was isolated from the mutants using protocols given in the literature (Burgstaller 2012) and the gene knock-out was verified with PCR using gene-specific primers as shown in Table. 4.3.

Table 4.3: List of primers used in this study

S. No.	Primers name	Sequence	Reference
1	erm_F	5' GGGAAAGGATCCTGCTGACTTGCACCATATC ATAAAAAT 3'	this study
2	erm_R	5' GGGAAAGGATCCACCTCTTTAGCTCCTTGG AAGCTG 3'	this study
3	cyd_F	5' AATGGTGGCGAGTTTAGCGGT 3'	this study
4	cyd_R	5' GACGGGCATTTTCAGGTACTGGAC 3'	this study
5	cox_F	5' GTAAACCCAACGATGTCACTGACG 3'	this study
6	cox_R	5' AGTAGTCCTACGAGGACGTGTAG 3'	this study
7	cco_F	5' CCAATCACAAACATCCACC 3'	this study
8	cco_R	5' CTACCCGTTCTCTCAACT 3'	this study
9	omcs_F	5' GGGAAAGAATTCGAAGGAGTATACCTATA CATGAAGAAAGGCATGAAAGTTAGTCTGA 3'	Sekar et al 2016
10	omcs_R	5' GGGAAAGGATCCTTAATCTTTGGCGTGGC ATTTGTTAC 3'	Sekar et al 2016

Table 4.4: List of plasmids used in this study

S. No.	Plasmid name	Characteristics	Reference
1	pHBUV10	kanamycin resistance gene replaces part of *cydB* and *cydB*	Golden Lab
2	pHBUV9	spectinomycin resistance gene replaces part of *coxB*, *coxC* and whole of *coxA*	Golden Lab
3	UGS3- F2-P11	chloramphenicol resistance gene replaces part of *ccoN*	Golden Lab
4	pTRKH2	source for erythromycin resistance gene	Addgene
5	pNR2	erythromycin resistance gene replaces part of *coxB*, *coxC* and whole of *coxA*	this study

Table 4.5: List of cyanobacterial strains used in this study

S. No.	Name	Parent	Transformed with plasmid	Relevant genotype	Reference
1	*wt*	*S. elongatus* PCC7942	none	wild-type	Golden Lab
2	*omcs*	*wt*	pNR1	OmcS	Sekar et al 2016
3	*cyd*$^-$	*wt*	pHBUV10	*cydBA*::*kan*^{r}	this study
4	*cox*$^-$	*wt*	pNR2	*coxBAC*::*erm*^{r}	this study
5	*cco*$^-$	*wt*	UGS3- F2-P11	*ccoN*::*cam*^{r}	this study
6	*cyd*$^-$*omcs*	*omcs*	pHBUV10	OmcS + *cydBA*::*kan*^{r}	this study
7	*cox*$^-$*omcs*	*omcs*	pNR2	OmcS + *coxBAC*::*erm*^{r}	this study
8	*cco*$^-$*omcs*	*omcs*	UGS3- F2-P11	OmcS + *ccoN*::*cam*^{r}	this study

4.2.4. Ferricyanide Reduction Experiment

Cyanobacterial strains grown in BG11 medium (100 ml) with appropriate antibiotics were harvested at an OD_{750} of 0.6, washed with fresh BG11 medium and re-suspended in the same medium. IPTG (1 mM) was used to induce the expression of OmcS. After 24 h, potassium ferricyanide (1 mM) was added to the cultures, and the samples were collected every 12 h to monitor the reduction of potassium ferricyanide. Each time, absorbance of 1 ml of the sample was measured at 750 nm and 665 nm to estimate the growth and chlorophyll concentration respectively. Another 1 ml of the collected sample was centrifuged and the absorbance of

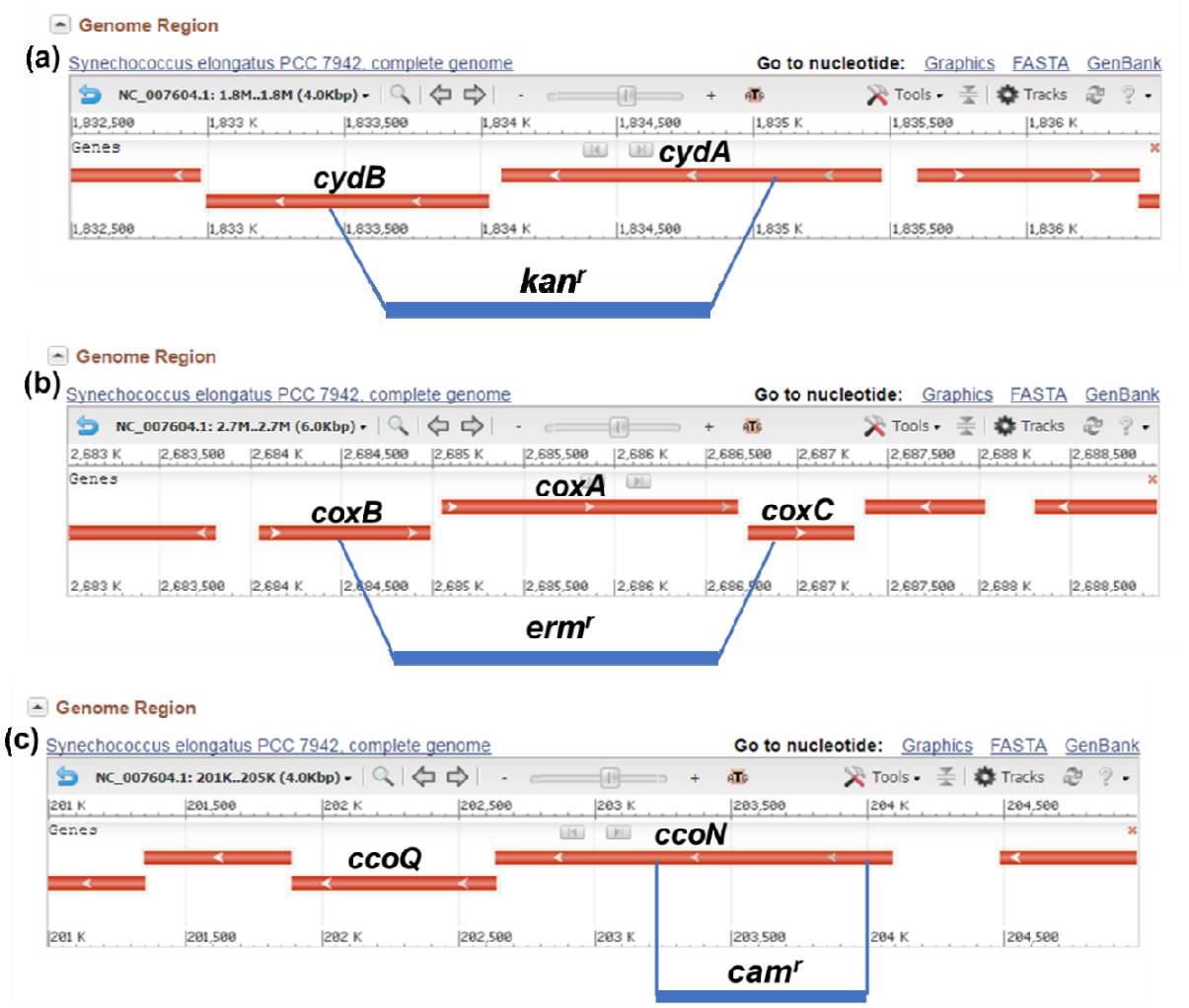

Figure 4.1: Schematic showing integration of the antibiotic resistance marker into genomic DNA of *S. elongatus* PCC7942 to replace the functional RTOs by double homologous recombination. The position of RTO genes are mined using NCBI genome website. Kanamycin resistance marker (kan^r) replaces parts of *cydB* and *cydA*; erythromycin resistance marker (erm^r) replaces parts of *coxB*, *coxA* and *coxC* and chloramphenicol resistance marker (cam^r) replaces *ccoN*

supernatant was measured at 420 nm to calculate the concentration of potassium ferricyanide. The experiments were conducted in triplicates under both light (80 µmol m^{-2} s^{-1}) and dark (incubator covered with black cloth) conditions and the rate of ferricyanide reduction for 24 h, normalized with the chlorophyll content, was calculated as explained Appendix F.

4.2.5. Electrochemical Experiments

The photocurrent generating ability of the knock-out mutants was evaluated by chrono-amperometry in a three-electrode electrochemical cell setup. The cyanobacteria on the multi-walled carbon nanotubes modified electrodes was used as working electrode, with a platinum wire counter electrode and Ag/AgCl (Sat. KCl) reference electrode. The CNT modified working electrode was prepared as mentioned in Sekar et al (2014), and the current was measured by applying a constant voltage (over-potential of 100 mV vs. Ag/AgCl) with respect to the corresponding open circuit potential.

1.15 Results and Discussion

4.3.1. PCR Verification of Single Knock-out Mutants

The single knock-out mutants were constructed and verified by PCR using gene specific primer sets as mentioned in Table 4.3. In the PCR verification (Figure 4.2), specific band corresponding to the respective gene (*cyd*, *cox* or *cco*) was observed only in *wt* and *omcs*. However, in all three cases (Figure 4.2a, b, c), band corresponding to the truncated gene portion was observed for all the single knockout mutants such as *cyd*$^-$, *cyd*$^-$*omcs* (Figure 4.2a) and *cox*$^-$, *cox*$^-$*omcs* (Figure 4.2b). For *cco*$^-$, *cco*$^-$*omcs* (Figure 4.2c), the size of chloramphenicol resistance marker gene was similar to that of the portion of *ccoN* replaced and did not show any obvious change in the band in gel image. Further, the presence of *omcS* gene was confirmed in *omcs*, *cyd*$^-$*omcs*, *cox*$^-$*omcs* and *cco*$^-$*omcs* (Figure 4.2d). This gene specific PCR verification is an important step that

confirms the homozygosity of all the single knock-out mutants. Because, *S. elongatus* is known to contain multiple copies of genomic DNA and it is critical to make sure that the gene was knocked out in all copies of the genomic DNA present inside the cell.

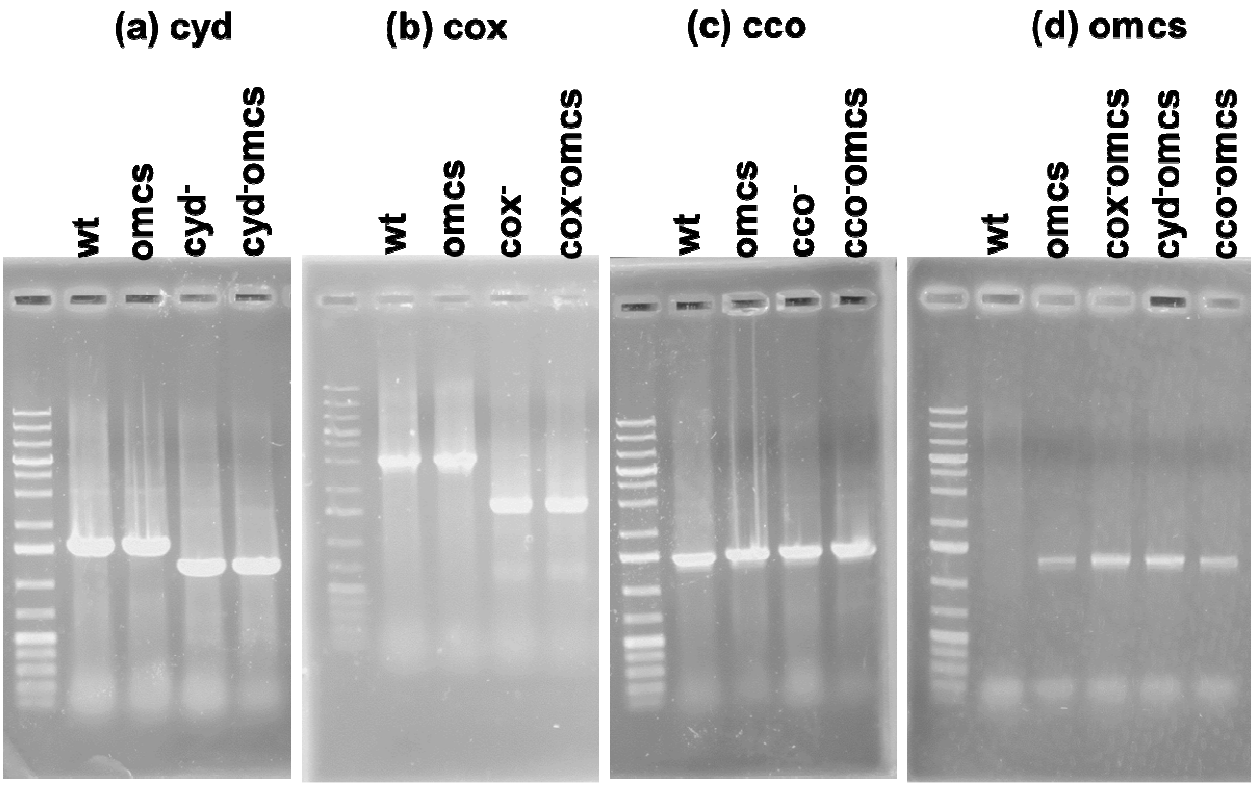

Figure 4.2: Verification of single knockout mutants by PCR using (a) cyd_F and cyd_R primers; (b) cox_F and cox_R primers; (c) cco_F and cco_R primers; (d) omcs_F and omcs_R primers; the lanes are labeled with the corresponding strain name. lane 1 in all the four panel contains 1 kb DNA ladder

4.3.2. Ferricyanide Reduction Assay

Extracellular electron transfer happening at the cellular outer envelope can be precisely studied using ferricyanide reduction assay. Potassium ferricyanide, being completely soluble, could not cross the cell membrane and was used to probe the electron transfer reactions that happen at the cell membrane. CB can use potassium ferricyanide as an alternate electron acceptor while

growing as a shake flask culture. Ferricyanide reduction rate of growing cultures of all the mutants was measured in the presence of light as shown in Figure 4.3. It is to be noted that the ferricyanide reduction rate (normalized with the respective chlorophyll content) of the mutants was compared with that of the wild-type (Figure 4.3), and the following interpretations were found:

1. *omcs* reduced more ferricyanide than that by *wt* (~twice), confirming our earlier data (Sekar et al. 2016) reported in chapter 3.
2. Among the single mutants without *omcs*, *cyd*$^-$ performed better followed by the *cco*$^-$, both of which reduced ferricyanide more than the *wt*. This observation could be attributed mainly to the presence of both cyd (bd-quinol oxidase) and cco (cbb_3 type cytochrome oxidase) in the thylakoid membrane (TM). While cco is present only in TM (Burgstaller 2012), cyd has been reported to be present in both TM and CM (Berry et al. 2002; Hart et al. 2005). So, knocking-out these two oxidases had increased the electron flux towards EET by decreasing the electron flux through R-ETC for oxygen reduction.
3. Following *cyd*$^-$ and *cco*$^-$, the *cox*$^-$ mutant reduced less ferricyanide, roughly similar to that of the *wt*. This observation might also be correlated to the presence of cox (aa_3 type cytochrome oxidase) only in the CM. Moreover, the ferricyanide reduction rate of *cox*$^-$ versus *cox*$^-$*omcs* was very similar to that of *wt* versus *omcs*.
4. It is surprising to note that the *cyd*$^-$*omcs* and *cco*$^-$*omcs* performed less EET than that of the corresponding single mutants: *cyd*$^-$ and *cco*$^-$.
5. Further, the same set of experiments under dark (Figure 4.4) did not provide any addition evidence to resolve the discrepancy mentioned above (in 4). In Figure 4.4, the trend was found to be almost similar to that under light condition, if not same at the magnitude.

6. Together, it can be concluded that the effect of knock-out mutations and the effect of cloning OmcS might not be cumulative, especially for the RTOs present in the TM.

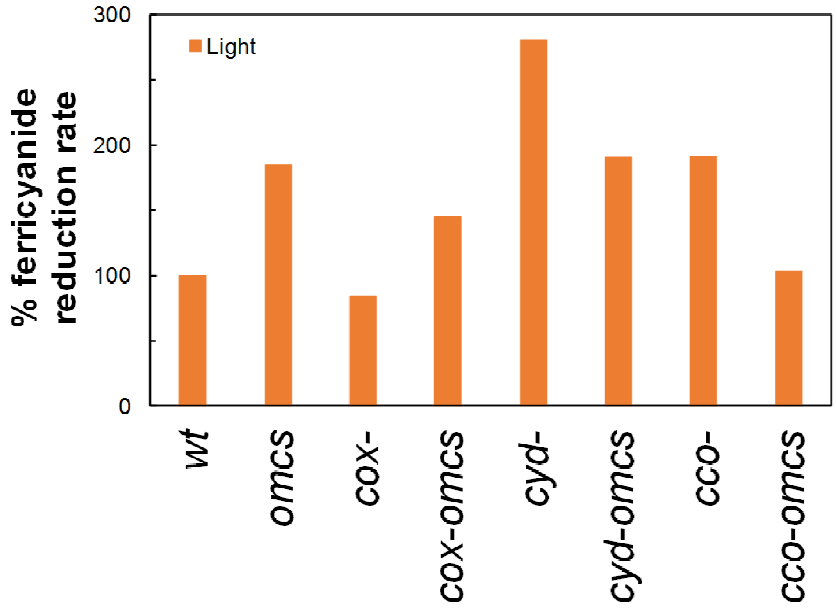

Figure 4.3: Ferricyanide reduction rate of single knock-out mutants under illumination. All the reduction rates, calculated as given in Appendix F, are normalized with that of the wild-type (wt) for ease of comparison (shown here is the representative data of the duplicate experiments)

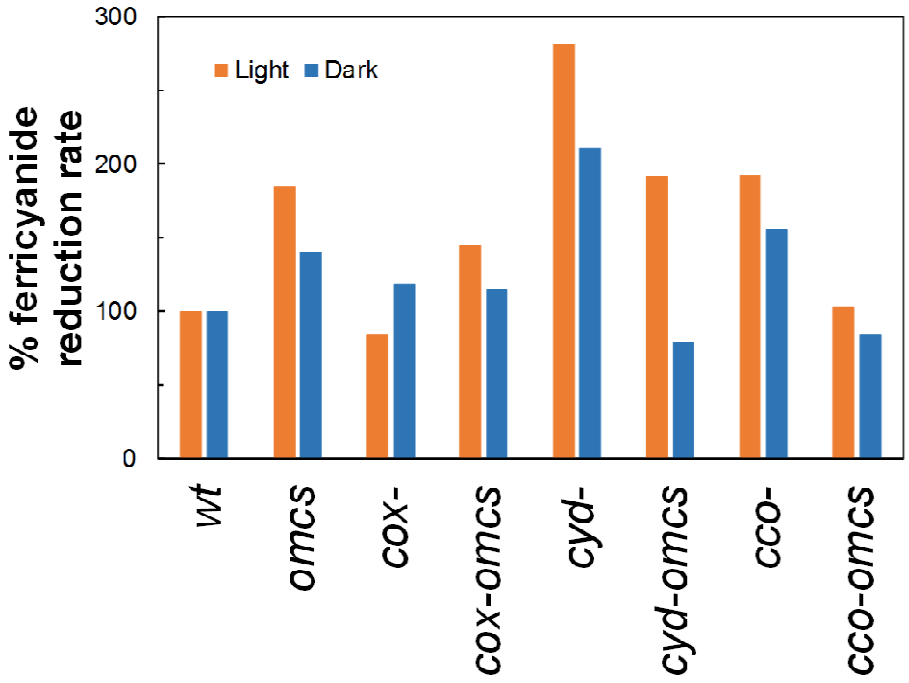

Figure 4.4: Comparison of ferricyanide reduction rate of single knock-out mutants under light and dark conditions. All the reduction rates, calculated as given in Appendix F, are normalized with that of the corresponding wild-type (wt) for ease of comparison (shown here is the representative data of the duplicate experiments)

4.3.3. Photocurrent Measurement

The light dependent electrochemical behavior of all the single mutants, *wt* and *omcs* was evaluated by measuring the photocurrent generation in the presence of light in electrochemical half-cell set up using chrono-amperometry. Initially the open circuit potential (OCP) was measured over time in alternate light and dark cycles and the average OCP of the all the strains is given in Table 4.6. Chrono-amperometry was performed using the I-time function in the potentiostat, which measured the current generated by the strains as shown in Figure 4.5 under alternate light-dark cycles by applying over-potential of 0.1 V with respect to the corresponding OCP (Table 4.6).

Table 4.6: Measurement of open circuit potential (OCP) in the electrochemical half-cell that contained CB (*wt*/*omcs*/different mutants)

Strain	Open Circuit Potential V *vs* Ag/AgCl	Applied Potential V *vs* Ag/AgCl
wt	0.07	0.17
cox$^-$	0.18	0.28
cyd$^-$	0	0.10
cco$^-$	0.23	0.33
omcs	0.03	0.13
cox$^-$*omcs*	0.02	0.12
cyd$^-$*omcs*	0.24-0.12	0.28
cco$^-$*omcs*	0.24	0.34

(Note that the OCP mentioned in the table were the stabilized OCP values over 1500 s; for the case (cyd$^-$omcs), in which the OCP changed from 0.24 to 0.12, the average value of 0.18 was used to calculate the over-potential i.e., 0.28).

Figure 4.5 shows the photocurrent measured over time under alternate light and dark cycles (300 s each, starting with dark). A clear light dependent electrogenic activity was observed for all the strains. The magnitude of current increased in the presence of light as shown in Figure 4.5 could not be correlated for a comparative analysis among the eight strains, since the OCP and the applied potential were diverse for all the strains.

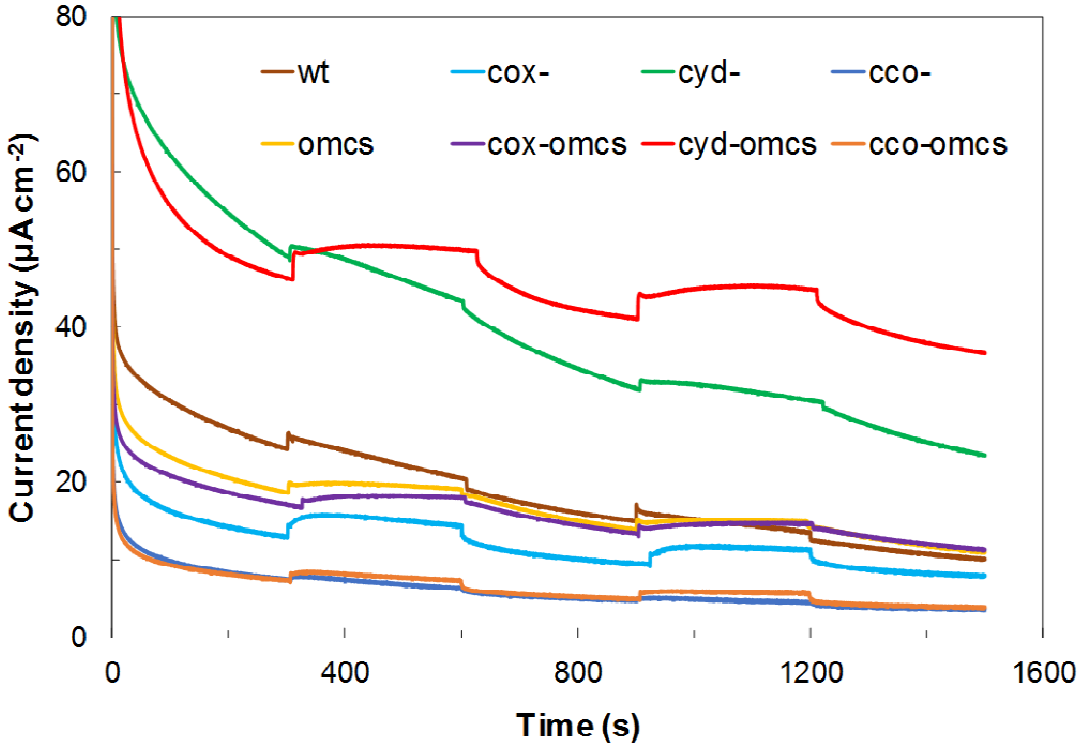

Figure 4.5: Photocurrent generation by single knock-out mutants by applying over-potential of 0.1 V with respect to the corresponding OCP (mentioned in Table 4.6). The experiment was started in dark and proceeded with alternate light/dark cycle of 300 s. Triplicate experiments were conducted and the representative data is shown here.

In summary, the following interpretations can be made:

1. The *cyd*$^-$*omcs* generated more photocurrent among all the eight strains, followed by the *cox*$^-$, particularly considering the fact that the applied potential was same for both the cases.
2. Both the *cco*$^-$ and *cco*$^-$*omcs* did not generate significant photocurrents compared to all the remaining six strains.
3. Comparison among *wt*, *omcs*, *cyd*$^-$, *cox*$^-$*omcs* is inconclusive from the conducted experiments.

4.3.4. bd-quinol oxidase diverts more electrons from P-ETC

Ferricyanide reduction experiment was conducted by adding potassium ferricyanide to the growing culture of CB in shake flasks. CB reduced the potassium ferricyanide through EET by using it as an alternate electron acceptor in shake flask cultures. On the other hand, photocurrent was measured, using a three-electrode electrochemical system, by applying a constant potential, in which CB would be forced to use EET. Amidst varying discrepancy, Figure 4.3 shows that *cyd*$^-$ exhibited higher EET biochemically (ferricyanide reduction), and Figure 4.5 shows that *cyd*$^-$ *omcs* generated higher photocurrent. It is also noteworthy that, followed by *cyd*$^-$, *cyd*$^-$*omcs* exhibited next higher EET (similar to the *omcs* control) as shown in Figure 4.3.

In CB, the bd-quinol oxidase couples the oxidation of plastoquinone and the reduction of O_2. Plastoquinone (PQ) was found to be major electron carrier in both the P-ETC and R-ETC. Moreover, PQ pool plays multiple roles in the ETC: (1) PQ are the electron acceptors immediately downstream of PSII in P-ETC; (2) PQ and ferredoxin are the electrons carriers in cyclic P-ETC that occur around PSI, and (3) PQ are known to present in both thylakoid and cytoplasmic membranes. The flux of electrons from PQ pool towards photocurrent generation is the maximum among all the pathways deciphered so far, as evident from its effect in decreasing the photocurrents (upto ~80 %) (Sekar et al. 2014), when the PSII was blocked by DCMU (DCMU binds to the Q_B site of PSII, similar to PQ). Among the three RTOs, bd-quinol oxidase diverts the electrons from the PQ pool to the R-ETC. Thus, knocking-out the bd-quinol oxidase increased the EET (biochemically through reducing more ferricyanide) and photocurrent generation (Figure 4.6). This also confirms the fact that bd-quinol oxidase was not involved in

transferring electrons from PQ pool to the cellular exterior, as previously hypothesized in Chapter 2 and Chapter 3 and the same has been updated in the schematic in Figure 4.6. Research work reported in (Berry et al. 2002; Hart et al. 2005; Howitt and Vermaas 1998; Lea-Smith et al. 2016; McCormick et al. 2015; Pils et al. 1997; Pils and Schmetterer 2001) and our research work (Sekar et al. 2016; Sekar et al. 2014) were collectively reviewed to draw the schematic shown in Figure 4.6. It is interesting to note that augmenting *cyd*$^-$ with OmcS resulted in generating more photocurrents than the corresponding controls such as *wt*, *cyd*$^-$ and *omcs*. Furthermore, it is to be noted that the interaction of OmcS with the P-ETC and/or R-ETC in CB is unknown, warranting further investigations. The role of other two RTOs towards EET could not be ascertained from the experimental evidences reported in this work. Further, the double knock-out and triple knock-out mutants and their combinations in *omcs* background would provide much more evidences to clearly understand the role of RTOs in CB for EET, which should be the goal of any future work in this area.

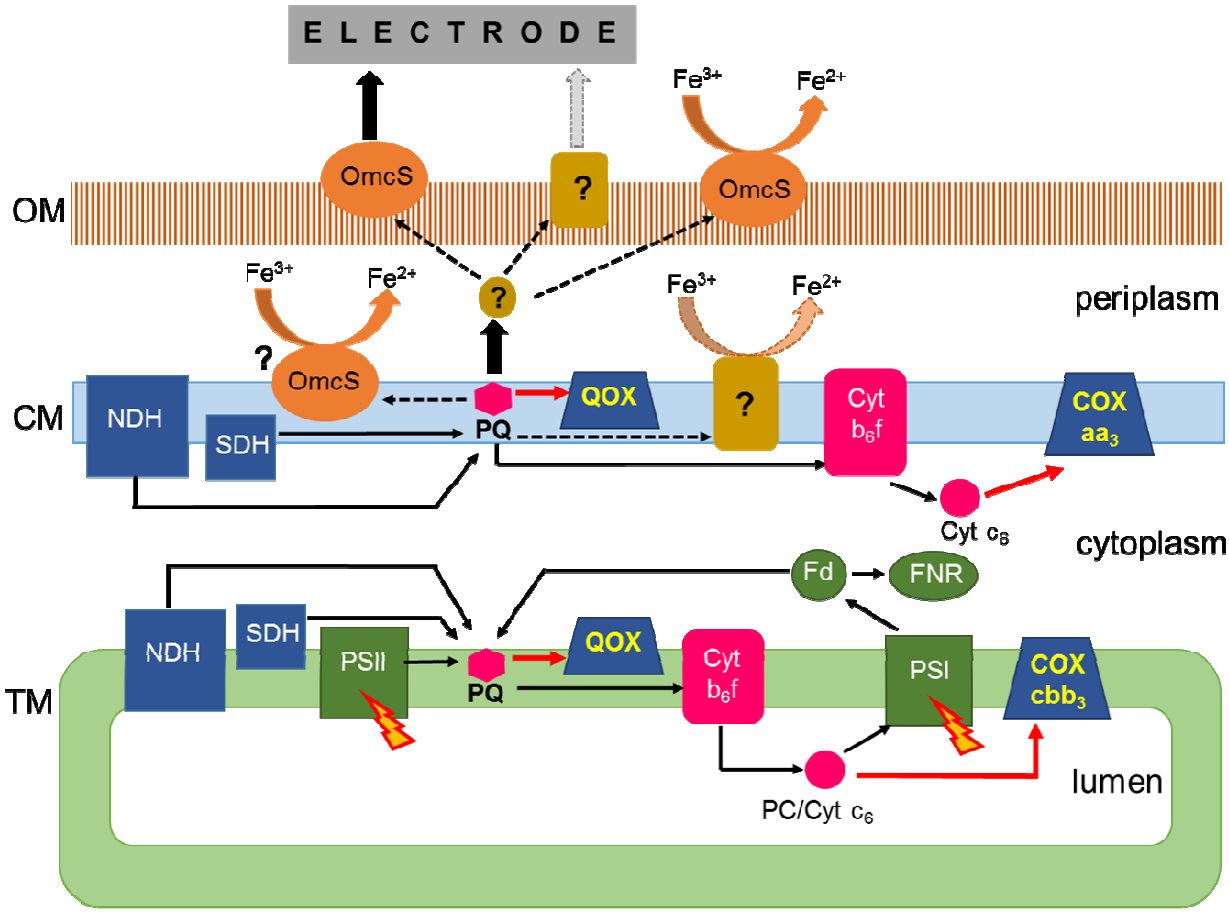

Figure 4.6: Schematic showing the exoelectrogenicity of *S. elongatus*: green shapes (PSII, PSI, Fd, FNR) take part in photosynthetic electron transport chain in TM; blue shapes (NDH, SDH, QOX, $COXcbb_3$, $COXaa_3$) take part in respiratory electron transport chain in CM and TM; pink shapes (PQ, Cyt b_6f, PC, Cyt c_6) take part in both photosynthetic and respiratory electron transport chains; black solid lines represent pathways happening in the wild-type *S. elongatus*; black broken lines and question marks were predicted to occur, but no experimental evidence is yet available; red solid lines are the pathways disrupted in knock-out mutants (*cyd*$^-$:QOX; *cox*$^-$: $COXaa_3$; *cco*$^-$: $COXcbb_3$); the three respiratory terminal oxidases are represented in yellow text inside the blue trapezoid; (Abbreviations: OM: outer membrane; CM: cytoplasmic membrane; TM: thylakoid membrane; NDH: NADH dehydrogenase; SDH: succinate dehydrogenase; QOX: quinol oxidase; $COXcbb_3$: cbb_3 type cytochrome oxidase; $COXaa_3$: aa_3 type cytochrome oxidase; PSII: photosystem I; PSI: photosystem II; Fd: ferredoxin; FNR: ferredoxin NADP reductase; PQ: plastoquinone; Cyt b_6f: cytochrome b_6f complex; PC: plastocyanin; Cyt c_6: cytochrome c_6; OmcS: outer membrane cytochrome c-type cytochrome S)

1.16 Conclusions

In this work, single knock-out mutants were constructed by knocking-out the three terminal respiratory oxidases (bd-quinol oxidase, aa_3-cytochrome oxidase and cbb_3-cytochrome oxidase), one at a time, in two different backgrounds such as wild type *S. elongatus* and the *S. elongatus* genetically engineering to express the heterologous outer membrane cytochrome called OmcS. Totally, eight different strains (*wt*, *cox*$^-$, *cyd*$^-$, *cco*$^-$, *omcs*, *cox*$^-$*omcs*, *cyd*$^-$*omcs*, *cco*$^-$*omcs*) were evaluated for their ability to do exoelectrogenicity by studying their ferricyanide reduction in growing culture and photocurrent generation in electrochemical cell. It was observed that *cyd*$^-$ (the mutant lacking bd-quinol oxidase) exhibited the best EET by reducing more ferricyanide and *cyd*$^-$*omcs* (the *cyd*$^-$ mutant containing OmcS) generated the most photocurrents. These two experiments clearly confirmed that the bd-quinol oxidase diverts more electrons from the photosynthetic electron transport chain to oxygen reduction and knocking it out would certainly enhance the exoelectrogenicity in cyanobacteria.

CHAPTER 5

ELECTRICITY GENERATION BY *PYROCOCCUS FURIOSUS* IN MICROBIAL FUEL CELL OPERATED AT 90 °C

This chapter contains text modified from the following two publications:

Narendran Sekar, Chang-Hao Wu, Michael W. W. Adams and Ramaraja P. Ramasamy. Submitted to *Biotechnology and Bioengineering*, 09/14/2016.

Narendran Sekar, Chang-Hao Wu, Michael W. W. Adams and Ramaraja P. Ramasamy. 2016. *ElectroChemical Society Transactions*. 72 (30):1-7.

Reprinted here with permission of the publisher.

Abstract

Hyperthermophiles are microorganisms that thrive in extremely hot environments with temperatures near and even above 100 ^{o}C. They are the most deeply rooted microorganisms on phylogenetic trees suggesting they may have evolved to survive in the early hostile earth. The simple respiratory systems of some of these hyperthermophiles made them potential candidates to develop microbial fuel cells (MFC) that can generate power at temperatures approaching the boiling point. We explored extracellular electron transfer ability of the hyperthermophilic archaeon *Pyrococcus furiosus* (*Pf*) by studying its ability to reduce alternate electron acceptors such as Fe(III) oxide and Fe(III) citrate as well as to generate electricity in a two-chamber MFC. *Pf* reduced Fe(III) oxide during its growth at 90 °C, and the *Pf* culture re-suspended in MOPS buffer (pH 7.5) was found to reduce Fe(III) citrate significantly using H_2 as an electron donor. *Pf* growing in defined medium functioned as an anolyte in a MFC operated at 90 ^{o}C, generating a maximum current density of 2 A m^{-2} and a peak power density of 225 mW m^{-2} without the addition of any external redox mediator. Electron microscopy and electrochemical impedance spectroscopy of the anode with the attached *Pf* biofilm demonstrated bio-electrochemical behavior that led to electricity generation in MFC via direct electron transfer. This proof of concept study reveals for the first time that a hyperthermophile such as *Pf* can generate electricity in an MFC at extreme temperatures. This may have relevance to its survival in high-temperature niches and advance our understanding of the biogeochemistry of the early hot environment and potentially of exobiology.

Keywords: Hyperthermophile, *Pyrococcus furiosus*, microbial fuel cell, electricity, exoelectrogenicity, iron reduction.

1.17 Introduction

Exoelectrogenicity is the ability of microorganisms to transfer electron extracellularly to insoluble electron acceptors. It has been suggested to be the earliest known mode of energy conservation exhibited by the primordial living forms that evolved in hot, volcanic environment of the early earth (Vargas et al. 1998). For example, many hyperthermophilic microorganisms that grow optimally at 80°C and above, such as *Pyrobaculum islandicum* and *Thermotoga maritima,* are known to conserve energy by coupling the oxidation of hydrogen gas with concomitant reduction of insoluble iron oxide (Fe_2O_3) in hot environments that lack soluble electron acceptors, such as oxygen or nitrate (Vargas et al. 1998). In fact magnetite (Fe_3O_4) formation in the ancient rock can be correlated to the signature of exoelectrogenic activity of hyperthermophiles (Lovley 2004; Weber et al. 2006). Exploring the interaction of such microorganisms with their abiotic environment not only helps us to understand the biogeochemistry and evolution of microbes in various extreme environments, but it could also play an important role in biotechnological applications, such as the design of microbial fuel cells and microbial biosensors, bioremediation and production of high value chemicals.

A microbial fuel cell (MFC) is an electrochemical device containing microorganisms in the anode chamber. They oxidize organic substrates and transfer the electrons to the anode, which generates electricity when connected through an external load to a cathode where a suitable terminal electron acceptor is reduced. Although MFC has been known for over two decades, the low power densities achievable in MFC make them less viable for commercial power generation. The low power density can be attributed mainly to various energy losses that occur in an MFC (Clauwaert et al. 2008; Logan et al. 2006). Major effort has therefore been undertaken to

improve the performance of MFCs by reducing ohmic and mass transfer losses through optimization of their design, configuration and operation. However, a comprehensive knowledge of the electron transfer mechanism occurring at microbe-electrode interfaces that addresses the significant kinetic loss is still lacking. Studying microbial interactions with the electrode and their exoelectrogenicity could possibly help to optimize and enhance the extracellular electron transfer thereby pushing the boundaries of MFC power densities by several orders of magnitude.

In the past decade, many anaerobic microorganisms belonging to Gram negative Proteobacteria, including the extensively studied *Geobacter* sp. (Busalmen et al. 2008; Reguera et al. 2006) and *Shewanella* sp. (Gorby et al. 2006; Marsili et al. 2008), as well as cyanobacteria (McCormick et al. 2011; Sekar et al. 2014) have been explored for electricity generation in MFCs and their possible extracellular electron transfer pathways have been elucidated (Lovley 2008; Pisciotta et al. 2011). All these microorganisms are mesophilic and grow optimally at moderate temperatures, ranging from 20 ^{o}C to 45 ^{o}C. Recently, thermophilic microorganisms such as *Thermincola* sp. strain JR (Wrighton et al. 2008), *Thermincola ferriacetica* (Marshall and May 2009), and *Calditerrivibrio nitroreducens* (Fu et al. 2013) were shown to generate electricity in MFCs that are operated at a temperature greater than 50 ^{o}C. Operating an MFC at an elevated temperature has many advantages over ambient temperature systems, such as higher reaction rates (both chemical and electrochemical), minimal risk of contamination from ubiquitous mesophilic microorganisms and maintenance of reducing anaerobic conditions due to lower solubility of oxygen at higher temperatures (Mathis et al. 2008; Wrighton et al. 2008). Recently, a mixed microbial culture obtained from the sub-surface of a petroleum reservoir was used as biocatalyst to examine electricity generation in a MFC that was operated at temperatures above

80 ^{o}C (Fu et al. 2015). In addition, a MFC was installed at a hydrothermal vent field and continually operated for six months (Girguis and Holden 2012). However, no pure culture of an anaerobic microorganism has been reported so far to generate electricity in a MFC operated above 80 ^{o}C.

In this study, a hyperthermophilic archaeon named *Pyrococcus furiosus* (*Pf*), which grows optimally at 100 ^{o}C (Fiala and Stetter 1986), was examined for its ability to carry out exoelectrogenicity via its biochemical reduction of insoluble (Fe_2O_3) and soluble iron (ferric citrate), and electricity generation in an MFC at 90 °C. Besides the advantages offered by high temperature, *Pf* itself offers many advantages for MFC operation, such as its ability to metabolize a wide range of carbohydrates including maltose, cellobiose, laminarin and chitin, and peptides (Koning et al. 2001; Lee et al. 2006). In addition, it contains a simple respiratory electron transport chain that consists of a single enzyme complex in the form of a 14-subunit membrane bound hydrogenase (MBH) (Sapra et al. 2003). Morphologically, *Pf* cells appear irregular coccoid in shape, about 0.8-2 μm in size, with a tuft of flagella up to 50 in number (Wirth et al. 2011) attached to one end of the cell and have a proteinaceous S-layer as outer cellular envelope (Fiala and Stetter 1986). The S-layer consists of a monomolecular array of glycoproteins that are anchored to the cell membrane beneath (Sara and Sleytr 2000).

A schematic of the major biochemical pathways of *Pf* that utilizes the disaccharide maltose as the carbon source is shown in Figure 5.1. Maltose is transported into the cell via trehalose/maltose binding protein (TMBP) (Koning et al. 2001) and hydrolyzed to glucose, which enters the modified ADP-dependent glycolytic pathway (Kengen et al. 1996). The major

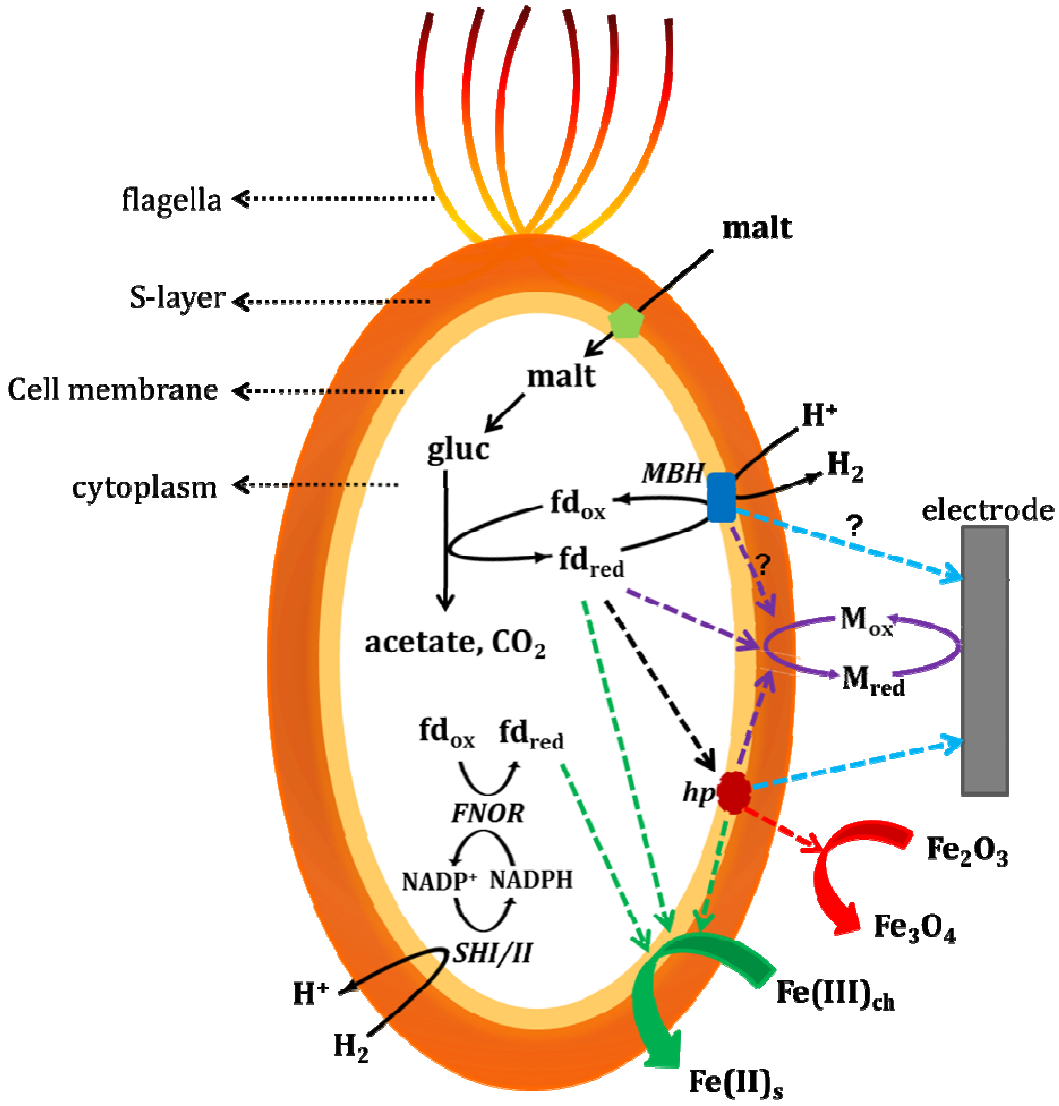

Figure 5.1: Schematic of various hypothesized electron transfer pathways showing exoelectrogenicity of *P. furiosus*: Black solid arrows represent the physiological biochemical pathways of the wild type *Pf* and broken arrows represent the possible extracellular electron transfer pathways leading to biochemical reduction of Fe_2O_3 (red) and $Fe(III)_{ch}$ (green) and the electron transfer routes to the electrode (blue). Purple arrows represent the electron transfer to exogenous redox mediators; (Abbreviations: malt-maltose; gluc-glucose; fd_{ox}-oxidized from of ferredoxin; fd_{red}-reduced form of ferredoxin; MBH-membrane bound hydrogenase; hp-hypothetical protein with ferric reductase activity; SHI/II-soluble hydrogenase I and II; FNOR-ferredoxin $NADP^+$ oxidoreductase; $Fe(III)_{ch}$-soluble chelated form of Fe(III) such as ferric citrate; $Fe(II)_s$-soluble form of Fe(II); M_{ox} and M_{red}-oxidised and reduced forms of mediators respectively

metabolic end-products are acetate, CO_2 and H_2 (Figure 5.1). The iron-sulfur containing redox proteins - ferredoxins, rather than NADH, are the reducing equivalents generated by *Pf* during sugar oxidation, and the ferredoxin connects central carbon metabolism and respiratory chain. Reduced ferredoxin directly transfers electrons to MBH, which both reduces protons to hydrogen gas and pumps H^+ and Na^+ ions to generate an ion gradient for ATP synthesis (Sapra et al. 2003). In addition to MBH, two cytoplasmic hydrogenases (SHI and SHII) are present in *Pf* and these are thought to consume H_2 to generate NADPH, which is required for anabolic pathways (van Haaster et al. 2008), and these enzymes thereby function as a safety value (Silva et al. 2000). Furthermore, as a model hyperthermophile, the complete genome of *Pf* was one of the first hyperthermophiles to be sequenced (Poole et al. 2005) and various genetic engineering tools have been recently developed for the metabolic engineering of *Pf* to produce high value industrial chemicals (Keller et al. 2013). Given the large amount of information available on this microorganism, it is the ideal hyperthermophile to explore exoelectrogenicity and the prospect of understanding and developing MFC operation at high temperature.

1.18 Materials and Methods

5.2.1. Materials

Iron (III) oxide, 3-(2-Pyridyl)-5,6-diphenyl-1,2,4-triazine-p, p′-disulfonic acid monosodium salt hydrate a.k.a. ferrozine and ferric citrate were purchased from Sigma Aldrich. AvCarb G200 battery felt and Nafion 115^{TM} were purchased from Fuel Cell Store. Titanium wire (0.25 mm diameter) and potassium ferricyanide were purchased from Alfa Aesar and Acros respectively.

5.2.2 Strain and Growth Conditions

The genetically tractable laboratory strain *Pyrococcus furiosus* COM1 (Lipscomb et al. 2011) was used for all the experiments. In addition, a double mutant ΔSHI/II strain (MW0015) that lacked two cytoplasmic soluble hydrogenases I and II was used for ferric citrate reduction experiment (Lipscomb et al. 2011). The composition of the rich medium was as follows: 1 × base salts, 1 × trace minerals, 0.255 μM sodium tungstate, 0.25 μg/mL resazurin, 0.5 % (w/v) yeast extract, 0.5 % (w/v) casein hydrolysate (enzymatic) and 0.5 % (w/v) maltose with added 0.5 g/L cysteine, 0.5 g/L sodium sulfide, 1 g/L sodium bicarbonate and 1 mM sodium phosphate buffer (pH 6.8). For the defined medium, yeast extract and casein hydrolysate were replaced with 2 × vitamin solution, 2 × 19-amino acid solution and 20 μM uracil. The chemical composition of the defined medium is therefore known whereas the rich medium contains undefined components such as yeast extract and casein hydrolysate. The stock solutions of base salt, trace minerals, vitamin solution and 19-amino acid stock solution were prepared as previously described (Adams et al. 2001; Lipscomb et al. 2011). The respective media were prepared and filter-sterilized using 0.22 μ filter. Liquid cultures were inoculated with a 1 to 2 % inoculum and then incubated at 90 ^{o}C in anaerobic culture bottles degassed with three cycles of vacuum and argon. For electrochemical experiments, resazurin, cysteine and sodium sulfide were omitted from the rich medium and resazurin and sodium sulfide were omitted in the defined medium. The suspension buffer contained 100 mM MOPS and 1 x base salt (pH 7.5).

5.2.3. Iron Oxide and Ferric Citrate Reduction

Iron reduction experiments were conducted in both rich medium and suspension buffer containing either 15 mM iron (III) oxide (Fe_2O_3) or 20 mM ferric citrate. All the experiments were performed in biological triplicates and incubated at 90 °C with shaking. The 0.5 mL overnight culture was inoculated into 50 mL rich medium and samples were collected to monitor cell growth (A_{600}) and concentration of Fe(II). For experiments in suspension buffer, the 500 mL overnight culture was centrifuged (5000 rcf, 10 min, 4 °C), washed twice with the suspension buffer and re-suspended in 50 mL of the same buffer. The head space was H_2-CO_2 (80:20, v/v). HCl-extractable Fe(II) was measured using ferrozine assay as previously described (Lovley 1987). Briefly, 0.5 mL of sample was mixed with equal volume of 0.5 M HCl at room temperature for 15 min and 10 µL of the extract was added to 490 µL ferrozine reagent (2 mM ferrozine in 50 mM HEPES, pH 7.0) and the absorbance was measured at 562 nm using UV-Vis spectrophotometer (Genesys 10S, Thermo Scientific). Ferrous ethylene diammonium sulfate was used as standard for the ferrozine assay following the same procedure as mentioned above.

5.2.3. Electrochemical Experiments

The conventional H-shaped two-chamber MFC setup was used with a working volume of 70 mL for both the anolyte and catholyte. The AvCarb G200 battery felt, 3 cm x 3 cm, wetted with 30 % ethanol and washed twice with water, was used as electrode and titanium wire sewn through the felt was used as current collector. Nafion membrane 115^{TM}, treated with 5 % H_2O_2, water and 8 % sulfuric acid at 80 ^{o}C for half an hour each with intermittent washing with water after each

step (Yang et al. 2010), was used a separator between anode and cathode chamber. Either the growth medium or suspension buffer was used as the anolyte while 50 mM potassium ferricyanide in 50 mM phosphate buffer (pH 6.8 in the growth medium and pH 7.5 in the suspension buffer) was used as the catholyte. The MFC setup, anolyte and catholyte solutions were autoclaved before each experiment. The 2 mL overnight culture of *Pf* was inoculated into the anode chamber and the MFC was incubated at 90 ^{o}C throughout the experiment. The MFC with un-inoculated anolyte was used as the abiotic control.

Both anode and cathode chamber were tightly fitted with butyl rubber stopper and their headspaces were filled with Argon. A 100 Ω resistance (resistance decade box, EXTECH Instruments 380400) was used as a load between the anode and the cathode, and the MFC voltage was monitored continuously using Arbin Instrument. From the voltage and the resistance values, the current generated by the MFC was calculated. Polarization curve was generated by measuring the current at different applied voltages using MITS PRO software program in Arbin Instrument. Impedance of the MFC was measured at open circuit potential with cathode as a working electrode and anode as both reference and counter electrodes using CHI potentiostat (CH Instrument, model 920C). Cyclic voltammetry was carried out using a glassy carbon electron as working electrode, platinum wire as counter electrode and Ag/AgCl (saturated KCl) as reference electrode using a CHI potentiostat (CH Instruments, model 920C). The electrode used for studying mediated electron transfer was prepared by drop-casting *Pf* cells onto multi-walled carbon nanotubes (CNT) modified carbon electrode as previously described (Sekar et al. 2014). For electron microscopy imaging, the MFC anode was aseptically removed, dried at room temperature in a sterile Petri dish for two days and imaged using scanning electron microscope

(FEI Inspect F FEG-SEM). For the anolyte replenishment experiment, the anode chamber, inoculated as described above, was disassembled when the current reached a stable background value and the anolyte was replaced with fresh growth medium without disturbing the anode biofilm and no inoculum was added after changing the anolyte.

1.19 Results and Discussion

5.3.1. Reduction of Fe_2O_3 by *P. furiosus*

The exoelectrogenicity of *Pf* was studied by its ability to reduce the Fe(III) added to the growth medium. Two different forms of Fe(III) such as insoluble Fe(III) oxide (Fe_2O_3) and soluble chelated ferric citrate (Fe(III)Cit) were used. The growth of *Pf* in rich medium containing Fe_2O_3 and the concentration of soluble Fe(II) were monitored as shown in Figure 5.2. Figure 5.2a shows that the growth profile of *Pf* was almost the same in rich medium both with and without Fe_2O_3. *Pf* reduced nearly 36 μM of Fe_2O_3 to Fe(II) in 23 hours compared to the corresponding un-inoculated abiotic control (Figure 5.2b). The lower Fe_2O_3 reduction by *Pf* (36 μM) can be due to the insoluble nature of Fe_2O_3 that it could not permeate the outer S-layer enveloping the cell, thereby the chances of Fe_2O_3 getting reduced at the cell membrane was lower.

5.3.2. Reduction of Ferric Citrate by *P. furiosus*

The growth of *Pf* in rich medium with Fe(III)Cit as alternate electron acceptor as well as reduction of Fe(III)Cit by *Pf* showed a higher background noise (Figure 5.S1). The components

of the rich medium or any of the undefined products that complexed with the added Fe(III)Cit at 90 °C could be possible reasons for the observed higher background noise. Thus, to better understand the extracellular electron transfer by *Pf* to Fe(III)Cit, the reduction assay was performed as a cell suspension experiment instead of growing the culture. H_2 was used as an electron donor, since the suspension buffer did not contain any electron donor.

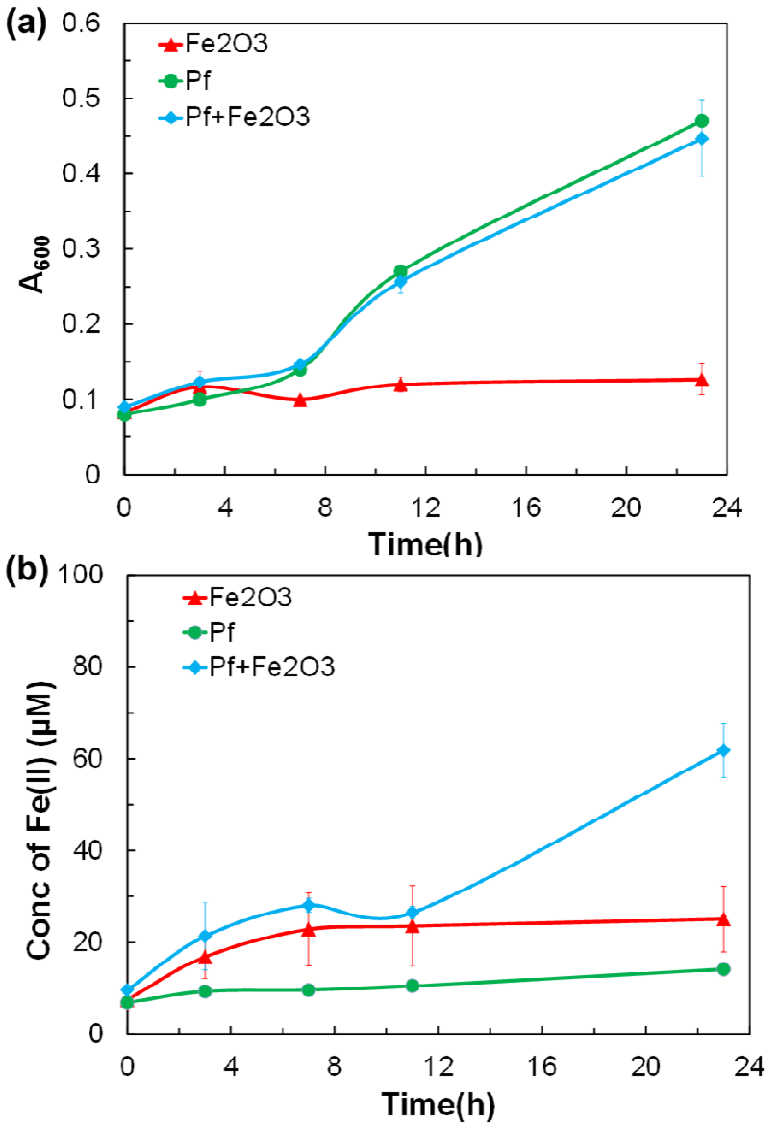

Figure 5.2: (a) Growth profile of *Pf* with and without Fe_2O_3 added to the rich medium at 90 ^{o}C; (b) Reduction of Fe_2O_3 to Fe(II) by *Pf* during its growth in rich medium at 90 ^{o}C

The *Pf* suspension culture showed significant reduction of Fe(III)Cit compared to the abiotic controls as shown in Figure 5.3. The usage of suspension buffer thus eliminated the possibility of complexation of Fe(III)Cit observed in the rich medium. Figure 5.3 shows that the *Pf* suspension culture with H_2 in headspace reduced ~3 mM Fe(III)Cit. However, *Pf* without H_2 in headspace and the double mutant ΔSHI/II (both with and without H_2) reduced relatively less Fe(III)Cit (~ 2 mM) as shown in Figure 5.S2. As explained in the Introduction section and Figure 5.1, the oxidation of H_2 can happen only with the help of soluble hydrogenases: SHI/II. The double mutant ΔSHI/II cannot uptake/oxidize H_2 physiologically. The suspension culture experiment revealed that H_2 was used as an electron donor by *Pf* for Fe(III)Cit reduction, but not solely, since a considerable amount of Fe(III)Cit reduction was also observed in the *Pf* culture without H_2 as well as in ΔSHI/II. This can be attributed to the presence of more reducing equivalents (ferredoxin/NADPH) in reduced state in the *Pf* cells during the overnight growth in rich medium prior to resuspension.

Further, it is noteworthy that the exoelectrogenicity of *Pf* observed with Fe(III)Cit (~3 mM) was 100-fold higher compared to that with Fe_2O_3 (36 μM). The apparent reason for this observation could be the ready accessibility of ferric citrate (soluble form of Fe(III)) for reduction at the cell membrane after permeating the outer S-layer (Figure 5.1).

5.3.3. Electricity Generation by *P. furiosus* through Direct Electron Transfer

After studying the ability of *Pf* to reduce Fe_2O_3 and Fe(III)Cit, the capability of *Pf* to transfer electrons extracellularly to the electrode was evaluated. The two-chamber MFC set up used to

study the electrochemical characteristics of *Pf* is shown in Figure 5.S3. Initially, the *Pf* cells were inoculated in the anode chamber with the rich medium as anolyte and the open circuit voltage was measured at 90 ^{o}C over time (Figure 5.S4a). In a separate MFC at 90 ^{o}C, the cells were inoculated in the anode chamber containing rich medium as the anolyte with a load of 100 Ω between the anode and cathode and the voltage was measured to calculate the current generated by the MFC (Figure 5.S4b). In both these cases (open circuit: Figure 5.S4a and closed circuit: Figure 5.S4b), the performance of the MFC was not significantly higher than the control (the uninoculated abiotic control). This could be attributed to the higher background noise from the

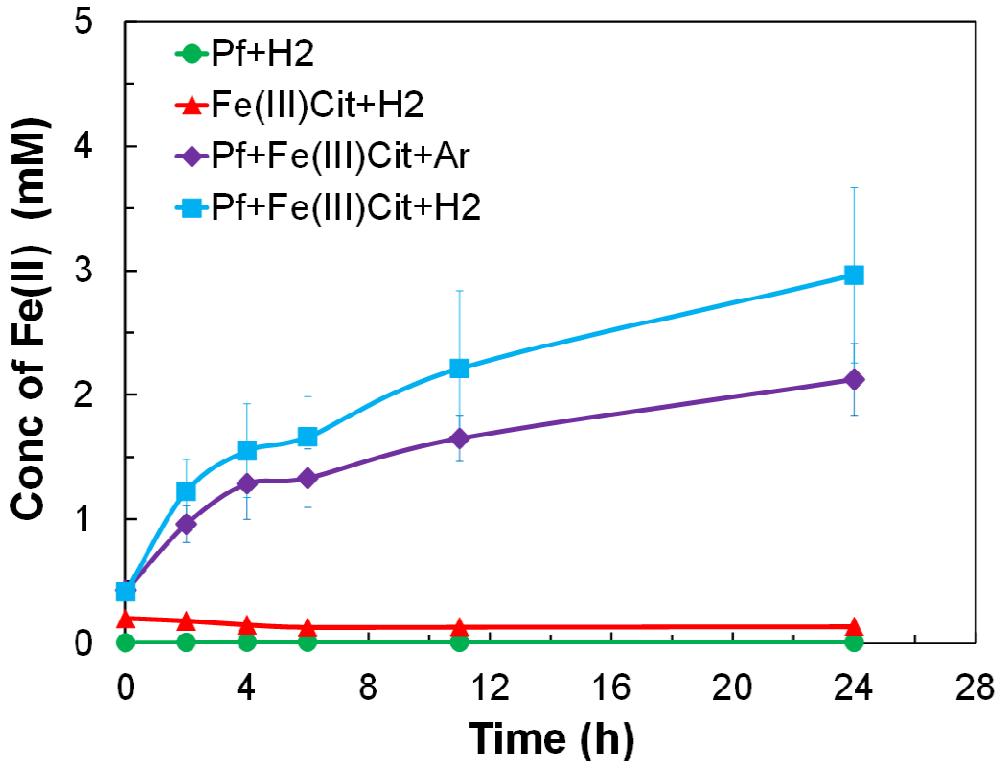

Figure 5.3: Reduction of Fe(III) citrate to Fe(II) by *Pf* suspension culture at 90 ^{o}C with and without H_2 as electron donor

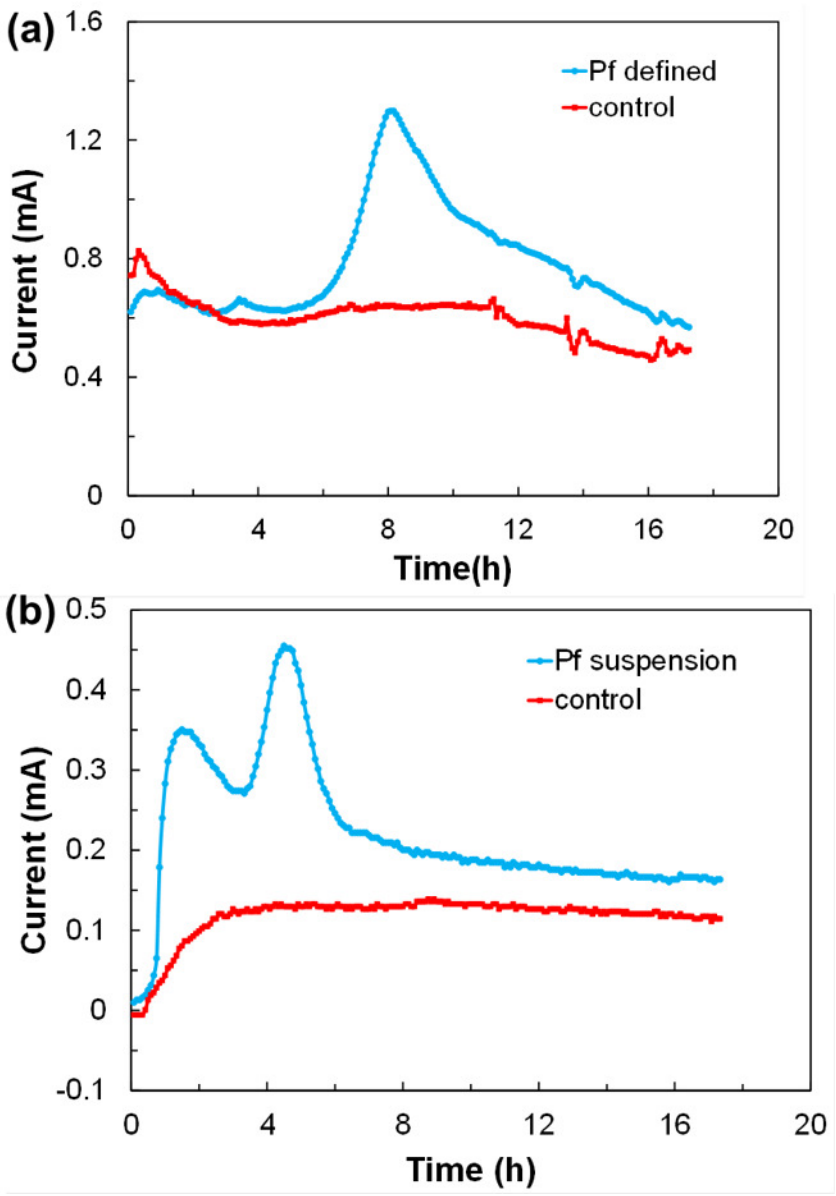

Figure 5.4: Current generation by (a) *Pf* growing in defined medium and (b) *Pf* suspension culture in two-chamber MFC operated at 90 ^{o}C along with the controls (uninoculated abiotic control); Representative data from triplicate experiments is shown here

undefined components of the rich medium, for example, yeast extract. However, when either defined medium or suspension buffer was used as the anolyte instead of the rich medium, a significant increase in current was observed compared to the uninoculated abiotic control. As shown in Figure 5.4a, the current measured in the MFC with *Pf* growing in the defined medium

steadily increased after four-hours post-inoculation, reached a maximum after eight hours, and then decreased steadily. Similarly, in the MFC that contained the *Pf* suspension culture (Figure 5.4b), two distinct current peaks were observed at approximately two and four hours after starting the MFC. The *Pf* growing in the defined medium took a relatively longer time to generate current as dictated by its growth in the defined medium. On the other hand, *Pf* cells suspended in the buffer generated current shortly after starting the MFC (< 2 hours later). We assume that this is because the cells did not need to first grow to carry out exoelectrogenicity; rather, they used the endogenous reducing equivalents (reduced ferredoxin) to generate the current. The decrease in first current peak of the suspension culture could be due to diminishing levels of the cellular reducing equivalents that could not be regenerated (Figure 5.4b). The second current peak current exhibited by the suspension culture is not an artifact since the data were highly reproducible. It should also be noted that temperature fluctuations (± 1 °C) were not observed throughout the MFC operation. The second current peak (Figure 5.4b) might be due to usage of H_2 as an electron donor by *Pf* to perform exoelectrogenicity once the endogenous reducing equivalents were used up. This observation is in agreement with the appearance of specific signal in the low frequency region of Nyquist plot obtained from impedance measurement (Figure 5.7b).

Following the MFC operation, the anode and the spent anolyte were analyzed. The anode was aseptically removed and subsequently examined using scanning electron microscope. This showed that the *Pf* cells were in direct contact with fibers of the carbon felt confirming biofilm formation on the anode (Figure 5.5a and 5.5b). *Pf* has previously been demonstrated to use its flagella to form cable like cell-cell connections as well as to adhere to solid surfaces like carbon

coated gold grids (Nather et al. 2006). No cells were seen in the anode from the uninoculated abiotic control (Figure 5.5c and 5.5d). Presumably biofilm formation facilitated direct electron transfer (DET) between *Pf* and the anode thereby generating a current in the MFC. Furthermore, the extracellular electron transfer by *Pf* was confirmed to be DET (rather than mediated electron transfer) by analyzing the spent anolyte for the presence of redox mediators using cyclic voltammetry between -0.8 and 0.6 V (*vs* Ag/AgCl). As shown in the cyclic voltammograms in

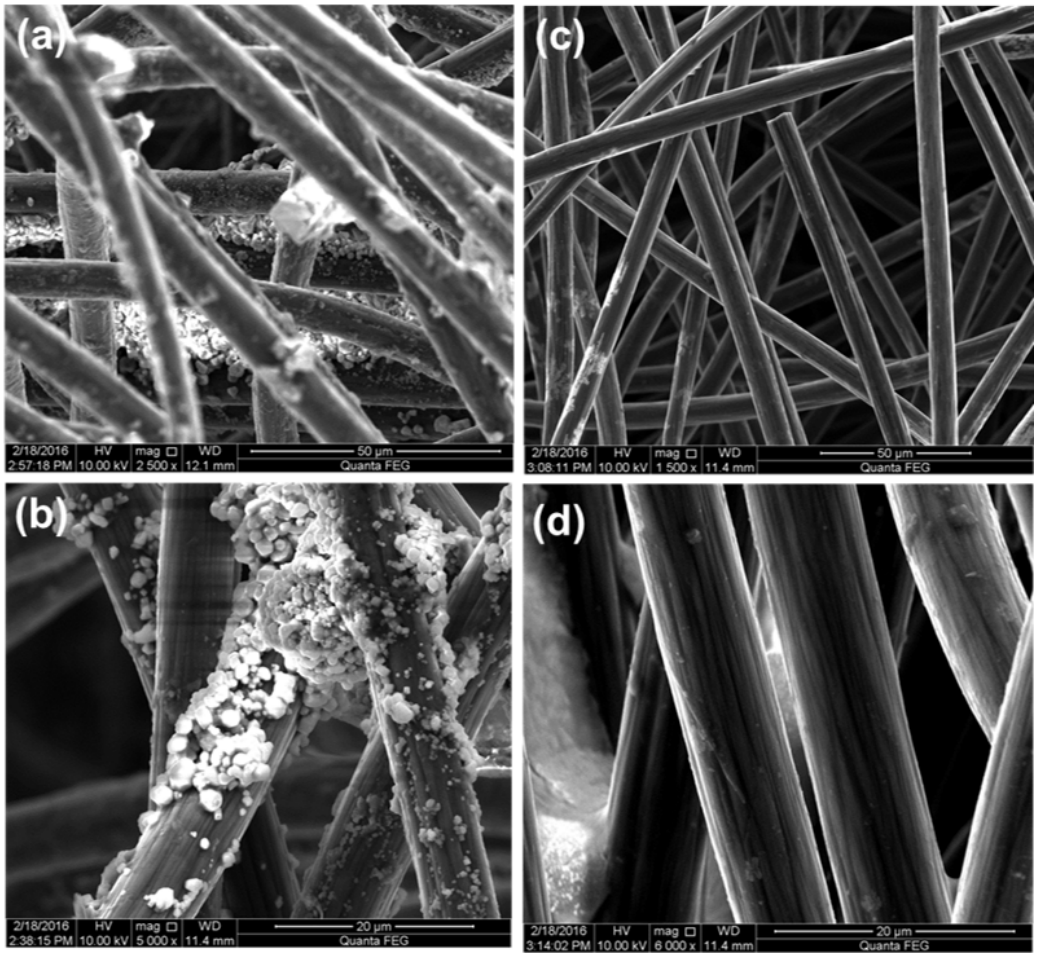

Figure 5.5: Scanning electron micrographs of (a and b) MFC anode with *Pf* growing in defined medium showing *Pf* biofilm on the carbon fibers and (c and d) anode from uninoculated abiotic control

Figure 5.S5, no specific redox peak attributable to a mediator was found using the spent anolyte from MFCs that contained *Pf*. Moreover, the voltammograms were identical to the voltammograms of spent anolyte from the uninoculated control MFC. The presence of electroactive *Pf* biofilm on the anode was investigated for its ability to generate current upon replenishing the spent anolyte with fresh growth medium (defined medium) but without adding an inoculum. The *Pf* cells in the biofilm not only served as an inoculum but the MFC exhibited a similar electrochemical response to that of the first inoculum (Figure 5.S6). This observation corroborates the fact that the biofilm-forming microorganisms that generate current by DET could be used for a sustained current generation in an MFC as long as the substrate/reductant (in this case, the maltose) is available in the feed solution. The current generation in the MFC via mediated electron transfer (MET) usually decreases upon anolyte change due to the depletion of soluble redox mediators. However, such a phenomenon was not observed here and the current generation in the second batch was roughly the same as that of the first, which further validates that DET and not the MET is the predominant mode of extracellular electron transfer from the *Pf* biofilm to the electrode.

5.3.4. Electrochemical Performance of MFC with *P. furiosus* as the Biocatalyst

In order to evaluate the performance of the MFC with *Pf* biofilm on the anode, polarization curve and impedance measurements were obtained post-inoculation at a) eight-hour for the MFC that contained the growing *Pf* culture and b) at four hours for the MFC that contained the *Pf* suspension culture. The electrochemical responses of the respective MFCs were at their maximum at those times (refer Figure 5.4a and 5.4b). The performance metrics of the two

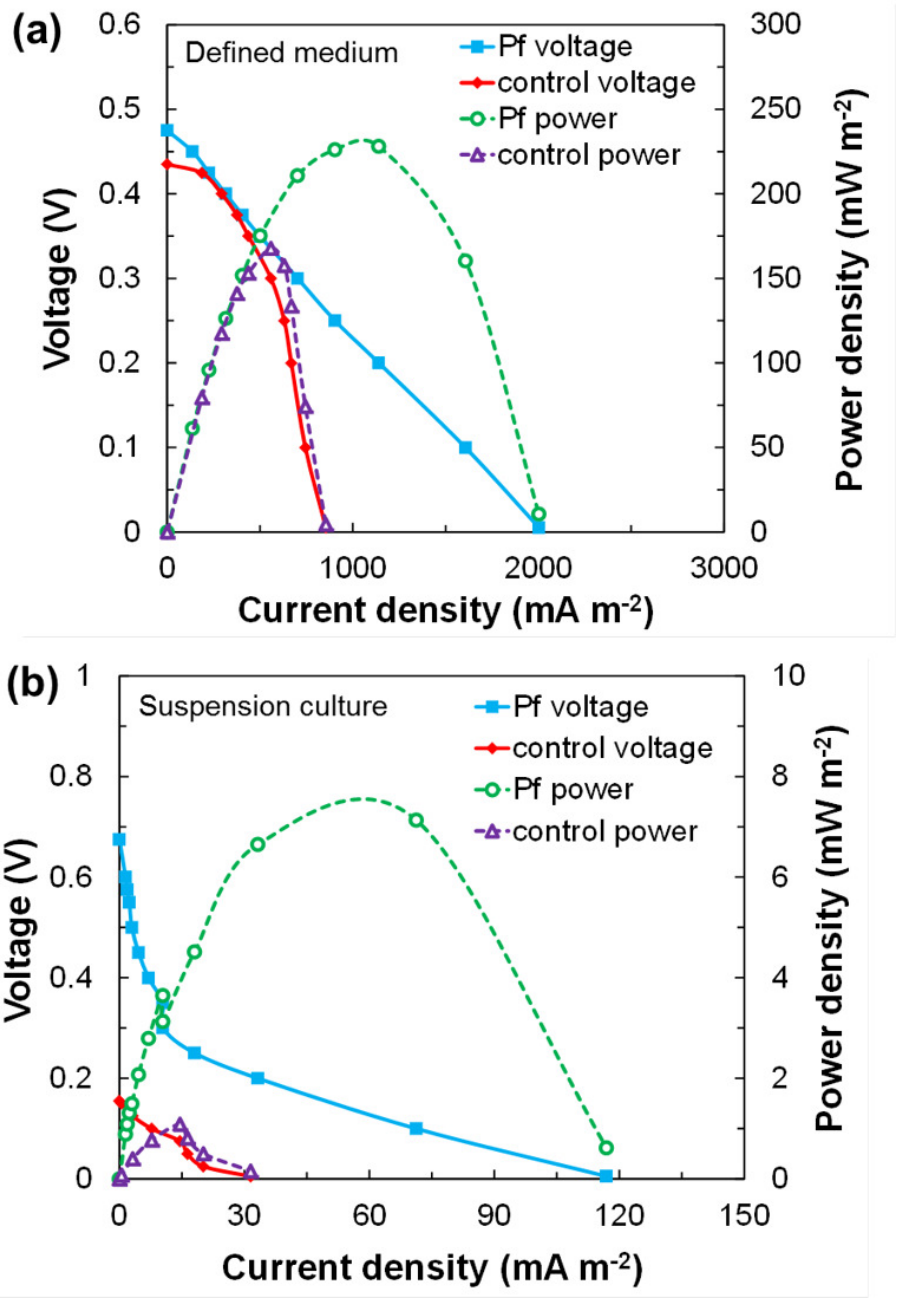

Figure 5.6: Polarization and power density curves for MFC with (a) *Pf* growing in defined medium and (b) *Pf* suspension culture along with the respective controls (uninoculated abiotic control); Representative data from triplicate experiments is shown here

different types of MFCs are summarized in Table 5.1. Figure 5.6a shows that the MFC with *Pf* culture growing in the defined medium generated a maximum current density of 2 A m^{-2} (two-fold higher than the abiotic control) and a peak power density of 225 mW m^{-2}. On the other hand,

for the MFC with the *Pf* suspension culture, even though the absolute value of maximum current density (120 mA m^{-2}) was lower than that generated by the growing culture, the performance was significantly better (four-fold higher) compared to the corresponding abiotic control (Figure 5.6b). Similarly, the peak power density achieved in suspension culture MFC (~ 8 mW m^{-2}) was nearly seven-fold higher than the corresponding control. Furthermore, comparing the shape of polarization curves, the electron transfer between *Pf* and electrode in the suspension culture MFC was found to be more kinetically limited compared to the growing culture. Presumably, various electroactive components (of the growth medium) might have facilitated the electron transfer kinetics. This could also be the likely reason for such a huge variation (nearly two orders of magnitude) in both the current density and power density values between the two different MFCs (growing *versus* suspended *Pf* cultures).

Electrochemical impedance spectroscopy (EIS) is a useful technique to determine the contribution of different internal resistances to the MFC performance and it also provides insight into the interaction between the electroactive species and the electrode (Sekar and Ramasamy 2013). EIS was performed when the MFC was operating at its maximal performance (maximum current density, see Figures 5.4a and 5.4b) and the resulting Nyquist data was fitted with the equivalent circuits (Figure 5.S7). As shown in the Nyquist (Figure 5.7a and 5.7b) and phase angle plots (Figure 5.7c and 5.7d), in both the defined medium and the suspension culture-based electrolytes, two time-constant regimes (indicated as I and II in Figure 5.7) were observed for the MFC with *Pf* cells whereas only a single time-constant was observed for the corresponding abiotic control. Clearly, the charge transfer resistance (R_{CT}) was lowered (see the diameter of the first semicircle in Nyquist plots, Figure 5.7a and 5.7b) due to the presence of the electroactive *Pf*

biofilm on the MFC anodes. Furthermore, the electrochemical response of the *Pf* biofilm was evident from the observation of a second regime (indicated as II in both plots) in the low frequency region, which was not seen in the control. An electroactive biofilm with slower electrochemical kinetics, (i.e., lower exchange current, I_o), is usually observed in the low frequency (high time-constant) region in EIS. Hence, the impedance measurement (Figure 5.7 and Table 5.1) was in direct correlation with the increased current generation by

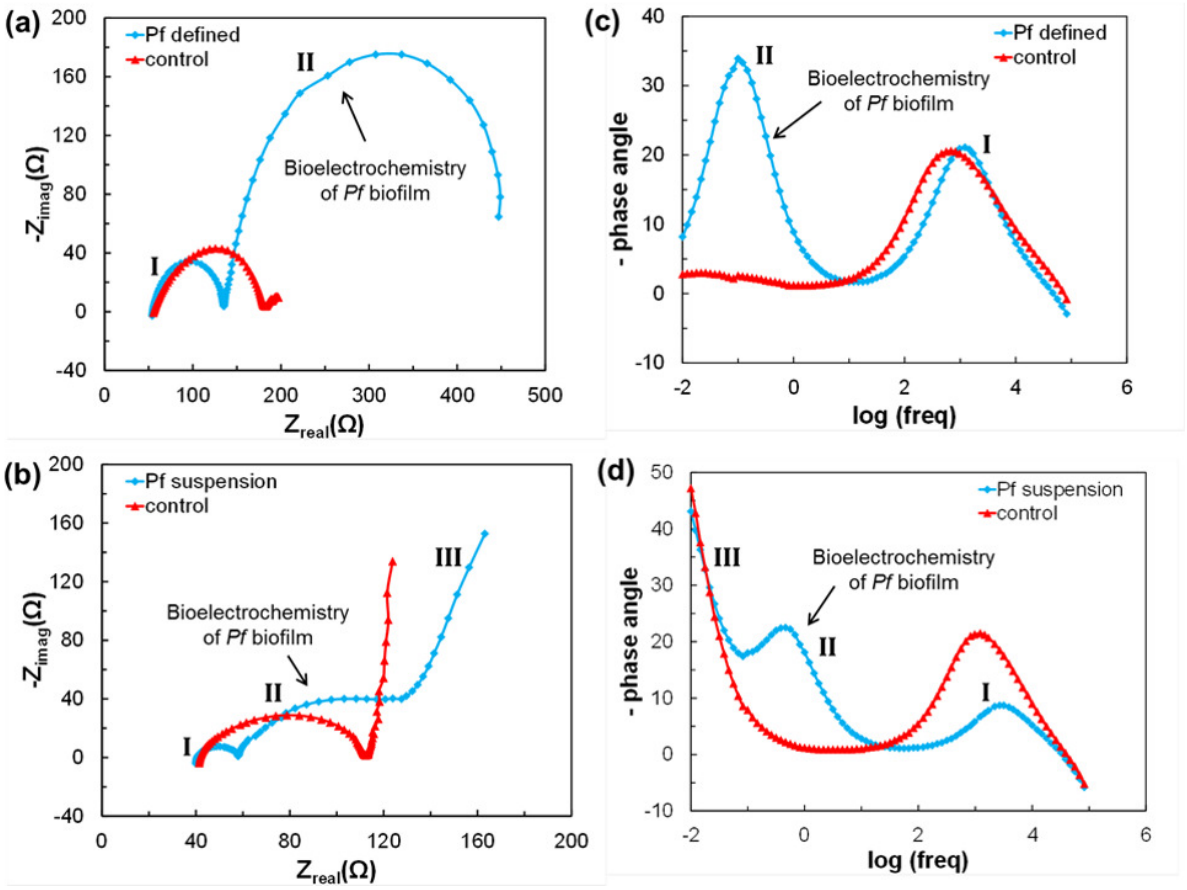

Figure 5.7: Nyquist plot for the MFC with (a) *Pf* growing in defined medium and (b) *Pf* suspension culture and the corresponding phase angle plots are shown in (c) and (d) respectively; control represents the corresponding uninoculated abiotic control; Equivalent circuits used to fit the measured impedance data are shown in Figure 5.S7 and the charge transfer resistance values are summarized in Table 5.1

Table 5.1: Performance metrics of two different types of MFC with *Pf* growing in the defined medium or as a suspension (defined medium and suspension buffer); E_{cell}-Full cell voltage; j_{max}-maximum current density; P_{peak}-peak power density; R_{CT}-charge transfer resistance

MFC Anolyte	**E_{cell} (V)**	**j_{max} (mA m^{-2})**	**P_{peak} (mW m^{-2})**	**R_{CT} (Ω)**
Defined medium (abiotic uninoculated control)	0.12	854	167	112.7
Pf growing in defined medium	0.64	2002	228	76.71*
Suspension buffer (abiotic uninoculated control)	0.425	31	1	56.63
Pf suspension culture	0.475	116	7.5	15.06*

* *Pf* growing in defined medium and *Pf* suspension culture, R_{CT1} are given.

the MFCs (Figure 5.4) that contained *Pf* cells. In addition, a third regime (indicated as III in Figure 5.7b) manifest by the *Pf* suspension culture could be correlated to a phenomenon, much slower than the biofilm electrochemical kinetics, such as diffusion of gases (H_2 in this case). H_2 might be subsequently utilized by the *Pf* suspension culture and used as an electron donor (via SHI and/or SHII), once all the endogenous reducing equivalents were used up. This would lead to current generation in the MFC corresponding to the second current peak observed in Figure 5.4b.

5.3.5. Potassium Ferricyanide Mediated Electron Transfer by *P. furiosus*

Besides demonstrating DET behavior by *Pf* cells, their ability to participate in MET was also studied using potassium ferricyanide as an exogenous redox mediator. Water-soluble redox mediators are generally used to probe electron transfer occurring at the cell membrane where they interact with electroactive redox proteins (such as c-type cytochromes) and mediate electron transfer, as previously discussed (Bombelli et al. 2011; Sekar et al. 2016). The *Pf* immobilized

CNT-modified electrode was used to study MET using a low scan-rate cyclic voltammetry (1 mV/s) at 90 ^{o}C. It is clearly evident from Figure 5.8 that potassium ferricyanide was used by *Pf* cells for MET as exemplified by the increased oxidation peak at 0.2 V (vs. Ag/AgCl) compared to the control electrode that did not contain *Pf*.

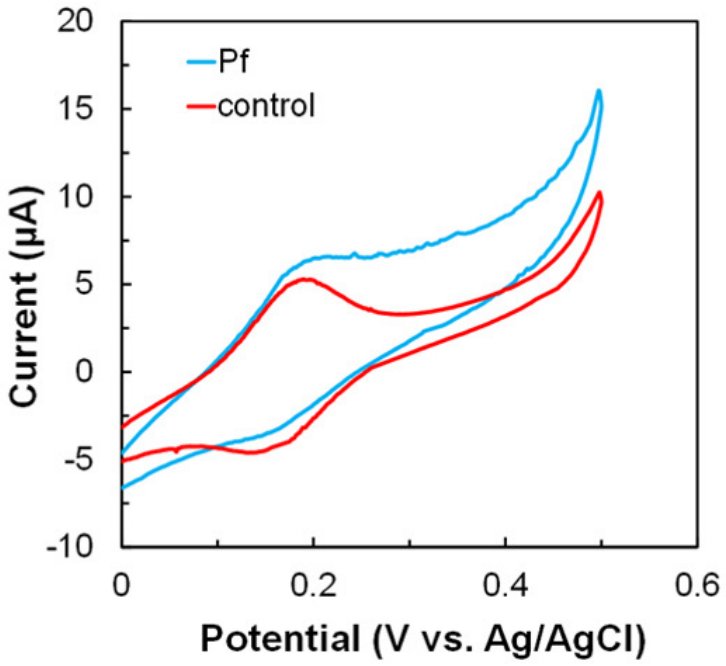

Figure 5.8: Cyclic voltammograms showing mediated electron transfer between *Pf* and multi-walled carbon nanotubes (CNT) modified electrode via potassium ferricyanide at 90 ^{o}C; Scan rate: 1 mV/s; (Representative data from triplicate experiments is shown here); control: CNT modified electrode without *Pf* cells

5.3.6. Extracellular Electron Transport Pathways of *P. furiosus*

The direct electron transfer between *Pf* cells and the electrode could be attributed to any hypothetical membrane protein present in the cell membrane and/or S-layer (Figure 5.1) that has ferric reductase activity similar to that found in iron-reducing microorganisms (Schroder et al.

2003). This hypothetical protein with ferric reductase activity could have coupled the oxidation of reduced ferredoxin and the reduction of alternate electron acceptors such as potassium ferricyanide and the electrode (Figure 5.1). While insoluble alternate electron acceptor like the electrode could be reduced only at the outer S-layer, the soluble electron acceptor such as potassium ferricyanide can permeate the S-layer and could be reduced at the cell membrane either by a membrane redox enzyme that itself is reduced by reduced ferredoxin. The involvement of NADPH as a possible electron carrier for exoelectrogenicity (Figure 5.1) cannot be excluded, since soluble hydrogenases (SHI and SHII) utilize H_2 to generate NADPH for anabolic processes (Ma and Adams 2001b; Ma et al. 2000; Ma et al. 1994). Consequently, ferredoxin $NADP^+$ oxidoreductase (FNOR) could catalyze electron transfer between NADPH and ferredoxin (Ma and Adams 2001a), diverting electrons from NADPH to the ferredoxin pool. Some MFCs were also demonstrated to contain microorganisms that produce H_2 either photosynthetically or fermentatively and the H_2 was oxidized *in situ* using the platinum coated anode (He et al. 2009; Rosenbaum et al. 2005a; Rosenbaum et al. 2005b). However, in the work presented herein, carbon fibers were used as MFC anode so the oxidation of H_2 at the anode surface is less likely due to the sluggish electro-kinetics of H_2 oxidation on carbon surfaces. The extracellular electron transfer pathways shown in Figure 5.1 were hypothetical and should be carefully studied by performing further experiments using an integrated biochemical and genetic engineering approaches which would be addressed in our future work.

Microbial reduction of Fe(III) by various hyperthermophiles belonging to widely divergent genera such as the archaea *Pyrobaculum islandicum*, *Pyrodictium abyssi* and *Methanopyrus kandleri* and the bacterium *Thermotoga maritima* has been reported (Vargas et al. 1998).

Interestingly, hyperthermophiles that do not reduce S^0, such as *Archaeoglobus fulgidus,* were also found to exhibit Fe(III)-reducing activity (Lovley 2004; Vargas et al. 1998). However, there is no evidence that these organisms conserve energy by iron reduction, i.e. carry out Fe(III) respiration, although this has been proposed to be the earliest evolved mode of energy conservation (Vargas et al. 1998). *P. furiosus* was also reported to reduce ferric citrate (Vargas et al. 1998) and artificial quinones such as anthraquinone-2, 6-disulfonate (AQDS) (Lovley et al. 2000) using H_2 as electron donor. In addition to Fe(III) reduction, *Pf* was also found to be involved in reductive precipitation of gold (Kashefi et al. 2001). All these studies pertaining to *Pf* were done to screen the capability of *Pf* along with other hyperthermophiles for the reduction of metals and quinones, and no attempts were made to understand the extracellular electron transport of *Pf*. Hence, herein we show for the first time that a pure culture *Pf* can interact with an electrode in an MFC operated at a temperature of 90 ^oC.

Table 5.2: Comparison of MFC power densities reported in the literature for thermophiles and hyperthermophiles with the results obtained in the current study

S. No.	**Anolyte culture**	**MFC working temperature ^oC**	**Power density (mW m^{-2})**	**Reference**
1	Mixed culture (anaerobic digester)	55	37	Wrighton et al 2008
2	*Thermincola ferriacetica*	60	146	Marshall et al 2009
3	Mixed culture (petroleum reservoir)	95	165	Fu et al 2015
4	*Pyrococcus furiosus*	90	228	This study
5	*Calditerrivibrio nitroreducens*	55	272	Fu et al 2013

A comparative analysis of power density achieved in MFC operated using thermophiles and hyperthermophiles is summarized in Table 5.2. The peak power density of 228 mW m^{-2} obtained in this study using *Pf* cells was higher than that measured by (Fu et al. 2015) who obtained 165 mW m^{-2} using a mixed microbial culture from a petroleum reservoir in a similar type of

MFC operated at 95 ^{o}C. Further, the maximum power density reported so far in MFCs operated above 55 ^{o}C is 272 mW m^{-2} using *Calditerrivibrio nitroreducens* (Fu et al. 2013). However, the MFC was operated in a fed-batch mode for ~400 h, so the results cannot be directly compared with the batch MFC studied here. It is also important to note that the current study is a proof of concept showing the interaction of *Pf* with MFC electrode to generate electricity and no optimization efforts were made to maximize the power density of the system. Furthermore, based on the experiments reported here, future studies of the exoelectrogenicity of hyperthermophiles such as *Pf* will help identify the possible electron acceptors that they can utilize. Potentially this will have a huge impact in bioremediation as well as in understanding physiological versatility of the microbe for energy conservation.

1.20 Conclusions

This study reports for the first time the usage of a pure culture of hyperthermophilic microorganism called *Pyrococcus furiosus* in a microbial fuel cell that was operated at 90 ^{o}C, showing significant electrochemical response compared to that of the control MFC. The extracellular electron transfer ability of *Pf* was also witnessed from its capability to reduce both Fe_2O_3 and ferric citrate biochemically. The proof of concept study highlights the potential of *Pf* to generate electricity in MFCs at high temperature locations. Moreover, such studies also help to advance our understanding in the field of biogeochemistry of the early hot environment and exobiology.

1.21 Supplementary Data

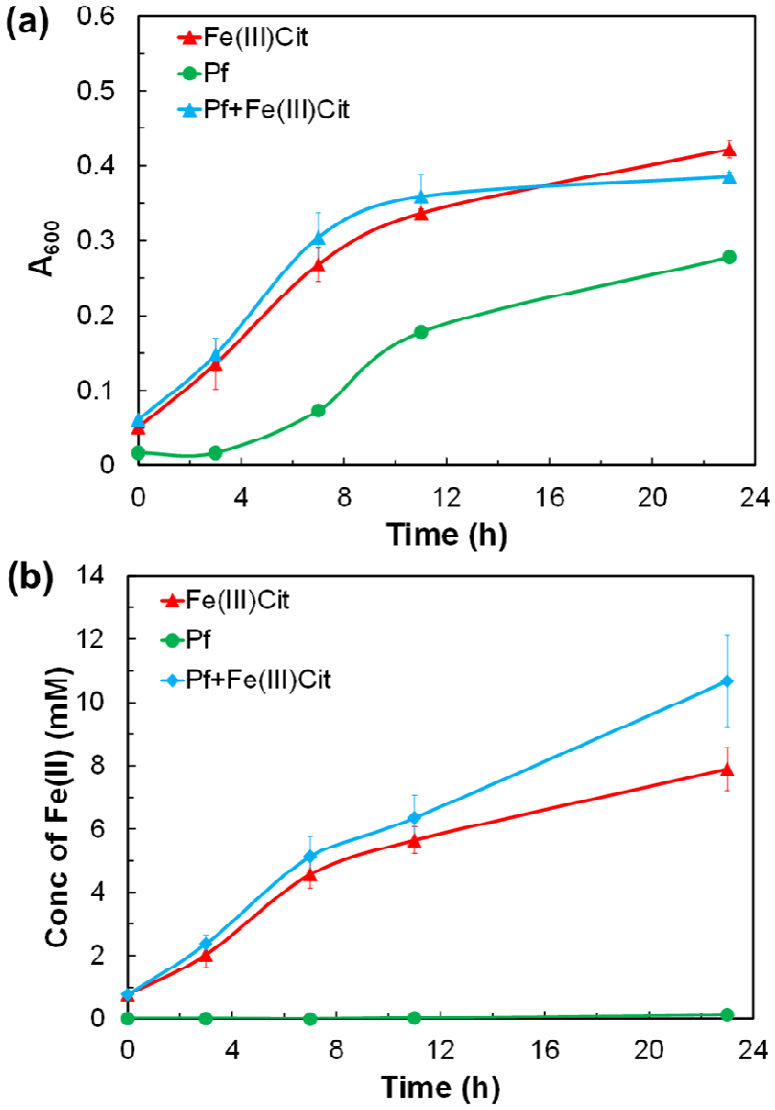

Figure 5.S1: (a) Growth profile of *Pf* with and without Fe(III) citrate added to the rich medium at 90 °C; (b) reduction of Fe(III) citrate to Fe(II) by *Pf* during its growth in rich medium at 90 °C

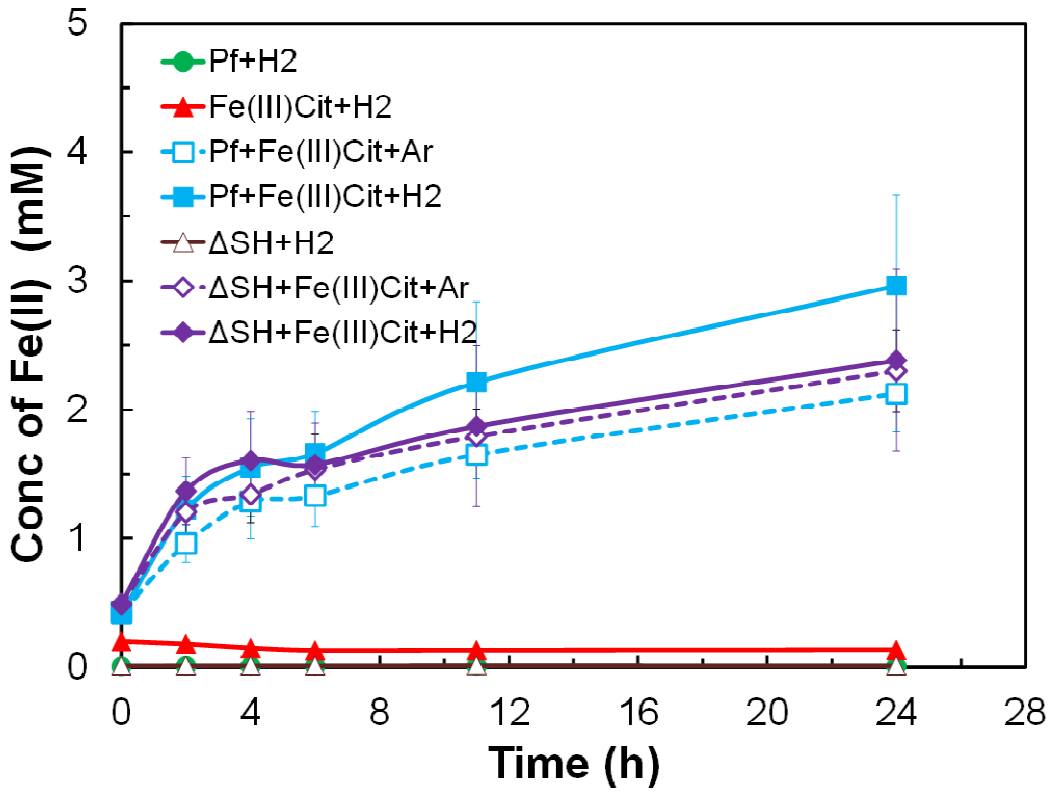

Figure 5.S2: Reduction of Fe(III) citrate to Fe(II) by *Pf* suspension culture and double mutant ΔSHI/II (ΔSH) suspension culture at 90 ^{o}C with and without H_2 as electron donor

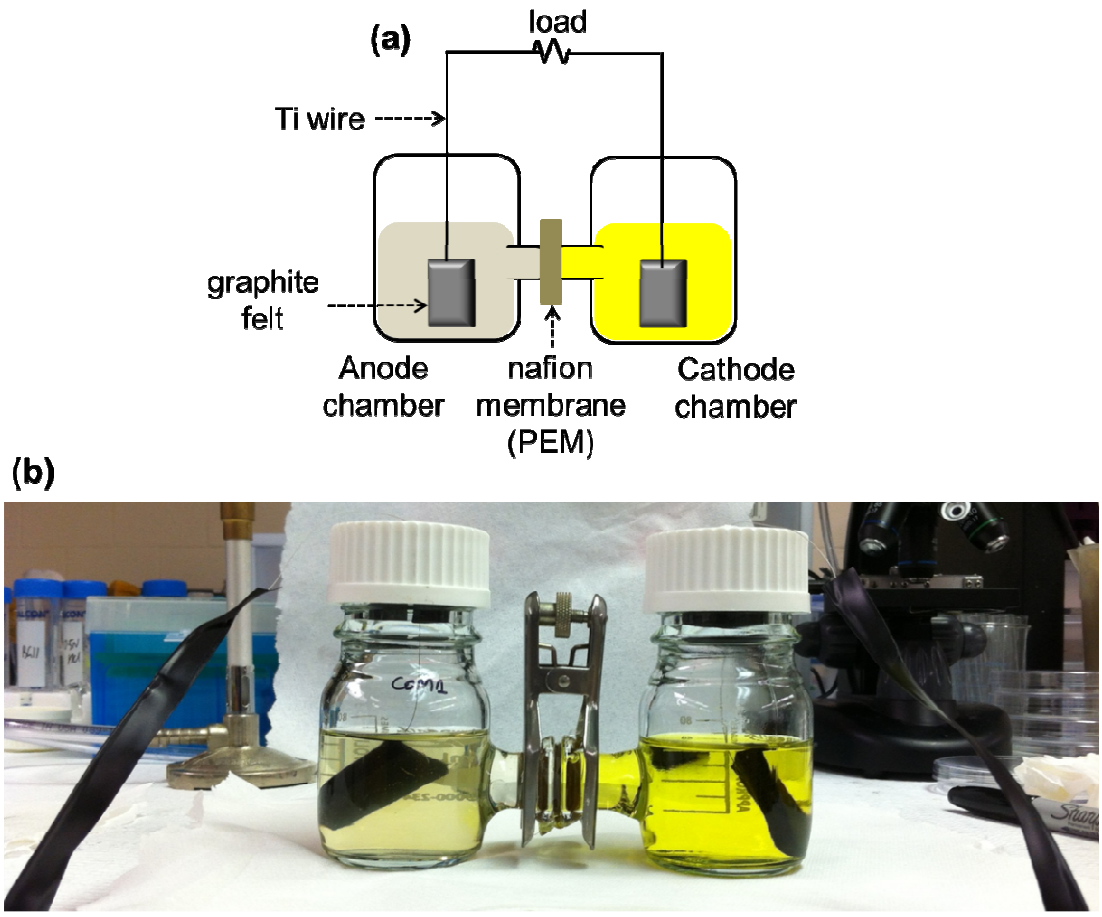

Figure 5.S3: (a) Schematic and (b) photograph of two-chamber H-shaped microbial fuel cell used in the study; PEM-proton exchange membrane; (Refer Materials and Methods section in the main text for more detailed information)

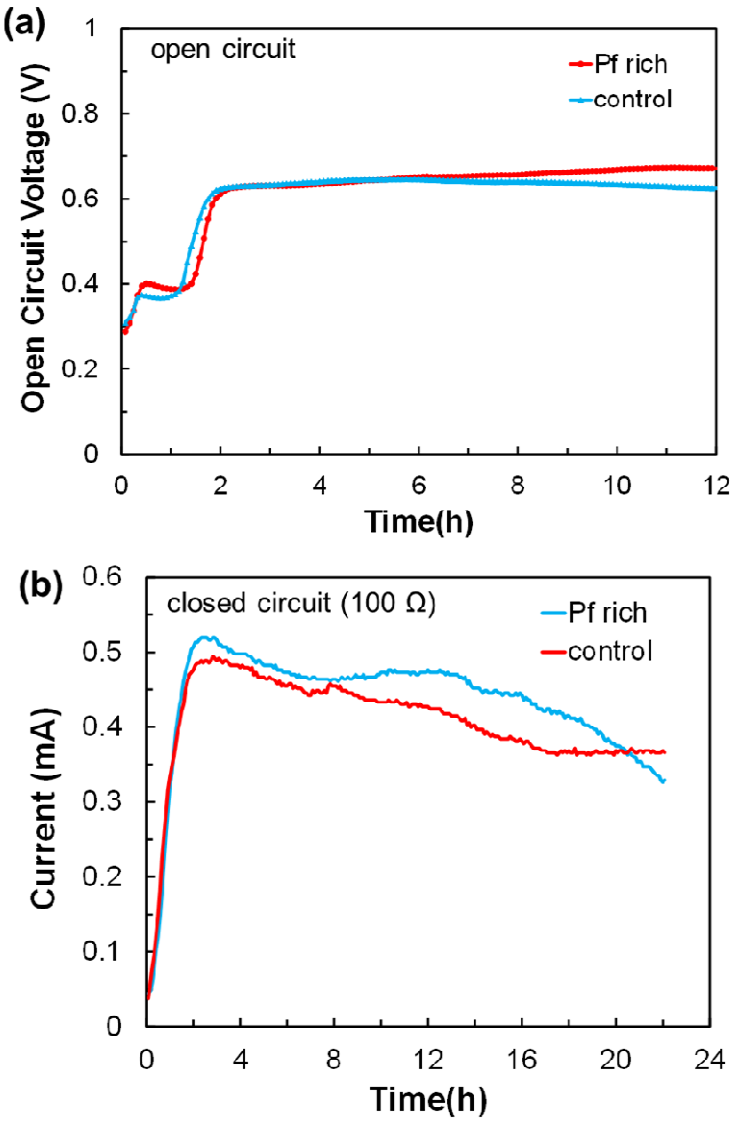

Figure 5.S4: (a) Open circuit voltage and (b) current generation by *Pf* growing in rich medium in two-chamber MFC operated at 90 °C; (Representative data from triplicate experiments is shown here); control: uninoculated abiotic control

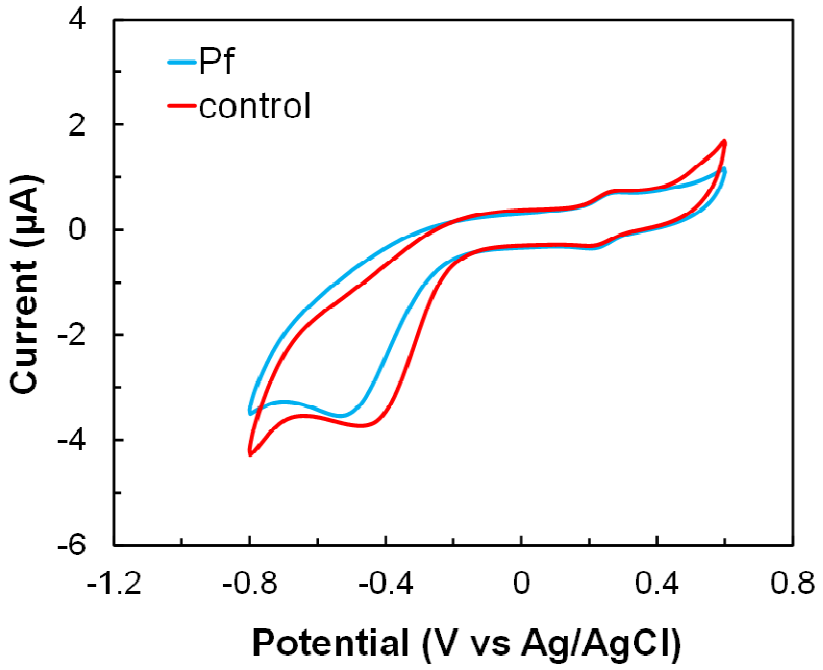

Figure 5.S5: Cyclic voltammograms of the spent anolyte from MFCs with *Pf* growing in defined medium and the uninoculated abiotic control

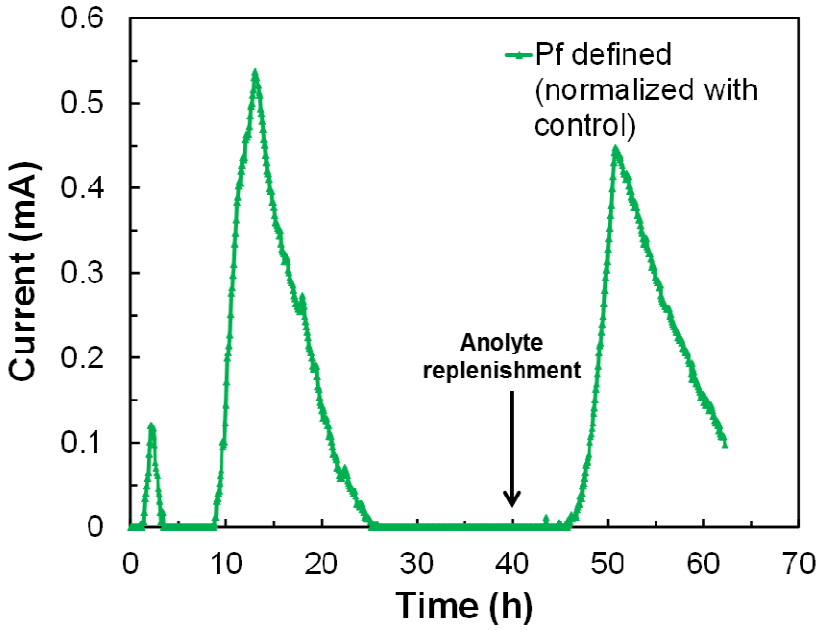

Figure 5.S6: Restoration of current generation by *Pf* after replenishing the spent medium with fresh defined medium in two-chamber MFC operated at 90 °C (the current shown here was normalized with the current from abiotic uninoculated control)

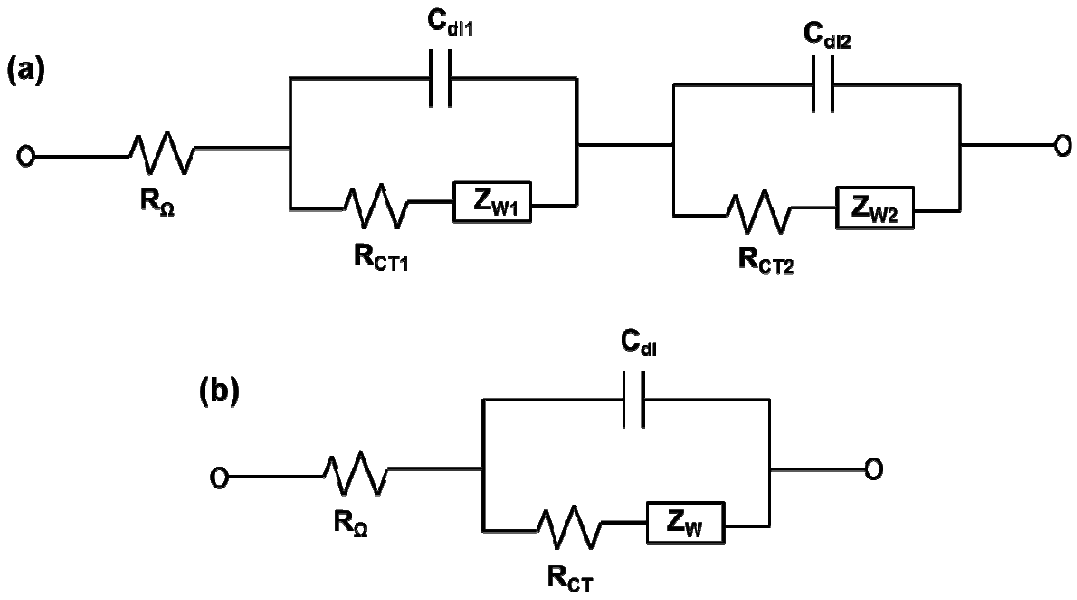

Figure 5.S7: Equivalent circuits used to fit the electrochemical impedance data measured for MFC (a) with *Pf* biofilm on the anode (two Randles circuits were used based on the two characteristic semicircular peaks observed in Nyquist plots, Figure 5.7a and 5.7b) and (b) the uninoculated abiotic control. (Abbreviations: R_Ω: ohmic resistance; C_{dl}: double layer capacitance; R_{CT}: charge transfer resistance; Z_W: Warburg impedance; For more information, refer Sekar and Ramasamy, 2013)

CHAPTER 6

STUDYING EFFECT OF LIGHT INTENSITY ON PERFORMANCE OF BIOFILM-BASED ANODE THROUGH A MATHEMATICAL MODEL

To be submitted to Journal of Electrochemical Society.

1.22 Introduction

Mathematical models are used to describe a system and/or a process quantitatively and have a great predictive power that is profoundly useful in design and optimization of the system under study. In engineering perspective, the prediction of mathematical models significantly reduces the time, energy and efforts for scale-up and commercial application of a technology. Particularly, modeling complex systems such as microbial fuel cells (MFC) has a greater value addition for advancing the technology in addition to the knowledge pool developed through the experimental data. MFC involves the interaction of various different phenomena such as physical, chemical, electrochemical and biological. Modeling MFC is a highly challenging task, and the results obtained from the modeling simulations have to be carefully investigated along with the measured experimental data (Ortiz-Martinez et al. 2015; Picioreanu et al. 2007). Modeling can be done to optimize the performance of either an anode or a cathode (half-cell system), and/or the full-cell system.

In this work, a mathematical model had been developed to describe a biofilm-based anode and to explicitly study the effect of incident light intensity on the anode performance. The current density generated at the electrode surface via both direct and mediated electron transfer had been characterized as a function of incident light intensity. The model developed in this work has greater implications to design and optimize the anode of photosynthetic MFC (P-MFC), where incident light intensity is a major contributing factor for the anode performance. The developed model could be extended by incorporating necessary factors to characterize the cathode, thereby facilitating the optimization of P-MFC in future.

1.23 Effect of Light Intensity

The influence of light intensity on the photosynthesis has been modeled in elaborate details in (Bechet et al. 2013; Ota et al. 2015; Zhang et al. 2015). Light intensity can be defined in three different terms as given below:

1. Incident light intensity (I_o): the light intensity that is incident onto the surface of the photo-bioreactor
2. Average light intensity (I_{av}): Inside the well mixed photo-bioreactor, all the cells receive different light intensities. I_{av} is the average of all those intensities.
3. Light intensity received at the cell surface (I): Due to factors such as light attenuation, reflectance by air bubbles, the incident light intensity (I_o) experienced by the cells is always diminished to I.

Both the I_{av} and I is a function of I_o and parameters such as geometry of photo-bioreactor, cell concentration and other operating parameters. For example, the light intensity received by the cell surface (I) can be defined as a function of incident light intensity (I_0) as given in Equation (6.1) (Zhang et al. 2015).

$$I = I_0 \exp\left[-\left\{\frac{3\,\alpha_g}{d_b} + \tau_c\, X\right\} z\right] \tag{6.1}$$

Table 6.1: List of parameters used to define light intensity received by the cell surface (I)

Parameter	Description	Dimension
α_g	Bubble volume fraction	-
d_b	Average bubble diameter	m
τ_c	Extinction coefficient of biomass	$m^2\ g^{-1}$
X	Biomass concentration	gDCW m^{-3}
Z	Thickness of photo-bioreactor	m

The following models (Equations (6.2) - (6.6)) have been commonly used so far to characterize the effect of light intensity on rate of photosynthesis. For simplicity, I_o is mentioned in all the models below and it could be extended to I_{av} and I depending on the experimental conditions.

Hyperbolic tangent model $$\mu = \mu_m \tanh\left[\frac{I_o}{k_I}\right] \quad (6.2)$$

Exponential model $$\mu = \mu_m \exp\left[-\frac{I_o}{k_I}\right] \quad (6.3)$$

Poisson model $$\mu = \mu_m \left[\frac{I_o}{I_{opt}}\right]\left\{1 - \exp\left[-\frac{I_o}{I_{opt}}\right]\right\} \quad (6.4)$$

Monod model $$\mu = \mu_m \left[\frac{I_o}{I_o + k_I}\right] \quad (6.5)$$

Light adaptation model $$\mu = \mu_m \left[\frac{I_o}{I_o + k_I + \frac{I_o^2}{k_{in}}}\right] \quad (6.6)$$

μ is the specific growth rate, μ_m is the maximum specific growth rate, k_I is the light saturation coefficient, k_{in} is the light photo-inhibition coefficient, I_{opt} is the optimum light intensity. Of all these models, Equation 6.5, the Monod model was found to better characterize the experimental value obtained from the photo-bioreactor (Ota et al. 2015). However, the light adaptation model (Equation 6.6) captures both the photo-inhibition effect and the Monod behavior (Zhang et al. 2015) and was adopted by us in the current modeling work reported here. In the current model also, I_o was used to characterize the influence of light intensity on the performance of P-MFC. In future, it could be extended to I_{av} and/or I based on the experimental conditions.

1.24 Governing Equations

Figure 6.1 explains the schematic representation of the model developed in this research work. The model considered a single biofilm domain of length 'L' with two interfaces: (1) bulk solution to the right of the biofilm and (2) the solid electrode to the left of the biofilm. The dependent variables were concentration of substrate (S), oxidized form of mediator (M_{ox}), reduced form of mediator (M_{red}) and the local biofilm potential (E) (Table 6.2). The independent variables were biomass concentration (X), polarized electrode potential (ε) and incident light intensity (I_o) (Table 6.3). j_D and j_M were current densities generated at the electrode surface via DET and MET respectively. The model adopted here and the values of all the constants in the model (Table 6.4) were similar to that explained in (Beyenal and Babauta 2015) with the inclusion of incident light intensity term to represent the influence of light intensity on the performance of anode that contain biofilm made up of photosynthetic microorganisms.

Mass balance for substrate (S) is given by Equation (6.7). This equation explains the rate of change of S in the form of Fick's second law. The left hand side term is the rate of change of S with respect to time 't', the first term on the right hand side is the concentration gradient of S with respect to biofilm length 'x' and second term on the right hand side is the overall substrate consumption rate by both mediated (q_M) and direct mode (q_D) of electron transfer. q_M and q_D are given by Equations (6.5) and (6.6).

$$\frac{\partial S}{\partial t} = D_{eS} \frac{\partial^2 S}{\partial x^2} - X\,(q_M + q_D) \tag{6.7}$$

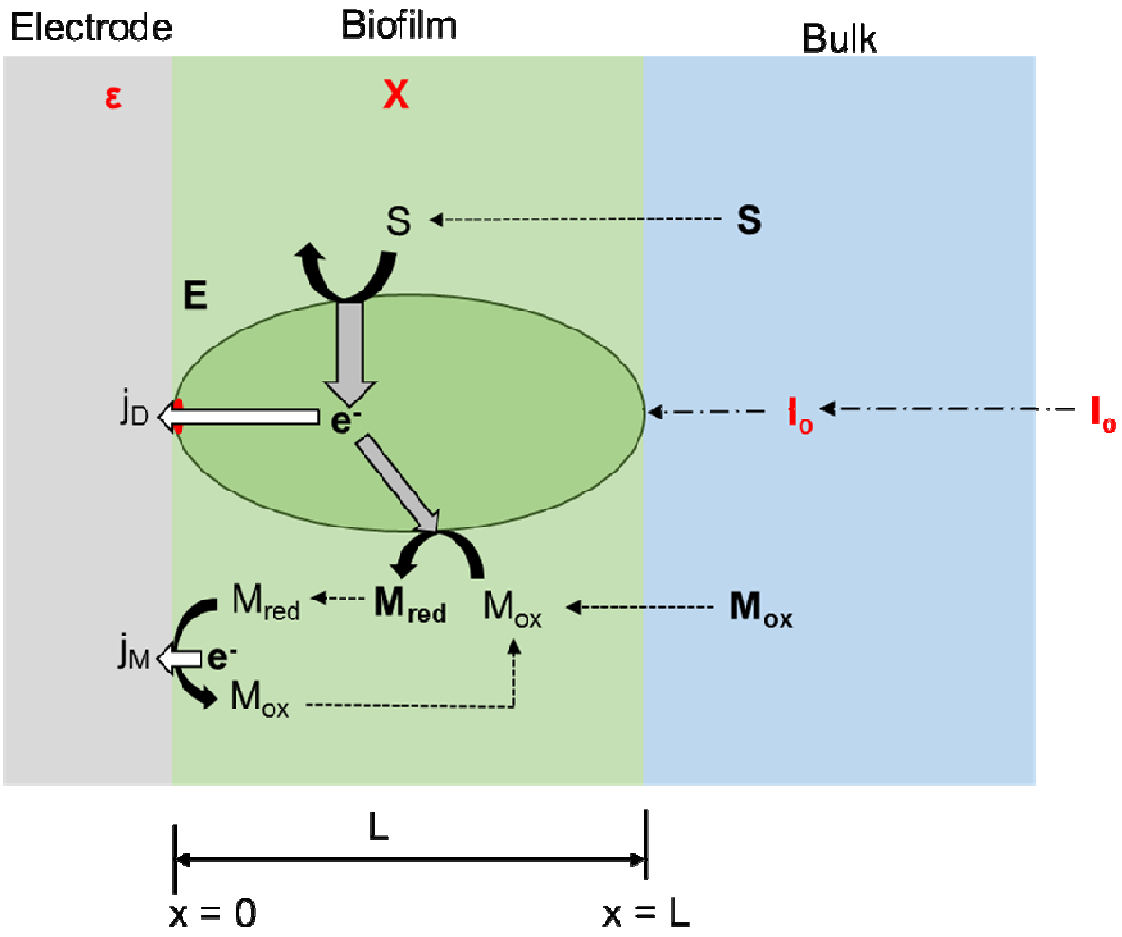

Figure 6.1: Schematic representation of the biofilm-based anode model with a single biofilm domain of length 'L' with two interfaces: (1) bulk solution to the right of the biofilm and (2) the solid electrode to the left of the biofilm. The dependent variables were represented in black: concentration of substrate (S), oxidized form of mediator (M_{ox}), reduced form of mediator (M_{red}) and the local biofilm potential (E). The independent variables were represented in red: biomass concentration (X), polarized electrode potential (ε) and incident light intensity (I_o). j_D and j_M were current densities generated at the electrode surface via DET and MET respectively

Mass balance for oxidized form of mediator (M_{ox}) is given by Equation (6.8). This equation explains the rate of change of M_{ox} in the form of Fick's second law. The left hand side term is the rate of change of M_{ox} with respect to time 't', the first term on the right hand side is the concentration gradient of M_{ox} with respect to biofilm length 'x' and second term on the right hand side is the reduction rate of M_{ox} in the biofilm.

$$\frac{\partial M_{ox}}{\partial t} = D_{eM} \frac{\partial^2 M_{ox}}{\partial x^2} - \frac{yf}{n} X q_M \quad (6.8)$$

Mass balance for reduced form of mediator (M_{red}) is given by Equation (6.9). This equation explains the rate of change of M_{red} in the form of Fick's second law. The left hand side term is the rate of change of M_{red} with respect to time 't', the first term on the right hand side is the concentration gradient of M_{red} with respect to biofilm length 'x' and second term on the right hand side is the reduction rate of M_{ox} in the biofilm.

$$\frac{\partial M_{red}}{\partial t} = D_{eM} \frac{\partial^2 M_{red}}{\partial x^2} + \frac{yf}{n} X q_M \quad (6.9)$$

Equation 6.4 shows the electron balance and is the reformulated form of Ohm's law ($J=\kappa E$), with J as current density, κ as conductivity (reciprocal of resistivity: $1/\rho$) and E as electric field, in this case anode potential. The first order derivative of the Ohm's law with respect to the space the biofilm length 'x' gives Equation (6.10). J_D is the current density generated through DET (Marcus et al. 2007) and E is the local biofilm potential. All the potential values mentioned in this chapter are with respect to Ag/AgCl unless otherwise mentioned.

$$\frac{\partial j_D}{\partial x} = -\kappa \frac{\partial^2 E}{\partial x^2} \quad (6.10)$$

Specific substrate utilization rate (q_M) via mediated electron transfer is given by Equation (6.11). It is a multiplicative Monod model in which q_M is defined as a function of S, M_{ox} and the incident light intensity I_o.

$$q_M = q_{max} \left[\frac{S}{S+k_S}\right] \left[\frac{M_{ox}}{M_{ox}+k_M}\right] \left[\frac{I_o}{I_o+k_I+\frac{I_o^2}{k_{in}}}\right] \quad (6.11)$$

Specific substrate utilization rate (q_D) via direct electron transfer is given by Equation (6.12). It is also a multiplicative Monod model in which q_D is defined as a function of S, E (Nernst-Monod term) (Marcus et al. 2007; Torres et al. 2008) and the incident light intensity I_o.

$$q_D = q_{max}\left[\frac{S}{S+k_S}\right]\left[\frac{1}{1+\exp\left\{-\frac{F}{RT}(E-E_{k_A})\right\}}\right]\left[\frac{I_o}{I_o+k_I+\frac{I_o^2}{k_{in}}}\right] \quad (6.12)$$

In both Equations (6.11) and (6.12), the effect of incident light intensity is included via term I_o, to explicitly characterize the photosynthetic microbial fuel cell (P-MFC) which is the novel term included in this model, since incident light intensity greatly affects the photocurrent generation (as evident from our earlier research work reported in chapter 2).

Current generated by MET is given by Equation (6.13)

$$j_M = F\,n\,(r_{ox} - r_{red}) \quad (6.13)$$

Where r_{ox} is the oxidation rate of M_{red} at the electrode surface and r_{red} is the reduction rate of M_{ox} at the electrode surface are given by Equations (6.14) and (6.15) respectively.

$$r_{ox} = M_{red}\,k_o \exp\left[(1-\alpha)\frac{nF}{RT}(\varepsilon - E^{\circ})\right] \quad (6.14)$$

$$r_{red} = M_{ox}\,k_o \exp\left[-\alpha\frac{nF}{RT}(\varepsilon - E^{\circ})\right] \quad (6.15)$$

Table 6.2: List of dependent variables used in the model

Dependent Variable	Description	Dimension
S	Substrate concentration	mol m^{-3}
M_{ox}	Concentration of oxidized form of mediator	mol m^{-3}
M_{red}	Concentration of reduced form of mediator	mol m^{-3}
E	Local biofilm potential	V
q_D	Specific substrate utilization rate via MET	mol $gDCW^{-1}$ s^{-1}
q_M	Specific substrate utilization rate via DET	mol $gDCW^{-1}$ s^{-1}
j	Total current density	A m^{-2}
j_D	Current density from DET	A m^{-2}
j_M	Current density from DET	A m^{-2}

Table 6.3: List of independent variables used in the model

Independent Variable	Description	Value	Dimension
X	Biomass concentration	1700	$gDCW^{-1}$ m^{-3}
I_o	Incident light intensity	0.8×10^{-3}	mol m^{-2} s^{-1}
ε	Polarized electrode potential	0.3	V

Table 6.4: List of constants used in the model

Constant	Description	Value	Dimension
D_{eS}	Effective diffusion coefficient of substrate	1.09×10^{-9}	m^2 s^{-1}
D_{eM}	Effective diffusion coefficient of mediator	0.43×10^{-9}	m^2 s^{-1}
y	Electron equivalence of substrate	4	-
f	Fraction of electron recoverable for current	0.6	-
n	Electron transferred per redox reaction of mediator	2	-
q_{max}	Maximum specific substrate utilization rate	2×10^{-6}	mol $gDCW^{-1}$ s^{-1}
k_S	Half-saturation constant for substrate	13.2	mol m^{-3}
k_M	Half-saturation constant for mediator	0.1×10^{-3}	mol m^{-3}
k_I	Light saturation coefficient	2.08×10^{-4}	mol m^{-2} s^{-1}
k_{in}	Light photoinhibition coefficient	3.33	mol m^{-2} s^{-1}
F	Faraday constant	96485	A s mol^{-1}
R	Universal gas constant	8.314	J K^{-1} mol^{-1}
T	Temperature	303.15	K
E_{KA}	Half maximum rate potential	-0.155	V
α	Transfer coefficient	0.5	-
k_o	Standard heterogenous rate constant	1.6×10^{-5}	m s^{-1}
E^o	Standard redox potential of the mediator	-0.2	V
κ	Biofilm conductivity	5×10^{-5}	A V^{-1} m^{-1}

Current generated by DET is given by Equation (6.16)

$$\frac{\partial j_D}{\partial x} = F\, y\, f\, X\, q_D \tag{6.16}$$

The total current is sum of the current generated by MET and DET is given by Equation (6.17).

$$j = j_M + j_D \tag{6.17}$$

1.25 Solving the PDEs in MATLAB

The governing equations are given in the form of four second order PDEs as Equations (6.7) – (6.10). The system of four second order PDEs was solved using the 'pdepe' solver in MATLAB. The detailed procedure for using the pdepe solver is described in Mathwork (Mathwork 2011). The initial condition and a set of two boundary conditions to solve the second order PDEs for all the four equations are given in Table 6.5. The concentration of substrate and the M_{ox} in the bulk solution were 25 mM and 1 μM respectively and there was no M_{red} present in the bulk solution. The applied anode potential was 0.3 V (vs Ag/AgCl).

The MATLAB returned the solution for all the PDEs and all the 3-D and 2-D graphs were generated using MATLAB. The source code used to solve the PDEs in MATLAB is given in Appendix K. The mesh size used were 100 x 100 (i.e. the biofilm length of 100 μm was divided into 100 intervals with 1 μm as each mesh dimension and the simulation time of 2 s was divided into 100 intervals with 0.02 s as each mesh dimension).

Table 6.6: Initial condition and boundary conditions used to solve the second order PDEs given in Equations (6.7) – (6.10)

Initial condition at t = 0	**Boundary condition 1 at x = 0**	**Boundary condition 2 at x = L**
S = S (bulk)	$\frac{\partial S}{\partial x} = 0$ Nuemann BC (no flux at electrode)	S = S (bulk) Dirichlet BC (defined concentration)
M_{ox} = 0	$\frac{\partial M_{ox}}{\partial x} = -\frac{1}{D_{eM}}(r_0 - r_r)$ Nuemann BC (Butler-Volmer flux at electrode)	$M_{ox} = M_{ox}$ (bulk) Dirichlet BC (defined concentration)
$M_{red} = M_{ox}$ (bulk)	$\frac{\partial M_{red}}{\partial x} = -\frac{1}{D_{eM}}(r_r - r_o)$ Nuemann BC (Butler-Volmer flux at electrode)	M_{red} = 0 Dirichlet BC (defined concentration)
E = ε	E = ε Dirichlet BC (defined potential at electrode)	$\frac{\partial E}{\partial x} = 0$ Nuemann BC (no electron flux beyond biofilm)

The current density generated via MET, j_M, was calculated using Equation (6.13). The current density generated via DET, j_D, was calculated as follows:

Integrating Equation (6.10) with respect to 'x' gives the following Equation (6.11)

$$j_D = -\kappa \frac{\partial E}{\partial x} + C \qquad (6.18)$$

At x = L, j_D = 0 and $\frac{\partial E}{\partial x} = 0$, which gives the value C =0. Applying this condition, the j_D was calculated using the following Equation (6.19). The local biofilm potential 'E' obtained by

solving the PDE (Equation (6.10)), was used to calculate the change of E over time t at the electrode surface (x=0).

$$j_D(x=0) = -\kappa \frac{\partial E}{\partial x}(x=0) \quad (6.19)$$

The total current density, j, was calculated from the Equation (6.17). The effect of light intensity on the total current density was obtained by calculating the total current density as mentioned above after each simulation at different incident light intensity.

1.26 Results and Discussion

The 3-D plots showing the change of concentration of S, M_{ox}, M_{red} and E are shown in Figure 6.2 to Figure 6.5. For ease of understanding, the 3-plots were converted to 2-D plots at four different boundaries (1) the electrode surface (x=0) and (2) the bulk (x=L i.e. 100 μm) over time, and (3) initial time (t=0) and (4) final time ($t=t_f$ i.e. 2 s) across the length of biofilm. The concentration of substrate in the bulk solution was 25 mM. The substrate concentration (S) was found to change over time at the electrode surface, whereas the S was maintained constant at the initial value in the bulk over time (Figure 6.2 and 6.6).

The concentration of M_{ox} in the bulk solution was 1 μM and there was no M_{red} present in the bulk solution. All the M_{ox} in the biofilm were reduced to M_{red} initially due to microbial exoelectrogenicity. Hence, at initial time (t=0), concentration of M_{ox} in the biofilm was 0 and the concentration of M_{red} in the biofilm was equal to 1 μM (similar to M_{ox} in bulk). At varying time, M_{red} would be oxidized at the electrode surface regenerating the M_{ox} back. Simultaneously, M_{ox} would also be reduced at the electrode surface. Thus, the concentration profiles of M_{ox} and M_{red}

were found to vary in contrasting manner across the length of biofilm over time, i.e., increasing concentration gradient of M_{ox} versus decreasing concentration gradient of M_{red} towards the electrode surface as well as bulk solution (Figure 6.3, 6.4, 6.7 and 6.8).

The applied anode potential was 0.3 V (vs Ag/AgCl). While the potential did not change over time at the electrode surface, the local biofilm potential was found to decrease over time across the length of biofilm (Figure 6.5 and 6.9). The local biofilm potential is a function of local concentration of M_{ox} and M_{red} as defined by Nernst equation, and thus was found to vary with varying concentration of M_{ox} and M_{red}. Even though the applied potential is always constant at the electrode surface, the potential changes locally throughout the biofilm and this phenomenon has a greater impact on the microbial exoelectrogenicity locally (Carmona-Martinez et al. 2013). It is interesting to note that the model could capture the change of local biofilm potential across the length of biofilm over time.

The current density generated via both MET (j_M) and DET (j_D) and the total current density (j) were shown in Figure 6.10. Both the j_M and j_D were found to increase over time at the electrode surface, but the magnitude of current densities was different. The current generated via MET was much higher compared to that generated via DET. Hence, the total current density, j, observed in Figure 6.10 bottom panel was almost similar to the j_M. This difference was mainly based on the value of constants used in the simulations. For example, just by increasing the biofilm conductivity, j_D can be increased. By incorporating the parameters measured in the experiments, the model can be made more sophisticated.

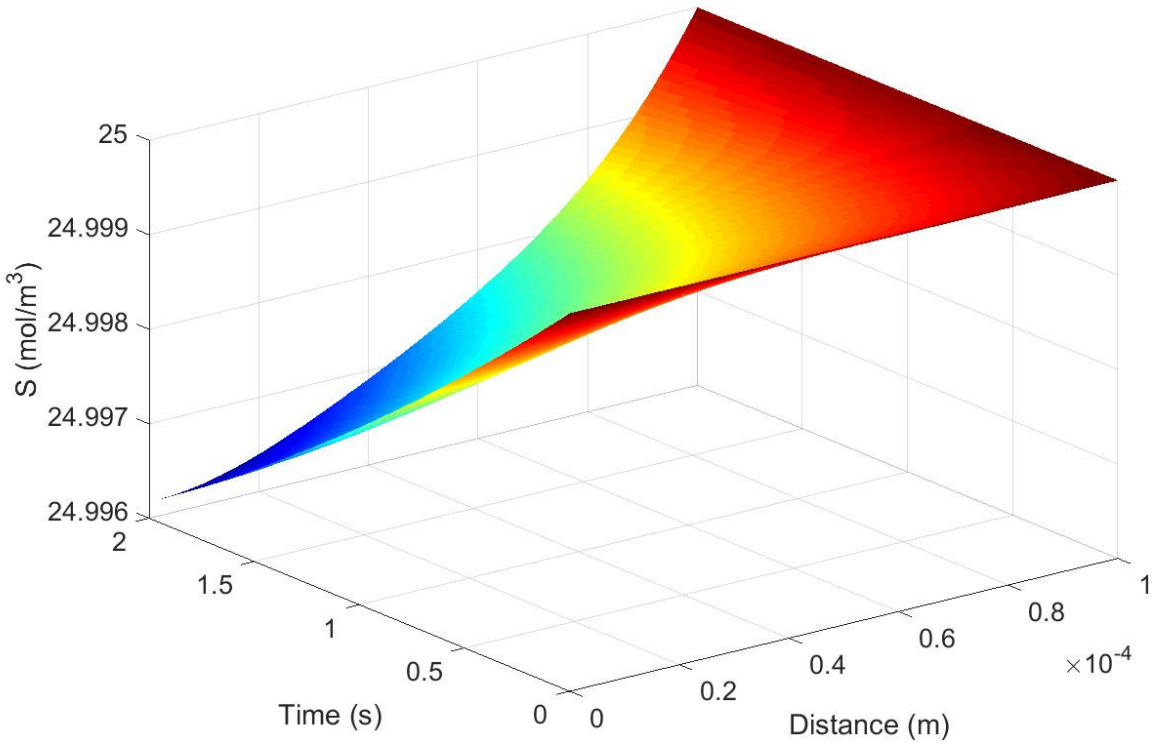

Figure 6.2: Simulated 3-D plot showing change of concentration of substrate over time and across length of biofilm

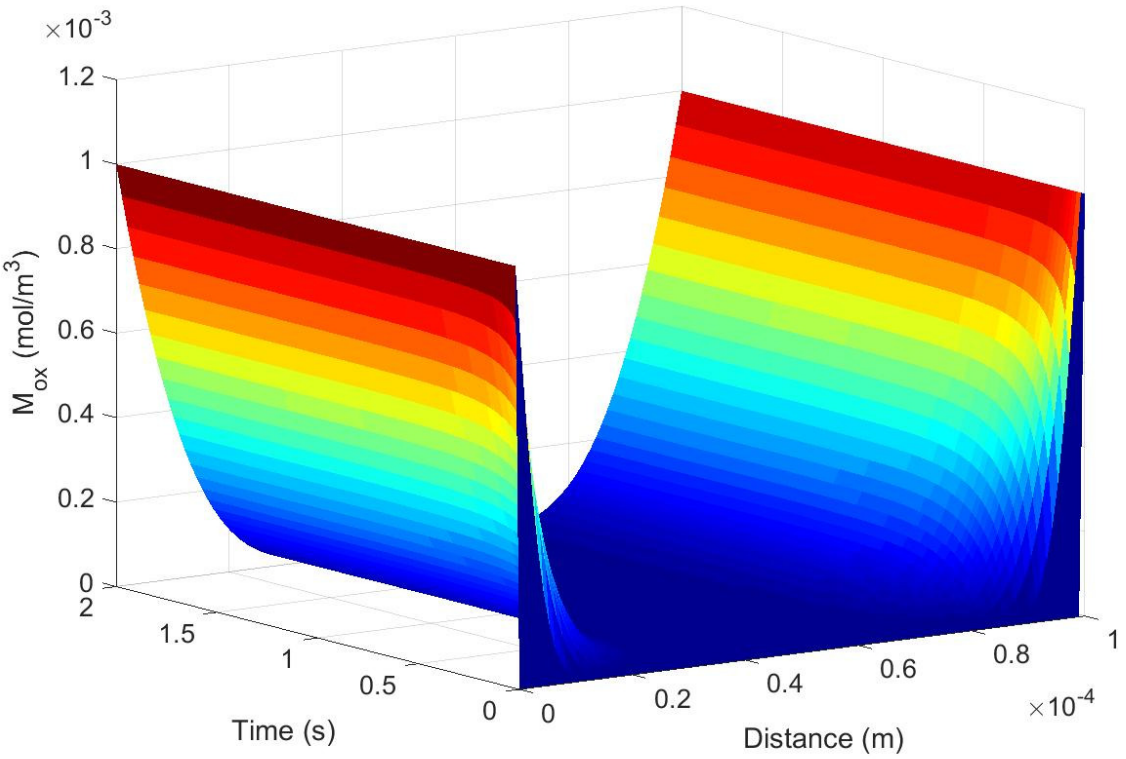

Figure 6.3: Simulated 3-D plot showing change of concentration of oxidized form of mediator over time and across length of biofilm

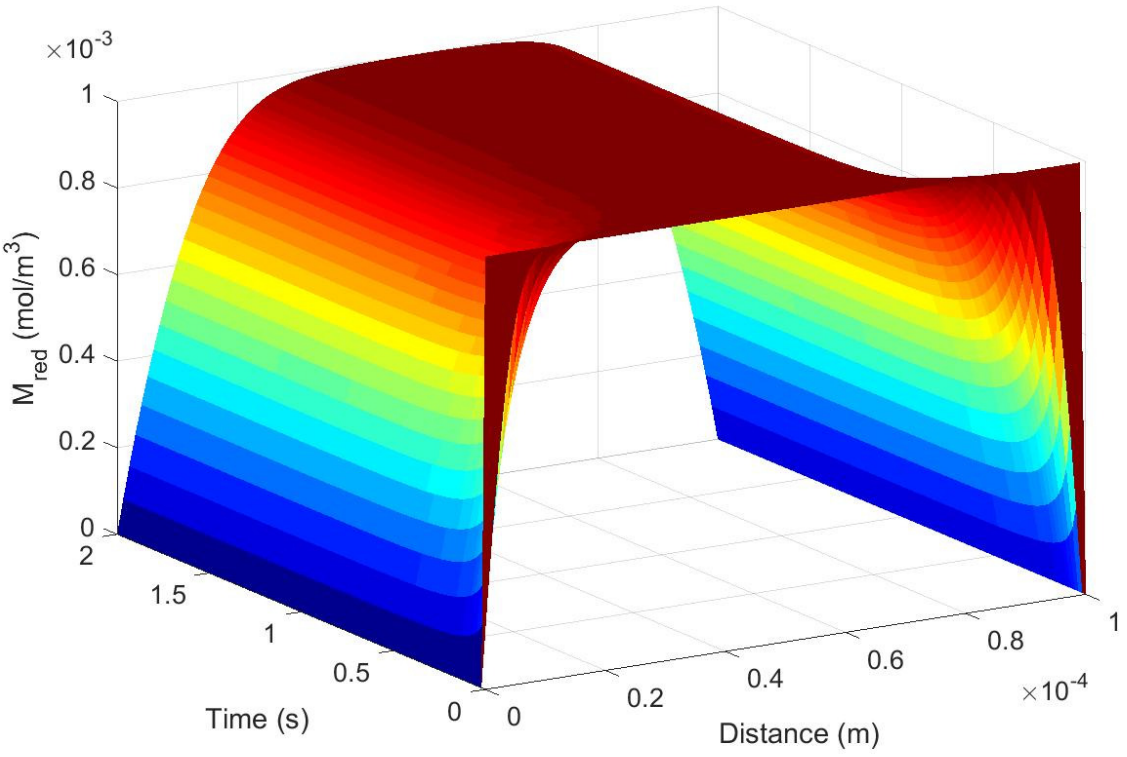

Figure 6.4: Simulated 3-D plot showing change of concentration of reduced form of mediator over time and across length of biofilm

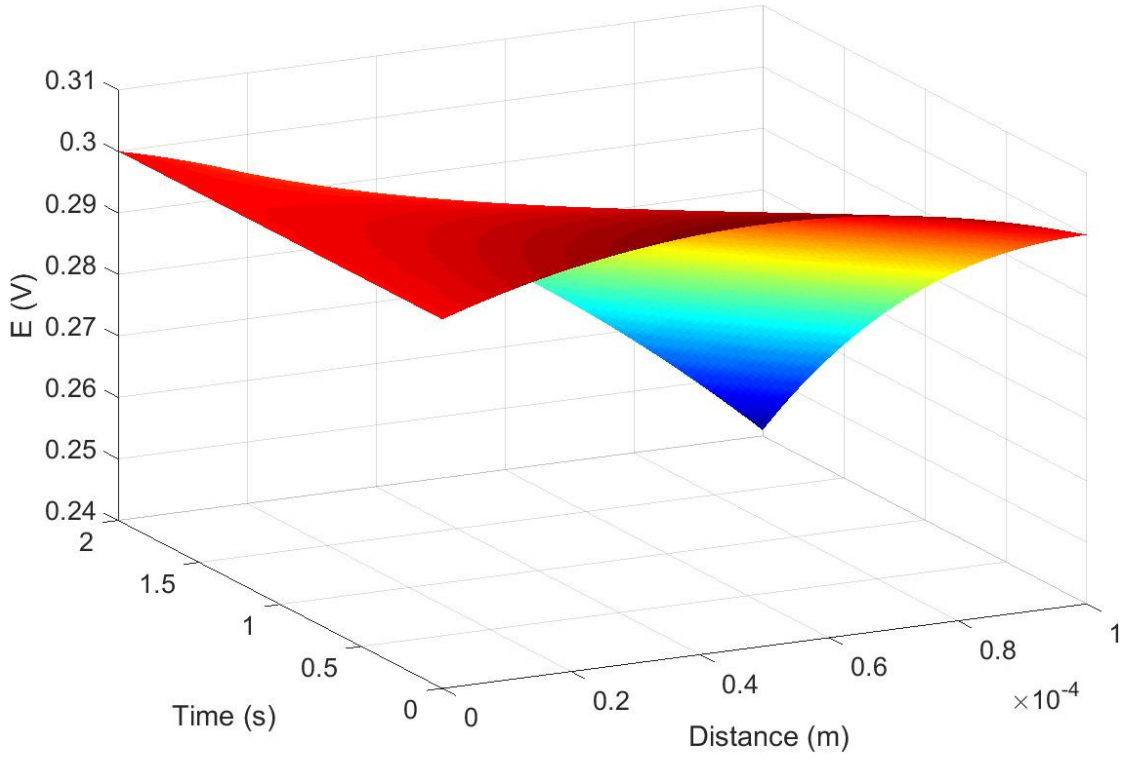

Figure 6.5: Simulated 3-D plot showing change of local biofilm potential over time and across length of biofilm

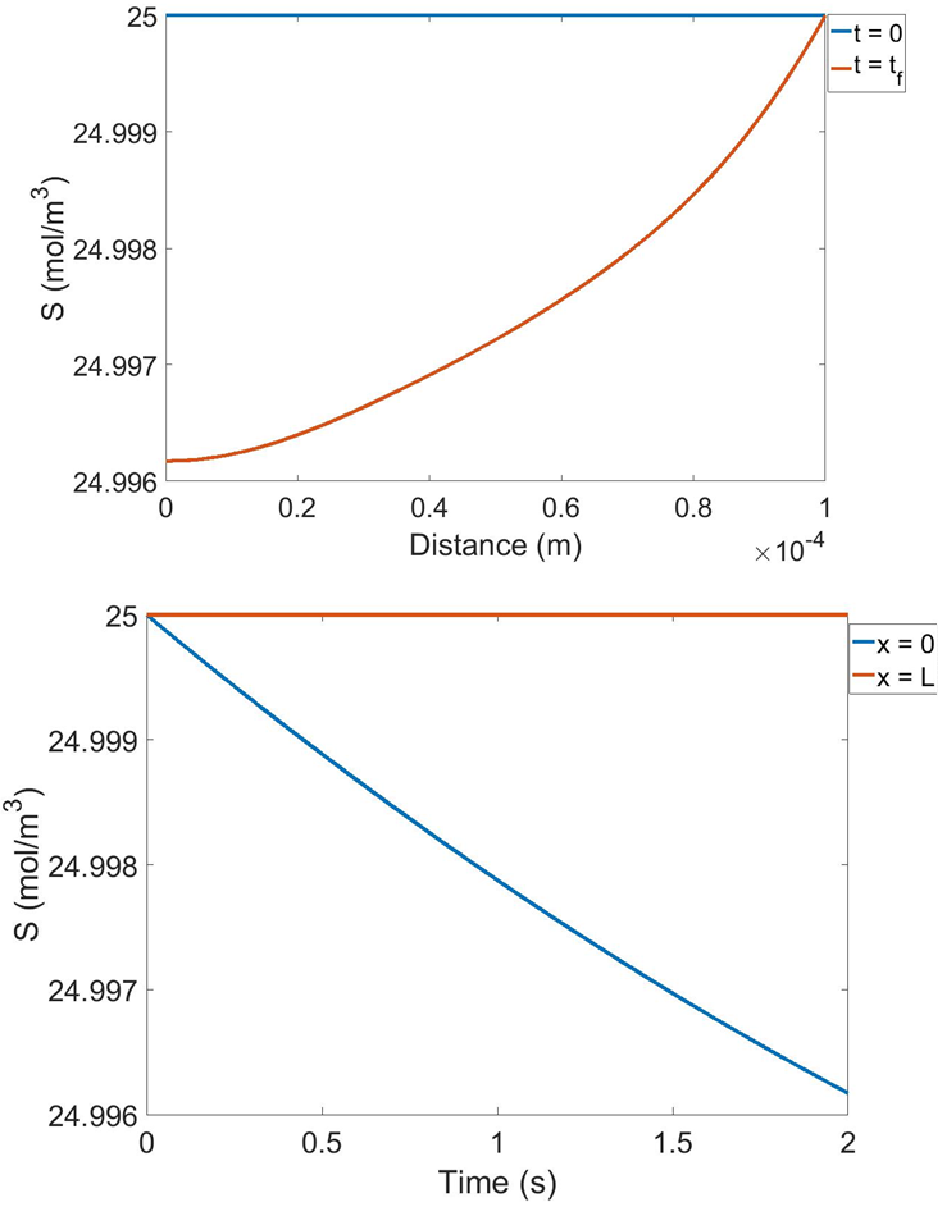

Figure 6.6: 2-D plots obtained from Figure 6.1 showing change of concentration of substrate across length of biofilm (top panel) and over time (bottom panel)

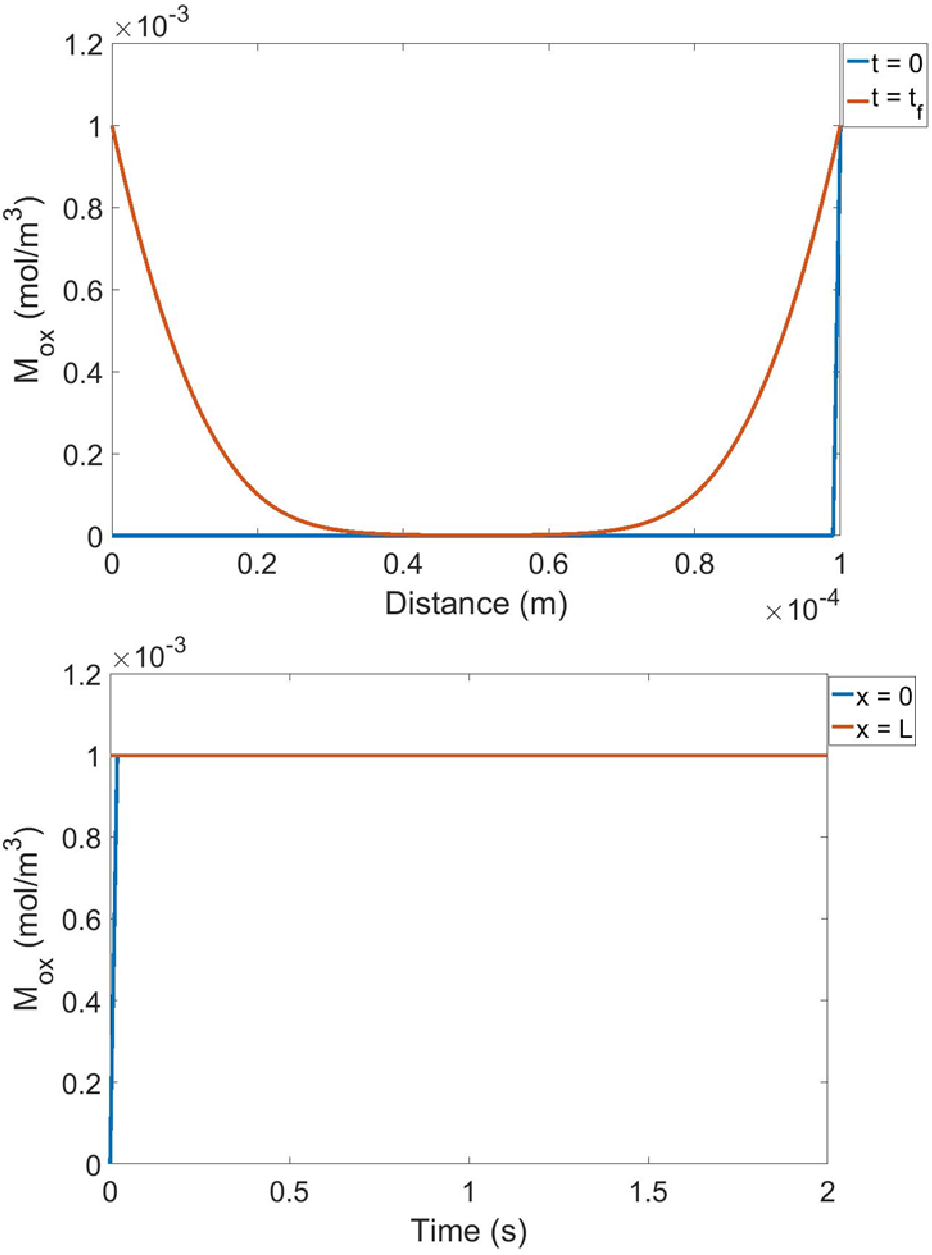

Figure 6.7: 2-D plots obtained from Figure 6.2 showing change of concentration of oxidized form of mediator across length of biofilm (top panel) and over time (bottom panel)

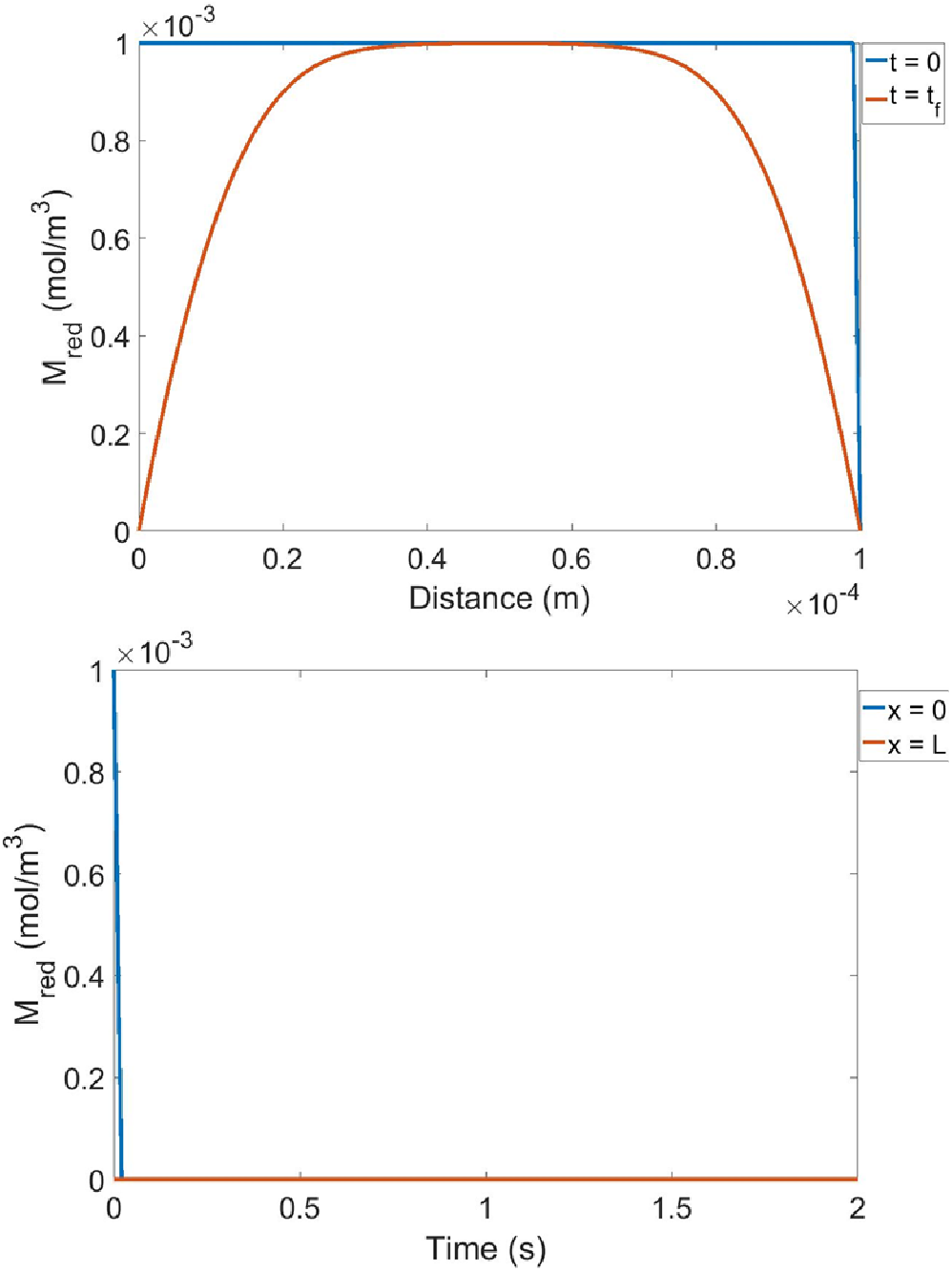

Figure 6.8: 2-D plots obtained from Figure 6.3 showing change of concentration of reduced form of mediator length of biofilm (top panel) and over time (bottom panel)

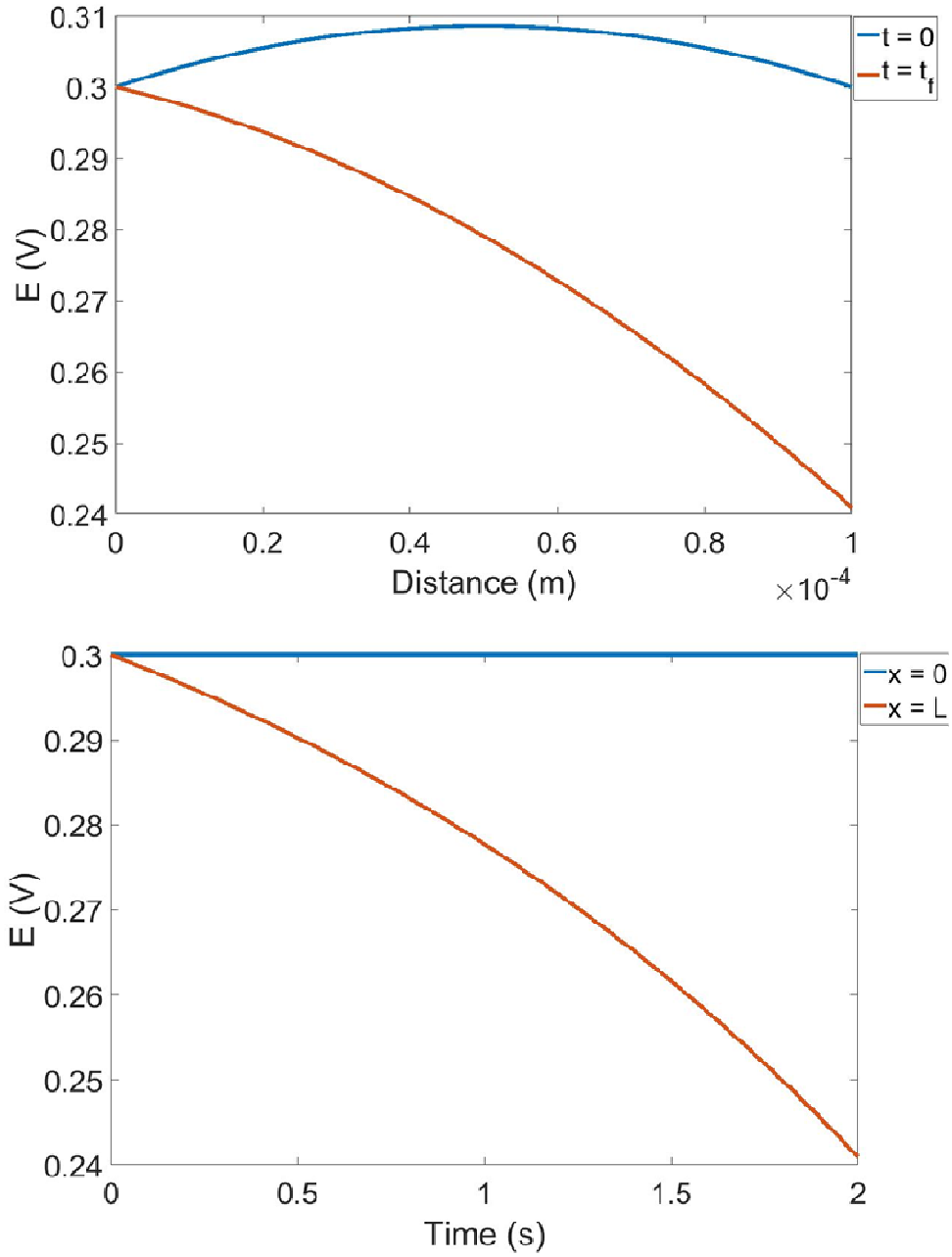

Figure 6.9: 2-D plots obtained from Figure 6.4 showing change of local biofilm potential across length of biofilm (top panel) and over time (bottom panel)

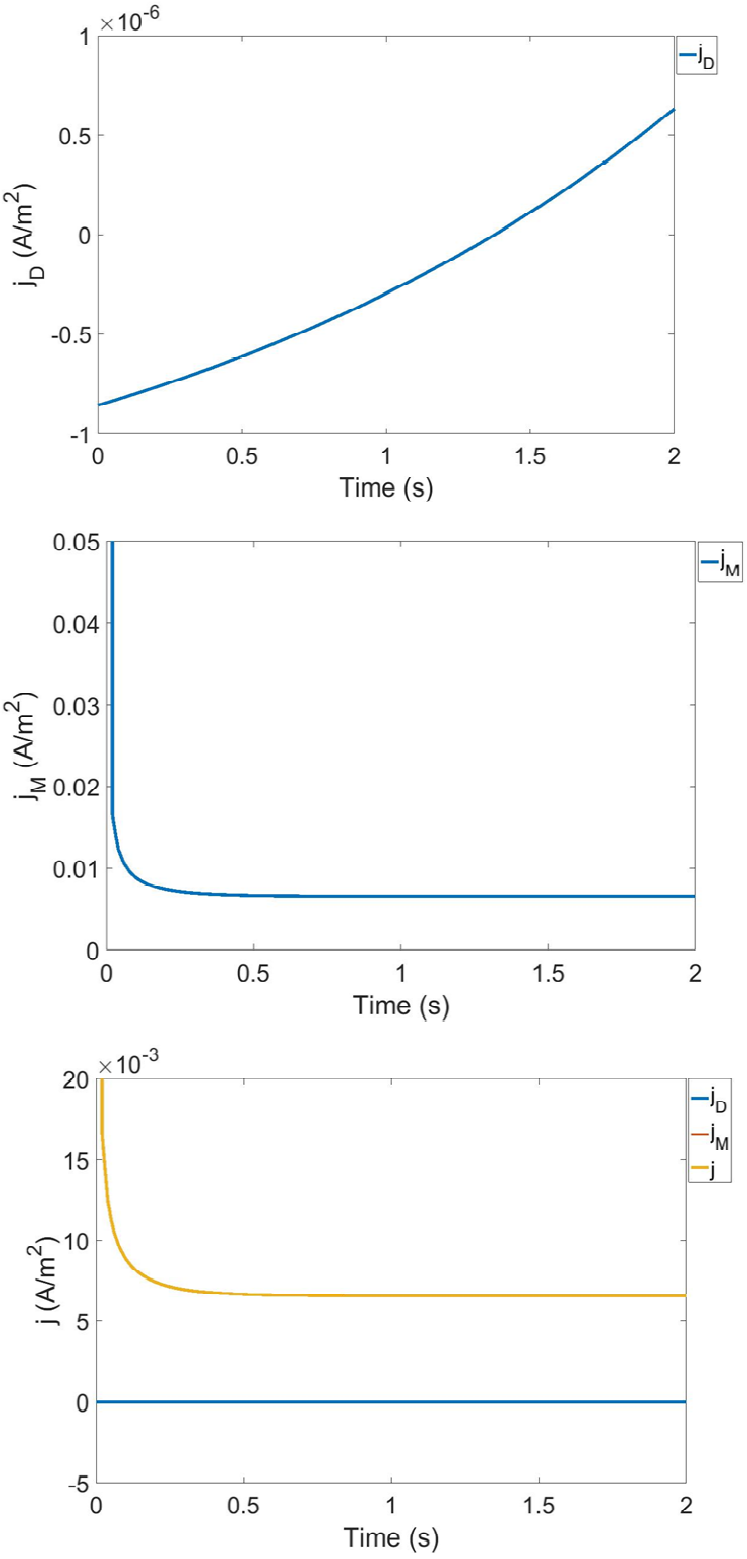

Figure 6.10: 2-D plots showing rate of change of current density generated via DET, j_D (top panel), via MET j_M (middle panel) and comparison of rate of change of total current density j with j_D and j_M (bottom panel) at the electrode surface

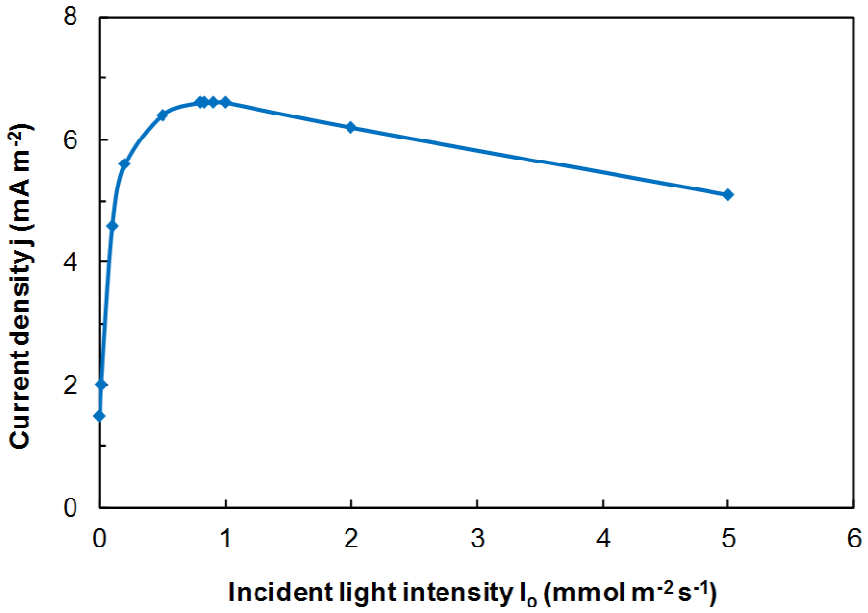

Figure 6.11: Effect of incident light intensity on the current density generated at the electrode surface (current densities mentioned in the y-axis are the total current density, j, calculated by varying the incident light intensity during each simulation)

With increasing incident light intensity, the current density generated at the electrode surface as found to increase initially, reach a plateau and decrease gradually as shown in Figure 6.11. This exactly follows the light saturation and the photo-inhibition kinetics. The model developed in this research work could efficiently capture the effect of light intensity on current generation at the electrode surface. The independent variable used in the model is the incident light intensity (I_o). The developed model can be extended in future by including parameters such as photo-bioreactor geometry, light attenuation, reflectivity, etc., so as to characterize the light dependence of P-MFC performance in practical applications and at higher scale.

1.27 Conclusions

A mathematical model was developed to describe the current generated by a biofilm-based anode via both direct and mediated electron transfer. Further, the effect of incident light intensity on the total current density generated by such system was modeled by including the light saturation and photo-inhibition terms. The developed model was found to capture the influence of light on the electrode performance efficiently in simulations and the model needs to be validated by conducting experiments that measure the current generation at different light intensities. While many complex models had been developed to characterize the MFC, no comprehensive model is available yet to characterize the current generation in the photosynthetic MFC. Considering the facts that the light intensity is one of the important factors influencing the performance of P-MFC and the ability of the developed model to efficiently describe such effect, this model can be considered as a good starting point for engineers to model and optimize the P-MFCs.

CHAPTER 7

CONCLUSIONS AND FUTURE DIRECTION

The electrochemical energy conversion by microorganisms generates electricity in microbial fuel cell. Though, the concept of MFC has been developed in early 1980s, advancement of the technology for a realizable practical application has been hampered mainly due to its limitation in generating lower power densities. Despite conventional engineering efforts undertaken so far, in terms of optimizing the design and the process at macroscopic level, the improvement achieved hitherto is already saturated. A multi-disciplinary approach to study MFC at microscopic level, especially at the microbe-electrode interface has huge advantages and scope to further push the upper limits of MFC performance. Such efforts have been carried out in the research work in three different dimensions:

(1) Enhancing the cyanobacterial exoelectrogenicity:

The research work reported in this dissertation is one such illustration of enhancing the extracellular electron transfer (EET) of microorganism, specifically that of cyanobacteria, by genetically engineering them to improve photocurrent generation in photo-bioelectrochemical cell.

Initially, light dependent exoelectrogenicity of a cyanobacterium named *Nostoc* sp. was studied by immobilizing it onto multi-walled carbon nanotubes modified carbon electrode. Different experimental parameters such as incident light intensity, wavelength of the incident light and biocatalyst loading (cyanobacterial cell concentration) were optimized for maximum photocurrent generation. A photo-bioelectrochemical cell (PBEC) containing *Nostoc* sp. on the multi-walled carbon nanotubes modified anode and an enzyme-based cathode was developed and found to generate a peak power density of 35 mW m^{-2} (18 mW m^{-2}/mW_{light}) without any exogenous mediator, which is the highest among similar photo-bioelectrochemical systems developed so far. However, the power density achieved in this study was lower compared to that generated by dissimilatory metal reducing bacteria (DMRB) in MFCs. Besides, extracellular electron transfer pathways between the cyanobacterium and the carbon nanotubes modified electrode had been elucidated with the help of site-specific photosynthesis inhibitors. Two major conclusions obtained from the study are as follows:

a) electrons were re-routed from the P-ETC of cyanobacteria to the electrode. Plastoquinones were found to contribute predominantly for the EET pathway. However, cyanobacteria did not possess any key players (redox proteins) on their outer membrane to efficiently perform EET.
b) electrons generated in the P-ETC of cyanobacteria were utilized by the competing R-ETC pathways that are simultaneously happening in the thylakoid membrane.

These two caveats were overcome in the subsequent work by genetically engineering the cyanobacteria to achieve specific objective and are concluded as given below.

Strategy 1:

Cyanobacterium named *Synechococcus elongatus* PCC7942 had been genetically engineered to express an outer membrane c-type cytochrome known as OmcS, similar to that present in DMRB. The expression of active OmcS in genetically engineered CB (Eng-CB) was confirmed through heme staining. Eng-CB was found to exhibit enhanced EET as evident from both the higher rate of ferricyanide reduction (~2 fold) and higher photocurrent generation (~ 9 fold) compared to the wild-type CB. The higher rate of ferricyanide reduction under both light and dark conditions by Eng-CB underlined the fact that the OmcS interacted with both P-ETC and R-ETC of the cyanobacteria. In a rudimentary PBEC, the Eng-CB was observed to generate ~ 5-fold higher power density than that generated by the wild-type CB.

Strategy 2:

Each of the three terminal respiratory oxidases (bd-quinol oxidase, aa_3-cytochrome oxidase and cbb_3-cytochrome oxidase) in *S. elongatus* was knocked-out, one at a time, to study the role of these oxidases for its exoelectrogenicity. The knock-out mutant *cyd*$^-$ (the mutant strain lacking bd-quinol oxidase) exhibited better EET as evident from its higher ferricyanide reduction rate. This experimental result clearly confirmed that the bd-quinol oxidase diverted more electrons from the P-ETC and thus knocking it out certainly enhanced the exoelectrogenicity in cyanobacteria.

Combining the above two strategies, the strain *cyd*$^-$*omcs* (i.e., CB that contain OmcS, but lack

bd-quinol oxidase) was constructed and was found to generate more photocurrent compared to the corresponding controls (*wt*, c*yd*$^-$ and *omcs*). This work highlights the scope for enhancing photocurrent generation in cyanobacteria through genetic engineering, thereby benefiting faster advancement of the P-MFC technology.

(2) Exploring the exoelectrogenicity of a hyperthermophile:

In addition to improving exoelectrogenicity of the model microorganisms such as DMRB and cyanobacteria, exploring microorganisms that possess unique metabolic capability to be employed in MFC would certainly advance the application of MFC in various environmental niches. Towards this endeavour, a pure culture of hyperthermophilic microorganism called *Pyrococcus furiosus* was investigated for the first time, in a MFC that was operated at 90 ^oC. Unlike CB, *P. furiosus* was found to generate H_2 by consuming sugars and peptides via the simplest respiratory chain. The MFC that contained anode with *P. furiosus* biofilm showed significantly higher electrochemical response compared to that of the control MFC. The EET of *Pf* was also witnessed from its capability to reduce both Fe_2O_3 and ferric citrate in growth medium and suspension culture respectively at 90 ^oC. The proof of concept study reported in this dissertation highlights the potential of *Pf* to generate electricity in MFCs at high temperature locations. Moreover, such studies also help to advance our understanding in the field of biogeochemistry of the early hot environment and exobiology.

(3) Developing a Mathematical Model for P-MFC

An important aspect of commercialization of any technology is scale-up the prototype, i.e., from a lab-scale system to a practical real-time device. Mathematical modelling is a powerful predictive methodology to design and optimize the performance of the device in the journey of scale-up. A mathematical model was developed to describe current generation by a biofilm-based anode that contained photosynthetic microorganism. The effect of incident light intensity on the photocurrent generation was modelled by incorporating important factors such as light saturation and photo-inhibition. The developed model was found to characterize the influence of light intensity on the electrode performance efficiently in simulations. While a lot of complex models had been developed to characterize the MFC, no comprehensive model is available yet to characterize the current generation in the photosynthetic MFC. Considering the facts that the light intensity is one of the important factors influencing the performance of P-MFC and the ability of the developed model to efficiently describe such effect, this model can be considered as a good starting point for engineers to model and optimize the P-MFCs.

Future Directions

The following directions emerged from the overall research work reported in this dissertation and provide scope for future experiments to better characterize and/or enhance the microbial exoelectrogenicity.

1) Where does the OmcS localize in the genetically engineered *S. elongatus*, i.e., the presence of OmcS in different membrane systems of cyanobacteria such as outer membrane, cytoplasmic membrane and/or thylakoid membrane?
2) How does the OmcS interact with the photosynthetic and respiratory electron transport chains? Whom does it talk to, inside the genetically engineering *S. elongatus*?
3) Construction of double and triple knock-out mutants that lack the combination of respiratory terminal oxidases and their characterization for EET.
4) Elucidate extracellular electron transport pathways in *P. furiosus* and the prospects for enhancing the same.
5) Extend the mathematical model to include cathode so as to describe and optimize the performance of photo-bioelectrochemical cell and validate the model through experiments.

REFERENCES

Acharya K, Zazubovich V, Reppert M, Jankowiak R. 2012. Primary Electron Donor(s) in Isolated Reaction Center of Photosystem II from Chlamydomonas reinhardtii. Journal of Physical Chemistry B 116(16):4860-4870.

Adams MWW, Holden JF, Menon AL, Schut GJ, Grunden AM, Hou C, Hutchins AM, Jenney FE, Kim C, Ma KS and others. 2001. Key role for sulfur in peptide metabolism and in regulation of three hydrogenases in the hyperthermophilic archaeon Pyrococcus furiosus. Journal of Bacteriology 183(2):716-724.

Ahmed J, Park W, Kim S. 2009. Photoelectric Activity of Thylakoid Layer Formed on Gold via Aminoalkanethiol Self-Assembled Monolayers. Bulletin of the Korean Chemical Society 30(10):2195-2196.

Badura A, Esper B, Ataka K, Grunwald C, Woll C, Kuhlmann J, Heberle J, Rogner M. 2006. Light-driven water splitting for (bio-)hydrogen production: photosystern 2 as the central part of a bioelectrochemical device. Photochemistry and Photobiology 82(5):1385-1390.

Badura A, Guschin D, Esper B, Kothe T, Neugebauer S, Schuhmann W, Rogner M. 2008. Photo-induced electron transfer between photosystem 2 via cross-linked redox hydrogels. Electroanalysis 20(10):1043-1047.

Basen M, Sun J, Adams MWW. 2012. Engineering a Hyperthermophilic Archaeon for TemperatureDependent Product Formation. mBio 3(2):1-8.

Bechet Q, Shilton A, Guieysse B. 2013. Modeling the effects of light and temperature on algae growth: State of the art and critical assessment for productivity prediction during outdoor cultivation. Biotechnology Advances 31(8):1648-1663.

Bedford NM, Winget GD, Punnamaraju S, Steckl AJ. 2011. Immobilization of Stable Thylakoid Vesicles in Conductive Nanofibers by Electrospinning. Biomacromolecules 12(3):778-784.

Bendall DS, Manasse RS. 1995. Cyclic photophosphorylation and electron-transport. Biochimica Et Biophysica Acta-Bioenergetics 1229(1):23-38.

Berry S, Schneider D, Vermaas WFJ, Rogner M. 2002. Electron transport routes in whole cells of Synechocystis sp strain PCC 6803: The role of the cytochrome bd-type oxidase. Biochemistry 41(10):3422-3429.

Beyenal H, Babauta JT. 2015. Biofilms in bioeelctrochemcial systems. Hoboken, NJ, US: John Wiley & Sons, Inc.,.

Blankenship RE, Tiede DM, Barber J, Brudvig GW, Fleming G, Ghirardi M, Gunner MR, Junge W, Kramer DM, Melis A and others. 2011. Comparing Photosynthetic and Photovoltaic Efficiencies and Recognizing the Potential for Improvement. Science 332(6031):805-809.

Boghossian AA, Ham MH, Choi JH, Strano MS. 2011. Biomimetic strategies for solar energy conversion: a technical perspective. Energy & Environmental Science 4(10):3834-3843.

Bombelli P, Bradley RW, Scott AM, Philips AJ, McCormick AJ, Cruz SM, Anderson A, Yunus K, Bendall DS, Cameron PJ and others. 2011. Quantitative analysis of the factors limiting solar power transduction by Synechocystis sp. PCC 6803 in biological photovoltaic devices. Energy & Environmental Science 4(11):4690-4698.

Bradley RW, Bombelli P, Lea-Smith DJ, Howe CJ. 2013. Terminal oxidase mutants of the cyanobacterium Synechocystis sp PCC 6803 show increased electrogenic activity in

biological photo-voltaic systems. Physical Chemistry Chemical Physics 15(32):13611-13618.
Bryant DA. 1994. Advances in photosynthesis: The molecular biology of cyanobacteria. The Netherlands: Kluwer Academic Publishers.
Burgstaller HM. 2012. Respiratory terminal oxidases of the cyanobacterium *Synechococcus* sp. strain PCC7942. Vienna: University of Vienna. 101 p.
Busalmen JP, Esteve-Nunez A, Berna A, Feliu JM. 2008. C-type cytochromes wire electricity-producing bacteria to electrodes. Angewandte Chemie-International Edition 47(26):4874-4877.
Calkins JO, Umasankar Y, O'Neill H, Ramasamy RP. 2013. High photo-electrochemical activity of thylakoid-carbon nanotube composites for photosynthetic energy conversion. Energy & Environmental Science 6(6):1891-1900.
Cape JL, Bowman MK, Kramer DM. 2006. Understanding the cytochrome bc complexes by what they don't do. The Q-cycle at 30. Trends in Plant Science 11(1):46-55.
Carmona-Martinez AA, Harnisch F, Kuhlicke U, Neu TR, Schroeder U. 2013. Electron transfer and biofilm formation of Shewanella putrefaciens as function of anode potential. Bioelectrochemistry 93:23-29.
Carpentier R, Lemieux S, Mimeault M, Purcell M, Goetze DC. 1989. A photoelectrochemical cell using immobilized photosynthetic membranes. Bioelectrochemistry and Bioenergetics 22(3):391-401.
Ciesielski PN, Scott AM, Faulkner CJ, Berron BJ, Cliffel DE, Jennings GK. 2008. Functionalized Nanoporous Gold Leaf Electrode Films for the Immobilization of Photosystem I. ACS Nano 2(12):2465-2472.
Clauwaert P, Aelterman P, Pham TH, De Schamphelaire L, Carballa M, Rabaey K, Verstraete W. 2008. Minimizing losses in bio-electrochemical systems: the road to applications. Applied Microbiology and Biotechnology 79(6):901-913.
Das R, Kiley PJ, Segal M, Norville J, Yu AA, Wang LY, Trammell SA, Reddick LE, Kumar R, Stellacci F and others. 2004. Integration of photosynthetic protein molecular complexes in solid-state electronic devices. Nano Letters 4(6):1079-1083.
David L. Nelson MMC. 2008. Lehninger Principles of Biochemistry. 5 ed: Palgrave Macmillan.
de Wijn R, van Gorkom HJ. 2001. Kinetics of electron transfer from Q(A) to Q(B) in photosystem II. Biochemistry 40(39):11912-11922.
Duysens LNM. 1963. Photosynthetic Mechanisms of Green Plants. Washington, DC: Publ 1145 NAS-NRC.
Enami I, Kaneko M, Kitamura N, Koike H, Sonoike K, Inoue Y, Katoh S. 1991. Total immobilization of the extrinsic 33-KDa protein in spinach photosystem-II membrane preparations - protein stoichiometry and stabilization of oxygen evolution. Biochimica Et Biophysica Acta 1060(2):224-232.
Faulkner CJ, Lees S, Ciesielski PN, Cliffel DE, Jennings GK. 2008. Rapid assembly of photosystem I monolayers on gold electrodes. Langmuir 24(16):8409-8412.
Fiala G, Stetter KO. 1986. Pyrococcus furiosus sp-nov represents a novel genus of marine heterotrophic archaebacteria growing optimally at 100 degrees C. Archives of Microbiology 145(1):56-61.
Fromme P, Jordan P, Krauss N. 2001. Structure of photosystem I. Biochimica Et Biophysica Acta-Bioenergetics 1507(1-3):5-31.

Fu Q, Fukushima N, Maeda H, Sato K, Kobayashi H. 2015. Bioelectrochemical analysis of a hyperthermophilic microbial fuel cell generating electricity at temperatures above 80 degrees C. Bioscience Biotechnology and Biochemistry 79(7):1200-1206.

Fu Q, Kobayashi H, Kawaguchi H, Wakayama T, Maeda H, Sato K. 2013. A Thermophilic Gram-Negative Nitrate-Reducing Bacterium, Calditerrivibrio nitroreducens, Exhibiting Electricity Generation Capability. Environmental Science & Technology 47(21):12583-12590.

Fuerst EP, Norman MA. 1991. Interactions of herbicides with photosynthetic electron-transport. Weed Science 39(3):458-464.

Fultz ML, Durst RA. 1982. Mediator compounds for the electrochemical study of biological redox systems - a compilation. Analytica Chimica Acta 140(1):1-18.

Furukawa Y, Moriuchi T, Morishima K. 2006. Design principle and prototyping of a direct photosynthetic/metabolic biofuel cell (DPMFC). Journal of Micromechanics and Microengineering 16(9):S220-S225.

Girguis PR, Holden JF. 2012. On the Potential for Bioenergy and Biofuels from Hydrothermal Vent Microbes. Oceanography 25(1):213-217.

Goldsmith JO, Boxer SG. 1996. Rapid isolation of bacterial photosynthetic reaction centers with an engineered poly-histidine tag. Biochimica Et Biophysica Acta-Bioenergetics 1276(3):171-175.

Gorby YA, Yanina S, McLean JS, Rosso KM, Moyles D, Dohnalkova A, Beveridge TJ, Chang IS, Kim BH, Kim KS and others. 2006. Electrically conductive bacterial nanowires produced by Shewanella oneidensis strain MR-1 and other microorganisms. PNAS 103(30):11358–11363.

Green MA, Emery K, Hishikawa Y, Warta W. 2010. Solar cell efficiency tables (version 35). Progress in Photovoltaics 18(2):144-150.

Guikema JA, Yocum CF. 1978. Evidence for Two Sites of Inhibition of Photosynthetic Electron Transport by Dibromothymoquinone. Archives of Biochemistry and Biophysics 189(2):508-515.

Guskov A, Kern J, Gabdulkhakov A, Broser M, Zouni A, Saenger W. 2009. Cyanobacterial photosystem II at 2.9-angstrom resolution and the role of quinones, lipids, channels and chloride. Nature Structural & Molecular Biology 16(3):334-342.

Hanke GT, Hase T. 2008. Variable Photosynthetic Roles of Two Leaf-type Ferredoxins in Arabidopsis, as Revealed by RNA Interference. Photochemistry and Photobiology 84(6):1302-1309.

Hart SE, Schlarb-Ridley BG, Bendall DS, Howe CJ. 2005. Terminal oxidases of cyanobacteria. Biochemical Society Transactions 33(4):832-835.

Hasan K, Yildiz HB, Sperling E, Conghaile PO, Packer MA, Leech D, Hagerhall C, Gorton L. 2014. Photo-electrochemical communication between cyanobacteria (Leptolyngbia sp.) and osmium redox polymer modified electrodes. Physical Chemistry Chemical Physics 16(45):24676-24680.

He Z, Kan J, Mansfeld F, Angenent LT, Nealson KH. 2009. Self-Sustained Phototrophic Microbial Fuel Cells Based on the Synergistic Cooperation between Photosynthetic Microorganisms and Heterotrophic Bacteria. Environmental Science & Technology 43(5):1648-1654.

Herrero A, Flores E. 2008. The cyanobacteria: Molecular biology, genomics and evolution. Norfolk, UK: Caister Academic Press.

Hoffert MI, Caldeira K, Benford G, Criswell DR, Green C, Herzog H, Jain AK, Kheshgi HS, Lackner KS, Lewis JS and others. 2002. Advanced technology paths to global climate stability: Energy for a greenhouse planet. Science 298(5595):981-987.

Hosler JP, Yocum CF. 1987. Regulation of cyclic photophosphorylation during ferredoxin-mediated electron-transport - effect of DCMU and the NADPH NADP+ ratio. Plant Physiology 83(4):965-969.

Howitt CA, Vermaas WFJ. 1998. Quinol and cytochrome oxidases in the cyanobacterium *Synechocystis* sp. PCC6803. Biochemistry 37:17944-17951.

Hsu BD, Lee JY, Pan RL. 1986 The two binding sites for DCMU in photosystem II. Biochemical and Biophysical Research Communications 141(2):682-688.

Ivleva NB, Bramlett MR, Lindahl PA, Golden SS. 2005. LdpA: a component of the circadian clock senses redox state of the cell. Embo Journal 24(6):1202-1210.

Izawa S, Kraayenhof R, Ruuge EK, Devault D. 1973. The site of KCN inhibition in the photosynthetic electron transport pathway. Biochimica et Biophysica Acta 314:328-339.

Jacobs J, Pudollek S, Hemschemeier A, Happe T. 2009. A novel, anaerobically induced ferredoxin in Chlamydomonas reinhardtii. FEBS Letters 583(2):325-329.

Joet T, Cournac L, Horvath EM, Medgyesy P, Peltier G. 2001. Increased sensitivity of photosynthesis to antimycin A induced by inactivation of the chloroplast ndhB gene. Evidence for a participation of the NADH-dehydrogenase complex to cyclic electron flow around photosystem I. Plant Physiology 125(4):1919-1929.

Kashefi K, Tor JM, Nevin KP, Lovley DR. 2001. Reductive precipitation of gold by dissimilatory Fe(III)-Reducing Bacteria and Archaea. Applied and Environmental Microbiology 67(7):3275-3279.

Katz E. 1994. Application of bifunctional reagents for immobilization of proteins on a carbon electrode surface: Oriented immobilization of photosynthetic reaction centers. J. Electroanal. Chem 365:157-164.

Katz E, Shkuropatov AY, Shuvalov VA. 1990. Electrochemical approach to the development of a photoelectrode on the basis of photosynthetic reaction centers. Bioelectrochem. Bioenerg. 23:239-247.

Katz E, Shkuropatov AY, Vagabova OI, Shuvalov VA. 1989. Coupling of photoinduced charge separation in reaction centers of photosynthetic bacteria with electron transfer to a chemically modified electrode. Biochim. Biophys. Acta 976:121-128.

Keller MW, Schut GJ, Lipscomb GL, Menon AL, Iwuchukwu IJ, Leuko TT, Thorgersen MP, Nixon WJ, Hawkins AS, Kelly RM and others. 2013. Exploiting microbial hyperthermophilicity to produce an industrial chemical, using hydrogen and carbon dioxide. Proceedings of the National Academy of Sciences of the United States of America 110(15):5840-5845.

Kengen SWM, Stams AJM, deVos WM. 1996. Sugar metabolism of hyperthermophiles. Fems Microbiology Reviews 18(2-3):119-137.

Kern J, Renger G. 2007. Photosystem II: Structure and mechanism of the water : plastoquinone oxidoreductase. Photosynthesis Research 94(2-3):183-202.

Koning SM, Elferink MGL, Konings WN, Driessen AJM. 2001. Cellobiose uptake in the hyperthermophilic archaeon Pyrococcus furiosus is mediated by an inducible, high-affinity ABC transporter. Journal of Bacteriology 183(17):4979-4984.

Kouchkovsky Y, Kouchkovsky F. 1974. Study of the photosynthetic electron transfer reactions in chloroplasts and algae with the plastoquinone antagonist dibromothymoquinone. Bioehimica et Biophysica Acta 368: 113-124.

Lam KB, Irwin EF, Healy KE, Lin LW. 2006a. Bioelectrocatalytic self-assembled thylakoids for micro-power and sensing applications. Sensors and Actuators B-Chemical 117(2):480-487.

Lam KB, Johnson EA, Chiao M, Lin LW. 2006b. A MEMS photosynthetic electrochemical cell powered by subcellular plant photosystems. Journal of Microelectromechanical Systems 15(5):1243-1250.

Larom S, Salama F, Schuster G, Adir N. 2010. Engineering of an alternative electron transfer path in photosystem II. Proceedings of the National Academy of Sciences of the United States of America 107(21):9650-9655.

Lau C, Adkins ER, Ramasamy RP, Luckarift HR, Johnson GR, Atanassov P. 2012. Design of carbon nanotube based gas diffusion electrode for O2 reduction by multi-copper oxidase. Advanced Energy Materials 2:162-168.

Lea-Smith DJ, Bombelli P, Vasudevan R, Howe CJ. 2016. Photosynthetic, respiratory and extracellular electron transport pathways in cyanobacteria. Biochimica et Biophysica Acta 3:247-255.

Leang C, Qian X, Mester T, Lovley DR. 2010. Alignment of the c-Type Cytochrome OmcS along Pili of Geobacter sulfurreducens. Applied and Environmental Microbiology 76(12):4080-4084.

Lebedev N, Trammell SA, Spano A, Lukashev E, Griva I, Schnur J. 2006. Conductive wiring of immobilized photosynthetic reaction center to electrode by cytochrome c. Journal of the American Chemical Society 128(37):12044-12045.

Lee HS, Shockley KR, Schut GJ, Conners SB, Montero CI, Johnson MR, Chou CJ, Bridger SL, Wigner N, Brehm SD and others. 2006. Transcriptional and biochemical analysis of starch metabolism in the hyperthermophilic archaeon Pyrococcus furiosus. Journal of Bacteriology 188(6):2115-2125.

Lin C-C, Wei C-H, Chen C-I, Shieh C-J, Liu Y-C. 2013. Characteristics of the photosynthesis microbial fuel cell with a Spirulina platensis biofilm. Bioresource Technology 135:640-643.

Lipscomb GL, Keese AM, Cowart DM, Schut GJ, Thomm M, Adams MWW, Scott RA. 2009. SurR: a transcriptional activator and repressor controlling hydrogen and elemental sulphur metabolism inPyrococcus furiosus. Mol. Microbiol. 71:332–349.

Lipscomb GL, Stirrett K, Schut GJ, Yang F, Jenney FE, Jr., Scott RA, Adams MWW, Westpheling J. 2011. Natural Competence in the Hyperthermophilic Archaeon Pyrococcus furiosus Facilitates Genetic Manipulation: Construction of Markerless Deletions of Genes Encoding the Two Cytoplasmic Hydrogenases. Applied and Environmental Microbiology 77(7):2232-2238.

Logan BE. 2009. Exoelectrogenic bacteria that power microbial fuel cells. Nature Reviews Microbiology 7(5):375-381.

Logan BE, Hamelers B, Rozendal RA, Schrorder U, Keller J, Freguia S, Aelterman P, Verstraete W, Rabaey K. 2006. Microbial fuel cells: Methodology and technology. Environmental Science & Technology 40(17):5181-5192.

Lovley DR. 1987. Organic-matter mineralization with the reduction of ferric iron - A review. Geomicrobiology Journal 5(3-4):375-399.

Lovley DR. 2004. Potential role of dissimilatory iron reduction in the early evolution of microbial respiration. Origins: Genesis, Evolution and Diversity of Life 6:301-+.
Lovley DR. 2008. The microbe electric: conversion of organic matter to electricity. Current Opinion in Biotechnology 19(6):564-571.
Lovley DR, Kashefi K, Vargas M, Tor JM, Blunt-Harris EL. 2000. Reduction of humic substances and Fe(III) by hyperthermophilic microorganisms. Chemical Geology 169(3-4):289-298.
Luque A, Hegedus S. 2003. Handbook of Photovoltaic Science and Engineering: John Wiley & Sons.
Ma KS, Adams MWW. 2001a. Ferredoxin : NADP oxidoreductase from Pyrococcus furiosus. Hyperthermophilic Enzymes, Pt C 334:40-45.
Ma KS, Adams MWW. 2001b. Hydrogenases I and II from Pyrococcus furiosus. Hyperthermophilic Enzymes, Pt B 331:208-216.
Ma KS, Weiss R, Adams MWW. 2000. Characterization of hydrogenase II from the hyperthermophilic archaeon Pyrococcus furiosus and assessment of its role in sulfur reduction. Journal of Bacteriology 182(7):1864-1871.
Ma KS, Zhou ZH, Adams MWW. 1994. Hydrogen-production from pyruvate by enzymes purified from the hyperthermophilic archaeon, Pyrococcus furiosus - a key role for NADPH. FEMS Microbiology Letters 122(3):245-250.
MacColl R. 1998. Cyanobacterial phycobilisomes. J Struct Biol. 124(2-3):311–334.
Marcus AK, Torres CI, Rittmann BE. 2007. Conduction-based modeling of the biofilm anode of a microbial fuel cell. Biotechnology and Bioengineering 98(6):1171-1182.
Marshall CW, May HD. 2009. Electrochemical evidence of direct electrode reduction by a thermophilic Gram-positive bacterium, Thermincola ferriacetica. Energy & Environmental Science 2(6):699-705.
Marsili E, Baron DB, Shikhare ID, Coursolle D, Gralnick JA, Bond DR. 2008. Shewanella Secretes flavins that mediate extracellular electron transfer. Proceedings of the National Academy of Sciences of the United States of America 105(10):3968-3973.
Mathis BJ, Marshall CW, Milliken CE, Makkar RS, Creager SE, May HD. 2008. Electricity generation by thermophilic microorganisms from marine sediment. Applied Microbiology and Biotechnology 78(1):147-155.
Mathwork. 2011. Global Optimization Toolbox: User's Guide (r2011b).
McCormick AJ, Bombelli P, Bradley RW, Thorne R, Wenzel T, Howe CJ. 2015. Biophotovoltaics: oxygenic photosynthetic organisms in the world of bioelectrochemical systems. Energy & Environmental Science 8(4):1092-1109.
McCormick AJ, Bombelli P, Scott AM, Philips AJ, Smith AG, Fisher AC, Howe CJ. 2011. Photosynthetic biofilms in pure culture harness solar energy in a mediatorless bio-photovoltaic cell (BPV) system. Energy Environ. Sci 4:4699–4709.
Mehta T, Coppi MV, Childers SE, Lovley DR. 2005. Outer membrane c-type cytochromes required for Fe(III) and Mn(IV) oxide reduction in Geobacter sulfurreducens. Applied and Environmental Microbiology 71(12):8634-8641.
Mershin A, Matsumoto K, Kaiser L, Yu DY, Vaughn M, Nazeeruddin MK, Bruce BD, Graetzel M, Zhang SG. 2012. Self-assembled photosystem-I biophotovoltaics on nanostructured TiO2 and ZnO. Scientific Reports 2:DOI:10.1038/srep00234.

Nather DJ, Rachel R, Wanner G, Wirth R. 2006. Flagella of Pyrococcus furiosus: Multifunctional organelles, made for swimming, adhesion to various surfaces, and cell-cell contacts. Journal of Bacteriology 188(19):6915-6923.

Noji T, Suzuki H, Gotoh T, Iwai M, Ikeuchi M, Tomo T, Noguchi T. 2011. Photosystem II-Gold Nanoparticle Conjugate as a Nanodevice for the Development of Artificial Light-Driven Water-Splitting Systems. Journal of Physical Chemistry Letters 2(19):2448-2452.

Obinger C, Knepper JC, Zimmermann U, Peschek GA. 1990. IDENTIFICATION OF A PERIPLASMIC C-TYPE CYTOCHROME AS ELECTRON-DONOR TO THE PLASMA MEMBRANE-BOUND CYTOCHROME-OXIDASE OF THE CYANOBACTERIUM NOSTOC MAC. Biochemical and Biophysical Research Communications 169(2):492-501.

Ortiz-Martinez VM, Salar-Garcia MJ, de los Rios AP, Hernandez-Fernandez FJ, Egea JA, Lozano LJ. 2015. Developments in microbial fuel cell modeling. Chemical Engineering Journal 271:50-60.

Ota M, Takenaka M, Sato Y, Smith Jr. RL, Inomata H. 2015. Effects of light intensity and temperature on photoautotrophic growth of a green microalga, Chlorococcum littorale. Biotechnology Reports 7: 24–29.

Ouitrakul R, Izawa S. 1973. Electron transport and photophosphorylation in chloroplasts as a function of the electron acceptor. Biochimica et Biophysica Acta 305:105-118.

Parimi NS, Umasankar Y, P. A, Ramasamy RP. 2012. Kinetic and mechanistic parameters of laccase catalyzed direct electrochemical oxygen reduction reaction. ACS Catalysis 2(1):38-44.

Picioreanu C, Head IM, Katuri KP, van Loosdrecht MCM, Scott K. 2007. A computational model for biofilm-based microbial fuel cells. Water Research 41(13):2921-2940.

Pils D, Gregor W, Schmetterer G. 1997. Evidence for in vivo activity of three distinct respiratory terminal oxidases in the cyanobacterium *Synechocystis* sp. strain PCC6803. FEMS Microbiology Letters 152:83-88.

Pils D, Schmetterer G. 2001. Characterization of three bioenergetically active respiratory terminal oxidases in the cyanobacterium *Synechocystis* sp. strain PCC 6803. FEMS Microbiology Letters 203:217-222.

Pisciotta JM, Zou Y, Baskakov IV. 2010. Light-Dependent Electrogenic Activity of Cyanobacteria. PLOS One 5(5):DOI:10.1371/journal.pone.0010821.

Pisciotta JM, Zou YJ, Baskakov IV. 2011. Role of the photosynthetic electron transfer chain in electrogenic activity of cyanobacteria. Applied Microbiology and Biotechnology 91(2):377-385.

Poole FL, Gerwe BA, Hopkins RC, Schut GJ, Weinberg MV, Jenney FE, Adams MWW. 2005. Defining genes in the genome of the hyerthermophilic archaeon Pyrococcus furiosus: Implications for all microbial genomes. Journal of Bacteriology 187(21):7325-7332.

Potts M. 1999. Mechanisms of desiccation tolerance in cyanobacteria. Eur. J. Phycol 34:319-328.

Qian X, Mester T, Morgado L, Arakawa T, Sharma ML, Inoue K, Joseph C, Salgueiro CA, Maroney MJ, Lovley DR. 2011. Biochemical characterization of purified OmcS, a c-type cytochrome required for insoluble Fe(III) reduction in Geobacter sulfurreducens. Biochimica Et Biophysica Acta-Bioenergetics 1807(4):404-412.

Quintana N, Van der Kooy F, Van de Rhee MD, Voshol GP, Verpoorte R. 2011. Renewable energy from Cyanobacteria: energy production optimization by metabolic pathway engineering. Applied Microbiology and Biotechnology 91(3):471-490.

Ramasamy RP, Gadhamshetty V, Nadeau LJ, Johnson GR. 2009. Impedance spectroscopy as a tool for non-intrusive detection of extracellular mediators in microbial fuel cells. Biotechnol Bioeng 104(5):882-91.

Ramasamy RP, Luckarift HR, Ivnitski D, Atanassov P, Johnson GR. 2010. High electrocatalytic activity of tethered multicopper oxidase-carbon nanotube conjugates. Chemical Communications 46(33):6045-6047.

Ramasamy RP, Sekar N; University of Georgia Research Foundation, Inc., , assignee. 2015 05/21/2015. ENGINEERED PHOTOSYNTHETIC CELLS, PHOTOSYNTHETIC ELECTRODES INCLUDING THE PHOTOSYNTHETIC CELLS, AND METHODS OF USING THE ENGINEERED PHOTOSYNTHETIC CELLS. U. S. patent 62/164,821.

Rasmussen M, Minteer SD. 2014. Thylakoid direct photobioelectrocatalysis: utilizing stroma thylakoids to improve bio-solar cell performance. Physical Chemistry Chemical Physics 16(32):17327-17331.

Reguera G, Nevin KP, Nicoll JS, Covalla SF, Woodard TL, Lovley DR. 2006. Biofilm and nanowire production leads to increased current in Geobacter sulfurreducens fuel cells. Applied and Environmental Microbiology 72(11):7345-7348.

Roberts AG, Bowman MK, Kramer DM. 2004. The inhibitor DBMIB provides insight into the functional architecture of the qo site in the cytochrome b(6)f complex. Biochemistry 43(24):7707-7716.

Roberts AG, Kramer DM. 2001. Inhibitor "double occupancy" in the Q(o) pocket of the chloroplast cytochrome b(6)f complex. Biochemistry 40(45):13407-13412.

Robinson HH, Crofts AR. 1983. Kinetics of the oxidation reduction reactions of the photosystem-II quinone acceptor complex, and the pathway for deactivation. FEBS Letters 153(1):221-226.

Rosenbaum M, He Z, Angenent LT. 2010. Light energy to bioelectricity: photosynthetic microbial fuel cells. Current Opinion in Biotechnology 21(3):259-264.

Rosenbaum M, Schroder U, Scholz F. 2005a. In situ electrooxidation of photobiological hydrogen in a photobioelectrochemical fuel cell based on Rhodobacter sphaeroides. Environmental Science & Technology 39(16):6328-6333.

Rosenbaum M, Schroder U, Scholz F. 2005b. Utilizing the green alga Chlamydomonas reinhardtii for microbial electricity generation: a living solar cell. Applied Microbiology and Biotechnology 68(6):753-756.

Roy J, Luckarift HR, Lau C, Falase A, Garcia KE, Ista LK, Chellamuthu P, Ramasamy RP, Gadhamshetty V, Wagner G and others. 2012. Riboflavin production by Shewanella oneidensis MR-1 in response to electron donor limitation. RSC Advances 2:10020-10027.

Sapra R, Bagramyan K, Adams MWW. 2003. A simple energy-conserving system: Proton reduction coupled to proton translocation. Proceedings of the National Academy of Sciences of the United States of America 100(13):7545-7550.

Sara M, Sleytr UB. 2000. S-layer proteins. Journal of Bacteriology 182(4):859-868.

Schopf S, Wanner G, Rachel R, Wirth R. 2008. An archaeal bi-species biofilm formed by Pyrococcus furiosus and Methanopyrus kandleri. Arch Microbiol. 190(3):371-377.

Schroder I, Johnson E, de Vries S. 2003. Microbial ferric iron reductases. Fems Microbiology Reviews 27(2-3):427-447.

Schut GJ, Boyd ES, Peters JW, Adams MWW. 2013. The modular respiratory complexes involved in hydrogen and sulfur metabolism by heterotrophic hyperthermophilic archaea and their evolutionary implications. FEMS Microbiol Rev 37:182-203.

Schut GJ, Bridger SL, Adams MW. 2007. Insights into the metabolism of elemental sulfur by the hyperthermophilic archaeonPyrococcus furiosus: characterization of a coenzyme A-dependent NAD(P)H sulfur oxidoreductase. J. Bacteriol. 189:4431–4441.

Sekar N, Jain R, Yan Y, Ramasamy RP. 2016. Enhanced photo-bioelectrochemical energy conversion by genetically engineered cyanobacteria. Biotechnology and Bioengineering 113(3):675-679.

Sekar N, Ramasamy RP. 2013. Electrochemical impedance spectroscopy for microbial fuel cell characterization. J Microbial Biochem Technol S6:004.

Sekar N, Ramasamy RP. 2015. Recent advances in photosynthetic energy conversion. Journal of Photochemistry and Photobiology C-Photochemistry Reviews 22:19-33.

Sekar N, Umasankar Y, Ramasamy RP. 2014. Photocurrent generation by immobilized cyanobacteria via direct electron transport in photo-bioelectrochemical cells. Physical Chemistry Chemical Physics 16(17):7862-7871.

Shibamoto T, Kato Y, Sugiura M, Watanabe T. 2009. Redox Potential of the Primary Plastoquinone Electron Acceptor Q(A) in Photosystem II from Thermosynechococcus elongatus Determined by Spectroelectrochemistry. Biochemistry 48(45):10682-10684.

Silva PJ, van den Ban ECD, Wassink H, Haaker H, de Castro B, Robb FT, Hagen WR. 2000. Enzymes of hydrogen metabolism in Pyrococcus furiosus. European Journal of Biochemistry 267(22):6541-6551.

Sjoholm KH, Rasmussen M, Minteer SD. 2012. Bio-Solar Cells Incorporating Catalase for Stabilization of Thylakoid Bioelectrodes during Direct Photoelectrocatalysis. Ecs Electrochemistry Letters 1(5):G7-G9.

Solov'ev AA, Katz E, Shuvalov VA, Erokhin YE. 1991. Photoelectrochemical effects for chemically modified platinum electrodes with immobilized reaction centers from Rhodobacter sphaeroides R-26. Bioelectrochem. Bioenerg. 26:29-41.

Summers LA. 1980. The Bipyridinium Herbicides. New York, NY: Academic Press.

Tanaka K, Tamamushi R, Ogawa T. 1985. Bioelectrochemical fuel-cells operated by the cyanobacterium, Anabaena variabilis. J Chem Technol Biotechnol 35B:191–197.

Terasaki N, Yamamoto N, Hiraga T, Sato I, Inoue Y, Yamada S. 2006. Fabrication of novel photosystem I-gold nanoparticle hybrids and their photocurrent enhancement. Thin Solid Films 499(1-2):153-156.

Terauchi AM, Lu SF, Zaffagnini M, Tappa S, Hirasawa M, Tripathy JN, Knaff DB, Farmer PJ, Lemaire SD, Hase T and others. 2009. Pattern of Expression and Substrate Specificity of Chloroplast Ferredoxins from Chlamydomonas reinhardtii. Journal of Biological Chemistry 284(38):25867-25878.

Thomas PE, Ryan D, Levin W. 1976. IMPROVED STAINING PROCEDURE FOR DETECTION OF PEROXIDASE-ACTIVITY OF CYTOCHROME-P-450 ON SODIUM DODECYL-SULFATE POLYACRYLAMIDE GELS. Analytical Biochemistry 75(1):168-176.

Torimura M, Miki A, Wadano A, Kano K, Ikeda T. 2001. Electrochemical investigation of cyanobacteria Synechococcus sp PCC7942-catalyzed photoreduction of exogenous quinones and photoelectrochemical oxidation of water. Journal of Electroanalytical Chemistry 496(1-2):21-28.

Torres CI, Marcus AK, Parameswaran P, Rittmann BE. 2008. Kinetic experiments for evaluating the Nernst-Monod model for anode-respiring bacteria (ARB) in a biofilm anode. Environmental Science & Technology 42(17):6593-6597.

Trammell SA, Spano A, Price R, Lebedev N. 2006. Effect of protein orientation on electron transfer between photosynthetic reaction centers and carbon electrodes. Biosensors & Bioelectronics 21(7):1023-1028.

Trebst A. 1978. Plastoquinones in Photosynthesis. Phil. Trans. R. Soc. Lond. 284:591-599.

Trubitsin BV, Ptushenko VV, Koksharova OA, Mamedov MD, Vitukhnovskaya LA, Grigor'ev IA, Semenov AY, Tikhonov AN. 2005. EPR study of electron transport in the cyanobacterium Synechocystis sp PCC 6803: Oxygen-dependent interrelations between photosynthetic and respiratory electron transport chains. Biochimica Et Biophysica Acta-Bioenergetics 1708(2):238-249.

Tsujimura S, Wadano A, Kano K, Ikeda T. 2001. Photosynthetic bioelectrochemical cell utilizing cyanobacteria and water-generating oxidase. Enzyme and Microbial Technology 29:225–231.

Ulas G, Brudvig GW. 2011. Redirecting Electron Transfer in Photosystem II from Water to Redox-Active Metal Complexes. Journal of the American Chemical Society 133(34):13260-13263.

van Haaster DJ, Silva PJ, Hagedoorn P-L, Jongejan JA, Hagen WR. 2008. Reinvestigation of the steady-state kinetics and physiological function of the soluble NiFe-hydrogenase I of Pyrococcus furiosus. Journal of Bacteriology 190(5):1584-1587.

Vargas M, Kashefi K, Blunt-Harris EL, Lovley DR. 1998. Microbiological evidence for Fe(III) reduction on early Earth. Nature 395(6697):65-67.

Velasquez-Orta SB, Curtis TP, Logan BE. 2009. Energy From Algae Using Microbial Fuel Cells. Biotechnology and Bioengineering 103(6):1068-1076.

Vermaas WFJ. 2001. Photosynthesis and Respiration in Cyanobacteria. Encyclopedia of Life Sciences.

Vittadello M, Gorbunov MY, Mastrogiovanni DT, Wielunski LS, Garfunkel EL, Guerrero F, Kirilovsky D, Sugiura M, Rutherford AW, Safari A and others. 2010. Photoelectron Generation by Photosystem II Core Complexes Tethered to Gold Surfaces. Chemsuschem 3(4):471-475.

Weber KA, Achenbach LA, Coates JD. 2006. Microorganisms pumping iron: anaerobic microbial iron oxidation and reduction. Nature Reviews Microbiology 4(10):752-764.

Weinberg MV, Schut GJ, Brehm S, Datta S, Adams MW. 2005. Cold shock of a hyperthermophilic archaeon:Pyrococcus furiosusexhibits multiple responses to a suboptimal growth temperature with a key role for membrane-bound glycoproteins. J. Bacteriol. 187:336–348.

Wirth R, Bellack A, Bertl M, Bilek Y, Heimerl T, Herzog B, Leisner M, Probst A, Rachel R, Sarbu C and others. 2011. The Mode of Cell Wall Growth in Selected Archaea Is Similar to the General Mode of Cell Wall Growth in Bacteria as Revealed by Fluorescent Dye Analysis. Applied and Environmental Microbiology 77(5):1556-1562.

Wraight CA, Clayton RK. 1973. The absolute quantum efficiency of bacteriochlorophyll photooxidation in reaction centres of Rhodopseudomonas spheroides. Biochemica et Biophysica Acta 333:246-260.

Wrighton KC, Agbo P, Warnecke F, Weber KA, Brodie EL, DeSantis TZ, Hugenholtz P, Andersen GL, Coates JD. 2008. A novel ecological role of the Firmicutes identified in thermophilic microbial fuel cells. Isme Journal 2(11):1146-1156.

Yagishita T, Horigome T, Tanaka K. 1993. Effects of light, co2 and inhibitors on the current output of biofuel cells containing the photosynthetic organism Synechococcus sp. Journal of Chemical Technology and Biotechnology 56(4):393-399.

Yagishita T, Sawayama S, Tsukahara K, Ogi T. 1997. Effects of intensity of incident light and concentrations of Synechococcus sp. and 2-hydroxy-1,4-naphthoquinone on the current output of photosynthetic electrochemical-cell. Solar energy 61(5):347-353.

Yang M, Lu S, Lu J, Jiang SP, Xiang Y. 2010. Layer-by-layer self-assembly of PDDA/PWA-Nafion composite membranes for direct methanol fuel cells. Chemical Communications 46(9):1434-1436.

Yang Y, Xu M, Guo J, Sun G. 2012. Bacterial extracellular electron transfer in bioelectrochemical systems. Process Biochemistry 47(12):1707-1714.

Yehezkeli O, Tel-Vered R, Wasserman J, Trifonov A, Michaeli D, Nechushtai R, Willner I. 2012. Integrated photosystem II-based photo-bioelectrochemical cells. Nature Communications 3:DOI:10.1038/ncomms1741.

Yu Y, Zuo F, Li C-Z. 2014. Mediator-assisted photocurrent extraction from the thylakoids. Electrochimica Acta 144:263-267.

Zhang D, Dechatiwongse P, del Rio-Chanona EA, Maitland GC, Hellgardt K, Vassiliadis VS. 2015. Modelling of light and temperature influences on cyanobacterial growth and biohydrogen production. Algal Research-Biomass Biofuels and Bioproducts 9:263-274.

Zhang HM, Primak A, Cape J, Bowman MK, Kramer DM, Cramer WA. 2004. Characterization of the high-spin heme x in the cytochrome b(6)f complex of oxygenic photosynthesis. Biochemistry 43(51):16329-16336.

Zou YJ, Pisciotta J, Billmyre RB, Baskakov IV. 2009. Photosynthetic Microbial Fuel Cells With Positive Light Response. Biotechnology and Bioengineering 104(5):939-946.

APPENDICES

APPENDIX A

Culturing Cyanobacteria

Composition of BG11 medium (for 1 L)

Na_2CO_3	0.02 g
$NaNO_3$	1.07 g
Stock solution I	10 mL
Stock solution II	10 mL
Stock solution III	10 mL
Microelement solution	1 mL

Adjust the pH to 7.5 and sterilize by autoclave.

Stock solution I (for 1 L)

Na_2Mg EDTA	0.1 g
Ferric ammonium citrate	0.6 g
Citric acid H_2O	0.6 g
$CaCl_2$ $2H_2O$	3.6 g

Autoclave and store at room temperature.

Stock solution II (for 1 L)

$MgSO_4$ 7 H_2O	7.5 g

Autoclave and store at room temperature.

Stock solution III (for 1 L)

K_2HPO_4 6.1 g

Autoclave and store at room temperature.

Microelement solution (for 1 L)

H_3BO_3	2.86 g
$MnCl_2$ 4 H_2O	1.81 g
$ZnSO_4$ 7 H_2O	0.222 g
$CuSO_4$ 5 H_2O	0.079 g
$CoCl_2$ 6 H_2O	0.05 g
$NaMoO_4$	0.018 g

Filter sterilize using 0.2µ filter and store the bottle in dark by wrapping with aluminum foil.

- 90 mL of the BG11 medium is poured into 250 mL Erlenmeyer flasks and sterilized by autoclave. Usually 10 mL of cyanobacteria was used as inoculum for 90 mL shake flask culture and incubated in shaker at 100 rpm.
- *Nostoc* sp and *Anabaena variabilis* were grown at 25 °C under 12: 12 h light–dark cycles.
- *Synechococcus elongatus* was grown at 32 °C under continuous illumination.
- Illumination was provided using fluorescent lamps at an intensity of 80 µmol m^{-2} s^{-1} measured at the platform of the incubator (four 6400 K T5 white fluorescent lamps kept at the top of the incubator provide sufficient illumination)
- Subculture the cyanobacteria before the culture starts to turn yellow. It is too late, if the culture is already yellow.
- For BG11 agar plate, add 1.5% agar to the BG11 medium before autoclave.

Reference: The composition has been used in Bioconversion Research & Education Center (BREC), UGA to cultivate cyanobacteria and algae

APPENDIX B

Transformation in Cyanobacteria

The following protocol was used to transform *S. elongatus* with plasmid DNA.

1. To 2 mL eppendorf tubes, add 2 mL of culture for every transformation reaction to be performed.
    a. *Synechococcus* are capable of undergoing natural transformation, so the cells do not have a competency period. You also do not need to worry about the age of the culture (growing culture, a stationary phase culture, a fresh culture, or an old culture). Older cultures sitting on your bench may have lower efficiencies. For efficient transformations, use the mid-log cultures.
    b. Do not forget to include a negative control.
2. Spin the cells down (5000 x g for 10 minutes, room temperature).
3. Remove supernatant and resuspend cells in 750 µL of 10 mM NaCl.
4. Spin the cells again.
5. Remove the supernatant and resuspend the cells in 250 µL sterile BG11 media.
6. Add 1 – 10 µL of your plasmid DNA or water (negative control)
    a. I generally use 5 µL of the 30 µL eluate (~100 µg/mL) from miniprep.
7. Wrap the tubes in aluminum foil and put them on a shaker at 30°C.
    a. Incubation periods of 4 hours will produce transformants, though transformation efficiencies increase with longer incubation periods up to approximately 24 hours. Dark step is not necessary, but increases transformation efficiency ~8 fold.

8. Plate transformation reactions onto BG11 selective antibiotic plates. Incubate plates at 30°C in light. Use low light (~40 μmol m^{-2} s^{-1}) if the expected transformant is light sensitive, otherwise medium light (~100 – 200 μmol m^{-2} s^{-1}) will be sufficient. Transformants sometimes do not grow if placed in high light (+350 μmol m^{-2} s^{-1}).

Reference: Golden and Sherman. "Optimal Conditions for Genetic Transformation of the Cyanobacterium *Anacystis nidulans* R2". Journal of Bacteriology (1983) 158: 36 – 42.

APPENDIX C

Isolation of DNA from Cyanobacterial Culture

The following protocol was used to isolate genomic DNA from growing culture of *S. elongatus*. This yields both genomic and plasmid DNA.

1. Grow cells as described in Appendix A.
2. Transfer the cell suspension to a 50 mL Falcon tube and centrifuge for 10 min at 4000 g and room temperature.
3. Discard the supernatant and resuspend the pellet in a final volume of 1.5 mL in a microcentrifuge tube and centrifuge for 10 min at 14000 x g and room temperature.
4. Discard the supernatant and resuspend the pellet by vortexing in 400 µl TE.
5. Add 150 µL sterile glass beads (250 µm, acid washed, from Supelco Analytical)
6. Add 20 µL of 10 % w/v SDS.
7. Add 450 µL phenol-chloroform (1:1, v/v).
8. Vortex the tube for 1 min and cool the tube on ice for 1 min. Repeat this cycle for 5 times
9. Centrifuge the tube for 15 min at 14000 g and 4 °C; transfer the supernatant to a new microcentrifuge tube.
10. Phenol extraction:
    a. Add 0.4 mL phenol, vortex the tube and centrifuge for 3 min at 14000 g and 4 °C; transfer the supernatant and the interphase to a new tube and repeat this step.

b. Add 0.4 mL phenol-chloroform (1:1, v/v), vortex the tube and centrifuge for 3 min at 14000 g and 4 °C; transfer the supernatant and the interphase to a new tube and repeat this step.
c. Add 0.4 mL chloroform-isoamyl alcohol (24:1, v/v), vortex and centrifuge for 1 min at 14000 g and 4 °C; transfer the supernatant to a new tube.
d. Add 0.4 mL chloroform, vortex and centrifuge for 1 min at 14000 g and 4 °C; transfer the supernatant to a new tube.

11. Add 0.1 volumes sodium acetate (3 M).
12. Add 2.5 volumes of ethanol (-20 °C) and precipitate the DNA for 15 min at -20 °C.
13. Centrifuge for 15 min at 14000 g and 4 °C; discard the supernatant and wash the pellet with 70 % v/v ethanol (-20 °C).
14. Centrifuge for a few seconds and discard the supernatant.
15. Dry the pellet on bench top for at least 30 min or until you do not smell ethanol.
16. Dissolve the pellet in 50 µl TE.

Composition of Tris-EDTA (TE) buffer

10 mM Tris HCl pH 8.0

1 mM EDTA pH 8.0

Preparation of buffered Phenol

Buffered saturated or equilibrated phenol is commercially available. For DNA purification, the pH of the buffered phenol should be slightly alkaline (say >7.6), whereas the

acidic phenol is used for RNA extraction. If the pH of your phenol solution is < 7, then equilibrate it using Tris (pH 8.0) as follow to make suitable for DNA extraction. The phenol solution was extracted several times with equal volume of 1 M Tris (pH 8.0) in a separatory funnel until the pH of the phenolic phase was >7.6. Then the phenol was extracted once with 100 ml 0.1 M Tris (pH 8.0) + 0.2 ml β -mercaptoethanol. This solution was overlayed with 0.1 M Tris (pH 8.0) and stored in a bottle wrapped in aluminium foil at 4 °C. This solution was also used to prepare phenol-chloroform and phenol-chloroform-isoamyl alcohol solutions.

Reference: This protocol was modified from the methods given in the thesis (Burgstaller, 2012)

APPENDIX D

Cloning in *E. coli*

1. Design of cloning strategy and primer design using the software. Selection of restriction enzymes and buffers.
2. *E. coli* XL-1 Blue chemical competent cells (stock maintained in -80°C freezer in vials, each vial of 50 µL competent cells).
3. Obtaining DNA fragment by PCR (using genomic DNA of the desired microorganism or using the plasmid containing the synthesized gene: usually the gene sequence is codon optimized for expression in the desired microorganism and synthesized in Genscript).
4. PCR product purification
5. Restriction digestion of the plasmid and the PCR product
6. Ligation, transformation and plating in antibiotic selective agar plates
7. Design of screening strategy: Grow the colonies, isolate the plasmid and do PCR verification

I. Plasmid Isolation: Plasmid Miniprep - Zippy Protocol

II. PCR: Phusion Polymerase (50 µL system)

H_20	30 µL
5×Phusion HF Buffer	10 µL
2mM dNTP	5 µL

Primer mix	3.5 µL
Template	1 µL
Phusion Polymerase	0.5 µL

Annealing Temperature (Tm) should be the lowest Tm + 3 °C

Extension Time: 30s/kb at 72 °C

Reaction:

Step 1: 98 °C – 45 sec

Step 2: 98 °C – 15 sec

Step 3: Tm °C – 30 sec

Step 4: 72 °C – 30s/kb

Repeat Steps 2-3, 30 cycles

Step 5: 72 °C – 5 min

Step 6: 10 °C --- Hold

III. PCR product purification: ZYMO Protocol

IV. Restriction Digestion

1. Purified PCR product, plasmid to be digested separately- choose the correct restriction enzymes and the compatible buffer (refer NEB buffer charts)
2. Restriction digestion Set up (50 µL system)

Water	24 µL
10x Buffer (1/2/3/4)	5 µL
10x BSA	5 µL

Restriction Enzyme 1 2 µL

Restriction Enzyme 2 2 µL

Vector/ DNA 12 µL

3. Incubate at 37°C for 2-4 hours in water bath.

V. Gel Extraction

1. Use fresh 1x TAE buffer.

   Run 50 µL digested samples + 10 µL loading buffer in 0.8% Agarose gel.

2. Observe under UV Transilluminator. (wear UV protective glasses)
3. Cut the fragments and place it in their respective centrifuge tubes.

   Vector fragment and DNA- right size in separate tubes.

4. Add 300 µl - 600 µl of ADB buffer
5. Incubate at 55 °C for 10 min in water bath or as long as it takes to melt.
6. After the gel melts place in spin column with collection tube.
7. Centrifuge at 8000 rpm for 1min
8. Add 200 µL of DNA wash buffer.
9. Centrifuge at 15,000 rpm for 30 sec
10. Transfer spin column to centrifuge tube and add 8 µL milli- Q water.
11. Wait for 2 min and spin at 15,000 rpm for 30 sec.

VI. Ligation

1. Use DNA Insert: Plasmid as 3:1 or 5:1
2. Set up (10 µL system)

2x Buffer	5 µL
Vector	1 µL
Fragment	3.5 µL
Ligase	0.5 Ml

3. Wait for 5-10 min (room temperature), and then proceed for transformation.

VII. Heat shock Transformation

1. 10 µL sample + 50 µL chemical competent cell. (XLBlue1)
2. Keep on ice for 20-30 min
3. Heat shock at 42°C for 60 sec
4. Keep on ice for 2-3 min
5. Add 700 µL LB
6. Keep in 37 °C shaker for 30-45 min, 250 rpm
7. Centrifuge at 6000 rpm for 3 min
8. Discard 600 µL supernatant
9. Resuspend the 100 µL culture.
10. Spread the 100 µL culture on LB plate with the appropriate antibiotic.
11. Place it in 37 °C oven incubator overnight.

VIII. Screening

1. Pick 3-9 colonies and make overnight culture for all, separately.
2. Extract the plasmid from all cultures.
3. Verification of clones/mutants by PCR

APPENDIX E

Heme Staining

Protein Gel Electrophoresis

1. Run the cell lysate in SDS-PAGE with the following modifications (Usual SDS-PAGE procedure can be found at standard Maniatis protocols)
2. Reduce the SDS concentration in the electrophoresis buffer to 0.1 %
3. Pre-electrophorese the gel overnight at 1 mA/gel to remove excess ammonium persulfate.
4. Do not add SDS during gel polymerization; SDS would be introduced into the gel by the pre-electrophoresis step.
5. Perform gel electrophoresis under subdued light at 10 °C using a constant current power supply. Initially run the gel at a constant current of 1 mA/gel and increase the current to 3 mA/gel when the sample has completely entered the gel.
6. After the run, do not stain the gel with coomassie stain.
7. Stain the gel for peroxidase activity (heme staining) by the following procedure.

Heme staining procedure

1. Prepare a fresh solution of 6.3 mM TMBZ (3, 3', 5, 5' tetramethyl benzidine) in methanol.
2. Immediately before use, mix 3 parts of the TMBZ solution with 7 parts of 0.25 M sodium acetate, pH 5.0.
3. Immerse the gel in the mixture at room temperature in the dark.

4. After 1 to 2 hr with occasional mixing (every 10-15 min), add H_2O_2 to a final concentration of 30 mM.
5. Staining will be visible within 3 min and increase in intensity over the next 30 min.
6. At this time or a few hours later, place the gel in acetate buffered 30 % isopropanol solution (isopropanol:0.25 M sodium acetate, pH 5.0, at a ratio of 3:7).
7. Replace the acetate-buffered 30% isopropanol solution once or twice with fresh solution to remove any precipitated TMBZ. The replacement of the staining solution with the acetate buffered 30% isopropanol also serves to clear the gel background and enhance the staining intensity.
8. Document the gel under gel-documentation system (Biorad).

Principle of heme staining

All the heme proteins contain peroxidase activity. When H_2O_2 and TMBZ are added, the peroxidase activity of heme proteins converts the TMBZ to tetramethyl benzidine diamine which is observed as a visible band in the gel.

Reference: Protocol adopted from Thomas et al., 1976

APPENDIX F

Ferricyanide Reduction Assay

1. Grow the cells as given in Appendix A
2. Harvest 100 mL of culture at an OD_{750} of 0.6 by centrifuging the cells at 5,000 rpm for 10 min at room temperature
3. Re-suspend the pellet in 100 mL of fresh BG11 medium.
4. Do not forget to induce the omcs cultures with IPTG (working concentration of 1 mM)
5. Add sterile potassium ferricyanide solution (working concentration of 1 mM made in BG11 medium) to the culture
6. Incubate the cultures under light (same as explained in Appendix A) or dark with the same conditions, but cover the entire incubator with a dark cloth (You can also cover the flask with aluminum foil, but I prefer to put the shake flasks in the incubators and cover the entire incubator with a black cloth to maintain dark conditions
7. Collect 2 mL of samples every 4 h/12 h based on the time-points you need for 48 h/72 h respectively
8. Use 1 mL to measure the absorbance at 750 nm (for growth) and 665 nm (to estimate chlorophyll). Centrifuge the remaining 1 mL sample at 10,000 rpm for 5 min at room temperature
9. Measure the absorbance of the supernatant at 420 nm

10. Make a standard curve using known concentration of potassium ferricyanide vs absorbance at 420 nm. Use the standard curve to calculate the concentration of potassium ferricyanide from the A_{420} of the sample.
11. Calculate the chlorophyll content (mM) from A_{665} as shown below

$$Chlorophyll\ content = \frac{A_{665} * 12.7}{893.49}$$

12. The rate of ferricyanide reduction (mM ferricyanide mM^{-1}chl h^{-1}) is calculated using the formula given below

$$Rate\ of\ ferricyanide\ reduction = \frac{f_{t2} - f_{t1}}{(C_{t1} + C_{t2}) * (t2 - t1)}$$

where, f_{t1} and f_{t2} are ferricyanide concentration at time t1 and t2 respectively and C_{t1} and C_{t2} are chlorophyll content at time t1 and t2 respectively.

Reference: Protocol modified from Bradley et al., 2013

APPENDIX G

omcS Gene Sequence

Codon optimized for expression in *S. elongatus* PCC 7942

ATGAAGAAAGGCATGAAAGTTAGTCTGAGCGTGGCGGCGGCAGCACTCCTGATGTC
GGCACCGGCAGCGTTCGCATTCCATTCGGGCGGCGTGGCTGAATGCGAGGGTTGTCA
CACCATGCATAACAGCCTCGGTGGTGCAGTCATGAACAGCGCAACGGCACAGTTCA
CCACGGGTCCAATGCTGCTCCAGGGTGCAACCCAAAGCTCGAGTTGCCTGAACTGTC
ACCAACATGCGGGCGATACGGGTCCCAGCTCGTACCACATCAGCACTGCTGAAGCA
GACATGCCCGCTGGCACCGCACCGTTGCAGATGACGCCTGGCGGTGATTTTGGCTGG
GTCAAAAAGACCTATACGTGGAACGTTCGCGGCCTGAATACGAGCGAAGGCGAGCG
CAAAGGTCACAACATTGTTGCGGGCGATTACAATTATGTGGCTGACACTACCCTCAC
GACTGCACCAGGTGGCACCTACCCAGCAAACCAGTTGCATTGCAGTAGCTGTCACG
ATCCGCATGGCAAATATCGCCGCTTCGTCGACGGCTCGATCGCAACCACGGGTCTGC
CGATTAAGAATAGCGGCTCGTACCAAAACAGCAATGATCCTACGGCATGGGGTGCA
GTTGGTGCTTACCGCATCCTCGGTGGCACCGGCTATCAGCCTAAAAGTTTGAGCGGT
TCGTATGCCTTTGCAAACCAAGTGCCGGCAGCAGTCGCACCTAGCACCTACAATCGC
ACGGAAGCGACTACCCAGACCCGCGTGGCTTATGGCCAGGGTATGAGTGAGTGGTG
CGCGAATTGTCACACCGATATCCATAACAGCGCTTACCCAACGAATCTGCGCCACCC
AGCCGGTAACGGTGCTAAGTTCGGTGCAACCATTGCCGGTCTGTACAATTCGTATAA
AAAGAGTGGCGATCTCACTGGCACCCAGGCTAGCGCATACTTGTCGCTGGCACCGTT
TGAAGAGGGCACTGCCGATTATACCGTTTTGAAAGGTCATGCAAAGATTGATGACA
CGGCACTGACTGGTGCAGACGCAACGTCGAACGTGAATTGCCTGAGTTGTCACCGC
GCTCATGCAAGTGGCTTTGATAGCATGACCCGCTTCAACCTCGCCTACGAATTTACG
ACTATCGCCGATGCGAGTGGCAACAGCATTTATGGTACGGACCCCAATACTTCGAGT
CTGCAAGGCCGCAGCGTCAATGAGATGACTGCTGCATACTATGGCCGCACCGCAGA
CAAGTTCGCACCCTACCAACGCGCCCTGTGTAACAAATGCCACGCCAAAGATTAA

Length: 1299 bp

Vector name: pUC57

Synthesized from Genscript

APPENDIX H

Culturing *P. furiosus*

Composition of Defined Medium

Component	Stock conc.	Final conc.
Pf base salts	5 X	1 X
trace minerals	1000 X	1 X
sodium tungstate (Na_2WO_4•$2H_2O$)	100 mM	10 µM
Resazurin	5 mg/mL	0.25 µg/mL
Pf vitamin mix	200 X	1 X
Pf amino acid solution 19 AA (no cys)	25 X	2 X
Maltose	10 %	0.5 %
Add in fume hood while monitoring pH:		
cysteine hydrochloride		1 g/L
sodium sulfide (Na_2S)		0.5 g/L
sodium bicarbonate ($NaHCO_3$)		1 g/L
Adjust pH to between 6.7 and 6.8 with 10 M NaOH and add:		
potassium phosphate buffer (pH 6.8)	1 M	1 mM

Composition of Rich Medium

Component	Stock conc.	Final conc.
Pf base salts	5 X	1 X
trace minerals	1000 X	1 X
sodium tungstate (Na_2WO_4•$2H_2O$)	100 mM	10 µM
Resazurin	5 mg/mL	0.25 µg/mL
yeast extract	10 %	0.5 %
casein hydrolysate (enzymatic)	10 %	0.5 %
Maltose	10 %	0.5 %
Add in fume hood while monitoring pH:		
cysteine hydrochloride		0.5 g/L
sodium sulfide (Na_2S)		0.5 g/L
sodium bicarbonate ($NaHCO_3$)		1 g/L
Adjust pH to between 6.7 and 6.8 with 10 M NaOH and add:		
potassium phosphate buffer (pH 6.8)	1 M	1 mM

5X *Pf* base salts

	1000 mL
NaCl	140.0 g
$MgSO_4 \cdot 7H_2O$	17.5 g
$MgCl_2 \cdot 6H_2O$	13.5 g
KCl	1.65 g
NH_4Cl	1.25 g
$CaCl_2 \cdot 2H_2O$	0.70 g
dH_2O	to 1 L

Filter-sterilize. Store at room temperature or 4ºC.

1000 X Trace minerals

	1000 mL
HCl (concentrated)	1.00 mL
Na_4EDTA (tetra sodium)	0.50 g
$FeCl_3$	2.00 g
H_3BO_3	0.05 g
$ZnCl_2$	0.05 g
$CuCl_2 \cdot 2H_2O$	0.03 g
$MnCl_2 \cdot 4H_2O$	0.05 g
$(NH_4)_2MoO_4$	0.05 g
$AlK(S0_4) \cdot 2H_20$	0.05 g
$CoCl_2 \cdot 6H_2O$	0.05 g
$NiCl_2 \cdot 6H_2O$	0.05 g
dH_2O	to 1 L

Add HCl and EDTA to ~900 mL dH_2O. Then dissolve remaining salts and fill volume to 1000 mL. Solution is clear yellow. Store at room temperature (do not autoclave). Filter sterilize, if desired.

200 X Vitamin mix

	1000 mL
Niacin	10 mg
Biotin	4 mg
Pantothenate	10 mg
Lipoic Acid	10 mg
Folic Acid	4 mg
p-Aminobenzoic Acid	10 mg

Thiamine B_1	10 mg
Riboflavin B_2	10 mg
Pyridoxine B_6	10 mg
Cobalamin B_{12}	10 mg
dH_2O	to 1 L

Filter-sterilize. Aliquot into 50-mL falcon tubes, wrapped in foil. Store at -20ºC.

25 X 19-amino acid mix (no cysteine)

	1000 mL
Alanine	1.875 g
Arginine	3.125 g
Asparagines	2.5 g
Aspartic acid	1.25 g
Glutamic acid	5.0 g
Glutamine	1.25 g
Glycine	5.0 g
Histidine	2.5 g
Isoleucine	2.5 g
Leucine	2.5 g
Lysine	2.5 g
Methionine	1.875 g
Phenylalanine	1.875 g
Proline	3.125 g
Serine	1.875 g
Threonine	2.5 g
Tryptophan	1.875 g
Tyrosine	0.3 g
Valine	1.25 g

Filter-sterilize into aliquots of 500 mL or less. Store at 4ºC, wrapped in foil.

APPENDIX I

Iron Reduction Assay in *P. furiosus*

Reduction of Fe(III) oxides

1. Add 15 mM iron (III) oxide (Fe_2O_3) to the sterile *Pf* rich medium (50 mL shake flask experiments)
2. Inoculate 0.5 mL overnight culture into the 50 mL rich medium containing Fe_2O_3
3. Perform all the experiments in triplicates and incubate at 90 °C with shaking.
4. Collect samples every four hours from the inoculation time to monitor cell growth and concentration of Fe(II)
5. Growth was monitored by measuring the absorbance of collected sample at 600 nm
6. Measure the Fe(II) (aqueous ferrous iron concentration) using the ferrozine assay as explained below

Reduction of Fe(III) Citrate

1. Centrifuge 500 mL of overnight grown *Pf* cells (grown in rich medium) at 4 °C, 5000 rcf, 10 min and resuspend the cell pellet in 50 mL of suspension buffer
2. Add 20 mM ferric citrate to the 50 mL of suspension buffer containing *Pf* cells
3. Fill the headspace with H_2: CO2 (80:20, v/v)
4. Perform all the experiments in triplicates and incubate at 90 °C with shaking

5. Collect samples every four hours to measure the concentration of Fe(II) (aqueous ferrous iron concentration) using the ferrozine assay as explained below

Ferrozine assay

1. Collect 0.5 mL of sample and mix with equal volume of 0.5 M HCl at room temperature for 15 min and store the sample at 4 °C until further processing
2. Centrifuge at 10,000 rpm for 5 min at room temperature
3. Add 10 µL of the supernatant to 490 µL ferrozine reagent (2 mM ferrozine in 50 mM HEPES, pH 7.0)
4. Measure the absorbance at 562 nm using UV-Vis spectrophotometer (Genesys 10S, Thermo Scientific).
5. Make a standard curve using known concentration of ferrous ethylene diammonium sulfate and A_{562}
6. Calculate the concentration of soluble ferrous ion using the standard curve

Reference: Modified form the protocol given in Lovley 1987

APPENDIX J

Electrochemical Experiments

Preparation of CB electrode (CB/MWCNT/CP) for photocurrent measurement

1. SpectraCarb 2050-L carbon paper (CP) was used as the base electrode for all the experiments that measure photocurrent
2. Treat the CP with a boiling mixture of 1 M HNO_3 and 0.5 M H_2SO_4 (1:4 ratio) for an hour and wash with dd water.
3. Prepare the multi-walled carbon nanotube (MWCNT) solution (1 mg mL^{-1}) in dimethyl formamide
4. Suspend the MWCNT in dimethyl formamide to make a uniform slurry by sonicating it for 15 min in ultrasonic homogenizer.
5. Add 5 µL of MWCNT solution on top of the CP, dry in oven (roughly around 70 °C) to make MWCNT modified CP
6. Air dry the MWCNT/CP on the bench top and wet the MWCNT/CP with a small quantity of phosphate buffer before adding CB
7. Wash cyanobacterial (CB) culture using phosphate buffer (100 mM, pH 7) and re-suspend in the same buffer (Use appropriate concentration, usually I shall concentrate the 5 mL CB culture with a OD_{750} of 2.0 to 50 µL)
8. Add 5 µL of the CB culture on top of MWCNT/CP and allow to air dry at room temperature

9. After the cells are dried, add another 5 µL of the CB culture and repeat to maximum of four loading of CB cells
10. The CB/MWCNT/CP is used as the working electrode in three electrode set-up (half-cell) or as the anode in the bioelectrochemical full-cell

Three Electrode System

The three electrode system or half-cell electrochemical system consists of three electrodes:

1. **Working electrode**: the electrode where the concerned electrochemical reaction under study happens.
    a. The working electrode will be the anode when an oxidation reaction happen resulting in generating oxidation current (positive current)
    b. The working electrode will be the cathode when a reduction reaction happen resulting in generating reduction current (negative current)

The glassy carbon electrode (cylindrical in shape with a dimension of –x--) is used as the working electrode in the entire research unless otherwise specifically mentioned. Rather than using the glassy carbon electrode, usually the glassy carbon is modified with different biocatalyst such as CB/MWCNT/CP or PF/MWCNT/CP.

2. **Reference electrode**: The potential at the working electrode is measured or a fixed constant potential is applied to the working electrode with respect to this reference electrode. In the entire thesis work, silver/silver chloride reference electrode (Ag/AgCl, sat. KCl) is used as the reference electrode. The equilibrium potential of the Ag/AgCl,

sat. KCl is + 0.197 V with respect to Standard Hydrogen Electrode (SHE, whose equilibrium potential is 0 V). All the potential values are reported with respect to the Ag/AgCl, sat. KCl unless otherwise specifically mentioned.

3. **Counter electrode**: Also called auxiliary electrode that closes the circuit for an electrochemical measurement. For example, if the oxidation happens at the working electrode, the reduction reaction will happen at the cathode and vice versa. A thin platinum wire is usually used as the counter electrode.

The three electrode system is not a device. It is an electrochemical system used to study the oxidation/reduction reaction that is happening at the working electrode with respect to the reference electrode (Ag/AgCl, sat. KCl). All the three electrodes are dipped into the electrolyte and the leads from the three electrodes are connected to the potentiostat. A specific function (explained below) in the potentiostat is chosen based on the type of electrochemical parameter measured.

Research work	Working electrode	Reference electrode	Counter electrode
CB	Glassy carbon electrode modified with CB/MWCNT/CP	Ag/AgCl, sat. KCl	platinum wire
Pf	Glassy carbon electrode modified with PF/MWCNT/CP	Ag/AgCl, sat. KCl	platinum wire

Full Cell Set Up (Microbial Fuel Cell)

The Full cell or the microbial fuel cell is an electrochemical device that consists of anode and cathode. Oxidation occurs at the anode and reduction happens at the cathode. When the two reactions are spatially separated and based on the potential difference between the anode and the

cathode, the electron transferred from the microorganism to the anode, flows through the external circuit and are used to reduce a specific electron acceptor at the cathode. A separate reference electrode is not needed for measuring current (unless to separately characterize the anode and cathode).

Research work	Anode	Cathode
CB	Glassy carbon electrode modified with CB/MWCNT/CP	Glassy carbon electrode modified with Lac/MWCNT/CP
Pf	Carbon felt suspended in *Pf* culture	Carbon felt suspended in buffer containing potassium ferricyanide

Open Circuit Potential

Open Circuit Potential (OCP) is the potential difference between the two electrodes (the anode and the cathode) measured without closing the circuit with an external load, i.e., no current is flowing through the circuit. OCP is the maximum potential difference between the anode and the cathode of the electrochemical device such as MFC. The voltage of the MFC decreases from the OCP when appropriate load (resistance) is connected to the external circuit. Throughout the research work, the OCP is measured by choosing the "*Open Circuit Potential - Time*" function in the potentiostat.

I-t Measurement

I-t measurement, also called chronoamperometry, is a technique that measures current by applying a fixed constant potential using the potentiostat. If the applied potential (E_{app}) is greater than the OCP, you will measure the oxidation current (as a result of oxidation reaction happening

at the electrode surface). If the E_{app} is lesser than the OCP, you will measure the reduction current (as a result of reduction reaction happening at the electrode surface). In all the CB and *Pf* experiments, the applied potential is always greater than the OCP, so that the desired oxidation current (transfer of electrons from the microorganism to the electrode) will be measured. Throughout the research work, the OCP is measured by choosing the "*Amperometric I-t curve*" function in the potentiostat.

Polarization Curve

Polarization curve is a plot of current density (A/m^2) on the x-axis versus potential (V) in the y-axis. This plot can be obtained in two ways:

1. Using a potentiostat, do the *Amperometric I-t curve* by applying a different constant potential at a time to measure the steady state current (you do not need a variable resistance box in the case)
2. Using a current measurement device (Arbin instruments or a simple multimeter), measure the current by varying the resistance attached to the external circuit. From the current (I) and resistance (R), calculate the potential (V) using Ohm's law (V=IR)

The polarization curve clearly explains the type of losses (such as ohmic losses, charge transfer losses and concentration losses) that predominates the electrochemical system and is very useful to improve the system performance.

Power Density Curve

The performance of the MFC is usually characterized by the power density curve. It is the plot of current density (A/m^2) on the x-axis versus power density (W/ m^2) in the y-axis. Power density (P) is calculated by multiplying the current density (I) with the potential (V) using the correlation P=IV. The peak power density and the maximum current density are the two parameters that are usually used to gauge the MFC performance.

APPENDIX K

Matlab Source Code

```
function [c,f,s]=mfc1pde(x,t,u,DuDx)
c=[1;1;1;0];
f=[1.09*10^-9;0.43*10^-9;0.43*10^-9;5*10^-5].*DuDx;
ks=13.2;
km=0.1*10^-3;
F=96485;
R=8.314;
T=303.15;
b=1700;
i=0.8*10^3;
ki=0.208*10^3;
kin=3.33*10^3;
nm=1/(1+exp((-F/(R*T))*(u(4)+0.155)));
iterm=i/(i+ki+(i^2/kin));
sterm=u(1)/(u(1)+ks);
mterm=u(2)/(u(2)+km);
qmax=0.002*10^-3;
qm=qmax*sterm*mterm*iterm;
qc=qmax*sterm*nm*iterm;
s=[-b*qm-b*qc;-1.2*b*qm;1.2*b*qm;2.4*F*b*qc];
end
```

```
function u0=mfc1ic(x)
u0=[25 ; 0 ; 0.001 ; 0.3];
end
```

```
function [pl,ql,pr,qr]=mfc1bc(xl,ul,xr,ur,t)
pl=[0;3287.79*ul(3)-(7.7864*10^-14)*ul(2);(7.7864*10^-14)*ul(2)-3287.79*ul(3);(ul(4)-0.3)];
ql=[1;1;1;0];
pr=[(ur(1)-25);(ur(2)-0.001);ur(3);0];
qr=[0;0;0;1];
end
```

```
>>m=0;
>> x=linspace(0,0.0001,100);
>> t=linspace(0,2,100);
>> sol=pdepe(m,@mfc1pde,@mfc1ic,@mfc1bc,x,t);
>> u1=sol(:,:,1);
>> u2=sol(:,:,2);
>> u3=sol(:,:,3);
>> u4=sol(:,:,4);
>>for i = 1:100;
slope (i) = [u4(i,2)-u4(i,1)]/(2/100);
end
>>jD = slope * (-5*10^-5);
>>jM = 96485*2*(u3(:,1)*3287.79-u2(:,1)*7.7864*10^-14);
>>j = jM + jD';
```